NASA CONTRACTOR REPORT

NASA CR-1566

RADIATION INDUCED NONLINEAR DEGRADATION OF TRANSISTOR GAIN

Prepared by
THE BOEING COMPANY
Seattle, Wash.
for Goddard Space Flight Center

NATIONAL AERONAUTICS AND SPACE ADMINISTRATION • WASHINGTON, D. C. • JULY 1970

NASA CR-1566

RADIATION INDUCED NONLINEAR DEGRADATION OF TRANSISTOR GAIN

Issued by Originator as Boeing Doc. D2-125680-3

Prepared under Contract No. NAS 5-10443 by
THE BOEING COMPANY
Seattle, Wash.

for Goddard Space Flight Center

NATIONAL AERONAUTICS AND SPACE ADMINISTRATION

For sale by the Clearinghouse for Federal Scientific and Technical Information
Springfield, Virginia 22151 – CFSTI price $3.00

ABSTRACT

This document constitutes the final report for NASA Contract NAS5-10443 and supersedes the interim reports D2-125680-1 and -2. Included is a description of research conducted during the period of June 23, 1967 to January 31, 1969. Work on the program was directed toward accomplishing the main objective which is the establishment of correlation and equivalence factors of radiation induced nonlinear degradation of transistor current gain. Research progressed in accordance with a modified program plan primarily as outlined in the Boeing technical proposal document D2-125398-1, "Radiation Induced Nonlinear Degradation of Transistor Gain," April 1967 (Ref. 1).

The research described in this report, Phase II, deals primarily with ionization induced surface effects on transistors. In addition there is included in this work the extension of data on equivalences for displacement damage initiated in Phase I of this program under contract NAS5-9578 and the establishment of the feasibility of conducting simultaneously combined radiation effects tests proposed for future Phase III work.

A one MeV electron exposure test of transistors was used to empirically formulate aspects of the dependence of nonlinear damage on radiation and to determine the influence of continuous electrical operation during exposure on the magnitude of device damage. Cobalt 60 - gamma radiation exposure of devices from the Phase I contract was extended to high doses to provide improved data on gamma radiation displacement equivalences. Separate electron tests and 15 MeV proton tests were conducted to determine the best test plan approach for combined synergistic tests. Proton testing at 15 MeV was extended to high fluences to further study the importance of ionization effects and to improve displacement equivalence values obtained under the Phase I contract.

The dependence of passive but not active transistors on collector current during measurement of current gain was found to be consistent with that theoretically predictable from increased carrier recombination rates at the surface of the base-emitter junction region. A statistical study of passive transistors revealed that effects on devices within a batch tend to behave similarly, while devices from separate batches are likely to behave dissimilarly if the batch numbers (i.e., the date codes) are very different.

In addition, devices from different manufacturers are likely to be dissimilar due to differences in surface preparation, geometry, etc.

The profile for buildup of damage with dose, analyzed in the form of $\Delta(1/h_{FE})$, does not consistently fit any of the anticipated exponential or simple power law relationships. Moreover, if some of the curves of active NPN devices are to be approximated by a power law then $x > 1$ values should be used. Analysis of data in the desirable "normalized" form of relative gain loss $\Delta h_{FE}/h_{FE_i}$ was also performed. Empirical fitting of relative gain loss to a hyperbolic tangent formulation was successful for the transistor types studied.

In general the concept of ionization equivalences for nonlinear damage works quite well. The only (but very significant) exception was the much greater damage sensitivity of passive npn transistors that had been exposed to the ionization effects of 15 MeV protons.

Various new insights into the source of nonlinear damage were revealed and are described in detail. Although increased recombination at the silicon oxide and semiconductor interface appears to account for most of the damage, certain effects observed on leakage current, gain, capacitance, and I_b versus V_{BE} analysis indicate that charge buildup of the oxide layer (particularly for active devices) can play a very significant role.

Significant differences in radiation sensitivity between passive and active NPN devices were observed and are discussed in detail. Latin cube analysis of the data from the multifactor experimental design was effective in showing no significant interdependence between dose and either current or voltage applied either during exposure or applied for measurement of gain after exposure. Dependence of nonlinear damage on dose, current, or voltage separately are desdribed in the text.

Data on nonlinear damage to transistors exposed to pulsed electrons from the Linac (in the combined beam mode) agreed well with steady state exposure from the Dynamitron indicating no significant rate effects. 15 MeV proton nonlinear damage (in the combined beam mode) to pnp transistors showed good agreement with electron exposed devices based on total absorbed dose. Proton effects on npn transistors, however, showed much greater damage than electron effects for the same dose. Thus proton exposures were extended to high fluences to determine when displacement effects dominate. An anomalous sensitivity to active biasing during proton exposure was also observed.

Results of separate Linac electron and Dynamitron proton testing (in the combined beam mode) have, however, established the feasibility of combined beam testing.

It is recommended that a Phase III effort to this program be planned. That phase should include simultaneously combined electron and proton exposures. Due to more severe proton damage and somewhat opposing results of electron damage (ratio of active bias to passive) to npn devices, it is suggested that significant additive synergistic effects will be observed. It is also recommended that the latest high reliability device types (typical of new space system utilization) be tested along with base line 2N1613 transistors. A captive assembly line could be utilized to assure processing control as well as identification and selection of various specific surface properties. In addition, due to the unpredicted response observed on the precursory testing of npn transistors actively operated during proton exposure, it is proposed that studies of proton damage as a function of active bias during exposure be conducted to complement similar studies already conducted with electrons.

TABLE OF CONTENTS

TABLE OF CONTENTS (continued)

LIST OF ILLUSTRATIONS

LIST OF ILLUSTRATIONS (continued)

LIST OF ILLUSTRATIONS (continued)

LIST OF ILLUSTRATIONS (continued)

LIST OF ILLUSTRATIONS (continued)

LIST OF ILLUSTRATIONS (continued)

LIST OF TABLES

1.0 INTRODUCTION

1.1 PURPOSE

The overall needs that relate to space mission radiation vulnerability of electronic systems include the ability to:

1. Extrapolate from laboratory-simulated radiation tests to space radiation performance;

2. Extrapolate from performance on an in-flight test to other space mission conditions;

3. Generalize from radiation effects on a limited number of transistors to the effects on many types; and

4. Develop techniques to allow for standardization in qualification testing of new devices.

This contracted study serves as the second phase of a planned effort directed toward meeting those needs listed above. In particular, it is the objective of this contract to establish correlation and equivalence factors for radiation induced nonlinear degradation of transistor current gain (ionization induced surface effects) for use in the evaluation of semiconductor devices for spacecraft missions.

1.2 PROGRAM SCOPE AND DESCRIPTION

Phase I of this program was completed under NASA Contract NAS5-9578. The objective of Phase I research was the establishment of valid space radiation equivalences for permanent displacement damage to silicon transistors. The results of that work (specifically the relative effectiveness of electrons and protons of different energies as well as Cobalt-60 gamma rays) were reported in NASA report CR-814, "Space Radiation Equivalences for Effects on Transistors," by R. R. Brown and W. E. Horne, July 1967. (Reference 2).

Phase II of this program was conducted under this contract NAS5-10443, "Radiation-Induced Nonlinear Degradation of Transistor Gain." The integration of efforts and goals of Phase I and Phase II are shown in Figure 1 as well as the proposed Phase III efforts.

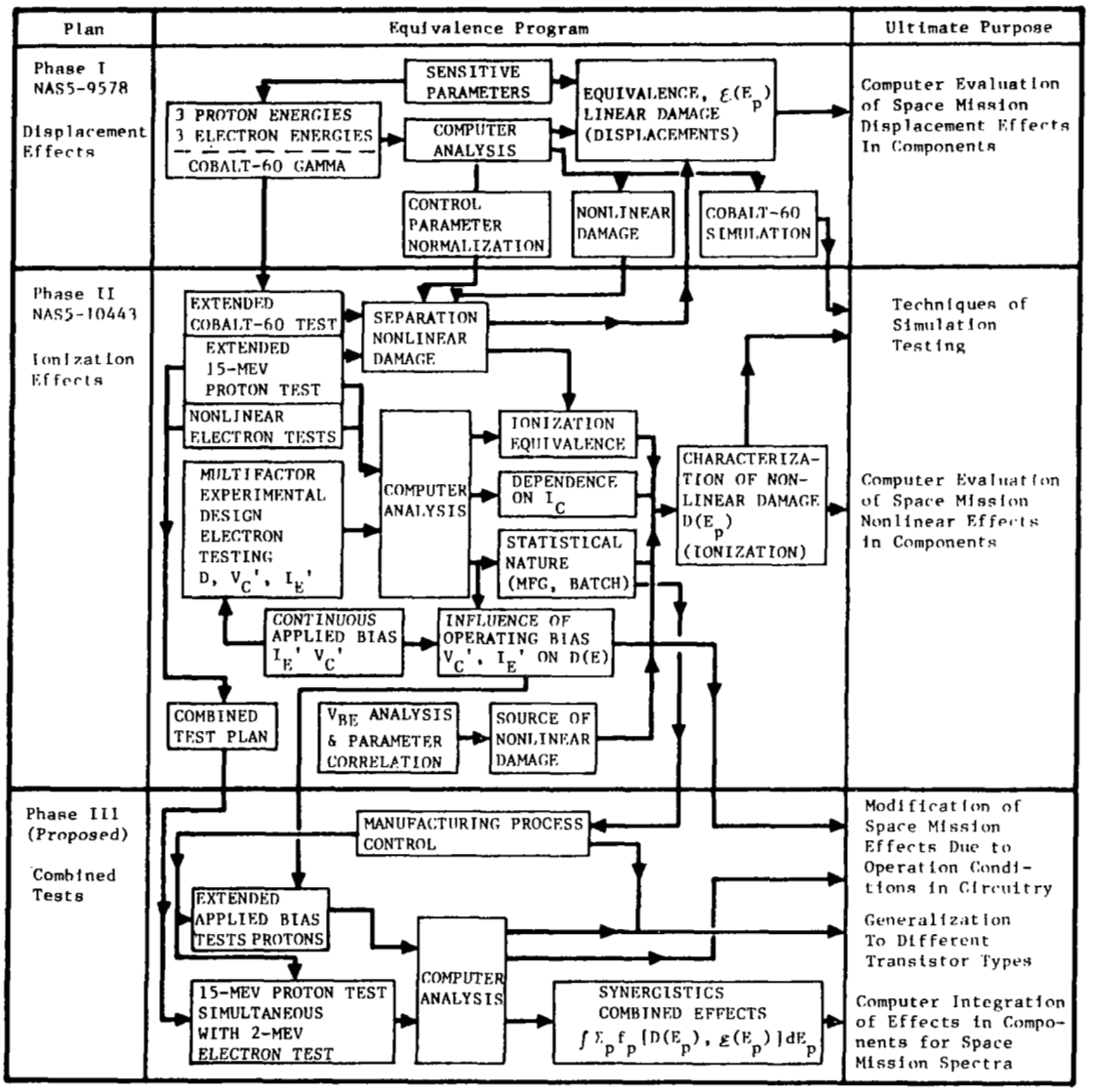

Figure 1: EQUIVALENCE PROGRAM

The work in Phase II was divided into three tasks.

Task A -- Empirically formulate the dependence of nonlinear damage on radiation, by:

1. Establishing the dependence of nonlinear gain degradation on the emitter current at which the gain is specified.

2. Determining the statistical spread in the increase of nonlinear damage with radiation exposure for: (a) one batch type; (b) different batch types; and (c) devices from manufacturers with different processing controls.

3. Establishing ionization equivalences for nonlinear damage.

4. Exploring the source of nonlinear damage by the use of V_{BE} versus I_B analysis and initial parameter correlation.

Task B -- Determine the influence on radiation equivalence for operation of devices under continuous electrical bias during exposure, by:

1. Using a multifactor experimental design to irradiate transistors under various combinations of: (a) particle exposure; (b) operating current, I_E'; and (c) bias voltage, V_C'.

2. Using a computer program for a statistical analysis of the functional dependence of gain degradation on particle exposure, I_E', and V_C'.

3. Modifying ionization equivalence values due to electrical operating conditions.

4. Recommending extended applied bias testing for proton ionization effects.

Task C -- Establish the feasibility of conducting combined effects tests to determine synergistics, by:

1. Integrating the Linac and Dynamitron beam handling systems in order to provide capability for simultaneously combined electron and proton exposure testing.

2. Conducting a separate electron test on transistors using the Linac (in a combined beam configuration) to determine if similar damage is obtained as that observed by steady state Dynamitron testing used in Tasks A and C.

3. Conducting a separate 15 MeV proton test to extended exposure levels (in a combined beam configuration) to assess the relative role of surface effects and displacement damage.

4. Recommending an appropriate approach for combined exposure testing based on results of Task B.2. and B.3.

1.3 SUMMARY OF WORK PERFORMED

Major tasks of this program were directed toward obtaining data important to the understanding of ionization induced surface effects (primarily gain degradation - nonlinear damage) on transistors. Efforts were primarily oriented toward applications of data important to the assessment of system vulnerability and prerequisite to design hardening.

Work was accomplished in accordance with the program description of Section 1.2. In general this included preparation of transistors for test by proper selection, burn in and culling, coupled with electrical characterization. Beside the measurements of 16 parameters (h_{FE} at various injection levels, I_{EBO}, I_{CBO}, V_{sat}...) on all devices, using an automatic transistor tester, special measurements (I_B vs. V_{BE}, I_{EBO} vs. V_R, I_{CBO} vs. V_R, C_{BE}, C_{BC}...) were also performed on selected groups of devices in order to aid in the interpretation of the data. Radiation tests performed on these devices include: 1) 1 MeV Dynamitron electrons, 2) Cobalt-60 gamma rays, 3) 2.9 MeV Linac electrons, and 4) 15 MeV protons. The behavior of selected devices, 2N1613 - NPN and 2N1132 - PNP, was monitored during exposure under both passive and active conditions. The results of these tests were analyzed by computer, wherever feasible, for each task.

The separation of nonlinear damage for 10 different types of transistors exposed to 0.5, 1.3, and 2.0 MeV electrons during the phase I contract (NAS5-9578) was completed. Further computer analysis of that data at I_E = 2.8, 5, and 10 ma was used to show that the relative increase in nonlinear h_{FE} degradation with decrease in the level of emitter injection during measurement was similar for widely different transistor types.

Extensive analysis of the current test data from the present contract (phase II of the program) was used to extend the study of the dependence of gain degradation on the collector current at which the gain was measured. This

dependence is given both in mathematical and in parametric representation. Although gain degradation was most drastic at the low current values, it was significant even at high currents. Plots h_{FE}, Δh_{FE}, $\Delta h_{FE}/h_{FE_i}$, $1/h_{FE}$, and $\Delta(1/h_{FE})$ as a function of I_C at different fluence levels and/or as a function of fluence for a family of different I_C values were studied. The general validity of the theoretically predictable dependence of degradation on I_C was verified for different types of radiation (for transistors exposed only passively to radiation). Transistor operation under active bias during exposure did not conform to the theoretically predicted formulation.

Both NPN and PNP transistors were procured from two manufacturers, Fairchild and Raytheon, with various date codes in order to study the differences in irradiation response among the devices within a given date code, between different date codes, and between manufacturers. The results of that study indicated first that the spread in damage in terms of relative gain loss of passive transistors was not great among all device batches tested. Even NPN and PNP transistors showed gain degradation of the same order. Furthermore, devices from one date code and manufacturer behaved similarly while dissimilarities between very different date codes was prevalent. Devices originating from different manufacturers were also subject to differences in surface processing techniques, etc.

Comparing devices from different sources, as to their radiation sensitivity, raised the problem of finding the proper quantity(ies) in terms of which the devices could be compared. Both $\Delta 1/h_{FE}$ and $\Delta h_{FE}/h_{FE_i}$ were used for such purposes. A considerable interest was focused recently on the problem of predicting nonlinear damage by finding the proper functional relation between gain degradation, in terms of $\Delta 1/h_{FE}$ and fluence (or dose). A simple power law of the form $\Delta 1/h_{FE} = \text{constant } \Phi^x$ $(0 < x < 1)$ is advocated by some workers. Our results, however, indicate that other functional forms may be more desirable. Moreover, if some of the curves for active NPN devices are to be approximated by a power law then $x > 1$ value should be included. An interesting and useful relation between gain loss Δh_{FE} and initial gain, h_{FE_i}, was noted experimentally, resembling a correlation between these two quantities in a certain fluence range. Consequently, an approximate prediction of gain

loss from initial gain is possible subject to some limitations and a form of normalization is effected by using relative gain loss $\Delta h_{FE}/h_{FE_i}$. Empirical formulations using the hyperbolic tangent provide a reasonable fit between relative gain loss and absorbed dose.

The degradation of the transistor parameters are interpreted in terms of the current models of the effects of ionizing irradiation on oxidized silicon surfaces. Namely in terms of the positive charge accumulation and of the new interface states. A tremendous difference in radiation sensitivity between the passive and active NPN devices was observed. The active bias during exposure strongly enhanced gain degradation. Charge accumulation on the SiO_2 surface was also enhanced by the active bias; the redistribution of these charges during off-beam and off-bias periods gave rise to slow drifts (recoveries) in the transistor parameters. No differences were noted, however, between the active and passive PNP devices.

The hypothesis of ionization equivalence for nonlinear damage to passive transistors was explored. In general, equivalences on the basis of total dose appear to hold for X-ray, gamma ray, electron, and proton exposure of passive PNP devices and all but proton exposure of passive NPN devices. An anomalous exception to the total dose equivalence concept for passive transistors was observed with 15 MeV proton nonlinear damage to NPN transistors.

Active operation during exposure significantly enhanced the sensitivity of NPN transistors to electron induced nonlinear damage. Latin cube computer analysis of the multifactor experimental design provided data on the dependence of damage on electrical biasing and revealed information on the interdependences between current, voltage, and dose. Because of the increase of damage for active NPN devices and because of post irradiation recovery, pulse tester techniques were developed for the 2.9 MeV electron test and the 15 MeV proton test. The pulse tester measurements were made in situ without disconnecting any bias voltages. In the 15 MeV proton test important anomalies in the ratio of active to passive NPN transistor damage was observed.

Displacement equivalence values were updated. Computer analysis of the old data (NAS5-9578) was also used to obtain damage constants at I_E = 2.8 ma and in turn equivalence values for displacement damage. The independence of

equivalence values on current injection level further extends the validity and usefulness of the equivalence concept. Damage constants for gamma ray displacements were revised by extended testing to high exposures.

Extended proton tests helped to clarify the relative role of ionization and displacement effects. Although nonlinear damage appears to dominate at low exposures, the concept of ionization equivalence appears to be violated by proton damage. The feasibility of combined testing (simultaneous proton plus electron) was established, the recommended test setup is described, and the need established. Conclusions from the phase II work and recommendations for a future phase III program are described and justified in Sections 2.0 and 4.0.

2.0 DETAILED DISCUSSION OF PHASE II WORK

Phase II work included extensive pre-test preparations of transistors, execution of four radiation tests, and detailed analysis of the test results. Radiation tests included steady state and pulsed electron exposures, extension of Phase I Cobalt-60 gamma ray exposure, and extended 15 MeV proton exposure. The radiation test plans were devised to provide data on: 1) the characterization of nonlinear damage, 2) the influence of electrical bias, during exposure, on damage buildup, 3) the updating of displacement equivalence information, and 4) the feasibility of conducting simultaneously combined radiation testing.

2.1 PREPARATION OF TRANSISTORS

Pretest preparation of transistors included selection, burn-in, and electrical characterization. Transistors were procured as specified by type, manufacturer, and date code. They were "burned-in" by high power stressing and culling was performed on the basis of both manufacturer specifications and instability of key electrical parameters. A detailed electrical characterization of all test transistors was performed.

2.1.1 Selection of Transistors

Emphasis of the Phase II program was placed on the npn (2N1613) and the pnp (2N1132) oxide passivated diffused planar transistor types. They were selected from the 10 silicon types previously studied under Phase I (NAS5-9578). In the process of Phase I work the importance of ionization-induced surface effects were emphasized, preliminary empirical characterization was attempted, and an hypothesis was made concerning its origin. In Phase II only two registered types of transistors were selected, in order to study more effectively the source of this surface effect and its dependence on the type and energy of incident radiation as well as its statistical dependence on date code and manufacturer.

A group of 356 transistors were procured for Phase II study. These transistors were selected from two different manufacturers (Fairchild and Raytheon) with specified lots of different series numbers. The transistor series numbers are related to the work items of Section 1.2 as indicated in Table 1.

Table 1. Identification of Phase II Transistors

Device and Manufacturer	Date Code	1 Mev Electron		2 Mev Electron		15 Mev Proton		Total Tested
		No Bias	Bias	No Bias	Bias	No Bias	Bias	
F-2N1613	701	10	20	8	2	13	6	59
F-2N1613	552	10	20					30
F-2N1613	615	10	10					20
F-2N1132	721	10						10
F-2N1132	736	10						10
F-2N1132	621	10						10
R-2N1613	446	10						10
R-2N1613	6545	10						10
R-2N1613	6625	10						10
R-2N1132	6523	10	20	8	2	8	2	50
R-2N1132	6649	8	20					30
R-2N1132	6710	10	10					20
	TOTAL	118	100	16	4	21	8	269

NOTE: F = Fairchild

R = Raytheon

Unbiased (passive) transistors included 38 Fairchild 2N1613, 30 Raytheon 2N1613, 36 Raytheon 2N1132, and 30 Fairchild 2N1132 used in the electron tests and 13 Fairchild 2N1613 and 8 Raytheon 2N1132 used in the 15 MeV proton test. Biased (active) transistors included 52 Fairchild 2N1613 and 52 Raytheon 2N1132 used in electron tests and 6 Fairchild 2N1613 and 2 Raytheon 2N1132 used in 15 MeV proton tests. The biased devices were used to reveal the influence of the different bias conditions on the nonlinear gain degradation. Date code series number selections were made not only to observe differences of damage for different series numbers, but also to provide more assurance that the semiconductor batch, the construction details, and the surface conditions within one test unit are the same. The date code marked on the device can is simply an indication of the year and the week when the device passed its final electrical test during manufacturing.

2.1.2 Burn-in and Culling of Transistors

All transistors were given a 75 hour "burn-in" test in order to eliminate those devices which were initially of potentially poor quality. Electrical biasing conditions for the burn-in was chosen (Table 2) in order to operate the devices at near maximum current and voltage stress.

Table 2. Biasing Conditions for Burn-in

Device Type	I_E (ma)	V_{CE} (volts)	Power Dissipation (mw)
2N1613	40	19	760
2N1132	30	19	570

The burn-in test was conducted using circuits as shown in Figure 2. Electrical parameters to be used for determining device stability were measured on the Fairchild Series 500 transistor tester both before and after burn-in. The criteria for culling of some transistors were either failure to meet manufacturer's specifications or excessive drifts in electrical parameters.

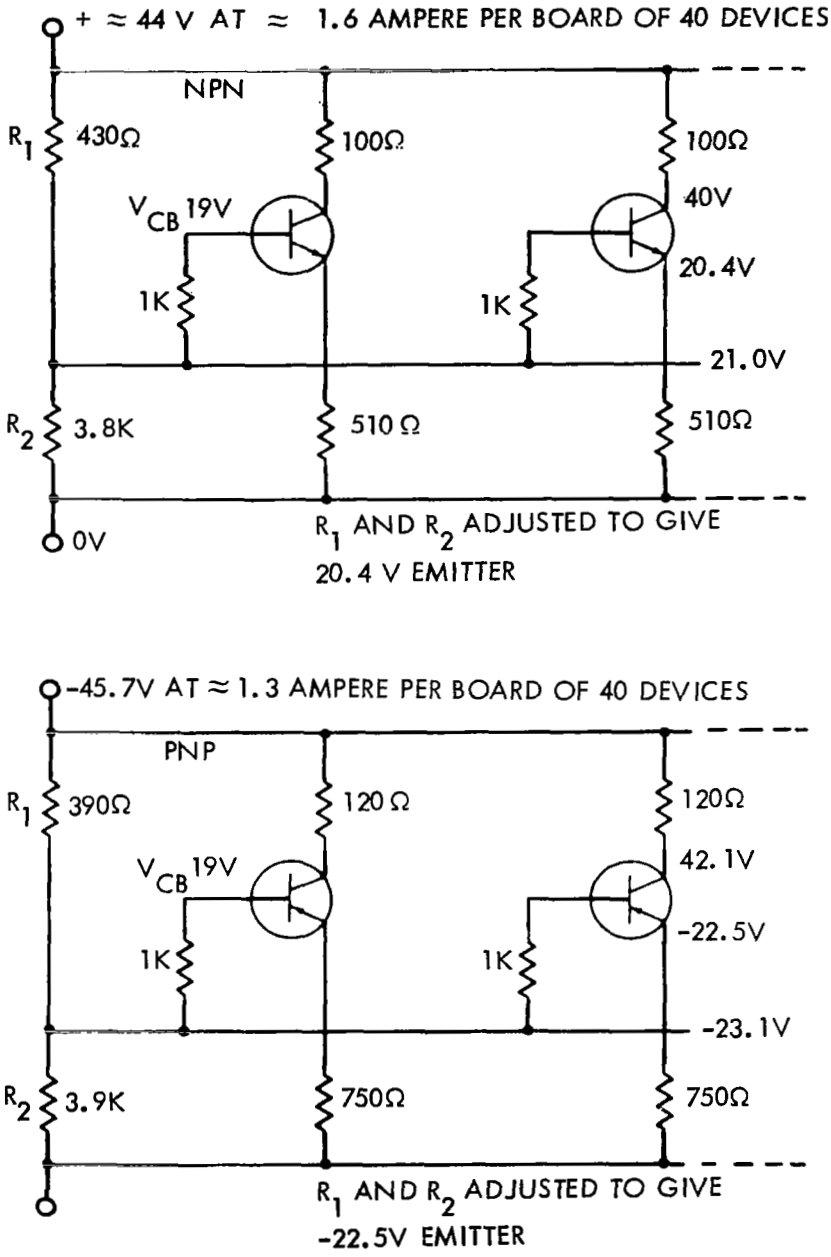

Figure 2. Burn-in Test Circuits

2.1.3 Electrical Characterization of Transistors

2.1.3.1 Fairchild Series 500 Test Data

The Fairchild Series 500 transistor tester was programmed to automatically perform 16 sequential measurements per transistor. Data from all transistors was automatically logged on IBM cards using a Fairchild Model Option K data logging module, and an IBM 526 Card Punch.

The Fairchild Series 500 test set was programmed to measure the following parameters: d.c. common emitter current gain, h_{FE}, at a collector voltage of 10 volts and at emitter currents of 10, 30, and 100 μa, 1, 3, 10, 20, and 40 ma; V_{CE}(sat) at h_{FE} = 10 for I_C = 150 ma; I_{CBO} at $-V_{CB}$ = 5, 20, and 60 volts for 2N1613's and $-V_{CB}$ = 5, 20, and 50 volts for 2N1132's; I_{EBO} at $-V_{EB}$ = 1, 3, and 6 volts (except for Fairchild 2N1132's which were tested at 1, 2, and 4 volts). Current gain values for collector currents of 2 ma and above were made using the short pulse mode (350 μsec) in order to limit device heating. A Wyle Environmental Chamber Model CN 1060640 is used to control the ambient transistor temperature to 35 $\pm$ 1/2°C during measurement. Following irradiation auxiliary equipment for low gain readings on the Fairchild (below a gain of 1.9) were occasionally required and used.

To verify instrument repeatability "standard" transistors were measured periodically and values are compared with those obtained earlier. Measurement of h_{FE} with and without corrections for increased leakage current were compared. In general increase in leakage current was too small to effect a change in h_{FE} values.

2.1.3.2 Special Measurements on Selected Devices

Table 3 summarizes the program of special transistor measurements made on selected devices for 1 MeV electron tests of Tasks A and B.

I_C and I_B Versus V_{BE} (at 35°C)

This type of measurement was useful in the past in locating the radiation damaged region of a transistor thus in providing clues about the source of the nonlinear damage. Early work has shown that the different base current components, originating in the different transistor regions, could be identified from the I_B versus V_{BE} measurements. (Ref. 3). The limits of interpretation, the significance of the data, together with the physical origin of I_B are discussed in Appendix I. The usefulness of the measurements in our work is demonstrated in Section 2.3.5.

Table 3. Special Measurements on Transistors

Measurement	Test Conditions	When Measured	Number of the Transistors in Types	
			2N1613	2N1132
I_C and I_B versus V_{BE}	T = 35°C V_{BE} = (0.1-0.72)V	Before and after irradiation ≈ After every third Φ_K	20 5	20 5
I_{EBO} and I_{CBO}	T = 35°C V_{BE} = 2V V_{BC} = 10V	After each Φ_K	10	10
I_{EBO}, I_{CBO} versus T	T = 35°C-200°C V_{BE} = 2V V_{BC} = 10V	Before irradiation	10	10
I_{EBO}, I_{CBO} versus V	T = 35°C T = 100°C	≈After every third Φ_K Before irradiation	5 5	5 5
C_{BE}(0V), C_{BC}(0V)	T = room temperature	After each Φ_K	10	10
C_{BE}, C_{BC} versus V	T = room temperature V_{BE} = (0-6)V V_{BC} = (0-24)V	Before and after irradiation	5	5
t_b from h_{FE}(db) tester	T = room temperature f = 30 MHz I_E = (0.7-40) ma	Before and after irradiation	70 (All No bias transistors in the 1 MeV electron test)	70

The measuring curcuit used is given in Figure 3. The current was measured by a Keithley Model 410 micro-microammeter below 3×10^{-4} ampere and by a Weston Model 62 milliampere meter above 3×10^{-4} ampere. The voltage source used was a Power Designs Model 2005 precision power supply. A special electrical circuit controlled the temperature of the copper-cylinder over ($35 \pm 0.1°C$) in which the transistors were positioned. A typical I_b and I_c versus V_{BE} curve is shown in Figure 4 for a 2N1132 transistor. Two base current components of I_B are identified in this figure.

C_{BE} and C_{BC} at Zero Bias and C_{BE} and C_{BC} Versus Reverse Bias (Room Temperature)

The measurements of the junction capacitances were also useful in studying nonlinear damage in transistors since they indicate the onset and existence of surface inversion during exposure.

The measurements were carried out by using the Boonton Model 74C-58 capacitance bridge with its built-in bias supply. The bias voltage was monitored by a Fluke Model 801 differential d.c. voltmeter. The 100 KHz signal level was $\simeq$ 20 mv as monitored by a Hewlett-Packard Model 400H a.c. voltmeter.

Figure 5 shows capacitance versus voltage data with and without an assumed value of the junction contact potential for a 2N1613 transistor. The slope of the lines gives the anticipated power law dependence of the capacitance on voltage, $C \propto V^K$. The K value for the 2N1613 transistor is -2.9. K values should be compared with those obtained from the power law dependence of the bulk space charge recombination-generation current on voltage since in both cases the power law dependence simply reflects the voltage dependence of the junction width.

Reverse Current (I_{EBO}, I_{CBO}) Measurements

The reverse currents by their physical origin (thermal generation currents in the different transistor regions; See discussion in the Appendix) are excellent monitors of surface conditions. Consequently, I_{EBO} (2V) and I_{CBO} (10V) data at 35°C were taken before and during the 1 MeV electron test. In addition, in order

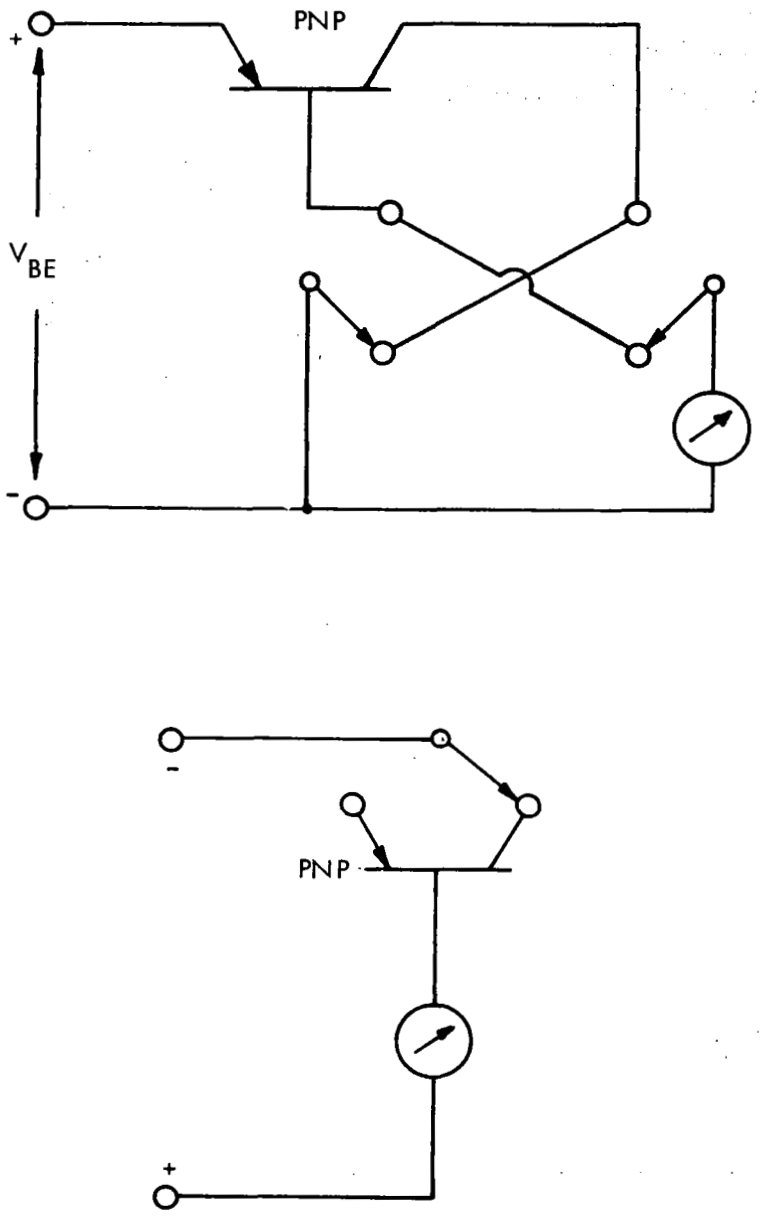

Figure 3. Circuit Diagrams for the I_C, I_B Versus V_{BE} and I_{EBO}, I_{CBO} Measurements

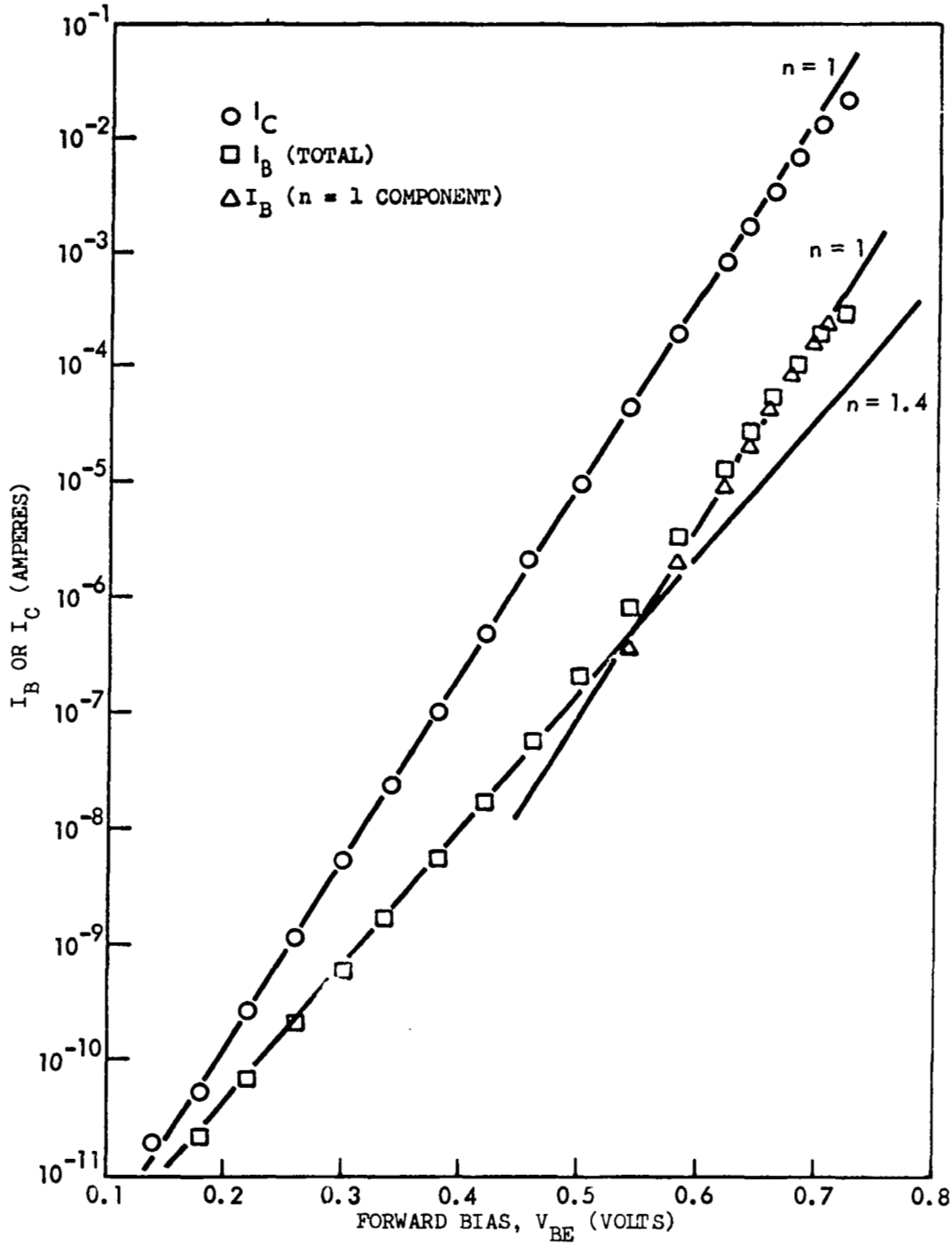

Figure 4. Typical I_C and I_B Versus V_{BE} Data (2N1132)

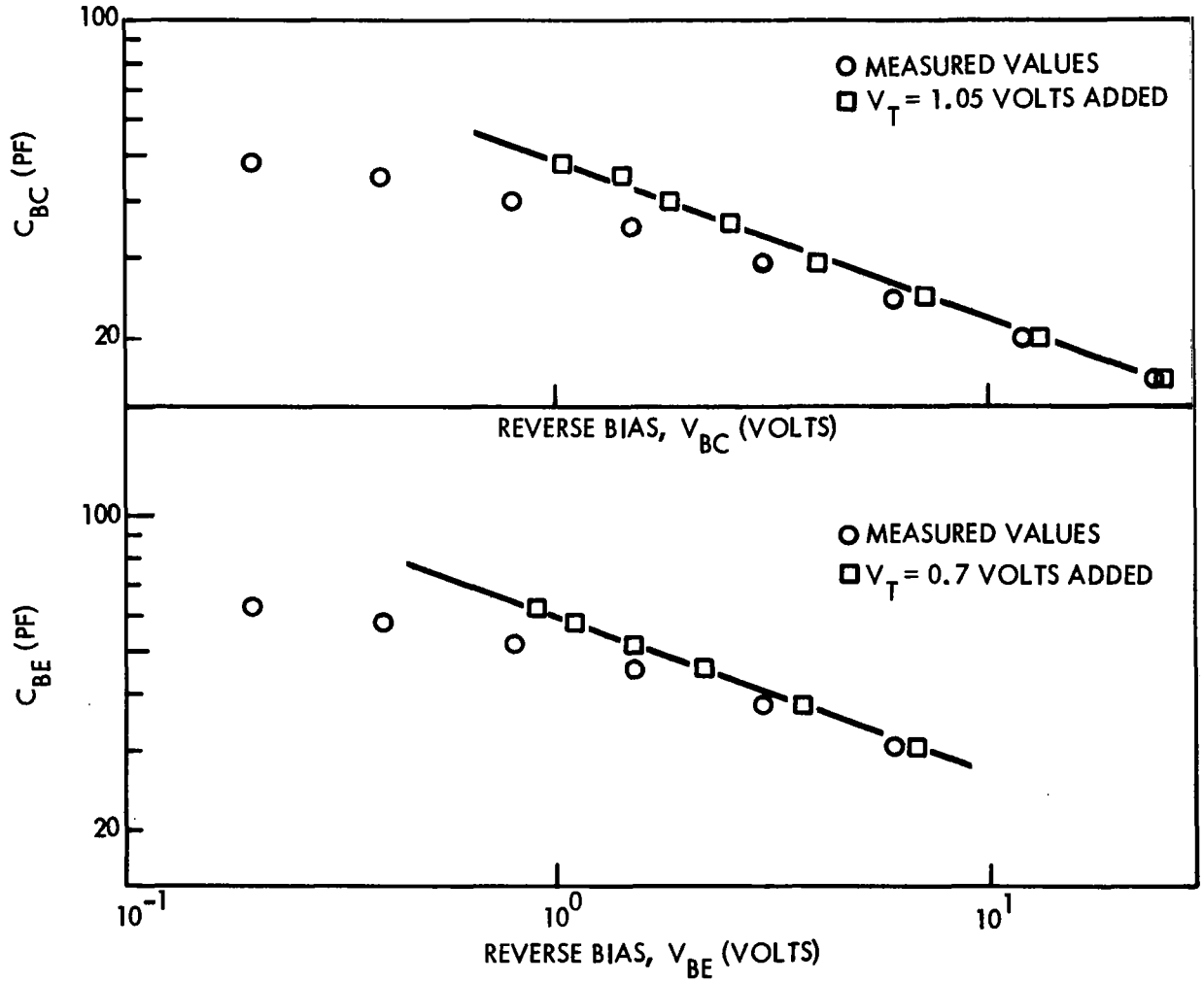

Figure 5. C_{BE} and C_{BC} Versus Reverse Bias (2N1613) (Data are shown with and without an assumed value for the junction contact potential, V_T)

to obtain a more complete characterization of our selected group of planar devices prior to irradiation, I_{EBO}, I_{CBO} versus Temperature and I_{EBO}, I_{CBO} versus Voltage measurements were also carried out. The information obtained was somewhat complementary to the I_B versus V_{BE} analysis, i.e., the relative importance of the different spatial components of the thermal generation currents was revealed. The following figures show that before irradiation the surface component of the reverse current was negligible for the NPN but not for the PNP devices.

I_{EBO} (2V) and I_{CBO} (10V) versus inverse temperature curves are shown in Figures 6 and 7 together with the activation energies characterizing different current components in different temperature ranges. The activation energies of ≈ 0.6 eV and ≈ 1.2 eV obtained from the slopes indicate the bulk space-charge region generation current, I_{BRG} and the diffusion current, I_D, respectively. The measuring circuit is shown in Figure 3. The instruments used were the same as those in the I_C and I_B versus V_{BE} measurements. A different temperature chamber was used, however, a new oven was constructed of aluminum to have a smaller thermal mass.

The I_{EBO} and I_{CBO} versus voltage measurements were carried out on 10 devices and are shown in Figures 8 through 11 for 35°C and 100°C respectively. At 35°C I_{BRG} is dominant over I_D. At 100°C I_D starts to dominate I_{BRG}. At 35°C the current values were so low that is was impractical to take I_{EBO} data below 100 mv and I_{CBO} data below 10 mv. For V_{CB} above about 100 mv the predicted power law dependence of $(I_{BRG})_{CBO}$ on voltage is clearly seen for the case of 2N1613 giving $I \propto V^K \approx V^{2.2}$. ($K = 2.9$ was obtained in the C_{BC} versus reverse bias measurement, the discrepancy is not understood.) The I_{CBO} versus V curve in Figure 9 for 2N1132 does not lend itself to simple power law analysis. This apparently indicates the presence of some other current component above 100 mv, presumably a surface generation current in the transition region.

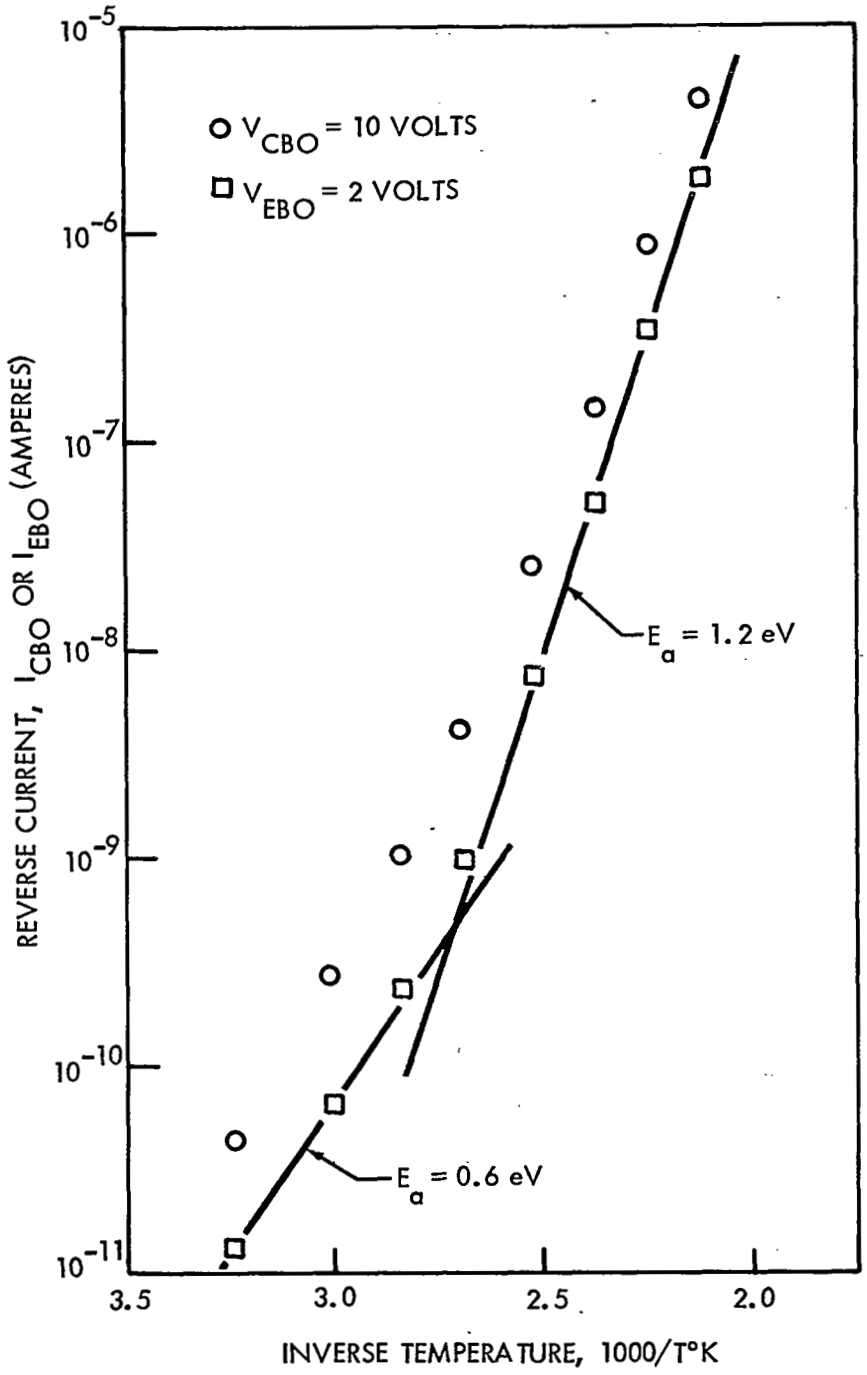

Figure 6. I_{EBO} and I_{CBO} Versus Inverse Temperature (2N1613)

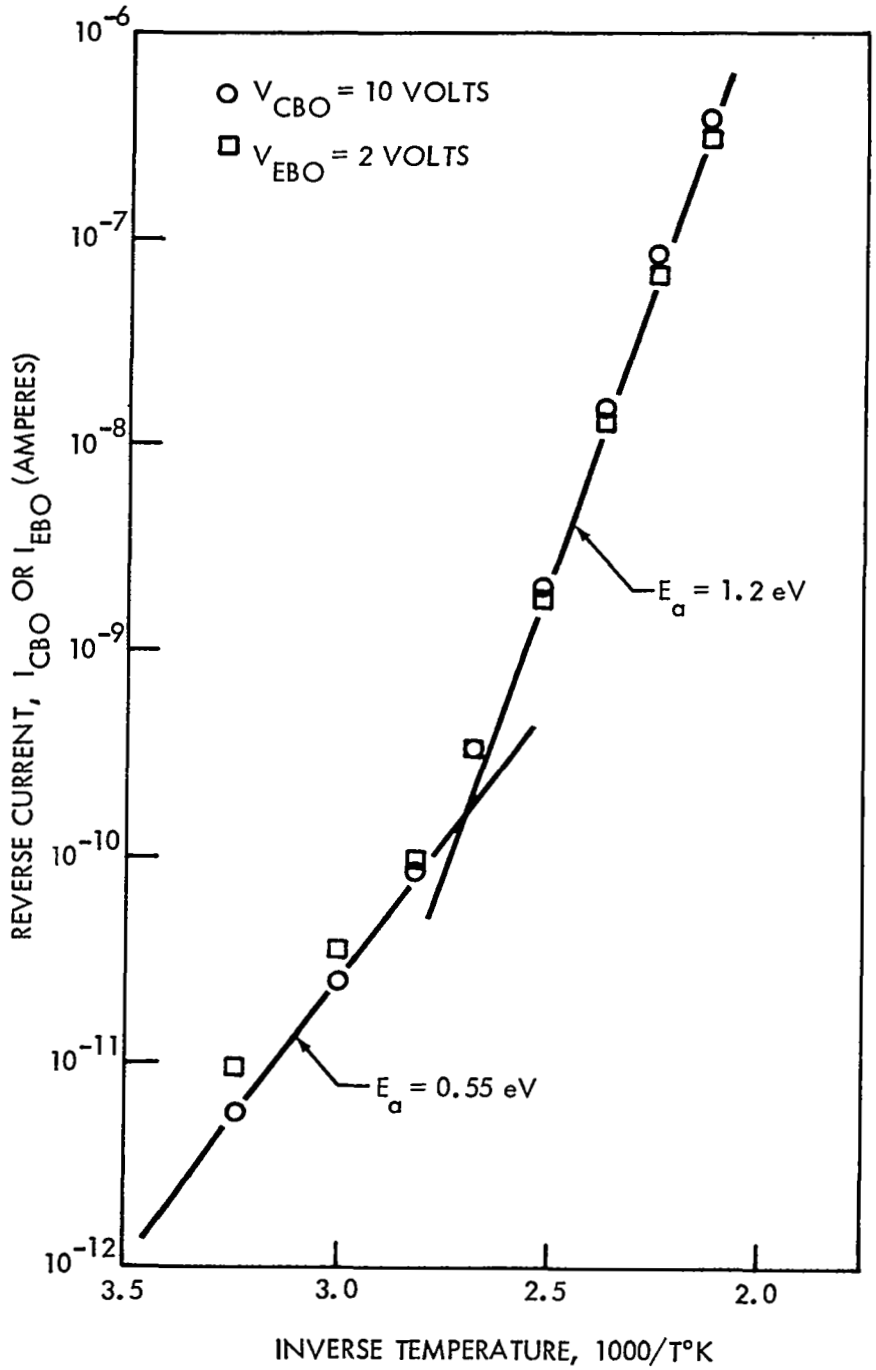

Figure 7. I_{EBO} and I_{CBO} Versus Inverse Temperature (2N1132)

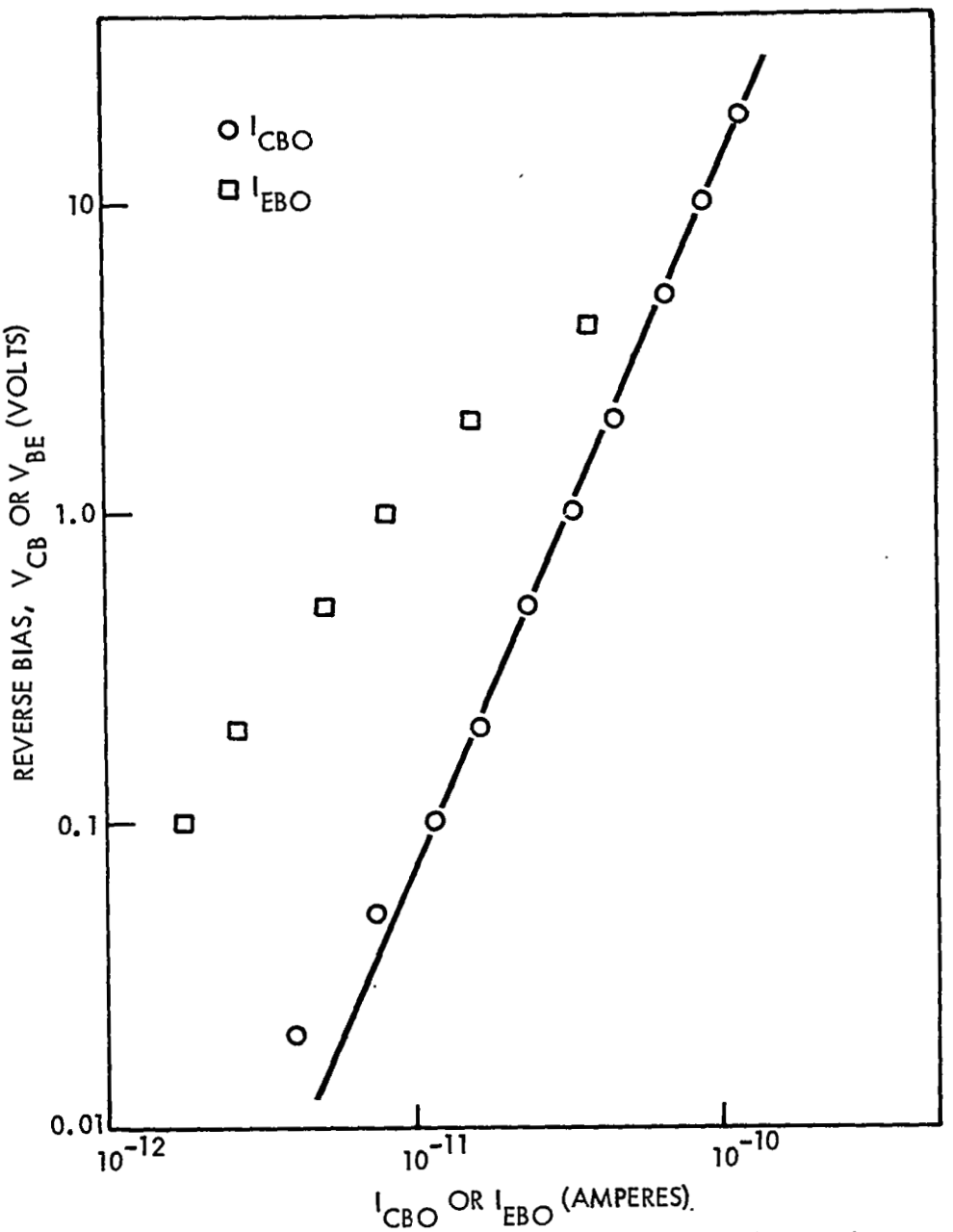

Figure 8. I_{EBO} and I_{CBO} Versus Voltage at 35°C (2N1613)

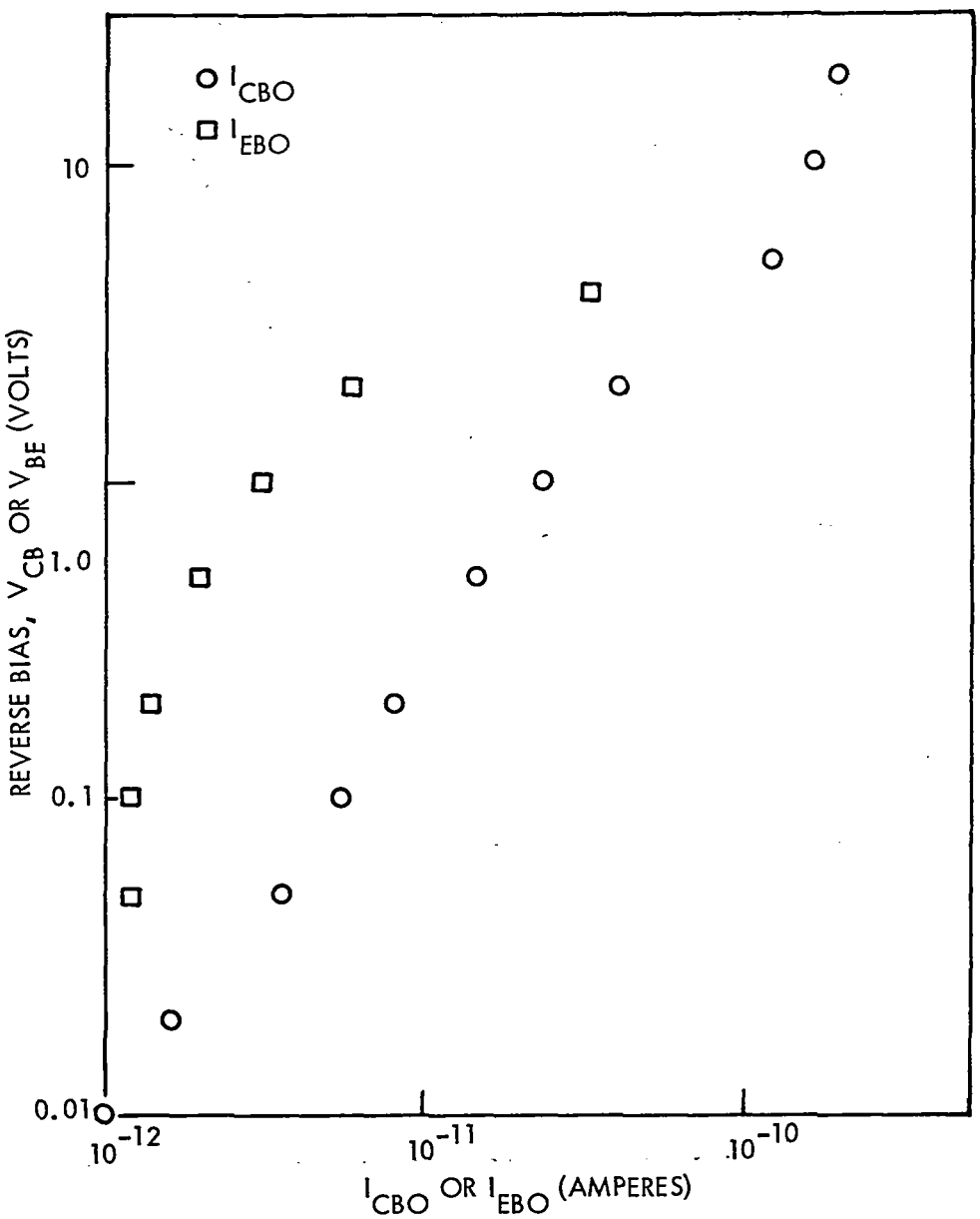

Figure 9. I_{EBO} and I_{CBO} Versus Voltage at 35°C (2N1132)

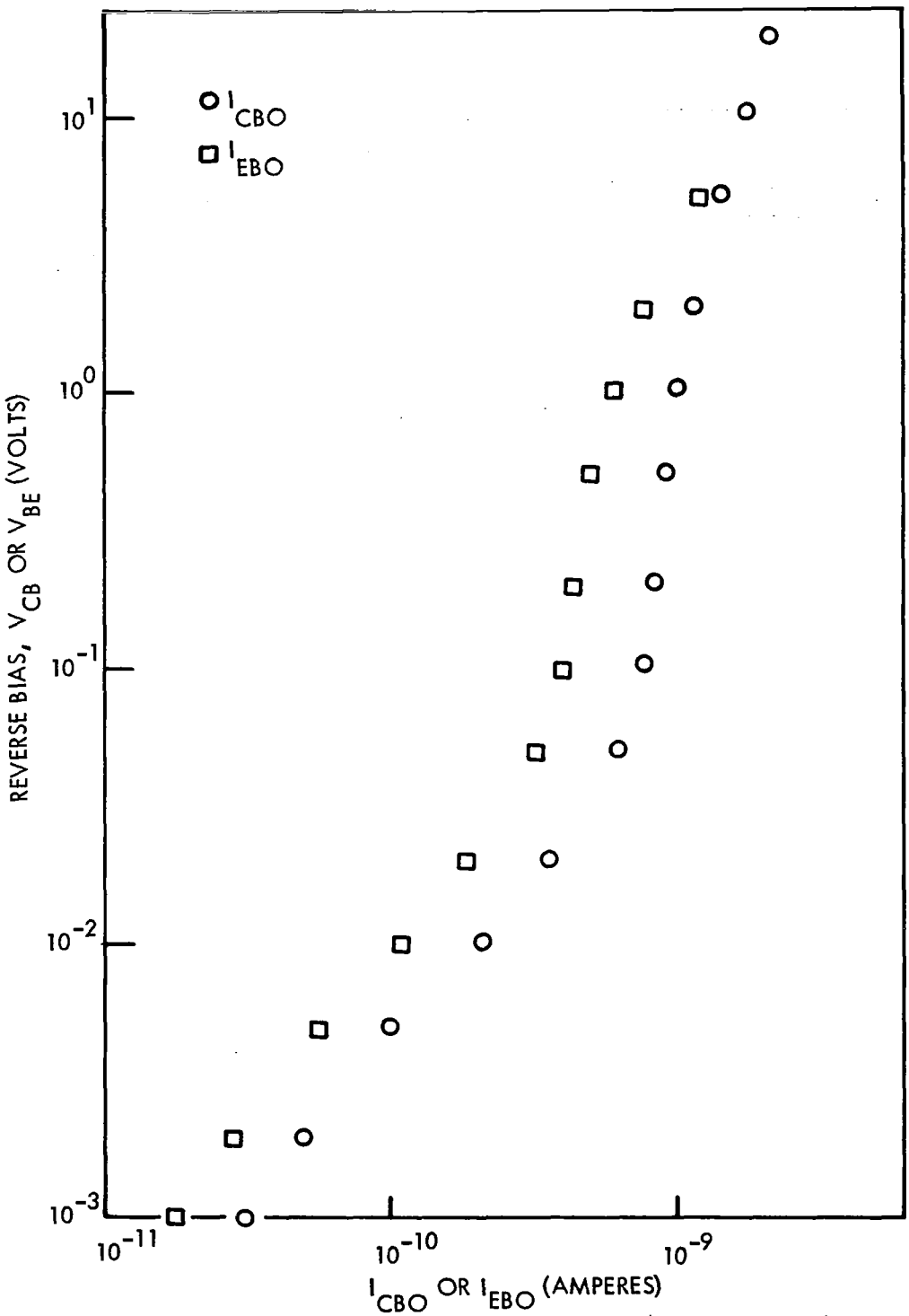

Figure 10. I_{EBO} and I_{CBO} Versus Voltage at 100°C (2N1613)

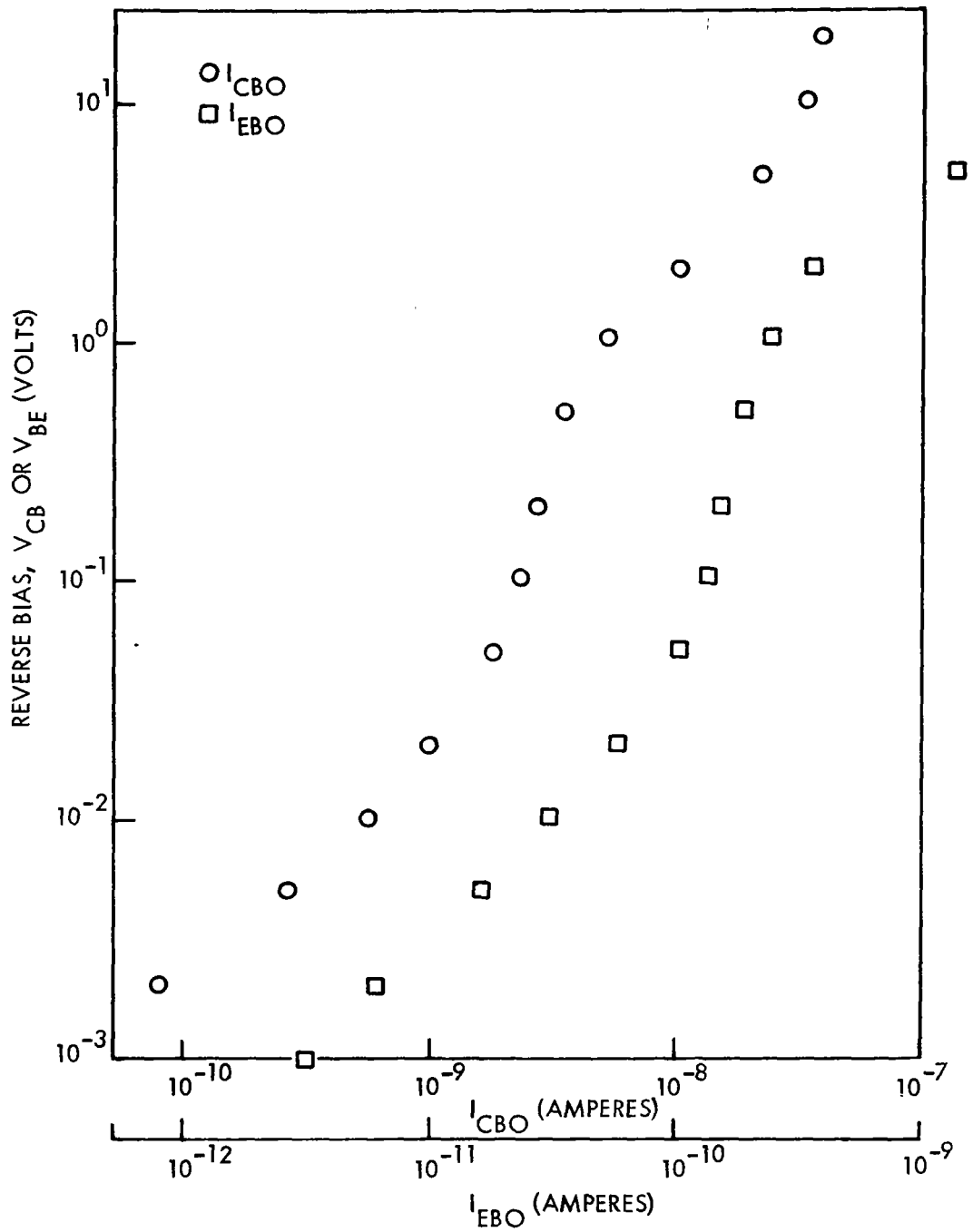

Figure 11. I_{EBO} and I_{CBO} Versus Voltage at 100°C (2N1132)

At 100°C the buildup of current between 1 mv and 100 mv is due to the diffusion current. Above 100 mv the current reaches saturation, at least for the 2N1613, indicating the absence and thus the relative insignificance of the I_{BRG} component in this temperature range.

t_b from h_{FE} Values

Base transit time values were determined from h_{FE} data. The whole procedure is described in complete detail in a later section where the method of obtaining base transit time values for devices used in the Phase I program is presented. Small signal a.c. current gain measurements were made, at room temperature, using a Fairchild Model 7515S h_{FE} tester. This instrument measures h_{FE} in db to the nearest 1/2 db.

Values of base transit time were used in Phase I studies to effectively normalize linear displacement damage. Consequently t_b values are useful in the effective separation of linear and nonlinear damage.

2.2 RADIATION TESTS

Four separate radiation tests were conducted during this program. These included steady state 1 MeV electron exposure using the Dynamitron accelerator, Cobalt-60 gamma exposure using the Gammacell 200, 2.6 MeV electron exposure using the Linac accelerator, and 15 MeV proton exposure using the Helium-3 deuterium reaction. The latter two tests were conducted in a combined beam configuration. Results of these tests are later summarized in this report according to the major tasks to be accomplished.

2.2.1 1 MeV Electron Test

The 1 MeV electron test provided most of the data for Task A on general characterization of nonlinear damage as well as data for Task B on the influence of continuous bias during exposure.

The electron test setup used in the initial Phase I work (NASA report, Ref. 2, NAS CR-814) was improved in preparation for the 1-MeV electron test. The beam handling system is essentially the same as that shown in Figure 12. Changes to this system include: 1) a four element slit system (current pickup capability on the slits) used to position and monitor the beam, 2) an automatic remote

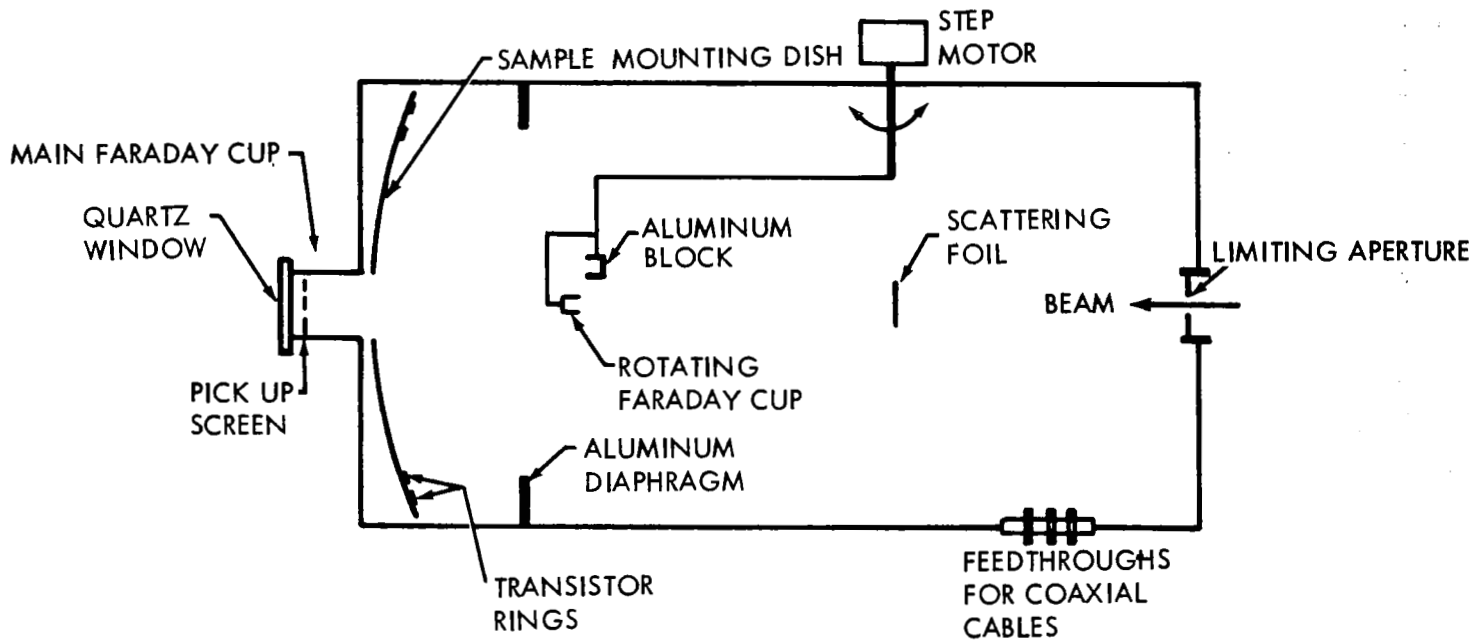

Figure 12. Electron Beam Handling System

controlled rotating Faraday cup for dosimetry mapping, 3) an aluminum block mounted beside the rotating Faraday cup. This can be rotated into a position to block and monitor the electron beam at its entrance to the test chamber, and 4) a one-fourth-inch thick aluminum diaphragm mounted so as to baffle electrons scattered at large angles and prevent them from increasing the low energy background at the transistor mounting plate.

A 10 mil aluminum foil was selected in order to obtain a reasonably uniform exposure of transistors positioned on a large diameter ring, cylindrically symmetrical to the beam axis. Scattered beam intensity versus scattering angle is shown in Figure 13. Rings of transistors were located at 22 and 26 degrees scattering angle.

TLD powder dosimeters were mounted in the test chamber during the beam mapping tests. Total dose as determined from measurement of the TLD powder, agreed well with fluence values calculated from current reading taken from the rotating Faraday cup.

Other relevant experimental details of the 1 MeV electron test are given below:

Source of electrons: The Dynamitron accelerator provided the DC electron beam. The beam energies were approximately 1.4, 1.3, and 1 MeV when incident on the 10 mil Al scattering foil, on the 8 - 11 mil Kovar transistor can and on the Si chip respectively. Although electrons with 1 MeV energy cause lattice displacements in silicon, the number of such events is relatively small below about 10^{15} electrons/cm^2 fluence. No effects on the transistor parameters due to lattice displacements were observed below the quoted fluence value. Fluence values noted on all plots are not for exposure on transistor cans, but rather corrected for transmission loss through the metal cans, i.e., exposure on the silicon chip.

Beam intensities: Exposure rate was increased by a factor of about 50 during the course of the experiment. (Initial stages: 1/2 μa; final stages: 24 μa incident beam on the scattering foil.) Such variation was a practical necessity in order to cover about 4 orders of magnitude in fluence values within reasonable times. The absence of rate effects was verified during the Linac electron tests.

Temperature of irradiation (as monitored by a Copper-Constantan thermocouple, fastened to the transistor cans): Temperature varied between 25 and 32°C for the unbiased transistors and between 35 and 41°C for the biased

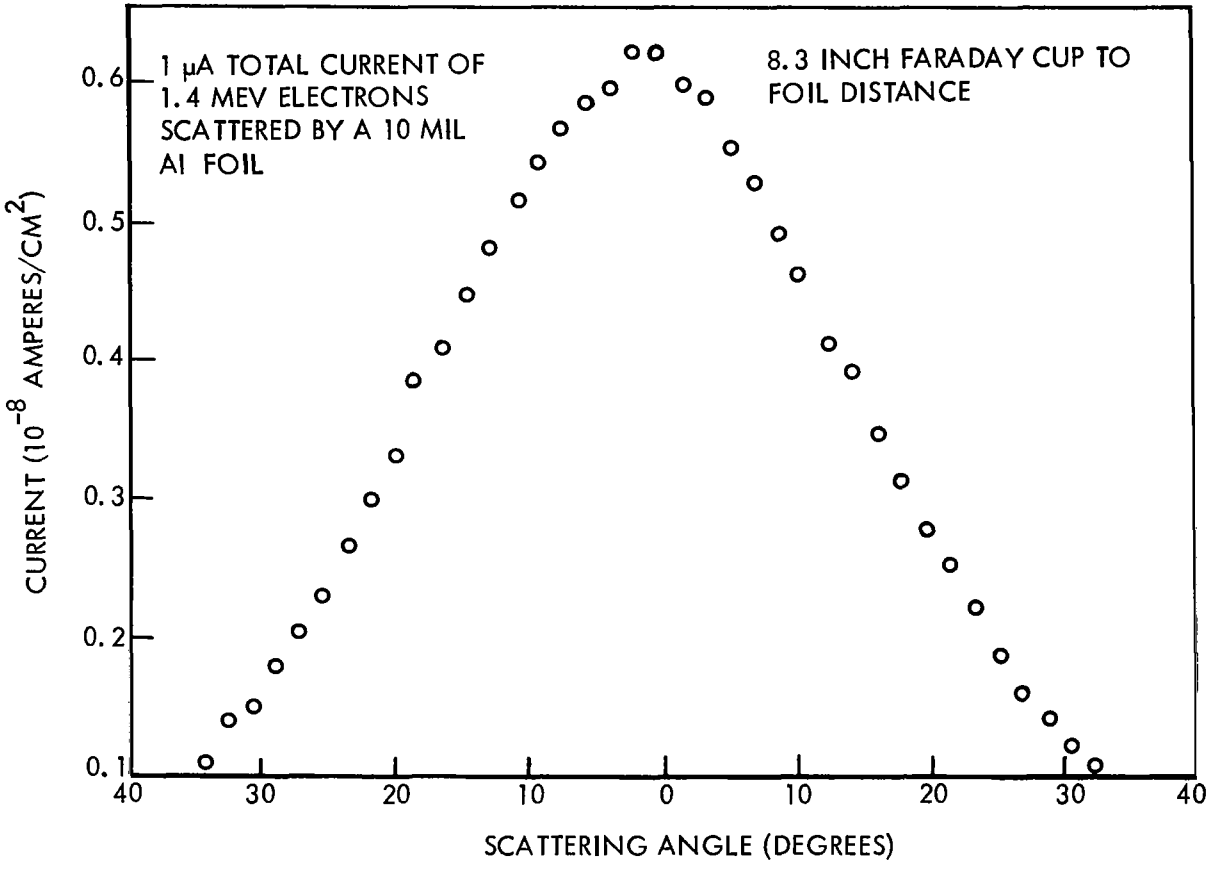

Figure 13. Angular Dependence of the Scattered Beam Intensity

transistors. T_{irr} increased gradually as higher and higher beam intensities were used. Most of the biased transistors were heatsinked in order to avoid excessive temperatures due to internal heating.

Fluence values: 17 fluence points were chosen in the range of about $3 \times 10^{11} - 3 \times 10^{15}$ electrons/cm^2. In the calculation of the actual fluence values the transmission losses suffered by the electrons, when traversing the transistor cans, were taken into account. Thus, all fluence values shown on plots and tables is for radiation incident on the semiconductor chip.

Measurement conditions after irradiation: The bias supply was turned off within two minutes after completion of a given irradiation. Generally, the pulse measurements of gain and other parameters were started on the Fairchild Series 500 within less than an hour and were completed within an additional 2-1/2 hours. Forward biasing of certain selected devices also took place from time to time during the I_B and I_C vs. V_{BE} measurements. The reason for stressing these conditions now is that in certain cases a recovery of surface damage was observed in-between irradiations, even at room temperature. This recovery might have been a simple function of time and/or it might have been initiated or accelerated by the measurement itself (due to the injection). Consequently, it was desirable to monitor the conditions.

2.2.2 Cobalt-60 Gamma Ray Test

The Cobalt-60 gamma ray tests provided data not only for revised values of displacement damage constants and equivalences but also provided further information on techniques for simulation testing.

Transistors were mounted on a cylindrical holder and lowered into the center of a cylindrical source array. The cylindrical source array was contained in a Gammacell 200, shown in Figure 14. The irradiation was conducted in air. No electrical bias was applied to the devices during irradiation. The radiation field was mapped using cobalt glass chips. These chips were read, using a Beckman DU spectrophotometer, to a relative accuracy of about 5.0 percent and an absolute accuracy of about 10.0 percent. Exposure dose rates for this configuration are shown in Table 4.

Exposure values were extended from that at the end of the Phase I contract (NAS5-9578), approximately 3×10^7 R to 6×10^8 R. The extended testing covered the period from July 1967 to August 29, 1968.

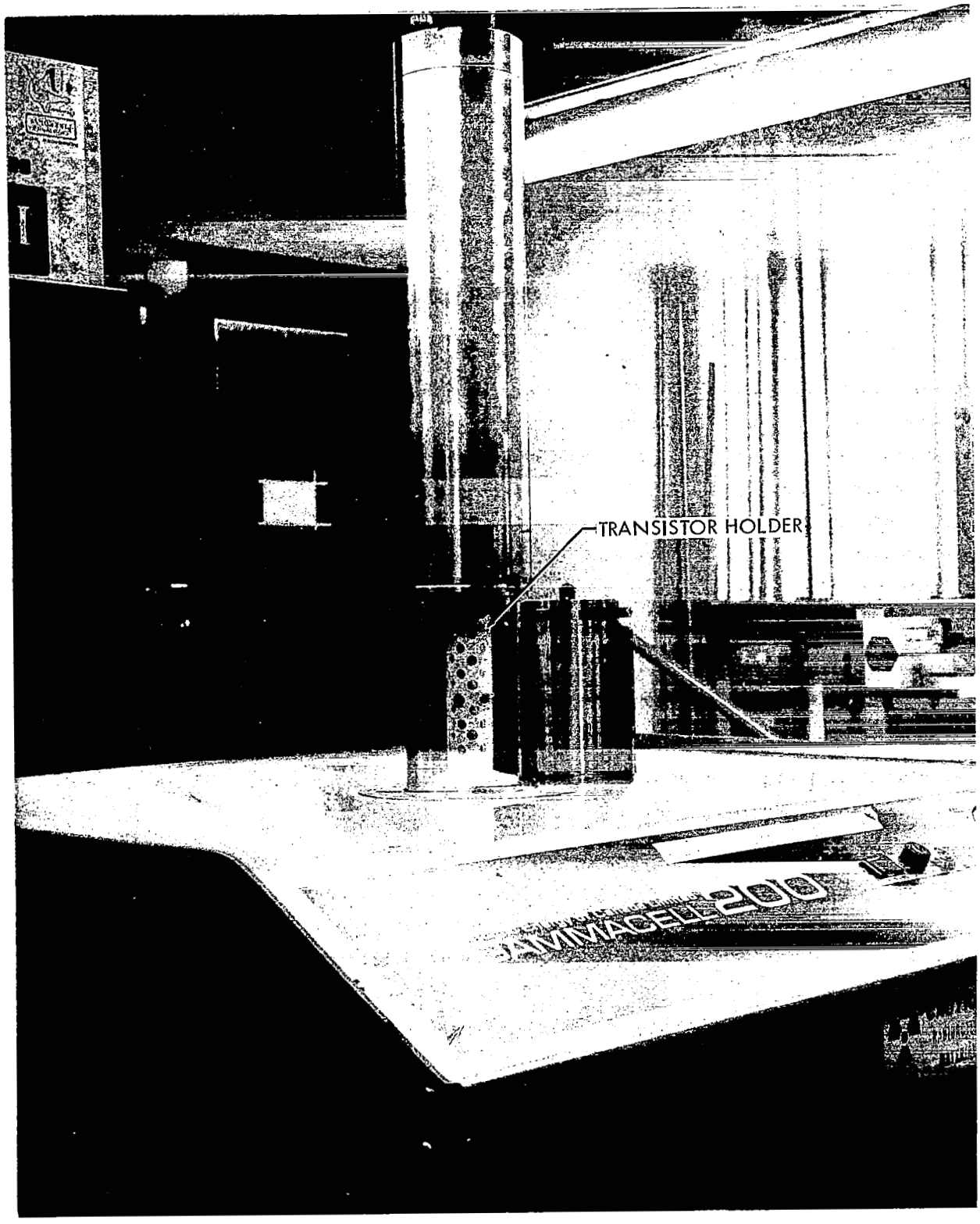

Figure 14: TRANSISTOR MOUNT FOR GAMMACELL 200

Table 4. Gammacell 200 Exposure Dose Rates

Transistor Type	Phase I Device No.	Dose Rate ($R\ hr^{-1}$)
2N1613	22	7.42×10^4
	23	6.95×10^4
	24	7.17×10^4
	25	6.56×10^4
2N1711	20	7.30×10^4
	21	6.63×10^4
	22	7.25×10^4
	23	6.85×10^4
2N2219	20	7.22×10^4
	21	7.32×10^4
	22	6.57×10^4
	23	6.95×10^4
2N1132	20	7.22×10^4
	21	6.57×10^4
	22	7.30×10^4
	23	6.85×10^4
2N2801	20	7.43×10^4
	21	6.95×10^4
	22	7.07×10^4
	23	6.53×10^4
2N2411	20	6.85×10^4
	21	6.63×10^4
	22	7.30×10^4
	23	6.53×10^4

2.2.3 2.9 MeV LINAC Electrons

The electron source for these tests was the LINAC which provided a four microsecond pulse of 2.9 MeV electrons at a repetition rate of either 15 or 30 pulses per second. The electron beam was scattered by a two mil titanium window. This foil isolated the LINAC vacuum system from the scattering chamber vacuum system where the samples were mounted and also served as the beam scatterer. A rotatable Faraday cup capable of being interposed between the LINAC and the test devices was used to sense the electron beam current and as an aid in tuning the LINAC. Rotating the Faraday cup out of the way, the scattered electron beam was detected by a calibrated photodiode (D_3 of Figure 15) mounted on the target aperature plate near the test transistors. Passive dosimetry was placed inside and outside transistor cans and the preliminary dosimetry taken correlating the absorbed dose (inside and outside the cans) with the photodiode response [Rads (Si)] per pulse times number of pulses). During the actual testing the photodiode was used as an aid for adjusting the target dose and actual dosimetry was taken using passive dosimeters placed near the transistors. The fluence of incident electrons per Rad (Si) absorbed by the transistor chip inside the can was 4.14×10^7 electrons cm^{-2}/Rad (Si).

2.2.4 15 MeV Protons

Figure 15 illustrates the test configuration for the 15 MeV proton test and serves as a detailed drawing of the general figures of Section 2.6. A two MeV He^3 beam from the Boeing Radiation Effects Laboratory Dynamitron was directed onto a deuterium loaded titanium target and the protons produced in the $He^3(D^2, p)He^4$ reaction were used for these tests. An initial horizontal mapping centered about the target and in the plane of Figure 15 was made to determine the angular distribution of the protons and their energy dependence on angle.

A detector system consisting of a 2000 micron thick Silicon surface barrier detector, a pre-amplifier and a 512 channel Nuclear Data pulse height analyzer was used to determine energy and resolution. The detector was mounted at the end of a rotatable support arm (the same support arm shown supporting the

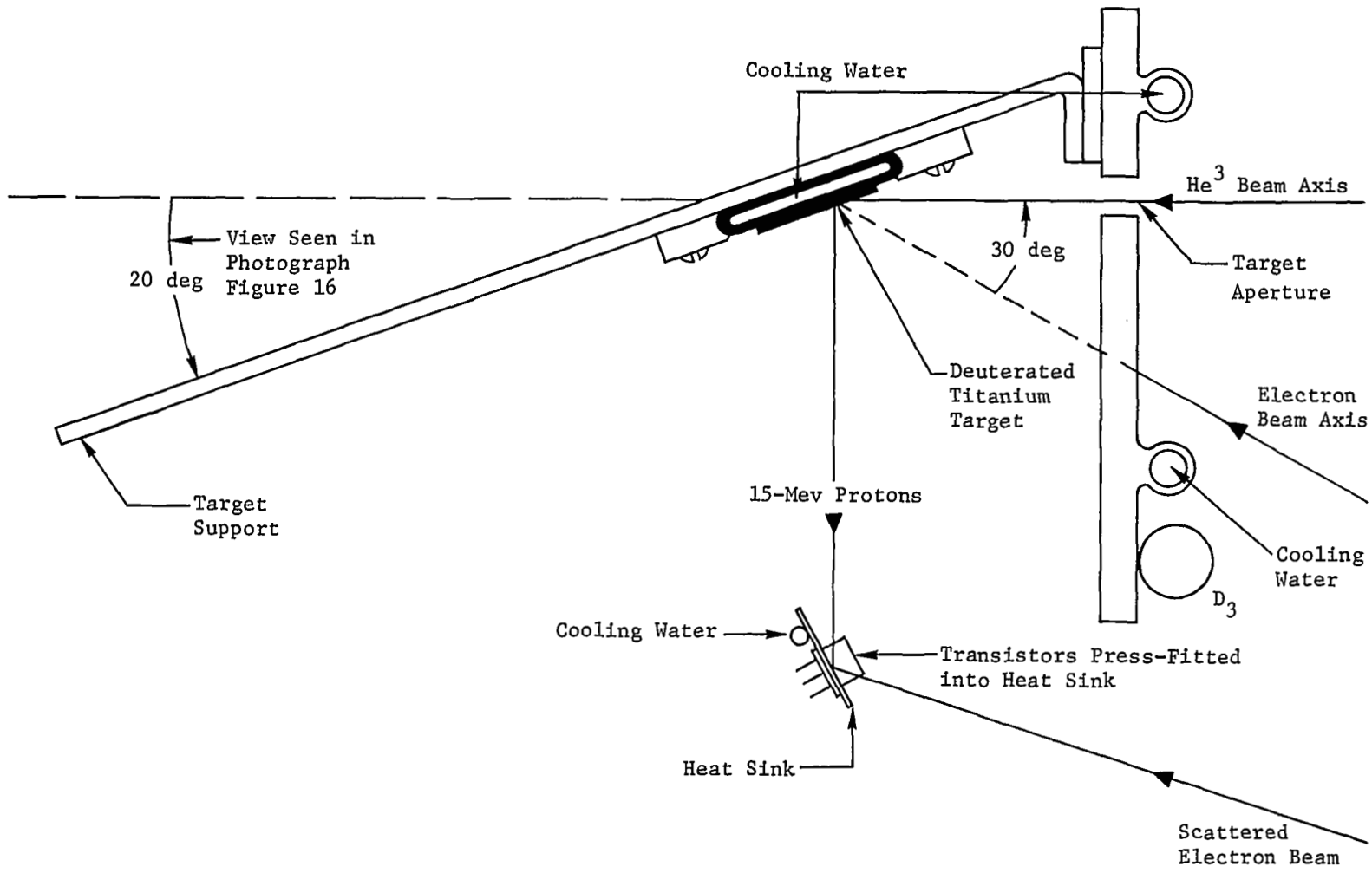

Figure 15: CROSS SECTION OF DEUTERATED TITANIUM TARGET

rotatable Faraday cup and D_2 in Section 2.6) whose pivot point was directly above the deuterated titanium target. It was determined that the 15 MeV protons emerged from the target at an angle of 90 degrees to the He^3 beam. A vertical mapping centered about the target at a radius of 2.2 inches was then made to determine flux uniformity at positions where the test transistor would be placed. The same detector system was used in this mapping (D_1 of Figure 99 of Section 2.6) and another monitor detector (D_2) was placed at 118 degrees to provide monitor counts correlated to the vertical mapping for use during the actual testing. A scintillation counter was mounted on the front face of the scattering chamber and it viewed the target through a hole in the target aperature. This counter was intended to be used in the same capacity as the monitor detector but it was found that its output (counts/min) was a function of beam position on the target and it was not used in this capacity. Instead its output, which was recorded on a strip chart recorder, was used as a tuning indicator for the Dynamitron. The chamber aperature, target aperature, target, and target support were insulated from ground and any He^3 beam striking any of these parts of the system was monitored in the control room to provide steering information for the He^3 beam.

After the preliminary dosimetry the vertical mapping detector was removed and the transistor mounting surface (see Figure 16) was attached to the target support structure. Passive dosimetry was then placed inside transistor cans which were taken from the same batch of transistors as the transistors which were tested. This provided dosimetry in terms of rads (Si) correlated to the monitor counts. The incident proton fluence per Rad (Si) absorbed by the transistor chip inside the can was 2×10^6 protons cm^{-2}/Rad (Si).

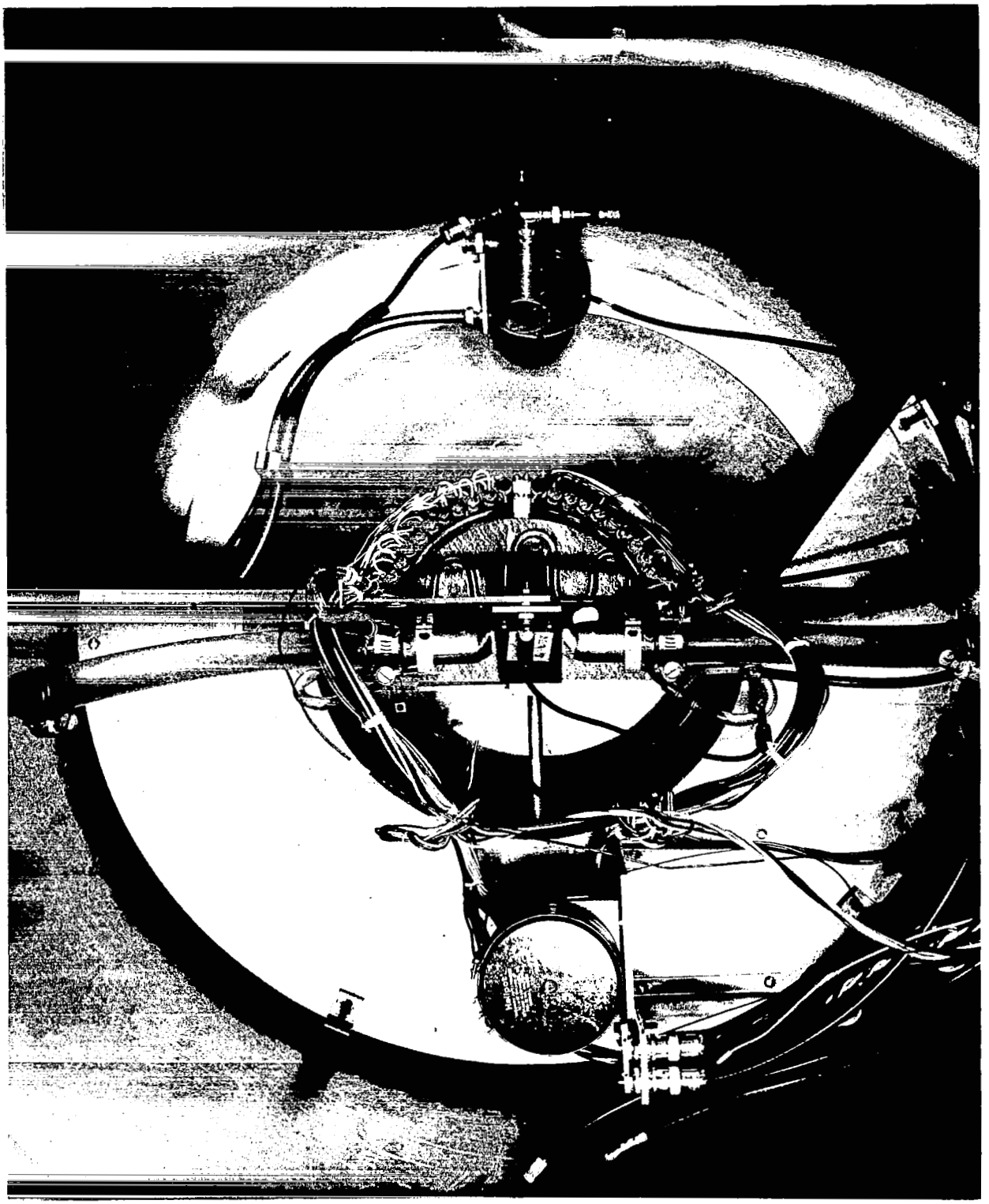

Figure 16: TRANSISTOR MOUNTING FIXTURE

2.3 TASK A CHARACTERIZATION OF NONLINEAR DAMAGE

2.3.1 Dependence of Nonlinear Damage on Measurement Current

One of the tasks of this contract was to evaluate empirically the dependence of nonlinear damage on the collector or emitter current, at which the current gain is measured. Some data were generated from extended analysis of the phase I tests, but most of the data resulted from new tests performed under this contract.

Computer analysis of test data obtained in contract NAS 5-9578 was performed in accordance with the technical proposal. This analysis provided further information on the dependence of nonlinear degradation on the value of collector current at which the gain was measured as well as further validity of equivalences for displacement damage (the latter will be discussed in Section 2.5). An example of the increase in nonlinear damage with decrease in the value the collector current (10, 5 and 2.8 ma) from the phase I test is shown in the computer plot of Figure 17. The separation of nonlinear damage for the 10 different types of transistors exposed to 0.5, 1.3, and 2.0 MeV electron irradiations have been completed and are shown in Section 2.3.3.1. The dependence of damage on measurement current found from extended computer analysis of the ten types of transistors from phase I tests was in agreement with more extensive data obtained on the two transistor types used in the new tests.

Measurements of gain for the 1 MeV electron and other phase II tests were made at collector currents from 10 μa to 40 ma. An example of how the significance of nonlinear damage increases at low measurement currents is illustrated in Figure 18. Data shown in that figure are values averaged from 30 2N1613 Fairchild transistors exposed passively during the 1 MeV electron test. The nonlinear character of the damage is indicated by the deviation from the "linear" displacement line. The basis of that line and equations relating to displacement effects are discussed in Section 2.5.

The fact that the nonlinear curves are nearly parallel can be explained qualitatively. The function $\Delta 1/h_{FE}$, which is plotted against Φ, can be expressed as

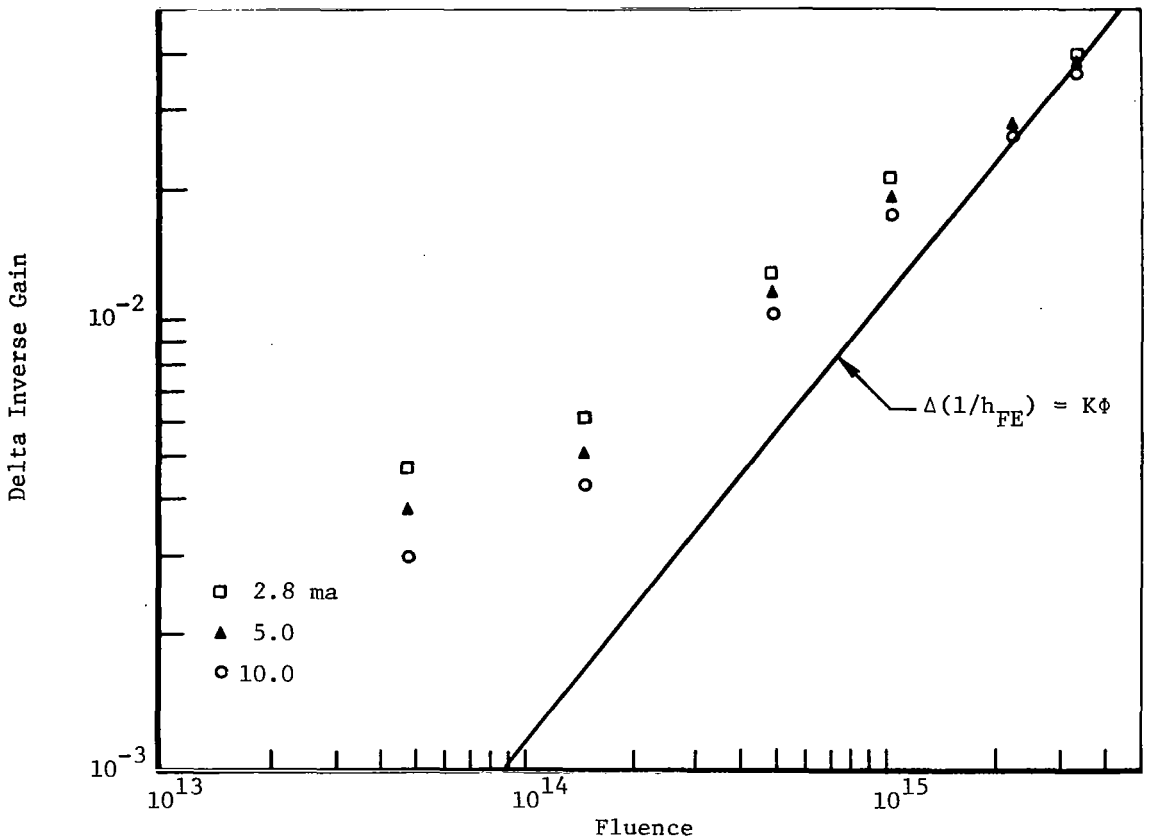

2N1711 Test 22 Position 2 1.3-Mev Electron Irradiation

Delta Inverse DC Gain vs Fluence, Family of Emitter Currents, Collector Voltage = 10.0

Test	Trans Type	Trans No.	Batch	Make	Cutoff	Nml Freq	Case
22	1711	8	513	FCLD	113.64	147.81	ON

Symbol	Curve	Current	Max Gain	Min Gain
□	1	2.8	0.04030	0.00244
▲	2	5.0	0.03825	0.00209
o	3	10.0	0.03657	0.00164

Tabulation of Array Points

Curve 1		Curve 2		Curve 3	
Fluence	Inv Gain	Fluence	Inv Gain	Fluence	Inv Gain
1.44+13	0.00244	1.44+13	0.00209	1.44+13	0.00164
4.80+13	0.00477	4.80+13	0.00383	4.80+13	0.00299
1.47+14	0.00611	1.47+14	0.00513	1.47+14	0.00434
4.88+14	0.01323	4.88+14	0.01190	4.88+14	0.01042
1.04+15	0.02118	1.04+15	0.01891	1.04+15	0.01757
3.36+15	0.04030	2.27+15	0.02819	2.27+15	0.02642
		3.36+15	0.03825	3.36+15	0.03657

Undefined Gains at the Following Fluences Were Not Plotted 2.27 + 15

Figure 17: CHANGE IN RECIPROCAL OF GAIN VERSUS FLUENCE (2N1711) (PHASE I DATA EXTENSION)

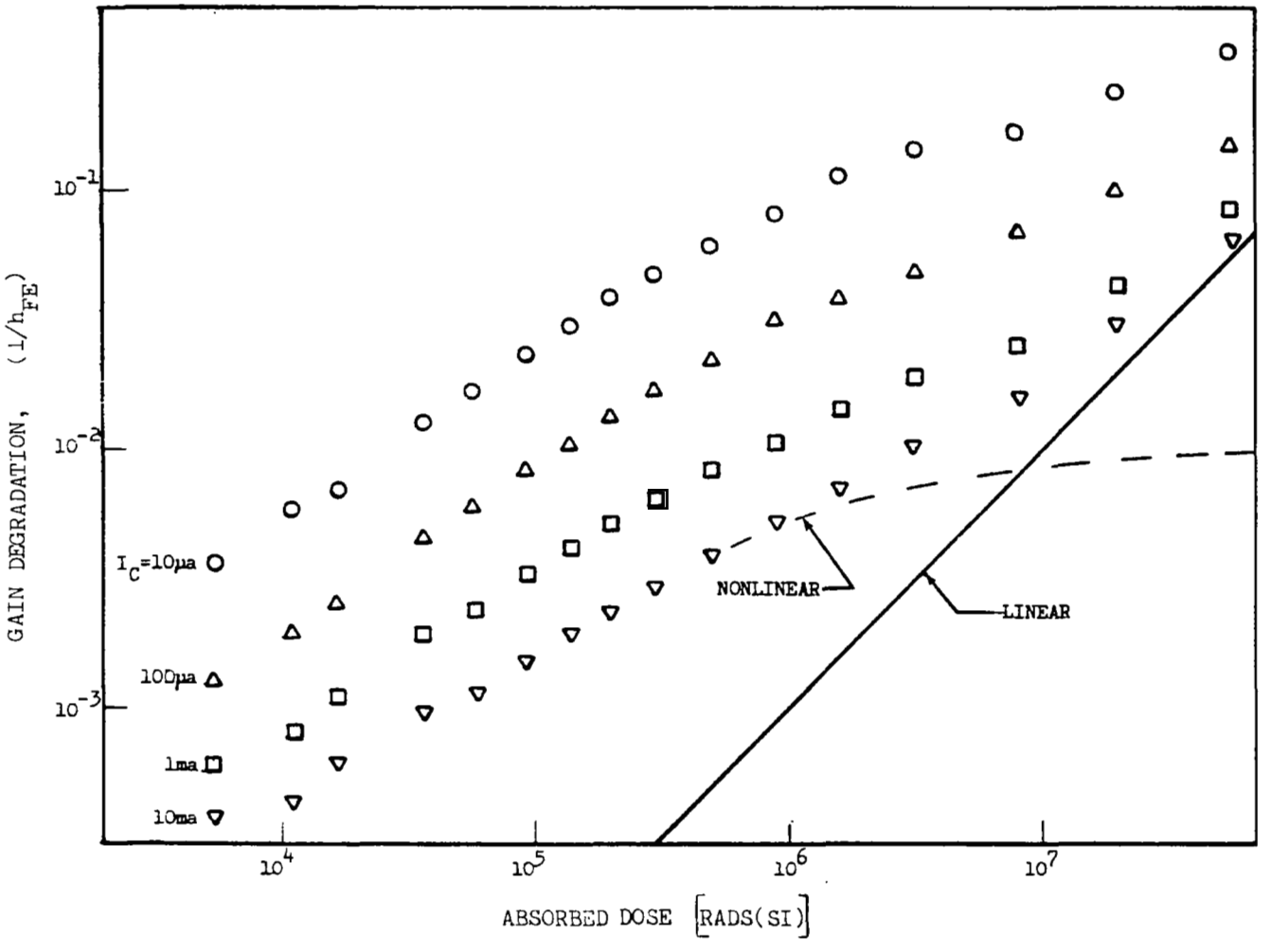

Figure 18. Nonlinear Damage of Passive 2N1613 Transistors

$$\Delta 1/h_{FE} = \frac{\sum I_{B_x}}{I_C} \tag{1}$$

where $\sum I_{B_x}$ is the sum of excess base current components built in by exposure to ionizing radiation. For two different I_C values at a given Φ, the ratio (i.e., the distance between them on log scale) is given by

$$\frac{(\Delta 1/h_{FE})_1}{(\Delta 1/h_{FE})_2} = \frac{\sum I_{B_{x1}}}{\sum I_{B_{x_2}}} \frac{I_{C_2}}{I_{C_1}} \tag{2}$$

Now the question is whether or not this ratio varies with fluence; if it remained nearly constant then the $\Delta 1/h_{FE}$ vs. Φ curves with different I_C values would be approximately parallel on a log-log plot. I_{C_1}/I_{C_2} is independent of fluence as well as the ratio of the extra base currents, at least when they are dominated by the surface components, since the ratio depends only on V_{BE}'s necessary to get the desired I_C values. The effect of increasing the number of interface states (ΔN_t) with dose should drop out, since both $I_{B_{X_1}}$ and $I_{B_{X_2}}$ are proportional to ΔN_t.

Gain plotted as a function of I_C before and after irradiation is shown in Figure 19. The 2N1711 transistor data given in Figure 19 are for a passive exposure to Cobalt-60 gamma radiation. More enhanced damage to npn transistors is observed when they are operated actively during irradiation (section 2.4).

It is also important to consider $\Delta h_{FE}/h_{FE_i}$ as a function of I_C since the relative gain loss is of interest to a circuit designer. An example of this type of data is shown in the computer plot of Figure 20 for a passive 2N1132. The figure expresses the fact, emphasized throughout the report, that although nonlinear gain degradation is usually most severe at low current levels nevertheless it can be significant even at higher current values. Characteristic plots of this type are similar for both 2N1613 and 2N1132 transistors. Relative gain loss initially built in rapidly at low current then as it begins to slow down the high current losses accelerate. Thus the slopes of $\Delta h_{FE}/h_{FE_i}$ plots do not provide a convenient functional relationship with I_C.

NPN Diffused Planar Transistor (2N1711)

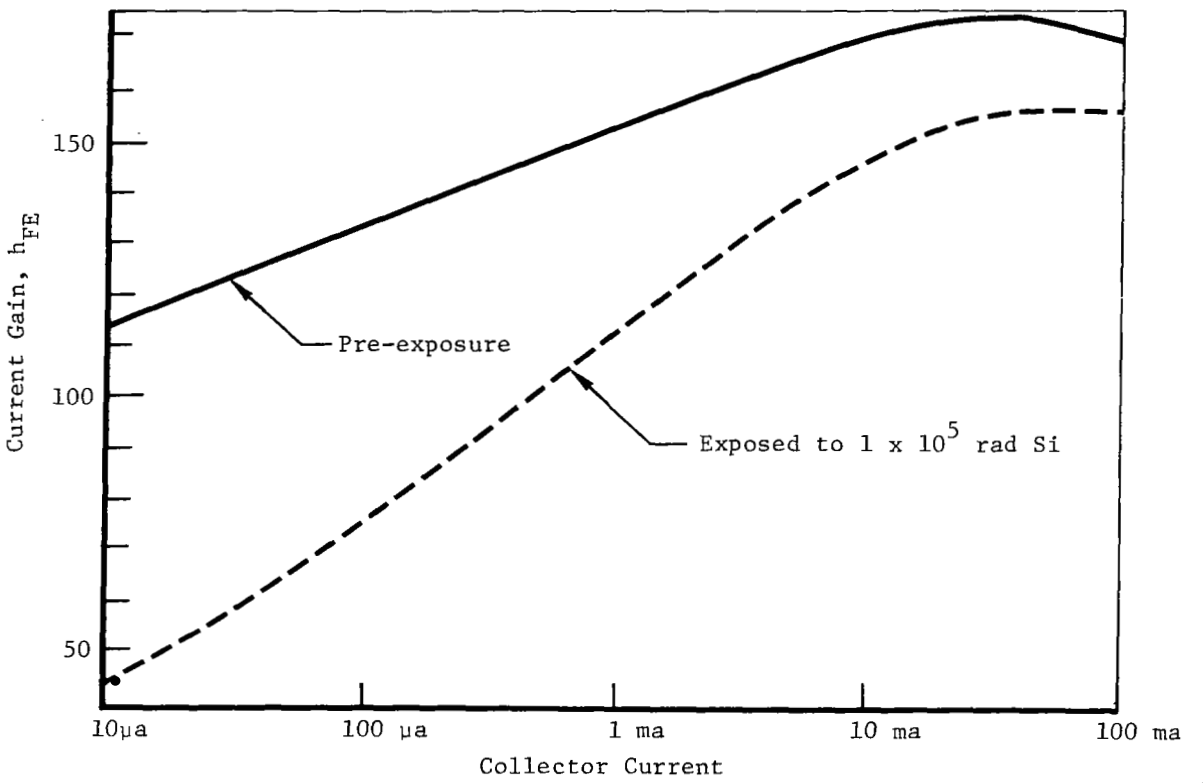

Figure 19: DEPENDENCE OF GAIN DEGRADATION ON COLLECTOR CURRENT

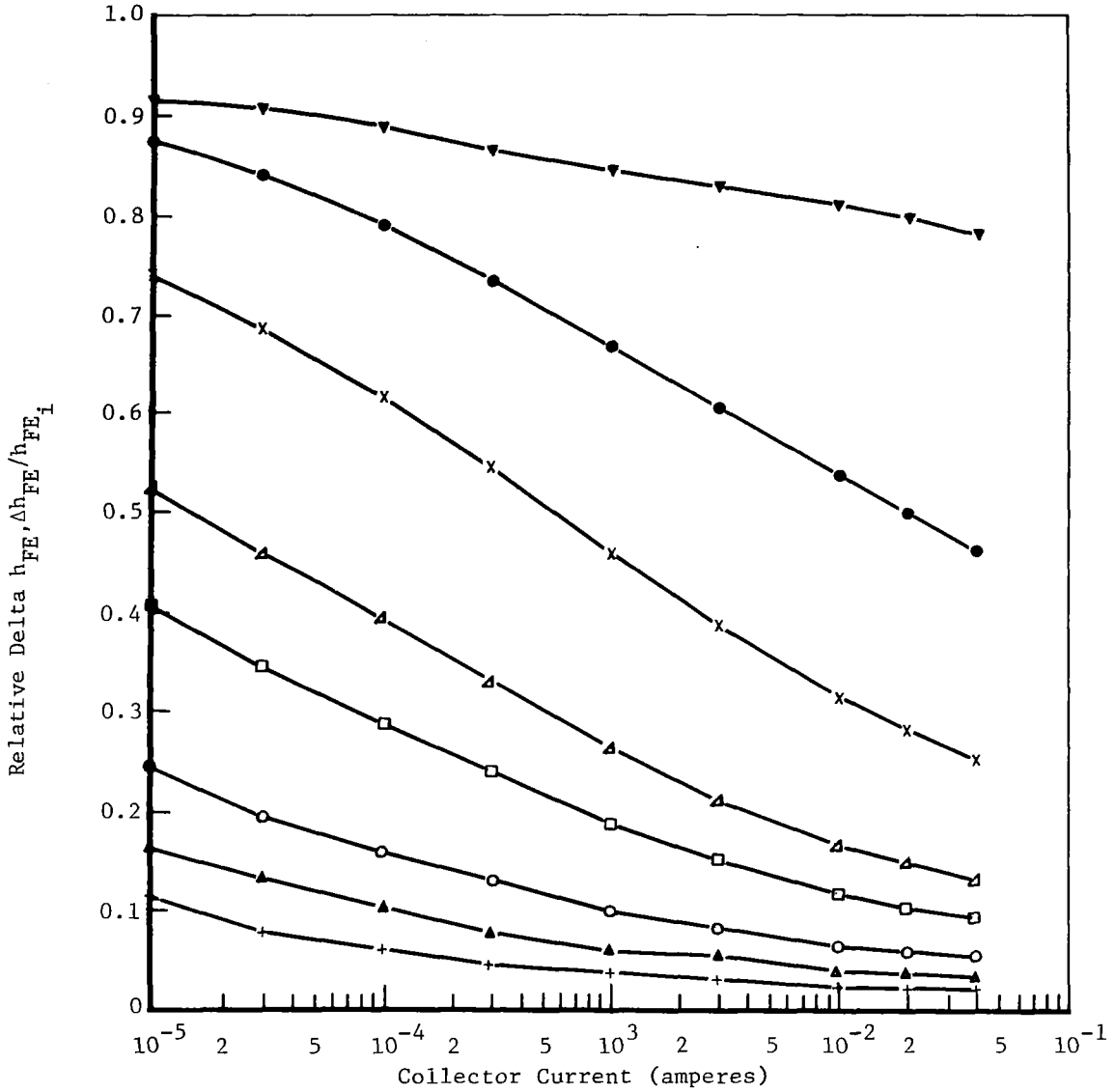

Change in DC Gain vs I_C, Family of Fluences, Type 2N1132, No. 198

Symbol	Fluence
*	0.00
+	2.35+11
▲	7.22+11
○	1.58+12
□	5.93+12
◿	1.29+13
x	6.81+13
●	3.41+14
▼	2.38+15

Figure 20: DEPENDENCE OF RELATIVE GAIN LOSS ON COLLECTOR CURRENT DURING MEASUREMENT

The most meaningful way to plot damage as a function of I_C, for empirical characterization, is shown in the computer plot of Figure 21. The functional relation between $\Delta 1/h_{FE}$ and I_C, subject to certain assumptions, is derived in Appendix I and is approximately given by

$$\Delta(1/h_{FE}) \cong \text{const. } I_C^{(1/n)-1} \tag{3}$$

This relation on a log-log plot would result in straight lines. Experimental data on passive transistors, at least at low currents and exposures where ionization induced surface effects dominate, did in general exhibit such straight line plots. The slopes of the lines furnish the "n" values which can identify the spatial origin of the dominant base current components at different fluences. That method of analysis is also discussed in Appendix I. In order to show the "n" value prior to irradiation, a $1/h_{FE_i}$ vs. I_C line is also included in Figure 21. From the flatness of the $1/h_{FE_i}$ line we see that initially $n \cong 1.3$ at I_C = 10 μa and $n \cong 1.0$ at 20 ma. For the 2N1613 transistor seen in Figure 21, $\Delta(1/h_{FE})$ data indicates that an n value of approximately 1.7 builds in for low exposures and low current. From that n value the spacing between the I_C curves of Figure 18 can be accounted for quantitatively. From Equation (3)

$$\frac{\Delta(1/h_{FE})_1}{\Delta(1/h_{FE})_2} \cong \left(\frac{I_{C_1}}{I_{C_2}}\right)^{(1/n-1)} \tag{4}$$

and with an n value of 1.7 for 2N1613 transistors we find for the ratio of currents $(\frac{10\ \mu a}{100\ \mu a}, \frac{0.1\ ma}{1\ ma}, \frac{1\ ma}{10\ ma})$ that

$$\frac{\Delta(1/h_{FE})_1}{\Delta(1/h_{FE})_2} \cong (10)^{0.41} \cong 2.6 \tag{5}$$

Actually

$$\Delta(1/h_{FE}) = 1/h_{FE} - 1/h_{FE_i} \tag{6}$$

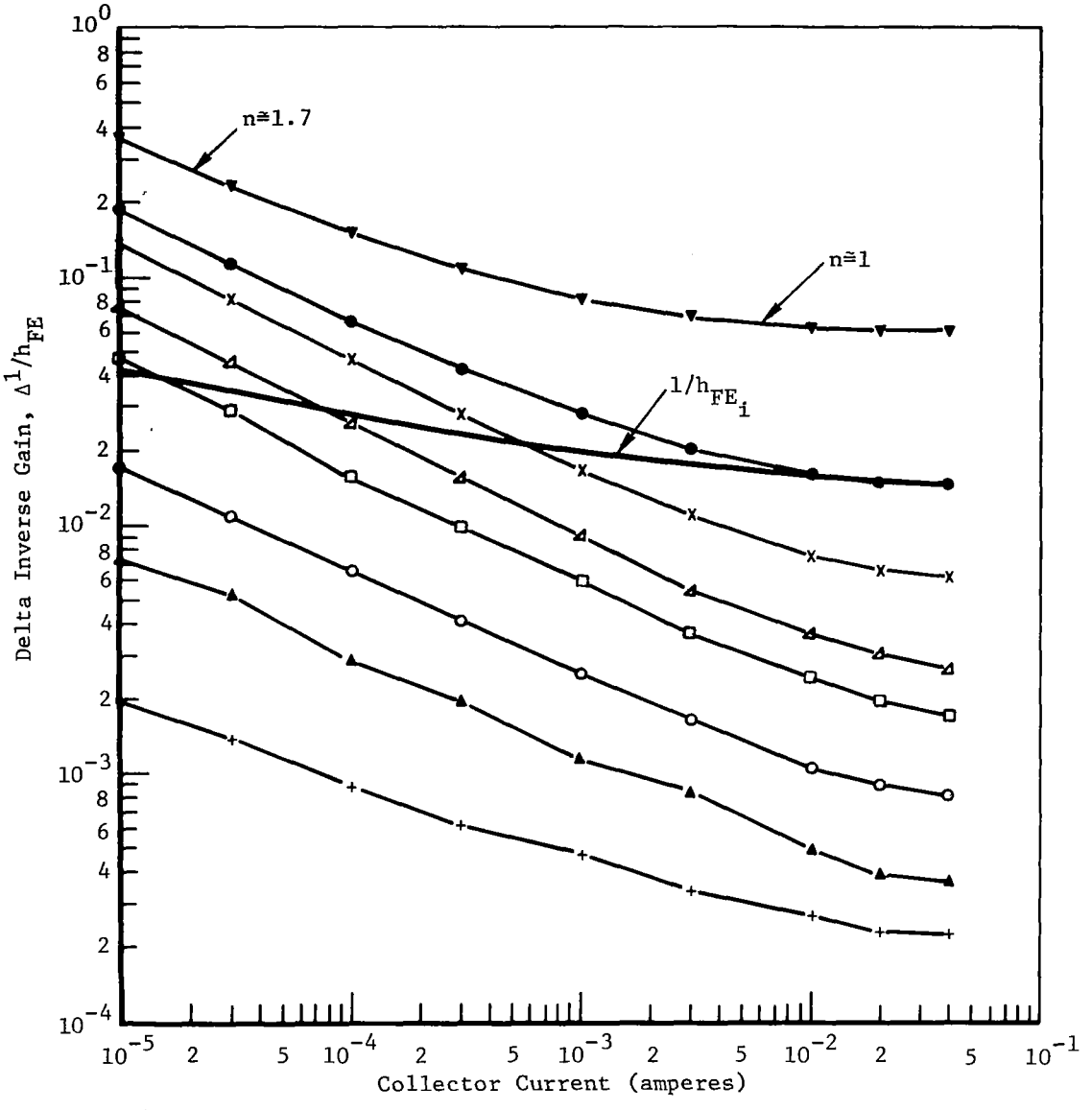

Change in DC Gain vs I_C, Family of Fluences, Type 2N1613, No. 2

Symbol	Fluence
*	0.00
+	2.35+11 (5.53 x 10^3 rad Si)
▲	7.22+11
○	1.58+12
□	5.93+12
◿	1.29+13
x	6.81+13
●	3.41+14
▼	2.38+15 (5.5 x 10^7 rad Si)

Figure 21: DEPENDENCE OF NONLINEAR DAMAGE ON THE COLLECTOR CURRENT DURING MEASUREMENT (FAIRCHILD 2N1613---PASSIVE)

where h_{FE_i} is also a function of I_C. Thus, the value of Equation (5) fits Figure 18 best at low currents and high exposures where

$$\Delta 1/h_{FE} \cong 1/h_{FE} \tag{7}$$

Eventually at high enough electron exposure the dominate component of n value for high currents corresponds to n = 1 typical of displacement damage in the bulk of the base region. The fluence at which this occurs (n = 1 in Figure 21) is the same as the fluence at which the electron damage of Figure 18 becomes "linear". N values for nonlinear damage to passive transistors varied from about 1.4 to 1.7, typical of that expected for recombination at the surface of the base-emitter junction regions (Ref. 3). In general, Fairchild transistors had steeper $\Delta(1/h_{FE})$ vs. I_C plots than Raytheon devices, i.e., a stronger dependence on I_C. Raytheon 2N1132 and 2N1613 transistors had n values of approximately 1.5 while Fairchild 2N1613 and 2N1132 had n values closer to 1.7 for nonlinear damage. Devices from both manufacturers, however, tended toward n = 1 when displacement damage began to dominate.

Results for nonlinear damage caused by Cobalt-60 exposure are shown in Figure 22 for $1/h_{FE}$ versus I_C. It should be noted that of course for low exposure $1/h_{FE} \cong 1/h_{FE_i}$ thus the n value for slope is close to n = 1. However as exposure increases to 1×10^6 rad Si the n value approaches 1.7 typical of the electron example of Figure 21.

Similar results (n = 1.7) for 15 MeV proton damage are shown for $\Delta(1/h_{FE})$ in Figure 23 for a 2N1613 transistor in the low exposure region where nonlinear damage dominates. For proton induced displacement damage, from the review of devices tested in phase I (as seen in section 2.5), the slope of $\Delta(1/h_{FE})$ vs. I_C is practically zero indicating a value of $n \cong 1$ as expected.

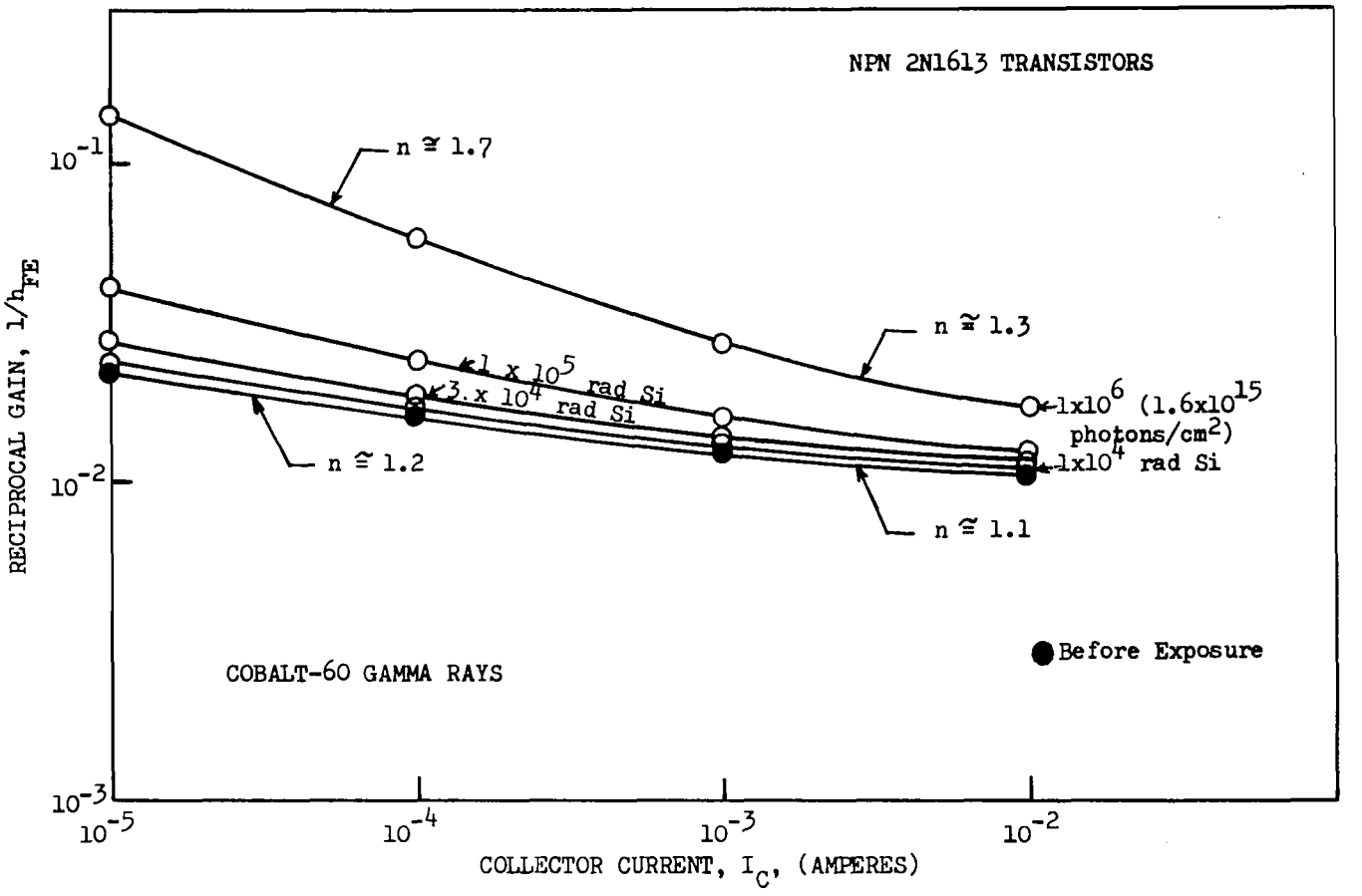

Figure 22. Dependence of Nonlinear Gamma Damage on Collector Current During Measurement

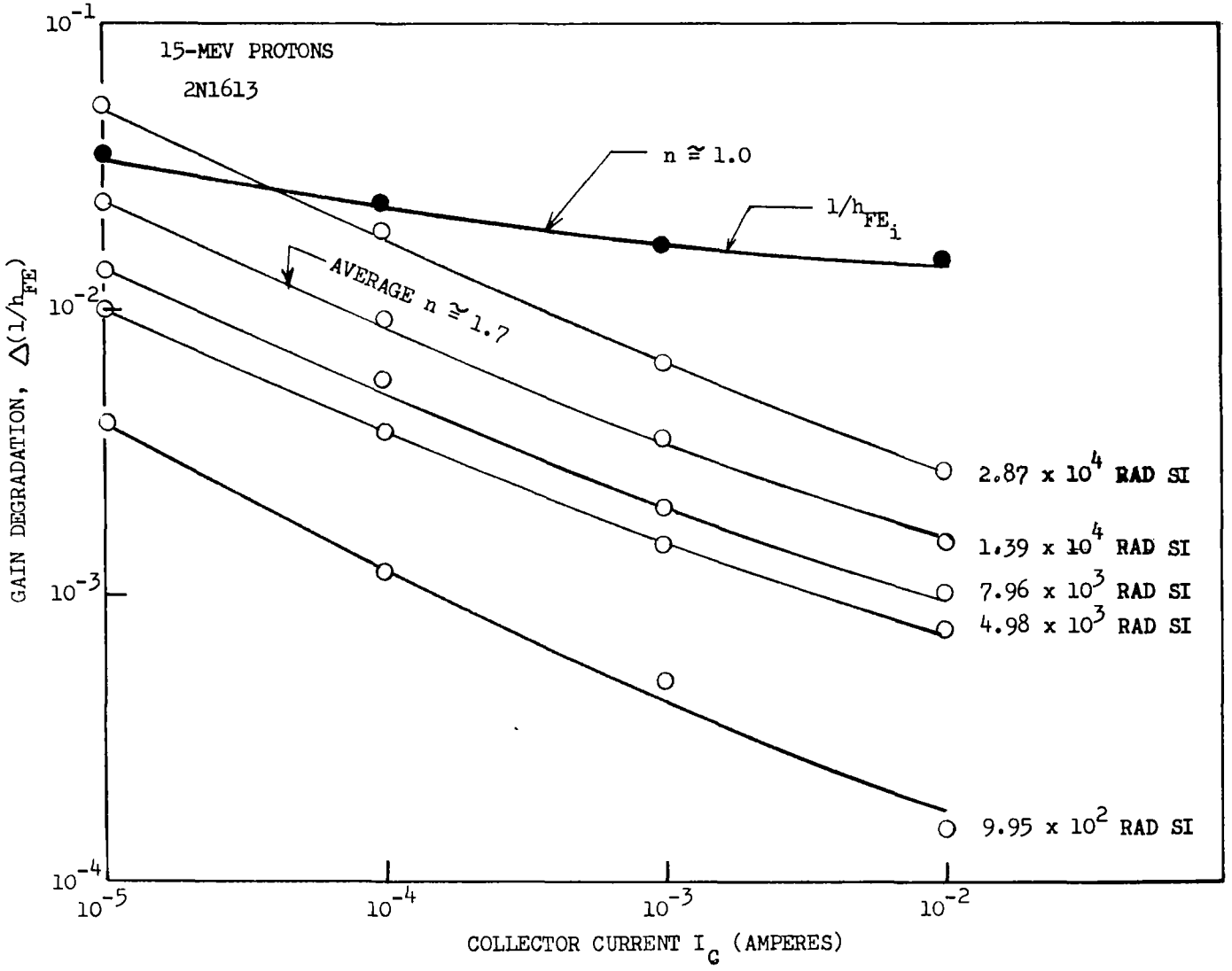

Figure 23. Dependence of Nonlinear Proton Damage on Collector Current During Measurement

2.3.2 Statistical Spread

For accurate predicting of transistor gain degradation due to ionizing irradiation, one should consider the statistical spread in response among presumably "identical" devices during identical exposure conditions. Spread in gain degradation is clearly expected among transistors, the question is how much. Initial surface conditions are critical for controlling certain transistor parameters and for influencing their degradation by surface ionization. More specifically, the oxidation conditions and surface cleaning techniques may determine not only the low current values of gain but also the degradation of that gain with exposure. Although the silicon chips are presumably subjected to "identical" fabrication conditions, it is not possible in practice to avoid some subtle differences in procedures (e.g. due to small differences in surface cleaning steps by different operators during assembly) consequently the surface conditions of the finished transistors can differ slightly.

In order to determine the size of the spread in transistor response during identical exposure, a statistical study was conducted on passive devices. 30 Fairchild 2N1613, 30 Raytheon 2N1613, 30 Fairchild 2N1132 and 30 Raytheon 2N1132 transistors were tested, actually each group of 30 came from three different date codes (10 devices each). This selection of transistors allowed us to observe differences among devices within a date code, between date codes, and between manufacturers. The actual date codes (year and week) of the devices used in the statistical study are listed in Table 5, and will be referred to by the batch designations assigned. A large selection of date codes was used (1964 to 1967). It is important to note here that although some interesting differences were observed, devices of the same register number but different batches (even between different manufacturers) generally showed similar sensitivity to radiation.

The results of the study are displayed in three different forms: h_{FE} vs. Φ, $\Delta h_{FE}/h_{FE_i}$ vs. Φ , and $\Delta 1/h_{FE}$ vs. Φ. All gain values shown in Section 2.3.2 refer to measurements at a collector current of 10 μa in order to maximize differences in damage. In each figure three curves will be superimposed. Each curve represents the mean value of the particular parameter taken for a given batch (10 devices). The vertical bars across the curves represent the standard deviations for the 10 devices. The curve for batch #1

Table 5. Summary of Batch or Date Code Designations

Passive Devices

2N1613 - NPN			2N1132 - PNP		
Batch Designation	Actual Date Code	Device Number	Batch Designation	Actual Date Code	Device Number
F1	701	1 thru 10	R1P	6523	111-120
F2	552	31- 40	R2P	6710	141-150
F3	615	61- 70	R3P	6649	161-168
R1	446	81- 90	F1P	721	189-198
R2	6545	91-100	F2P	736	199-207
R3	6625	101-110	F3P	621	208-218

will be left in its original position, the other two will be shifted horizontally for clarity in order to avoid overlap of the σ bars. The h_{FE} vs. Φ data illustrate the initial gain distributions within the batches as well as the changes of these distributions with fluence. The $\Delta h_{FE}/h_{FEi}$ vs. Φ data, since they are "normalized", as will be discussed in Section 2.3.3, are well suited to show up some inherent differences in surface conditions among the batches. Without such differences the curves should overlap. The $\Delta 1/h_{FE}$ vs. Φ data show the differences among the batches by using still another type of normalization as will also be discussed in 2.3.3.

Results in terms of the three forms of data display are shown in Figures 24 through 35. 2N1613 data is shown in the first six figures, 2N1132 data in the remainder. In each case the Fairchild devices are compared with the Raytheon devices in pairs of figures for each damage form h_{FE}, $\Delta h_{FE}/h_{FE_i}$, and $\Delta(1/h_{FE})$ versus fluence.

The following conclusions can be drawn from the figures:

i) Devices within a given batch:

Devices, as a general rule, tended to degrade in a very similar fashion within a given batch. Although the actual values of $\Delta 1/h_{FE}$ at given Φ were somewhat different for different devices, as the size of the σ bars testifies (e.g. Figures (28) and (29), the shape of the curves for the individual devices were very similar so that a given shape could almost serve as a marker for all the transistors within a batch. This will be emphasized more strongly in Section 2.3.3. Similar behavior during exposure presumably results in the devices bearing the same date code because they were fabricated together as a group, i.e., conditions were fairly similar for all of them. Although this is probably true it is not necessarily the case as discussions during a visit to the manufacturers revealed. Depending upon the number of devices produced within a particular week, the devices having the same date code may or may not come from the same "lot" (a group of wafers exposed to identical diffusion and oxidation conditions at the same time). If only a relatively small number of transistors were produced then they are likely to originate from the same lot. Devices with the same date code although coming

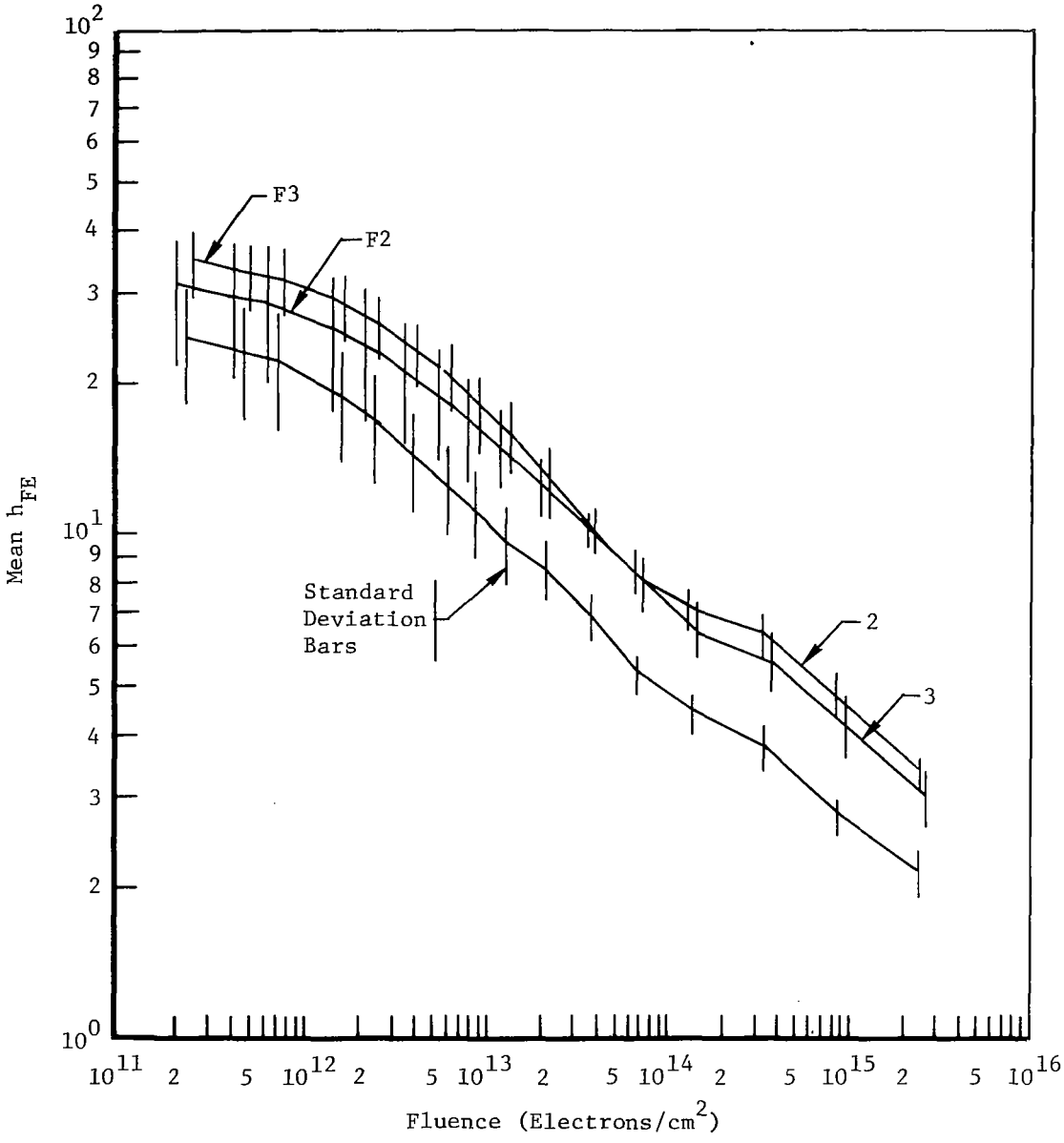

DC Gain at 0.01 ma vs Fluence, Type 2N1613 Batch F1, F2, F3

Figure 24: MEAN h_{FE} OF THREE BATCHES OF PASSIVE FAIRCHILD 2N1613 TRANSISTORS

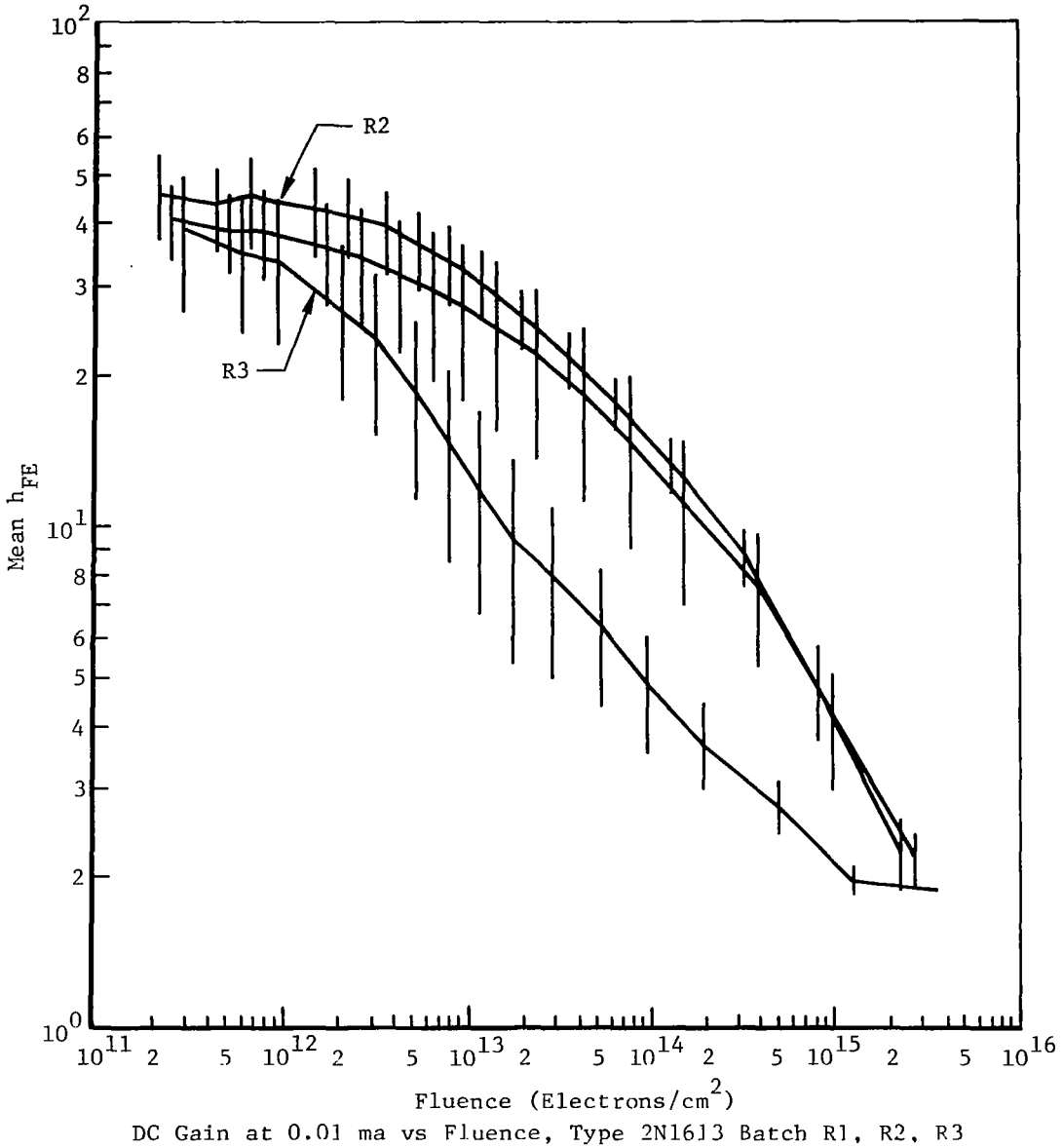

DC Gain at 0.01 ma vs Fluence, Type 2N1613 Batch R1, R2, R3

Figure 25: MEAN h_{FE} OF THREE BATCHES OF PASSIVE RAYTHEON 2N1613 TRANSISTORS

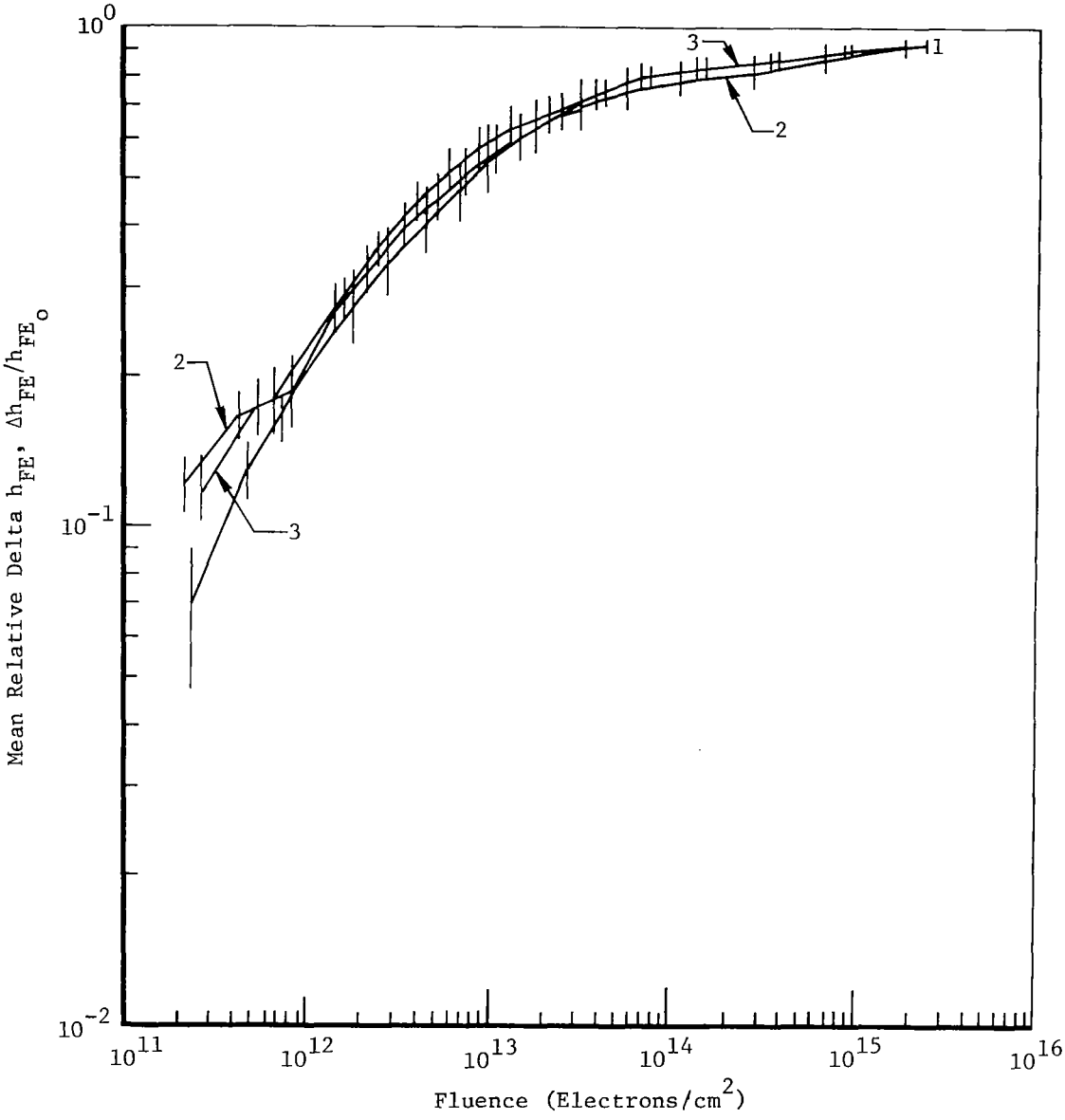

Change in DC Gain at 0.01 ma vs Fluence, Type 2N1613 Batch F1, F2, F3

Figure 26: MEAN RELATIVE GAIN LOSS OF THREE BATCHES OF PASSIVE FAIRCHILD 2N1613 TRANSISTORS

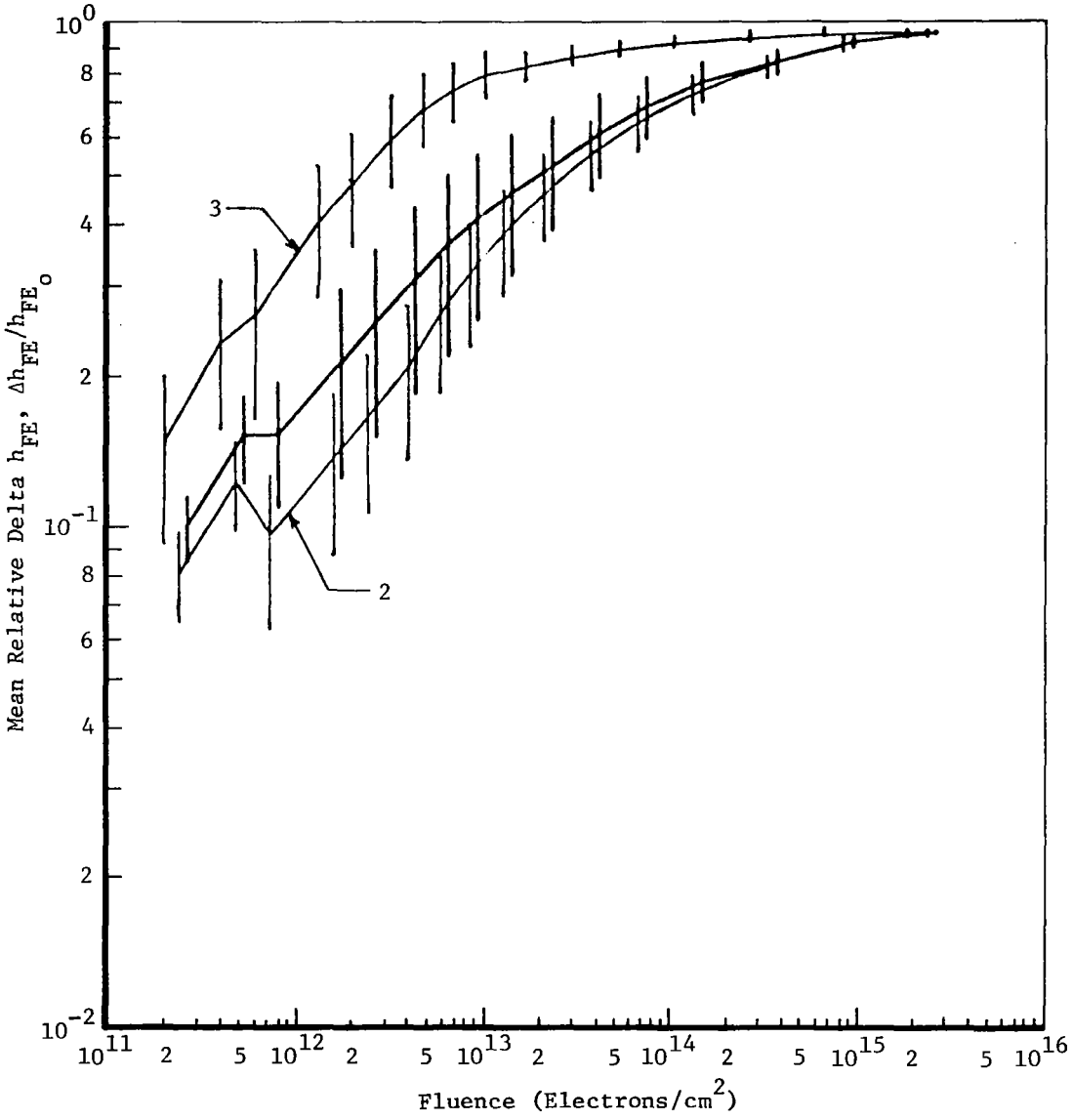

Change in DC Gain at 0.01 ma vs Fluence, Type 2N1613 Batch R1, R2, R3

Figure 27: MEAN RELATIVE GAIN LOSS OF THREE BATCHES OF PASSIVE RAYTHEON 2N1613 TRANSISTORS

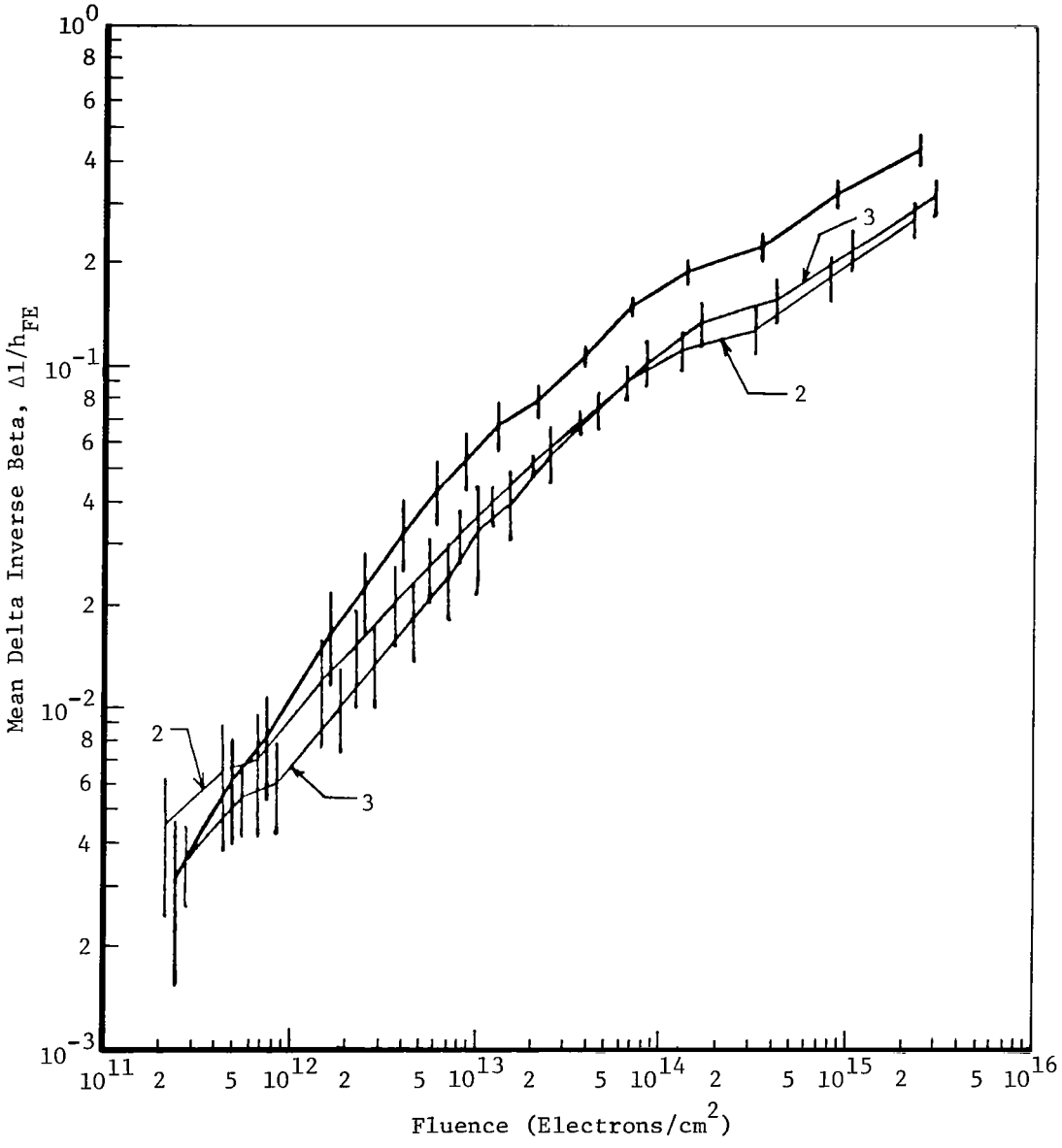

Change in DC Gain at 0.01 ma vs Fluence, Type 2N1613 Batch F1, F2, F3

Figure 28: MEAN $\Delta 1/h_{FE}$ OF THREE BATCHES OF PASSIVE FAIRCHILD 2N1613 TRANSISTORS

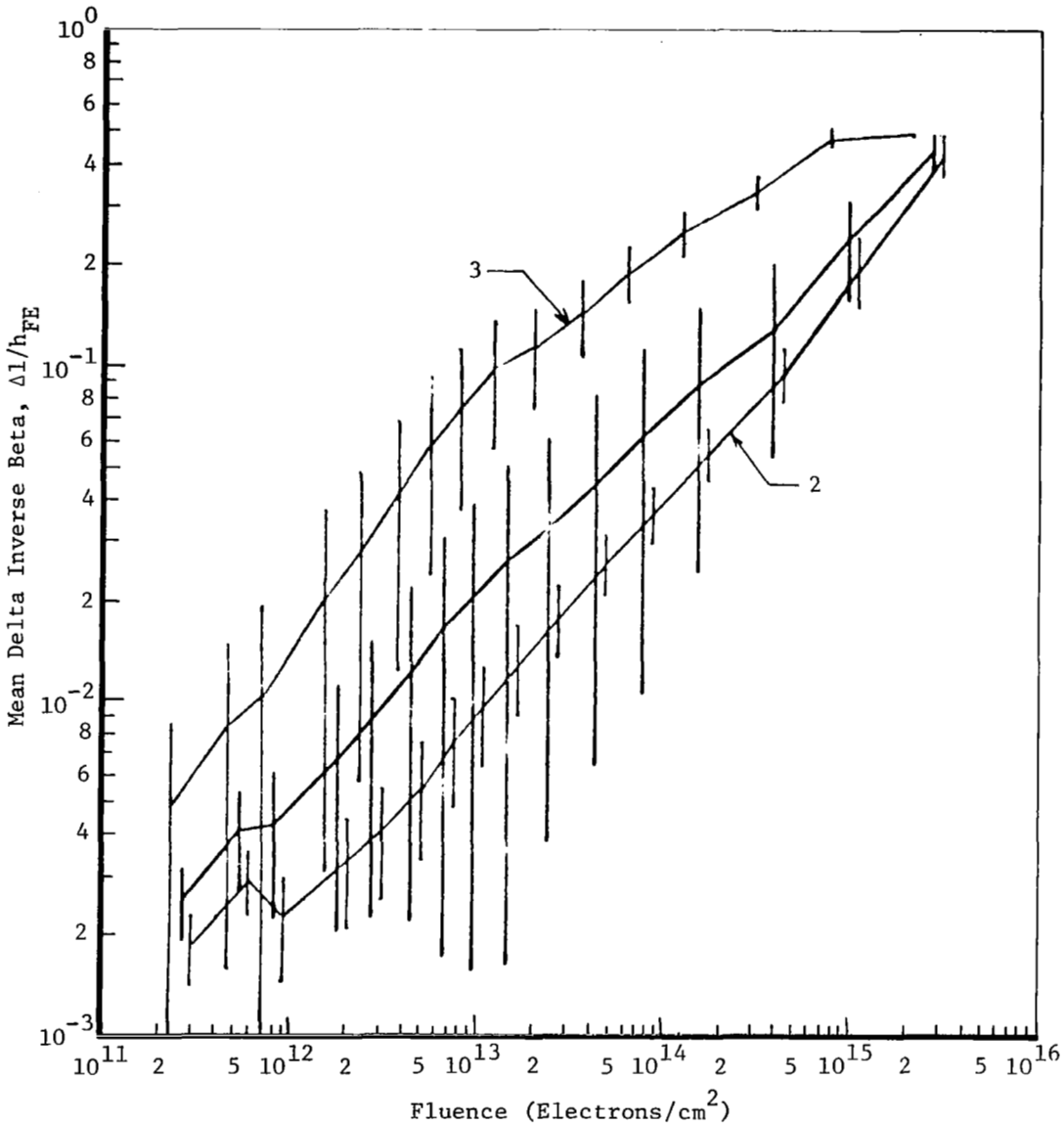

Change in DC Gain at 0.01 ma vs Fluence, Type 2N1613 Batch R1, R2, R3

Figure 29: MEAN $\Delta 1/h_{FE}$ OF THREE BATCHES OF PASSIVE RAYTHEON 2N1613 TRANSISTORS

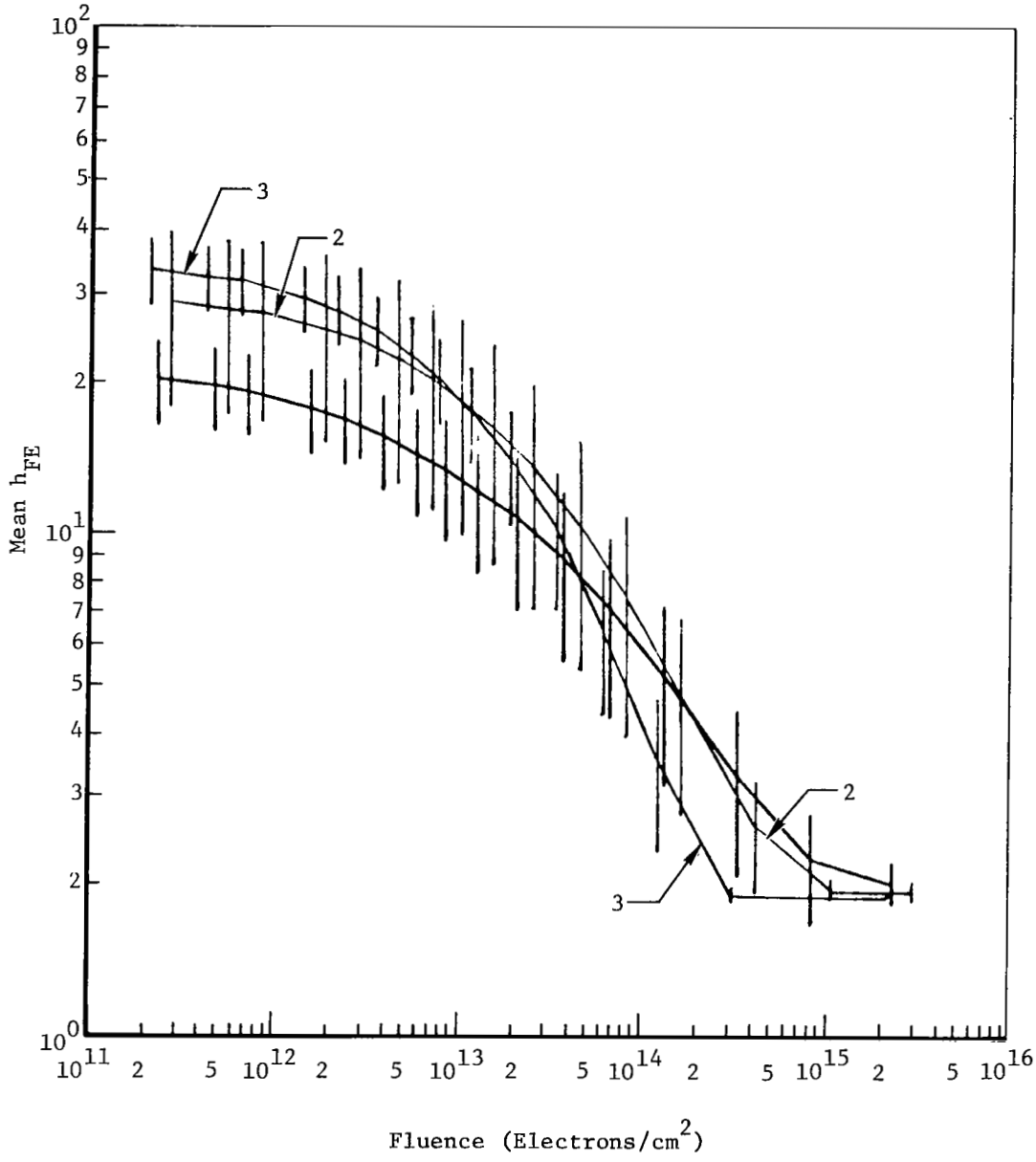

DC Gain at 0.01 ma vs Fluence, Type 2N1132 Batch R1P, R2P, R3P

Figure 30: MEAN h_{FE} OF THREE BATCHES OF PASSIVE RAYTHEON 2N1132 TRANSISTORS

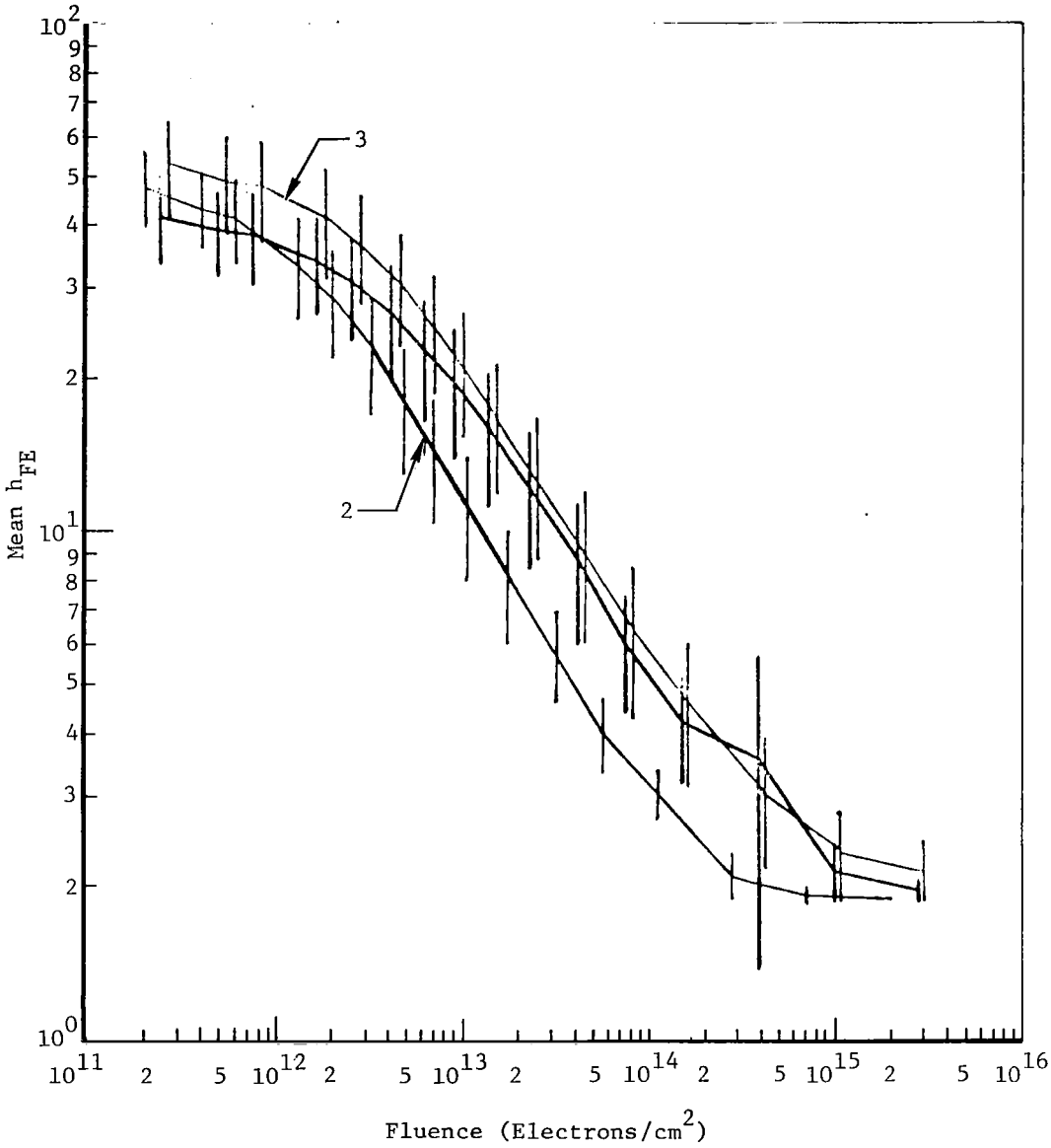

DC Gain at 0.01 ma vs Fluence, Type 2N1132 Batch R1P, R2P, R3P

Figure 31: MEAN h_{FE} OF THREE BATCHES OF PASSIVE RAYTHEON 2N1132 TRANSISTORS

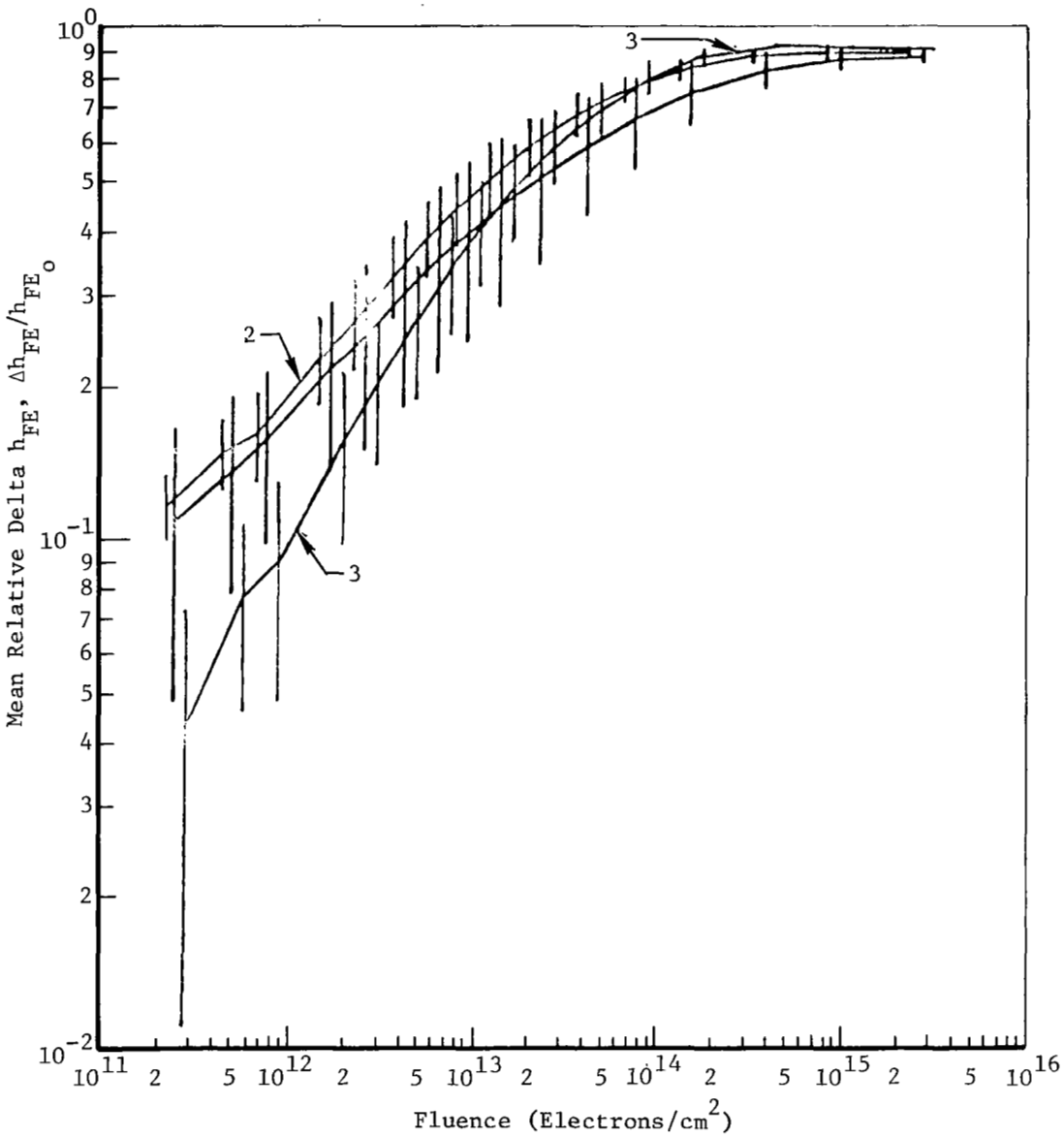

Change in DC Gain at 0.01 ma vs Fluence, Type 2N1132 Batch F1P, F2P, F3P

Figure 32: MEAN RELATIVE GAIN LOSS OF THREE BATCHES OF PASSIVE FAIRCHILD 2N1132 TRANSISTORS

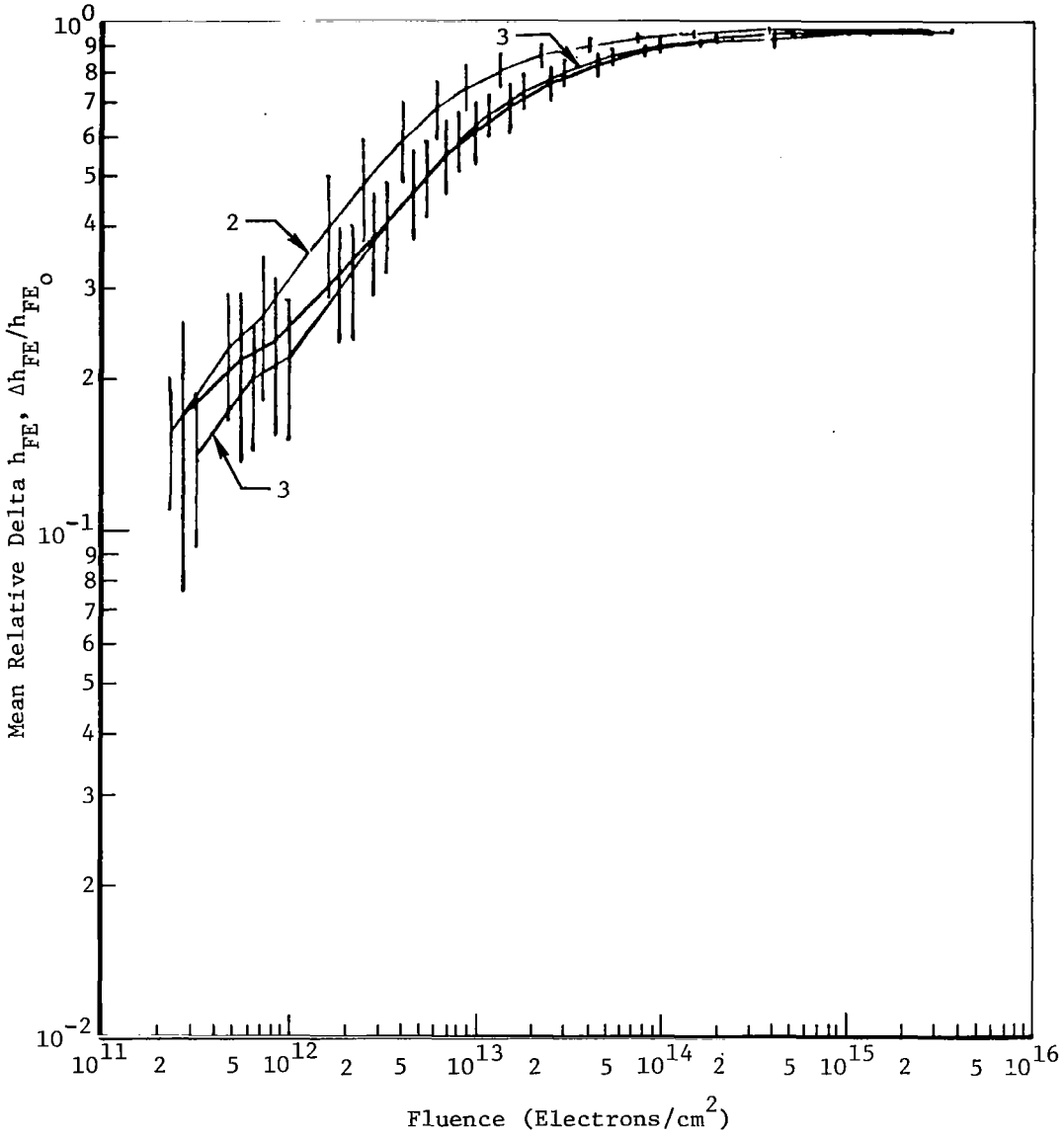

Change in DC Gain at 0.01 ma vs Fluence, Type 2N1132 Batch R1P, R2P, R3P

Figure 33: MEAN RELATIVE GAIN LOSS OF THREE BATCHES OF PASSIVE RAYTHEON 2N1132 TRANSISTORS

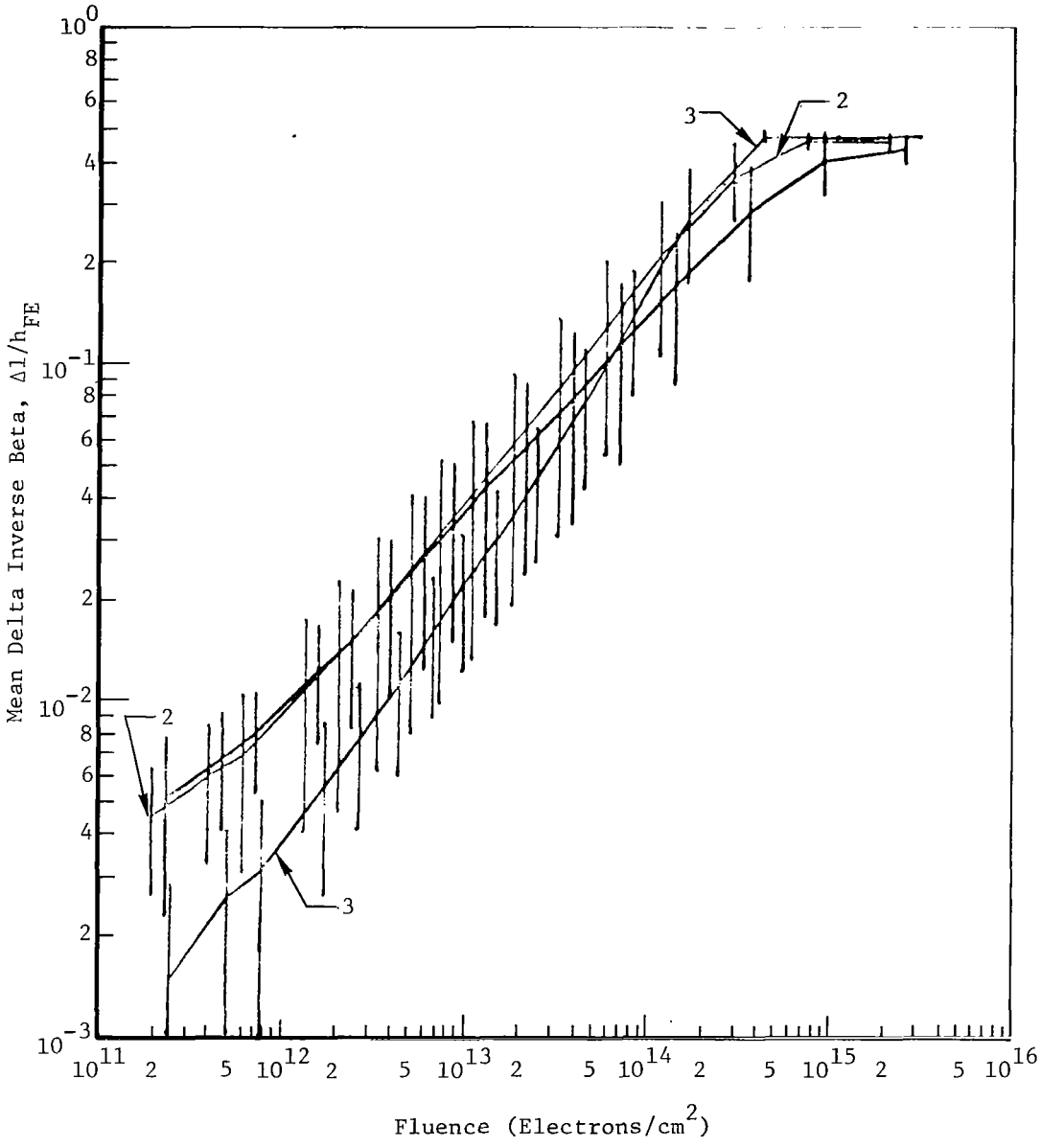

Change in DC Gain at 0.01 ma vs Fluence, Type 2N1132 Batch F1P, F2P, F3P

Figure 34: MEAN $\Delta 1/h_{FE}$ OF THREE BATCHES OF PASSIVE FAIRCHILD 2N1132 TRANSISTORS

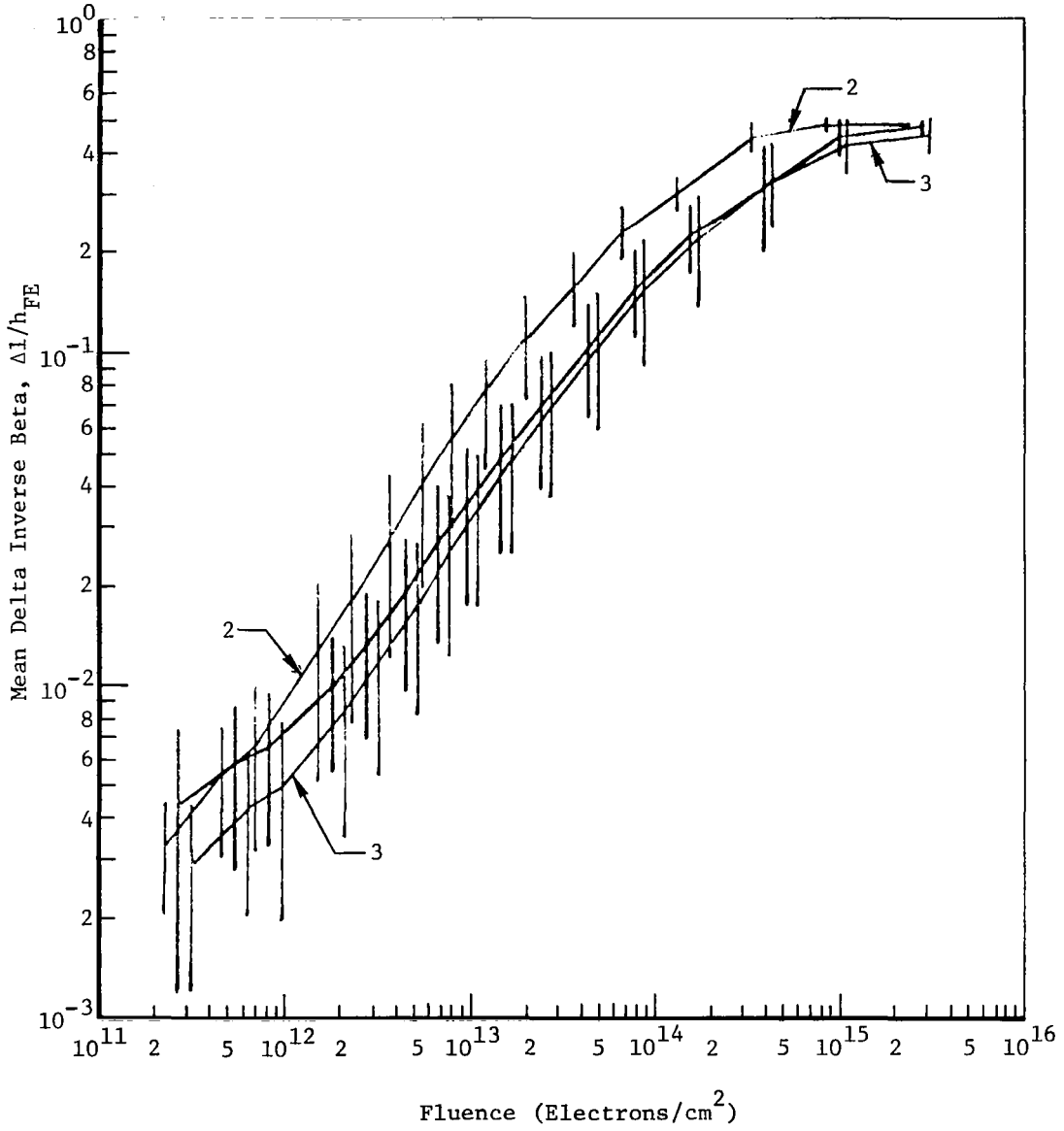

Change in DC Gain at 0.01 ma vs Fluence, Type 2N1132 Batch R1P, R2, R3

Figure 35: MEAN $\Delta 1/h_{FE}$ OF THREE BATCHES OF PASSIVE RAYTHEON 2N1132 TRANSISTORS

from different lots could, nevertheless, experience similar diffusion, oxidation and surface cleaning procedures within a week or so even though not exactly at the same time. To the contrary, devices having widely different date codes (by a year or more), probably experience slightly different fabrication conditions due to continuous improvement and changes in techniques (surface cleaning!) equipment, and operators during that time.

ii) Devices from different batches of the same manufacturer.

Differences in device response during irradiation for devices from different batches is expected especially if the date codes are far apart. Experimentally, this was indeed the case. By checking the date codes in Table 5 and comparing the curves representing separate batches in Figures (24) - (35) we observed the following:

a) NPN - Fairchild: The mean h_{FE} curves in Figure 24 representing batches F2 and F3 (only a few months apart) are fairly close while batch F1 (lower initial gain) is well outside the standard devication of the first two batches. This result might be expected on the basis of the date codes. When the nonlinear damage is plotted in a normalized fashion ($\Delta h_{FE}/h_{FE_i}$), then the curves of all batches superimpose as shown in Figure 26. However, the superposition of the curves in terms of the $\Delta 1/h_{FE}$ data in Figure (28) is not nearly as good, with F_1 still outside the standard deviation of F_2 and F_3.

b) PNP - Fairchild: The initial portion of the mean h_{FE} curves (Figure 30) representing F1P and F2P are far apart (different initial gains) while F3P is close to F2P. The superposition of the curves in terms of normalized form $\Delta h_{FE}/h_{FE}$ or even $\Delta 1/h_{FE}$ (Figures 32 and 34) is good for F1P and F2P (whose date codes are very close) but F3P which was manufactured a year earlier has a different sensitivity. Some small but significant differences probably exist between the exact surface conditions of transistor batches (F1P, F2P) and F3P.

c) NPN - Raytheon: Initial mean gain values of batches R1, R2, and R3, Figure 25, are very close in spite of about a year's separation in each of the date codes. But their irradiation responses are widely different both in terms of $\Delta h_{FE}/h_{FE_1}$ (Figure 27), and of $\Delta 1/h_{FE}$ (Figure 29). Interestingly though, R1 and R2 remain fairly close in the damage curves while batch R3 is much more sensitive to radiation even though it has the most recent date code.

d) PNP - Raytheon: R1P and R3P curves of mean h_{FE} are close in Figure 31 though the date codes are quite different. All curves are fairly close, as expected, when the nonlinear damage is normalized either in terms of $\Delta h_{FE}/h_{FE_i}$ or $\Delta 1/h_{FE}$ (Figures 33 and 35). However, the latest date code R2P was more radiation sensitive and often outside the standard deviation of the other two batches. This indicates that the surface conditions of the devices in batch R2P are significantly different in some way with respect to the other two batches. Discussions with the manufacturer could not reveal those fabrication differences, but revealed the desirability of identification of processing for correlation with effects (either by mil. spec. designation or captive line) on future radiation tests.

iii) Devices of the same register number from different manufacturers (Fairchild vs. Raytheon):

Differences in device response during exposure among devices coming from two manufacturers are certainly expected. There often are constructional differences between the devices and surface treatments can be entirely different (usually proprietary information) in spite of the fact that the devices are produced for the same function in an electrical circuit. These factors of course can have a large influence on the radiation hardness of the devices. In order to be able to select the most resistant transistors to an ionizing radiation environment it is important to determine what and how large are the differences in radiation response between devices from different manufacturers. The quantity $\Delta h_{FE}/h_{FE_i}$ was used primarily for comparing the devices of different manufacturers in order to normalize against differences in the emitter-base junction perimeters (see Section 2.3.3).

The following conclusions can be drawn from the figures:

2N1613 - NPN

Radiation resistance: Fairchild F_1, F_2, F_3 batches were grouped between Raytheon batches. (See the $\Delta h_{FE}/h_{FE_i}$ curves in Figures (26) and (27).) R1 and R2 were more resistant than Fairchild devices while R3 was more sensitive.

Statistical spread: The different Fairchild batches were much closer in overall behavior than the Raytheon ones. This was especially true in the $\Delta h_{FE}/h_{FE_i}$ curves which is equivalent to saying that there was a good correlation

between gain loss and initial gain for the Fairchild devices whereas absent for the Raytheon ones. Consequently the prediction of the gain loss, Δh_{FE}, or the relative gain loss, $\Delta h_{FE}/h_{FE_i}$, was possible for the Fairchild devices but not for the Raytheon transistors. Also the statistical spread among devices within a given batch is much wider for the Raytheon devices than for the Fairchild as seen from the size of the σ bars.

2N1132 - PNP

Radiation resistance: Fairchild batches were somewhat more resistant than the Raytheon ones. (See Figures (32) and (33).)

Statistical spread: Raytheon batches are slightly closer than the Fairchild ones, although the former batches cover over 1½ year period whereas the latter ones cover about a year. The standard deviation bars are approximately of the same size for both manufacturers. The correlation of the gain loss to the initial gain or equivalently the predictability of the relative gain loss, $\Delta h_{FE}/h_{FE_i}$ was approximately of the same degree for each manufacturer. (See Figures (32) and (33) or the Rank Coefficients of Correlation in Section 2.3.3.

In summary of this section we can say that in order to select transistors (given type and manufacturer) with the least expected spread in radiation response one should specify not only that the devices carry the same date code but also that they come from the same lot of Si wafers. As a compromise one may settle for the same date code only, although a somewhat higher statistical spread is then expected.

Of course, selecting the particular manufacturer is also a very important problem since the statistical spread even among different batches can be smaller for one manufacturer than that within one batch from another manufacturer. This is a statistical consideration only. It says nothing about the average radiation hardness (i.e., the radiation sensitivity) of the devices coming from different manufacturers which can be significantly different.

We wish to re-emphasize that this statistical study was carried out on passive transistors only. In actual space applications the devices are often active during exposure and as shown in Section 2.4 dmage is often far more severe, thus a similar statistical study carried out on biased devices would be highly desirable. On the basis of such a study, a much better prediction of the expected nonlinear gain degradation would be possible.

2.3.3 Correlations and Empirical Formulation

2.3.3.1 Properties of Formulations Relating $\Delta 1/h_{FE}$ and Dose

Displacement damage on transistor gain is often called linear damage because the buildup of $\Delta 1/h_{FE}$ is proportional to the fluence, Φ. Surface damage on transistor gain on the other hand is often called nonlinear damage because of the relation between $\Delta 1/h_{FE}$ and Φ is not linear as observed in Figure 16. Of course, for the purpose of predicting gain degradation with dose, it is of fundamental importance to know what the actual relation is. Is it a power law such as

$$\Delta(1/h_{FE}) = K\ D^m \tag{8}$$

(at least before saturation), where m is a constant and D is the dose; or perhaps an exponential relation

$$\Delta(1/h_{FE}) = K\ (1 - e^{-aD}) \tag{9}$$

where a is a constant? It has also been suggested that for 125 keV electron irradiation

$$\Delta 1/h_{FE} = K\ \ln(\Phi/\Phi_o) \tag{10}$$

where both K and Φ_o are constants.

For two practical reasons there has been no theoretical prediction of the $\Delta\ 1/h_{FE}$ vs. D or Φ relation. First, the electric field intensity and its distribution within the SiO_2 needs to be known for the exact description of the charge accumulation with dose. However, the fringing fields in the vicinity of the junctions due to biases are not very amenable to theoretical analysis. Second, it is not possible to relate $\Delta\ 1/h_{FE}$ <u>directly</u> to exposure phenomenon in a general manner, since gain changes can be affected by both the buildup of positive space charge in SiO_2 and the creation of new interface states. The relative importance of these two effects is still unsettled and probably depends on the particular experimental conditions. In any case, the theoretical

prediction of the buildup of interface states with dose is still missing, as discussed in Appendix I. Consequently, the buildup of the related quantity $\Delta 1/h_{FE}$ with dose cannot be theoretically predicted at present.

As far as the empirical form of the buildup is concerned, $\Delta 1/h_{FE}$ vs. Φ curves from this program showed a variety of very different shapes depending on transistor types, manufacturers, date codes and biasing conditions. These results have been summarized from Phase I and II work.

The separation of nonlinear damage from phase I displacement curves for 10 different types of transistors exposed to 0.5, 1.3, and 2.0 MeV electron irradiations were completed in phase II. Figures 36 through 38 show the typical results of this separation of damage. In Figure 39 transistor type 2N1132 is contrasted with type 2N2219 in typifying two transistor types which have different sensitivities to nonlinear damage. The horizontal axis of Figure 39 is shown in units of absorbed dose, rads(Si), which would allow us to superimpose the data corresponding to different electron energies if the nonlinear damage is primarily due to ionization effects. Two sets of data at one energy signify the difference in response between different species of identical transistors exposed to the same irradiation. The spread between these points is about the same as that between points corresponding to different energies; i.e., within the limits of error, all the data for the three energies superimpose. The shapes of these curves are not well enough defined to render them useful for more detailed analysis since the earlier experiments furnishing these data (NAS 5-9578) were designed to study linear rather than nonlinear damage.

Examples of $\Delta 1/h_{FE}$ degradation resulting from the 1 MeV electron test are summarized in Figures 40 through 44 in three different graphical forms. Most of our devices are represented in these figures. Since the Fairchild Series 500 Transistor Tester programs I_C instead of I_E and gain is measured as I_C/I_B data curves shown are for a family of I_C values. Corrections for the leakage current, I_{CBO}, (see Equation A1 of Appendix I) made very little difference in our data.

The fluence values, shown in these figures, can easily be converted into dose if desired, by dividing with a conversion factor of 4.24×10^7. That is to say

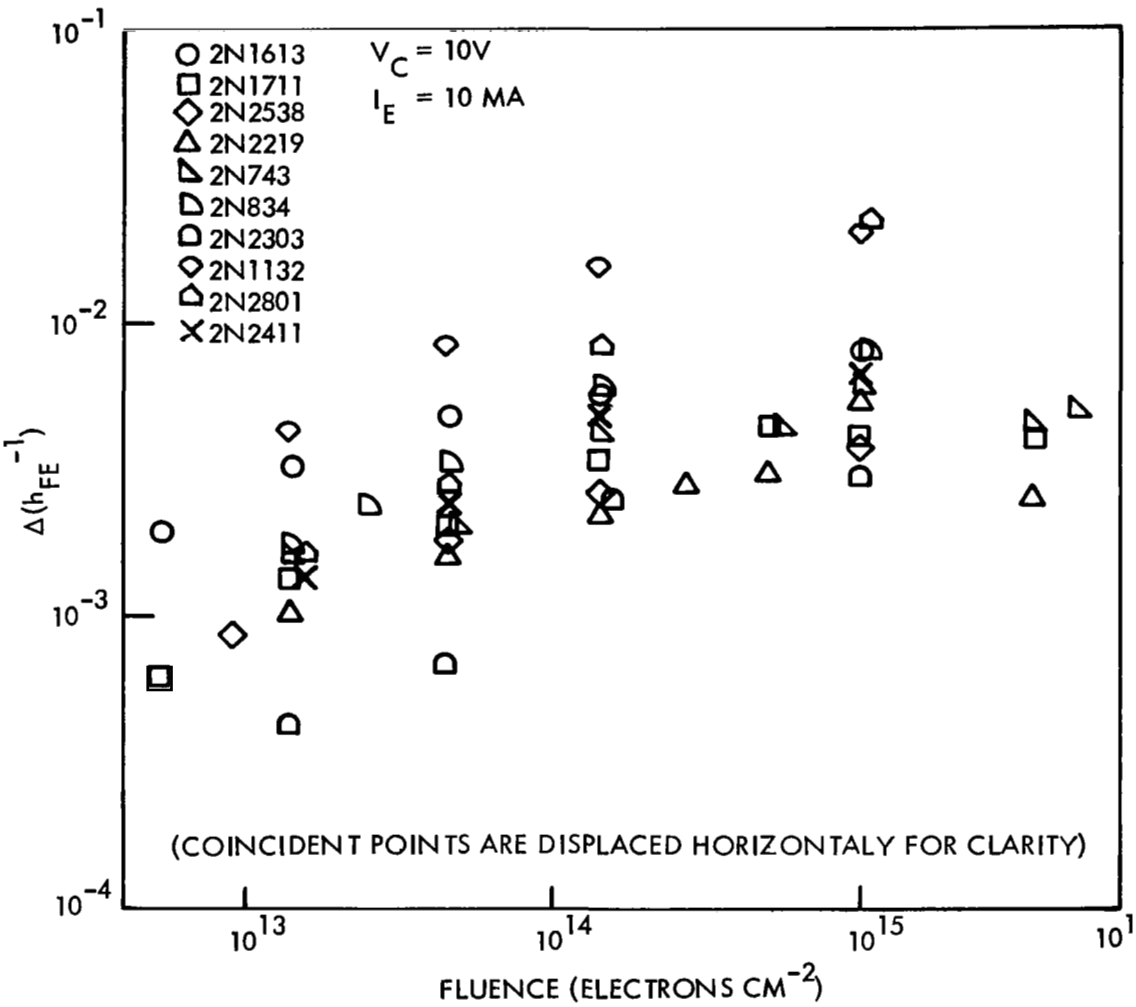

Figure 36. Nonlinear Damage in Transistors, as Separated From Total Damage, After 0.5 Mev Electron Irradiation (Extended Phase I)

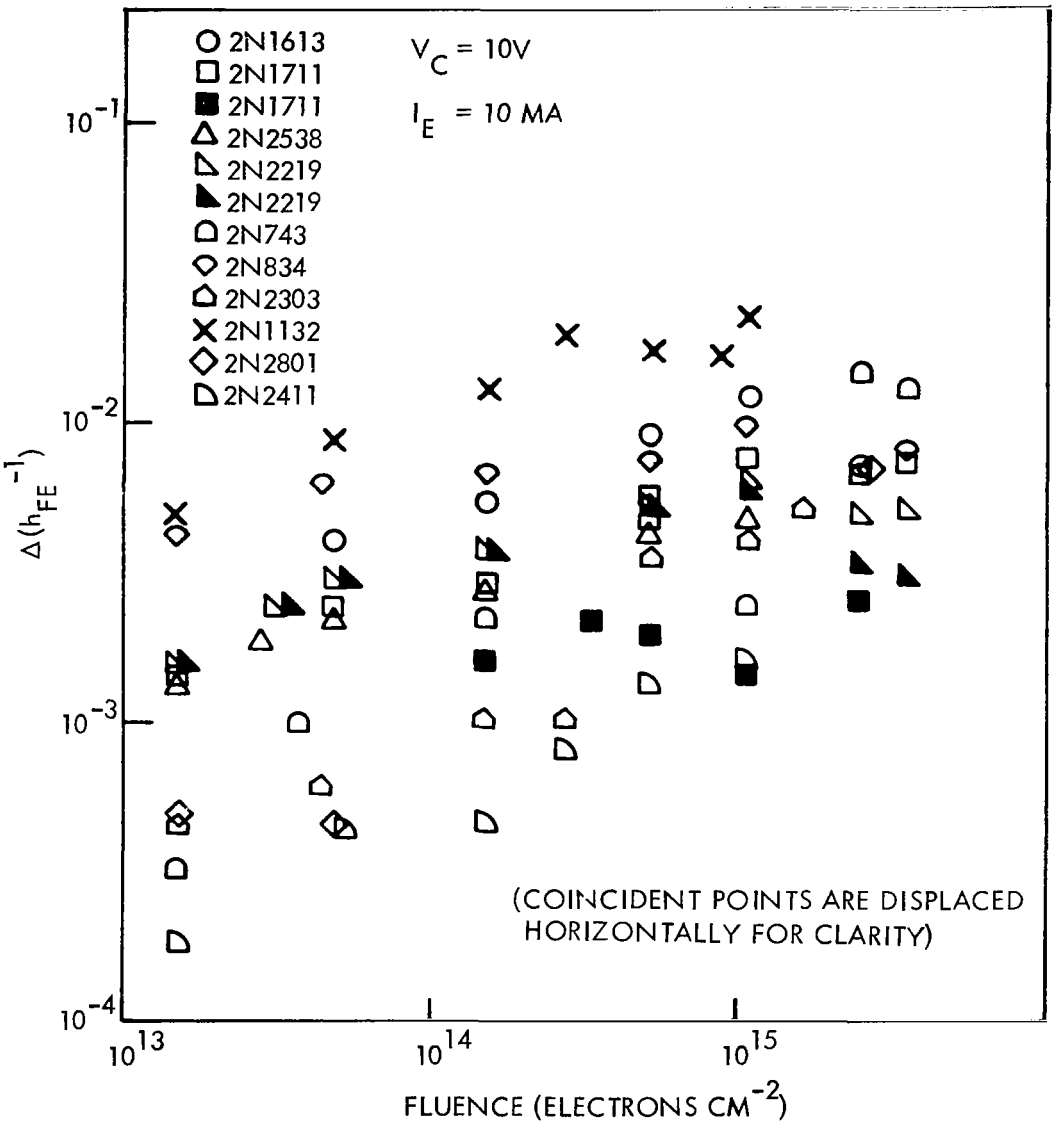

Figure 37. Nonlinear Damage in Transistors, as Separated From Total Damage, After 1.3 Mev Electron Irradiation (Extended Phase I)

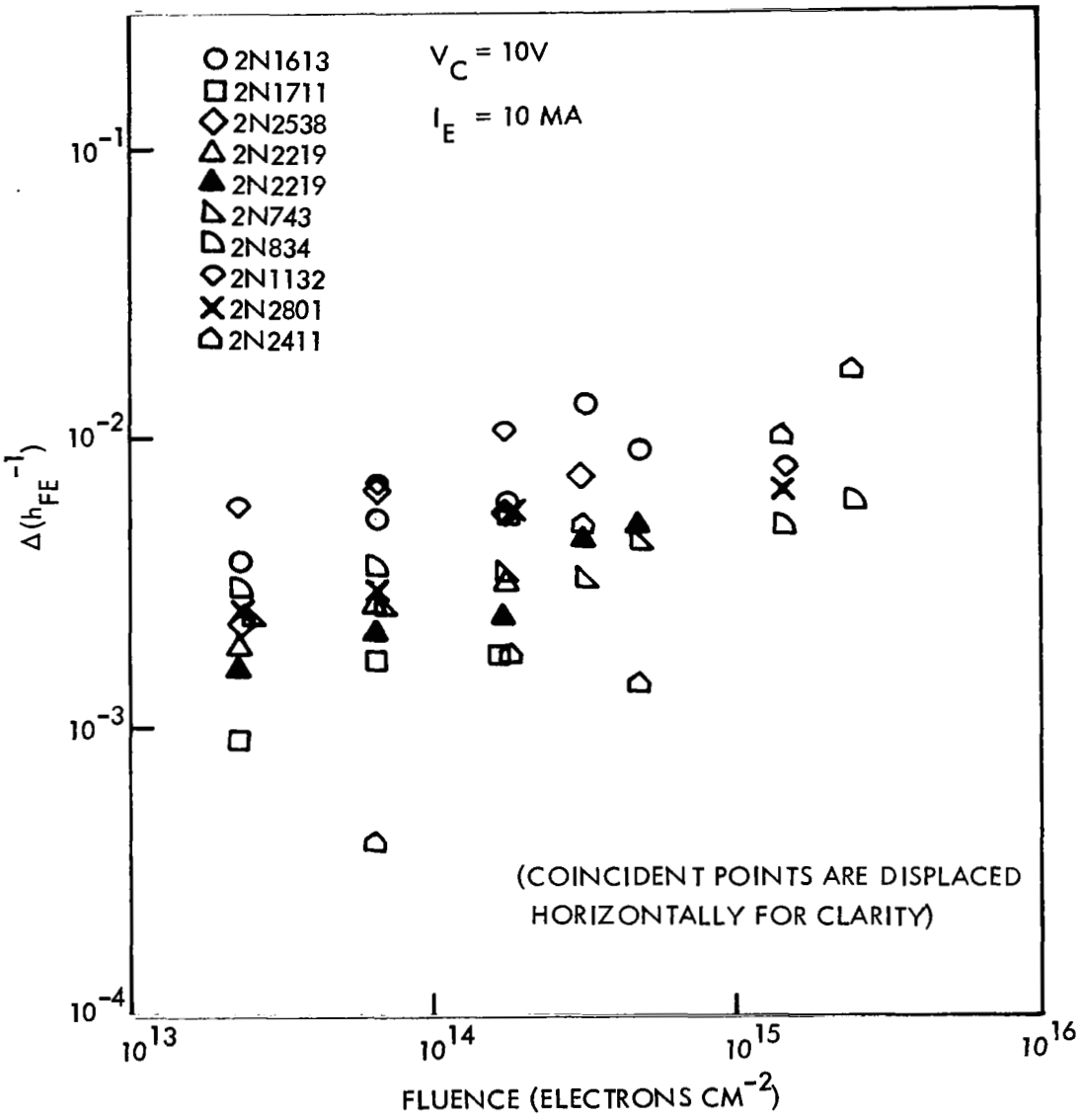

Figure 38. Nonlinear Damage in Transistors, as Separated From Total Damage, After 2 Mev Electron Irradiation (Extended Phase I)

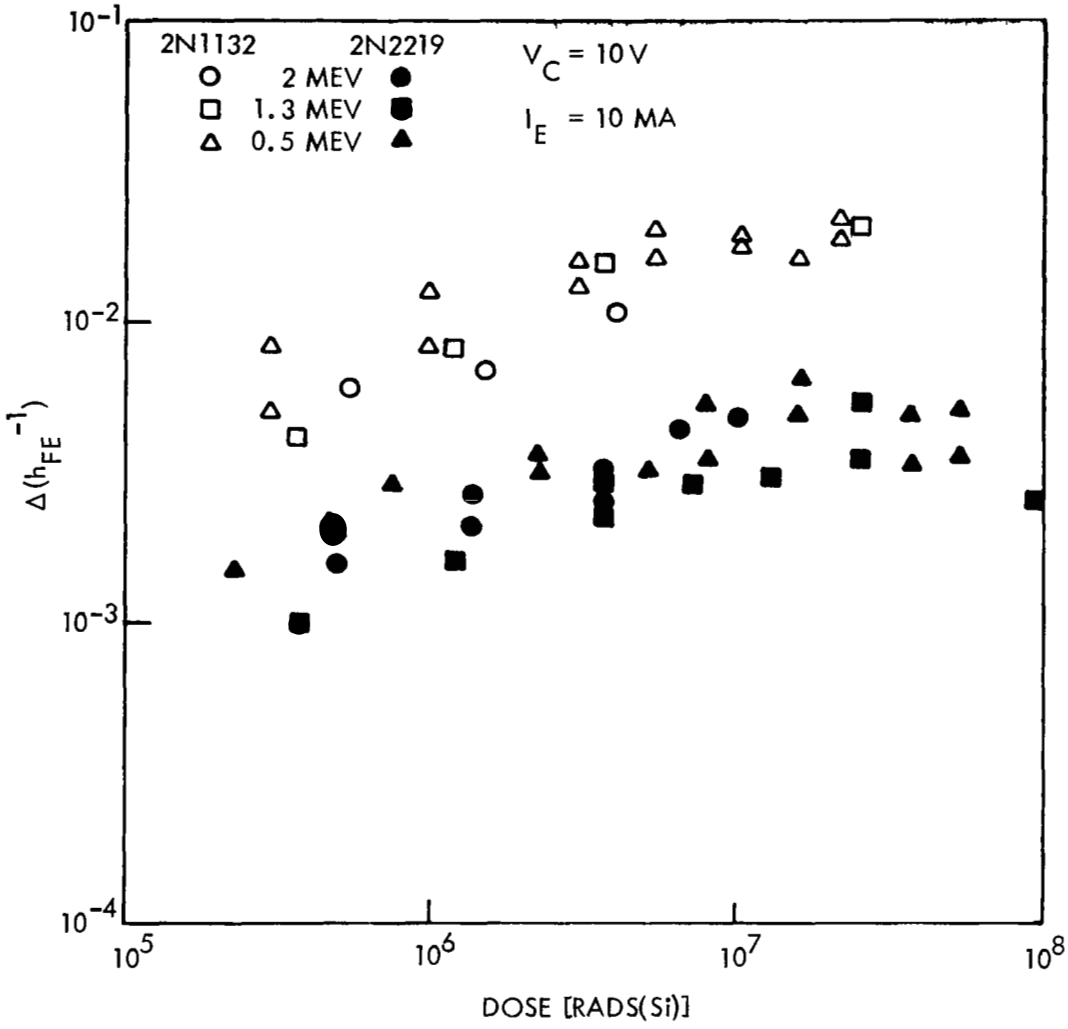

Figure 39. Comparison of Sensitivity of Two Types of Transistors to Nonlinear Damage (Extended Phase I)

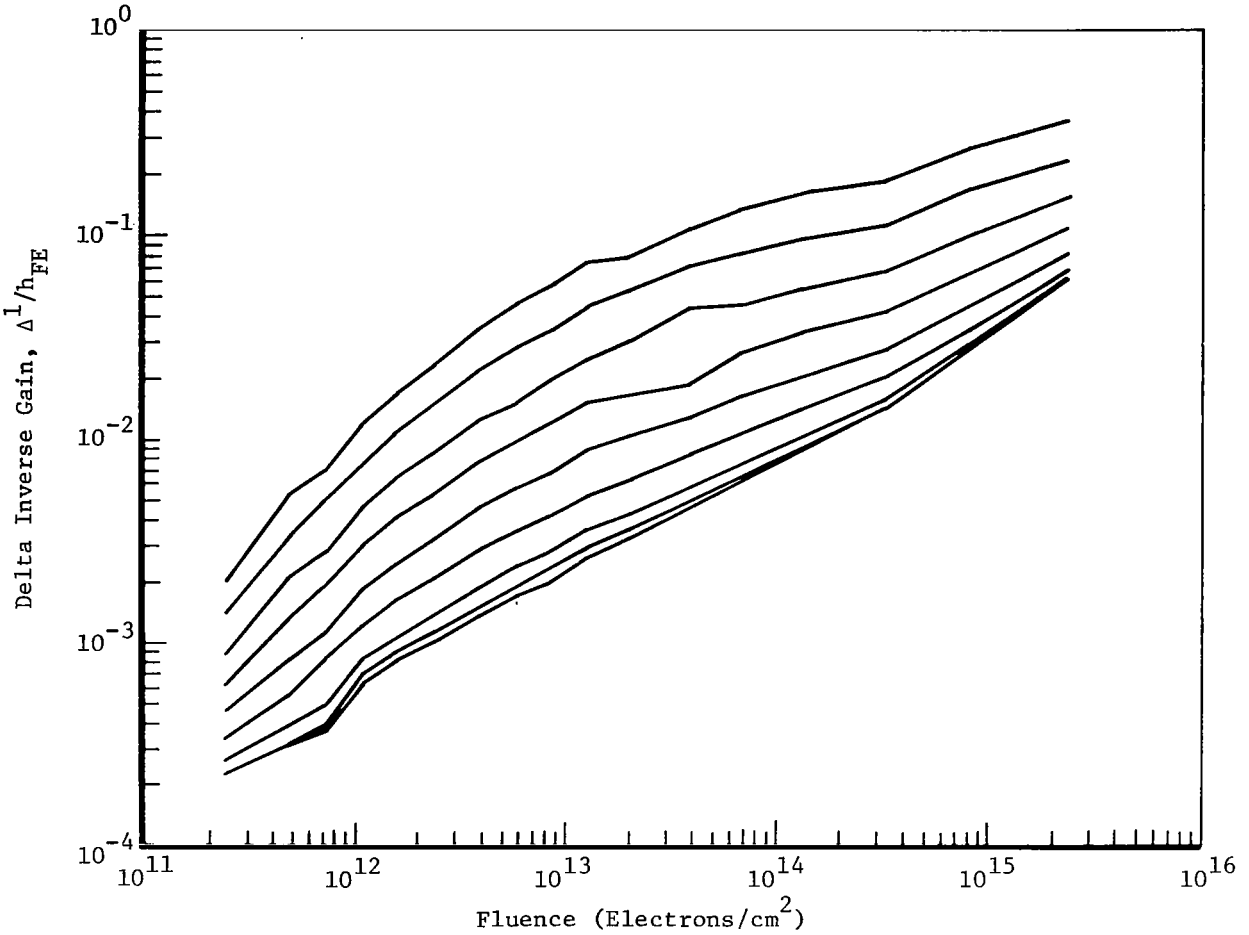

Figure 40: DEPENDENCE OF NONLINEAR DAMAGE ON INJECTION LEVEL DURING MEASUREMENTS IN PARAMETRIC FORM (FAIRCHILD 2N1613, PASSIVE, ONE BATCH; MEASUREMENT CURRENTS FROM TOP TO BOTTOM: 10-30-100-300 μa, 1-3-10-20-40 ma)

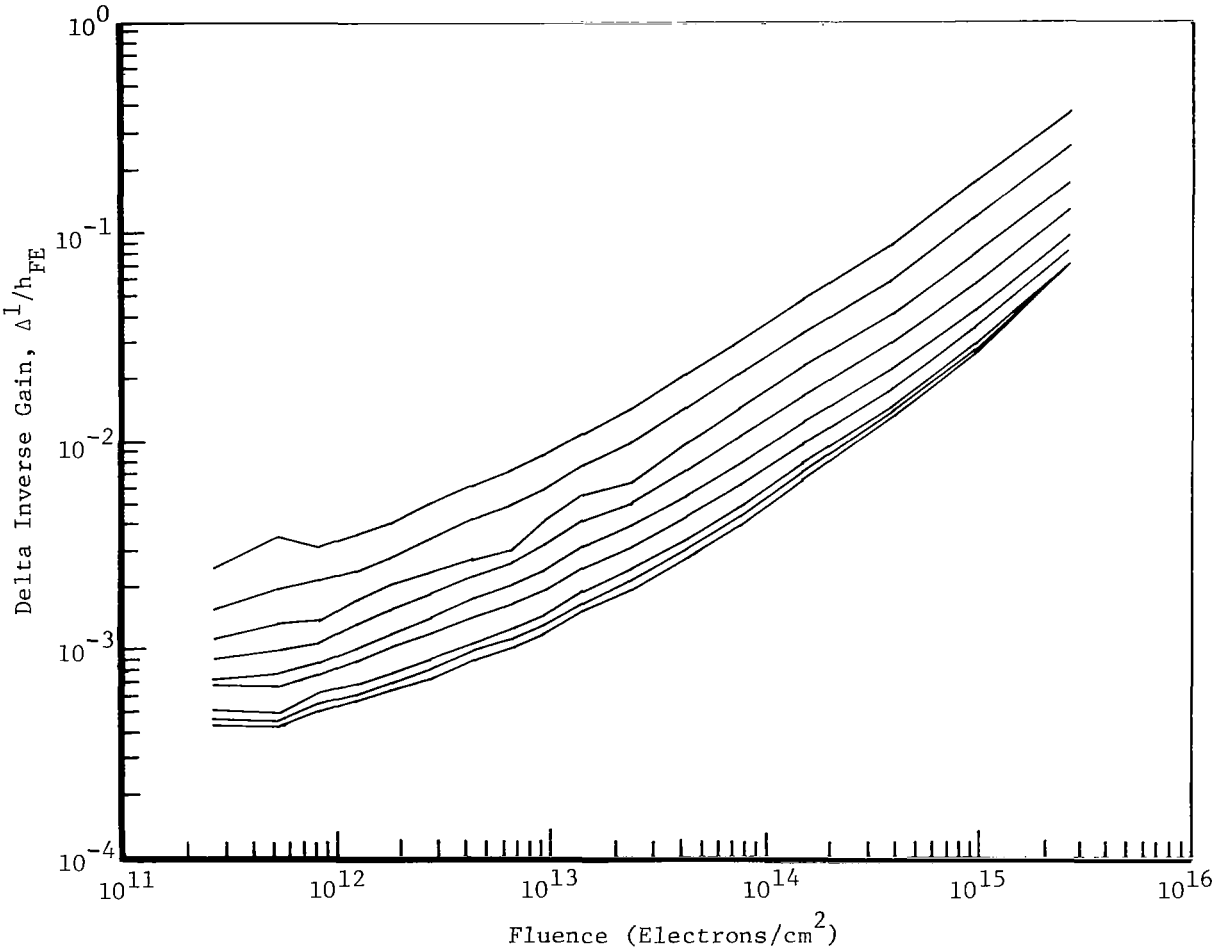

DC Gain vs Fluence, Family of Collector Currents, Type 2N1613, No. 82

Figure 41: DEPENDENCE ON NONLINEAR DAMAGE ON THE INJECTION LEVEL DURING MEASUREMENTS IN PARAMETRIC FORM (RAYTHEON 2N1613 PASSIVE, ONE BATCH; MEASUREMENT CURRENTS FROM TOP TO BOTTOM: 10-30-100-300 μa, 1-3-10-20-40 ma)

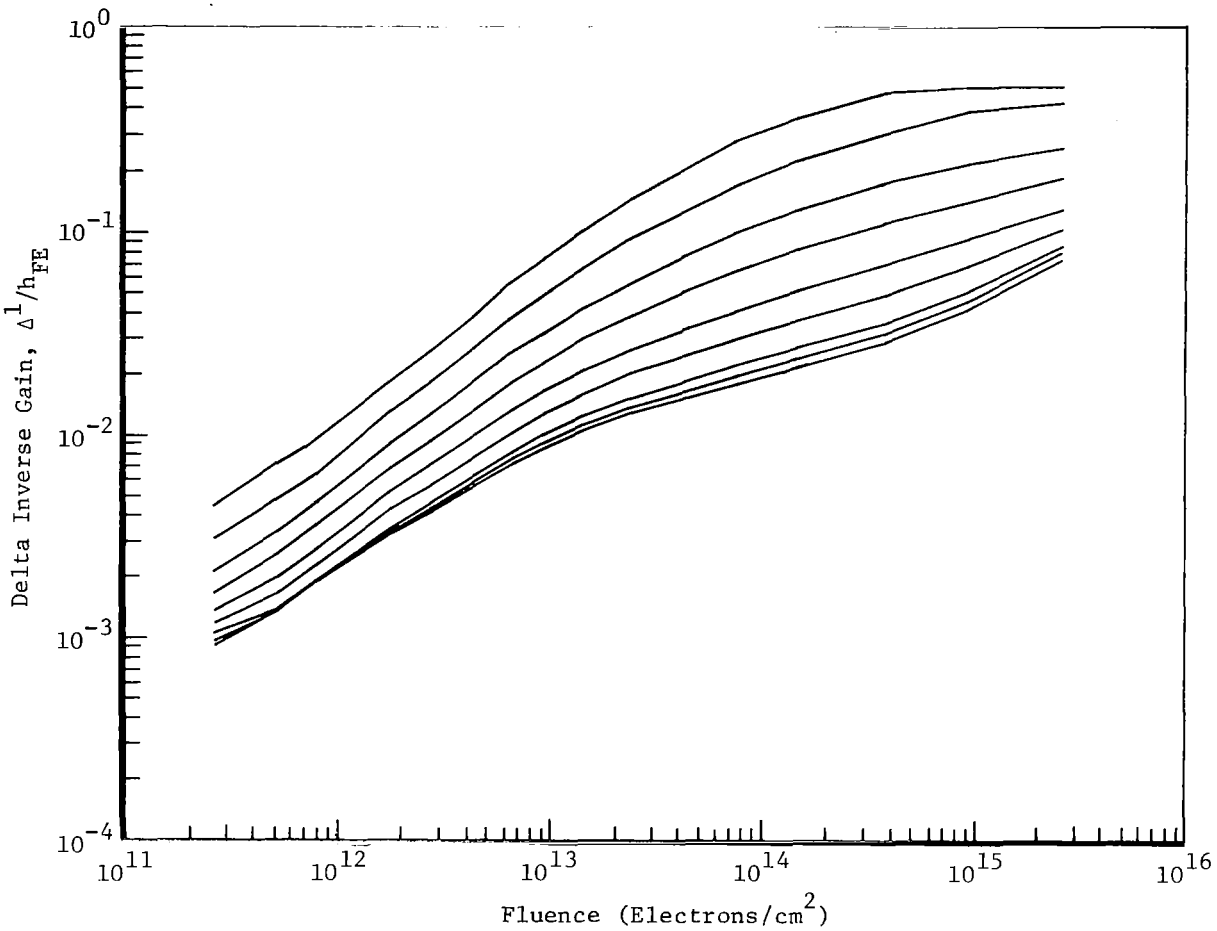

DC Gain vs Fluence, Family of Collector Currents, Type 2N1132, No. 146

Figure 42: DEPENDENCE OF NONLINEAR DAMAGE ON THE INJECTION LEVEL DURING MEASUREMENTS IN PARAMETRIC FORM (RAYTHEON 2N1132, PASSIVE, THREE BATCHES; MEASUREMENT CURRENTS FROM TOP TO BOTTOM: 10-30-100 μa; 1-3-10-20-40 ma)

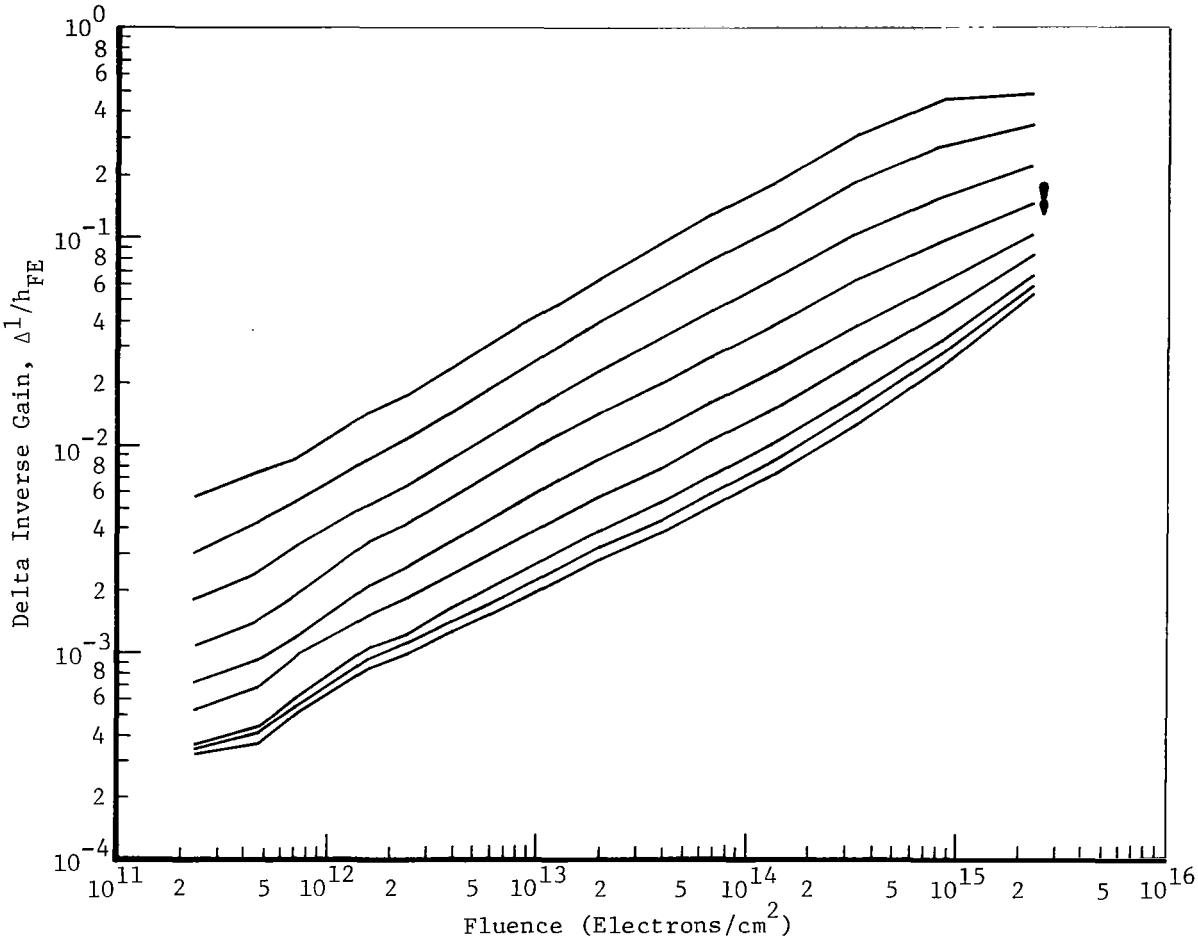

DC Gain vs Fluence, Family of Collector Currents, Type 2N1132, No. 198

Figure 43: DEPENDENCE OF NONLINEAR DAMAGE ON THE INJECTION LEVEL DURING MEASUREMENTS IN PARAMETRIC FORM (FAIRCHILD 2N1132, PASSIVE, PART OF TWO BATCHES--- SEE TEXT; MEASUREMENT CURRENTS FROM TOP TO BOTTOM: 10-30-100-300 μa, 1-3-10-20-40 ma)

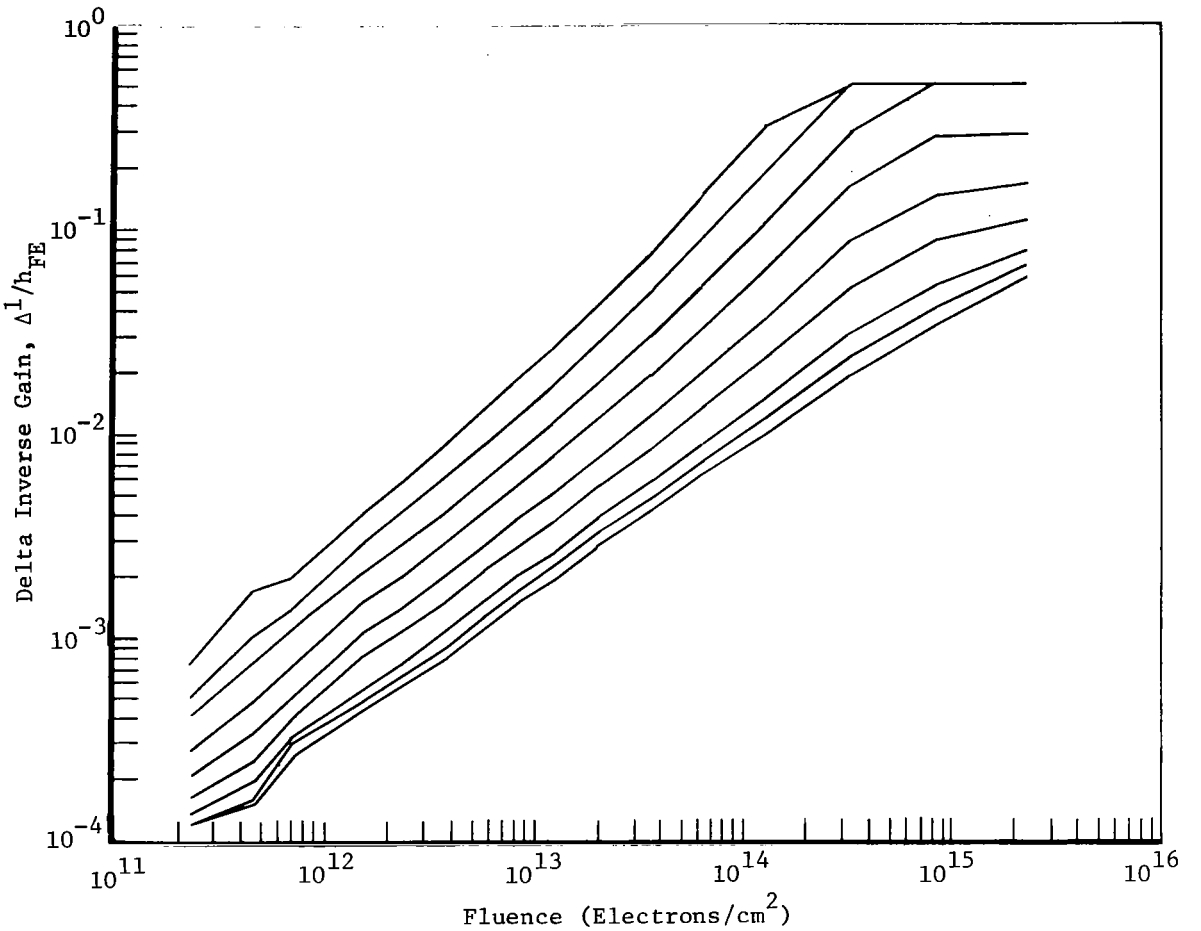

DC Gain vs Fluence, Family of Collector Currents, Type 2N1132, No. 215

Figure 44: DEPENDENCE OF NONLINEAR DAMAGE ON THE INJECTION LEVEL DURING MEASUREMENTS IN PARAMETRIC FORM (FAIRCHILD 2N1132, PASSIVE, ONE BATCH; MEASUREMENT CURRENTS FROM TOP TO BOTTOM: 10-30-100-300 μa, 1-3-10-20-40 ma)

$$\text{Dose (rads(Si))} = \frac{\text{Fluence (1 MeV electrons/cm}^2\text{)}}{4.24 \times 10^7 \left[\text{rads(Si)} \times \text{cm}^2\right]^{-1}} \qquad (11)$$

Note that the quoted fluence values on all figures are determined at the Si chip and not that incident on the transistor can. Transmission losses suffered by the electron beam when traversing the can were taken into account. In this way one is able to better compare the irradiation response of devices coming from different manufacturers and having different can thicknesses.

On a plot of the type $\Delta(1/h_{FE})$ vs. Φ for a family of I_C the "nonlinearity" of the gain degradation induced by surface effects is very apparent. The dependence of gain degradation on the measuring current (as discussed in section 2.3.1) is indicated graphically by a family of curves for nine different I_C values. These curves are almost parallel to each other and except for the very high current values, nearly equally spaced. This means, that at least for this type of a plot, measurements made at a small number of currents would be sufficient to characterize the I_C dependence and enable one to predict the curve at intermediate I_C values.

Figures 40 through 44 comprise a set showing the variety of different shapes of the $\Delta 1/h_{FE}$ vs. Φ curves, obtained under passive exposure. This representation by typical curves is possible since devices within a given date code generally had very similar curves hence one figure shown can represent the rest, and sometimes one device can represent all the devices from several date codes. Table 6 summarizes what figure is representative of devices in a given batch or batches. Of particular importance is the fact that the general shapes of the curves vary significantly (parallel, concave, convex) and consequently the slopes of $\Delta 1/h_{FE}$ vs. Φ curves are not a constant. Thus, none of the three formulations for $\Delta 1/h_{FE}$ given in Equations 8 through 10 can adequately serve as an empirical equation for nonlinear damage.

As shown in the figures, the I_C dependence of the gain degradation, however, does seem to be similar for all the devices represented, in spite of the differences in the graphical shapes of the $\Delta 1/h_{FE}$ vs. Φ plots (see section 2.3.1). This is not the case though for active NPN devices where dependence on I_C appears to also be a function of Φ. A tremendous difference in

the $\Delta 1/h_{FE}$ vs. Φ curves observed for passive and active NPN devices signify the drastic effect of the active bias during exposure in enhancing nonlinear gain degradation and will be discussed in section 2.4.

Table 6. Description of Passive Device Groups Represented in Figures 40-44

Figure No.	Device No.	Type	Manufacturer	Number of Date Codes Represented	Corresponding No. of Devices (10 dev./code)
40	2	2N1613 NPN	Fairchild	1	10
(Similar to Fig. 40 but less damage)		2N1613 NPN	Fairchild	2	20
41	82	2N1613 NPN	Raytheon	1	10
(Similar to Fig. 42 but greater spread I_C)		2N1613 NPN	Raytheon	2	20
42	146	2N1132 PNP	Raytheon	3	30
43	198	2N1132 PNP	Fairchild	2	20
(Similar to Fig. 42 less damage and more concave)		2N1132 PNP	Fairchild		
44	215	2N1132 PNP	Fairchild	1	10

A simple power law of the form of Equation 8 where $x < 1$, was shown in Figure 43. About 30 Fairchild transistors out of over 200 transistors tested did satisfy this relation. Our main conclusion is that it is difficult to make a specific statement about the shapes of the $\Delta 1/h_{FE}$ vs. Φ curves, except perhaps emphasizing their wide variety. We would like to stress this last point very strongly since it has been claimed (Ref. 5) that the buildup of nonlinear damage with fluence in dose can be approximated by

$$\Delta \frac{1}{h_{FE}} = \text{constant } \Phi^x \qquad 0 < x < 1 \qquad (12)$$

Indeed some of our passive devices did obey this simple relation. But not all of them. In fact, most of them did not. Of course, within a small dose range many of the $\Delta 1/h_{FE}$ vs. Φ curves can be approximated by a simple power law. However, this approximation fails when the whole dose range, below damage saturation, is considered. The second point is that in the proposed power law representation of the nonlinear damage with dose, the exponent, x, is claimed to be always less or at most equal to 1. In our experiments, most of the active NPN transistors exhibited faster than linear rise ($x > 1$) in part of the $\Delta 1/h_{FE}$ vs. Φ plots (see section 2.4). This means, of course, that in trying to predict nonlinear damage for such devices, in a given mission, with a less than linear power law, will badly underestimate the expected gain degradation. Due to the great importance of such prediction problems, further study would be clearly justified to clear up the discrepancies just discussed. (Interestingly enough, there appeared to be a slight voltage dependence of the exponent, x, being less than 1 or equal to 1 at the lower collector-base voltages. It is intriguing to speculate that the value of x, for whatever the power law approximation is worth, is dependent not only on device structure and processing variables, but also on the applied active biasing conditions. Note that in Reference 5 x is not assumed to be dependent on biasing, the authors simply increase the surface damage constant, k_s, to account for higher gain degradation of transistors with a reverse biased C-B junction.)

2.3.3.2 Correlation Studies and the $\Delta h_{FE}/h_{FE_i}$ Formulation

In trying to predict the response of bipolar transistors to ionizing irradiation it would be of considerable help if correlations between initial parameters and gain degradation could be found. Thus, correlation studies were conducted as summarized in Table 7. Parameters in question are listed as well as the degree of correlation expressed in terms of the Rank coefficients.

As shown in Table 7 and in Figures 45 and 46, good correlation was found only in one case, namely between the gain loss Δh_{FE} and the initial gain h_{FE_i}. Similar correlations were studied in an earlier contract with the Naval Radiological Defense Laboratory (Ref. 6). The word "correlation" is used in this report, in the context now described.

If $\sum I_{B_x}$ is defined as the sum of the extra base current components introduced by ionizing irradiation so that

$$I_b = I_{B_o} + \sum I_{B_x} \tag{13}$$

then

$$\frac{\Delta h_{FE}}{h_{FE_i}} = \frac{\sum I_{B_x}}{I_{B_o} + \sum I_{B_x}} \tag{14}$$

and

$$\Delta h_{FE} \simeq K \quad h_{FE_i} \text{ where } K \equiv \frac{1}{1 + \dfrac{I_{B_o}}{\sum I_{B_x}}} \tag{15}$$

This equation applies to each device separately and K values could be different for devices as their initial gains are different (excepting of course the very high dose case where $K \approx 1$ for all of them since $\sum I_{B_x} \gg I_{B_o}$). Interestingly enough, in certain cases K turns out to be approximately constant among devices, even at low exposures (Figures 45 and 46). In other words, the relative gain loss is approximately constant among devices regardless of the

Table 7. RANK CORRELATION COEFFICIENTS

Initial Parameter	h_{FE_i} (10 v, 0.01 ma)				$1/I_{EBO}$ ($\frac{6}{4}$ volts)			
Final Parameter	h_{FE_f}	Δh_{FE}	$\Delta h_{FE}/h_{FE_i}$	$\Delta 1/h_{FE}$	h_{FE_f}	Δh_{FE}	$\Delta h_{FE}/h_{FE_i}$	$\Delta 1/h_{FE}$
NPN								
a) NPN Fairchild, unbiased	.82	.95	.46	-.63	.03	.22	.27	.09
b) NPN Fairchild, biased	.21	.89	.22	-.11	.12	.23	.00	-.07
c) NPN Raytheon, unbiased	.44	.47	.07	-.20	.03	.20	.16	.06
PNP								
d) PNP Fairchild, unbiased	.77	.83	.07	-.36	-.42	-.45	-.06	-.16
e) PNP Raytheon, biased	.52	.81	.01	-.33	.34	.02	-.26	-.30
f) PNP Raytheon, unbiased	.44	.92	.42	.05	.37	.52	.29	.08

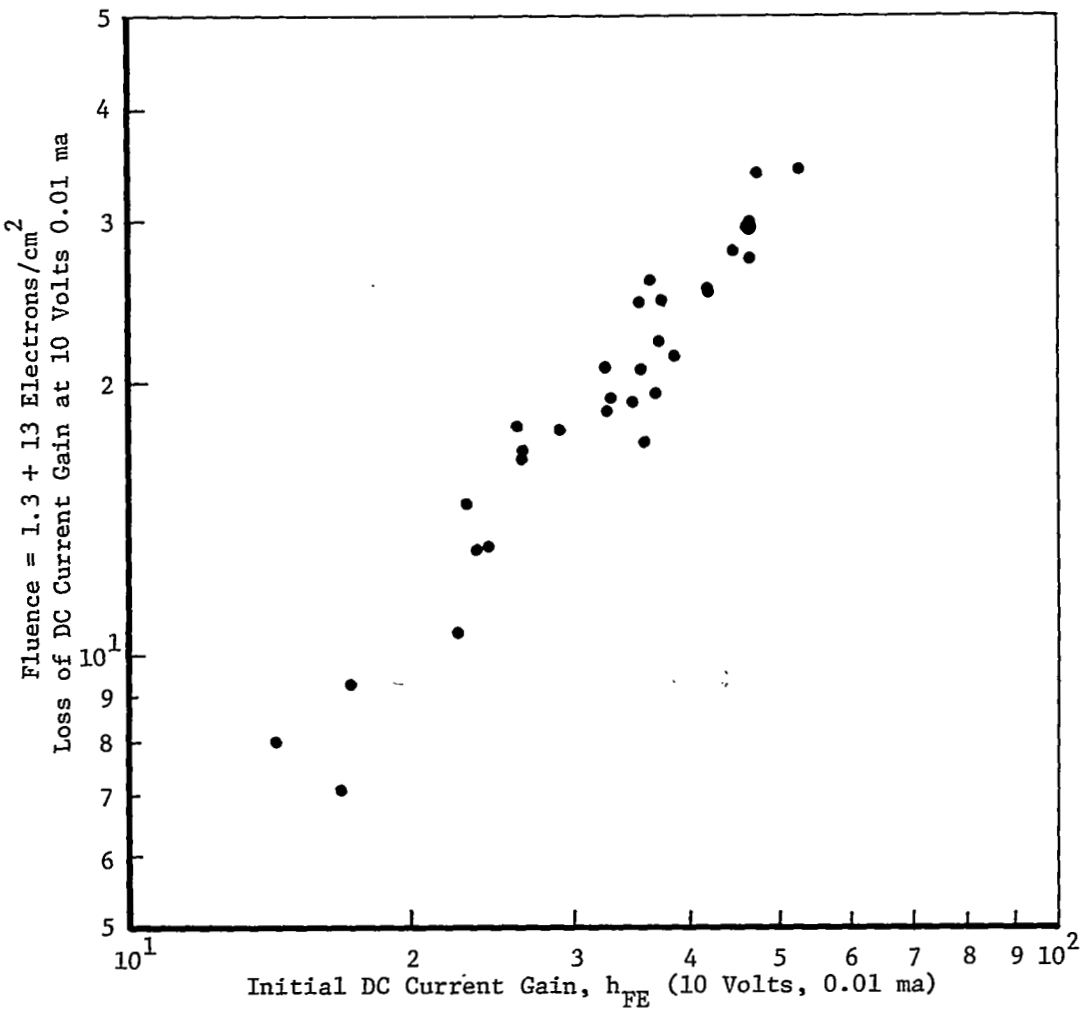

Type 2N1613, Fairchild Transistors
No Bias Applied
Rank Coefficient of Correlation = 0.95

Figure 45: CORRELATION OF GAIN LOSS WITH INITIAL GAIN (2N1613)

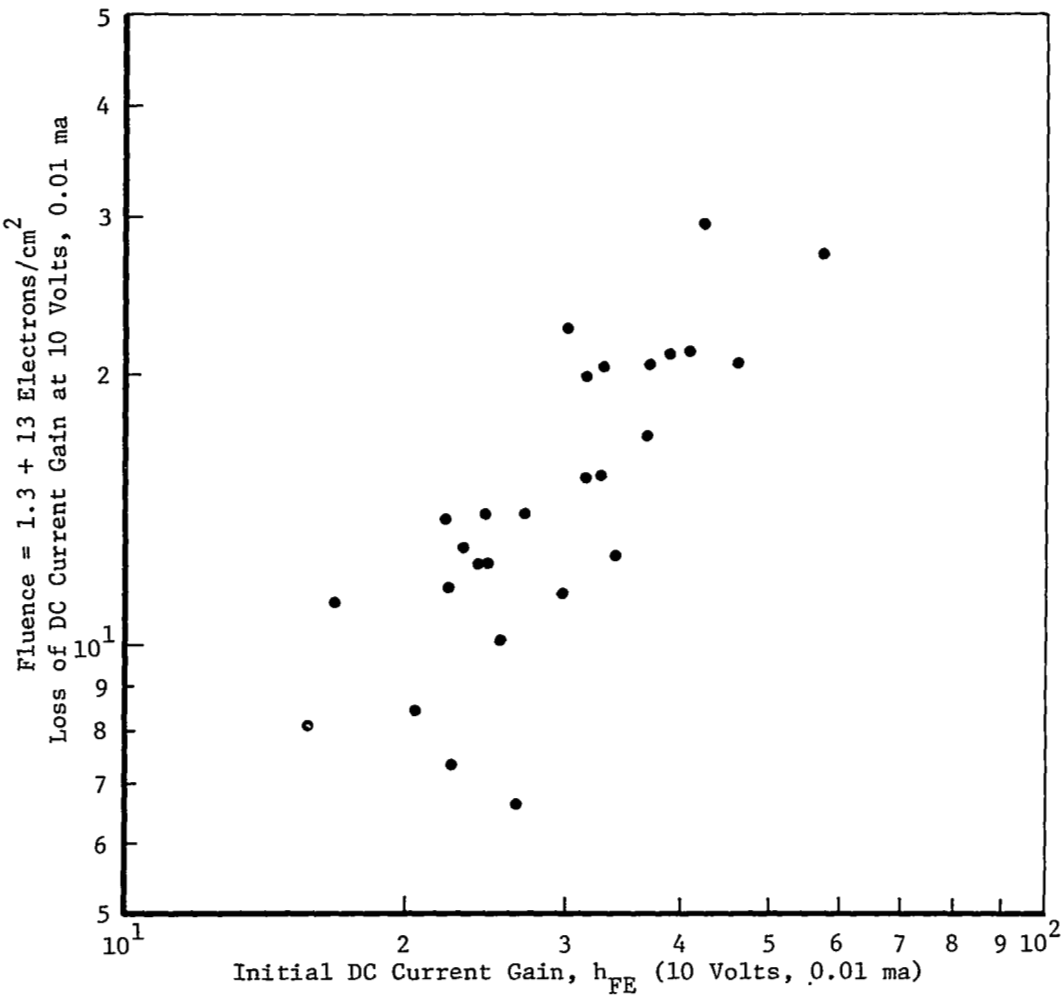

Type 2N1132, Fairchild Transistors
No Bias Applied
Rank Coefficient of Correlation = 0.83

Figure 46: CORRELATION OF GAIN LOSS WITH INITIAL GAIN (2N1132)

initial gains. This last sentence seems to imply that a "normalization" of the gain degradation of the different devices takes place when the results are compared in terms of $\Delta h_{FE}/h_{FE_i}$. Whether this is indeed the case, is still subject to discussion.

Certainly $\Delta 1/h_{FE}$ appears to be a good functional form for gain loss for some comparison purposes since it is equivalent to $\sum I_{B_x}/I_C$, and $\sum I_{B_x}$ is a direct measure of radiation sensitivity of the device. However, when the devices to be compared have different geometries, e.g., coming from separate manufacturers, it would appear that the quantity $\sum I_{B_x}/I_C$ ought to be modified in order to normalize the devices to the same geometrical dimensions. It appears that an expression like $\sum I_{B_x}/I_{B_o}$ would be appropriate since then the different geometrical factors should drop out. (E.g., the lengths of the emitter-base junction perimeters. The previous statement is strictly correct if both I_{B_o} and $\sum I_{B_x}$ are dominated by the same base current component. This is, however, usually the case in practice, because of the dominant role of the surface component in nonlinear damage.) Actually any expression involving $\sum I_{B_x}/I_{B_o}$ would be equally good, e.g., the relative gain remaining

$$\frac{\Delta h_{FE}}{h_{FE_i}} = \frac{1}{1 + \frac{\sum I_{b_x}}{I_{b_o}}} \qquad (16)$$

Note however, that it is just as wrong not to normalize against certain pertinent factors as to normalize against others which have nothing to do with the resultant gain degradation. Therefore we propose that if there is no correlation between I_{B_o} and $\sum I_{B_x}$ (i.e., between h_{FE_i} and $\Delta 1/h_{FE}$), then the comparison of presumably identical devices should be done in terms of $\Delta 1/h_{FE}$, whereas the comparison of others with known geometrical differences should be done in terms of $\Delta h_{FE}/h_{FE_i}$. On the other hand, if correlation between I_{B_o} and $\sum I_{B_x}$ do exist then the comparison of devices in terms of $\Delta h_{FE}/h_{FE_i}$ should always be superior to that in terms of $\Delta 1/h_{FE}$. An example of such correlations is shown in Figure 47 for a moderate exposure of 5×10^4 R. Furthermore in many of our experiments the quantity $\Delta h_{FE}/h_{FE_i}$ seemed to give a better normalization of the gain degradation. Data on statistical spread from section 2.3.2 illustrated advantages of using the form $\Delta h_{FE}/h_{FE_o}$ in order to reduce the standard deviation

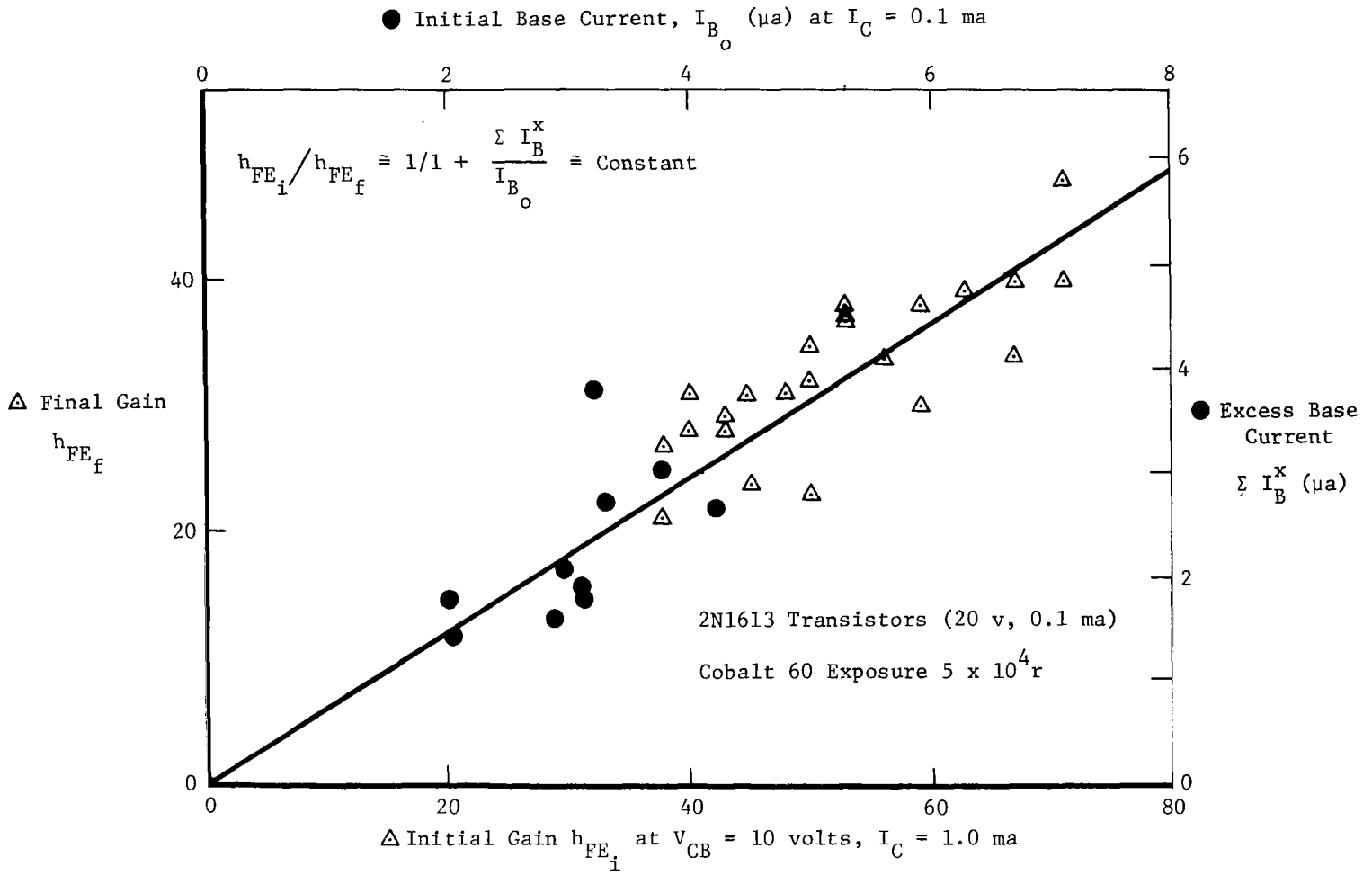

Figure 47: CORRELATION OF EXCESS BASE CURRENT WITH INITIAL BASE CURRENT

between transistor groups of the same or different date codes. Needless to say the problem merits further consideration. In particular, a thorough experimental study of correlation problems is sorely needed.

2.3.3.3 Empirical Formulation Equations

An empirical formulation of relative gain loss was developed to fit experimental results of the dependence on total absorbed dose. Relative gain loss was chosen on the basis of: 1) observed correlations between I_{B_o} and $\sum I_{B_x}$; 2) normalization of statistical spread in the sensitivity of transistors from the same or different batches; and 3) the desirability for using a form convenient for design engineers. Plots of the dependence of $\Delta h_{FE}/h_{FE_i}$ on fluence were shown in Figures 26, 27, 32, and 33. Relative gain loss by its nature as a fractional change must vary from 0 for no damage to 1 as a maximum of damage. Thus $\Delta h_{FE}/h_{FE_i}$ plotted against dose on a log plot must have the general form of a hyperbolic tangent which approaches 0 and 1 asymptotically at 0 and ∞ exposure respectively. Curve fitting to a hyperbolic tangent revealed that Equation 17 represented a reasonably consistent fit of the data available.

$$\Delta h_{FE}/h_{FE_i} = \tanh a\, D^m \tag{17}$$

Figure 48 shows how this functional relation fits the mean values of data on 30 passive 2N1132 Raytheon transistors measured at 10 ua collector current. In general all of the other transistor groups tested fitted Equation 17 with a power law dependence on dose given by $m \cong 0.4$

$$\Delta h_{FE}/h_{FE_i} \cong \tanh \left[K\, D\right]^{0.4} \tag{18}$$

Not all passive transistor types saturated at maximum relative gain losses when $\Delta h_{FE}/h_{FE_i} \cong 1$. Thus a saturation factor, f_s, was used to multiple Equation 18.

$$\Delta h_{FE}/h_{FE_i} \cong f_s \tanh \left[K\, D\right]^{0.4} = f_s \tanh K'\, D^{0.4} \tag{19}$$

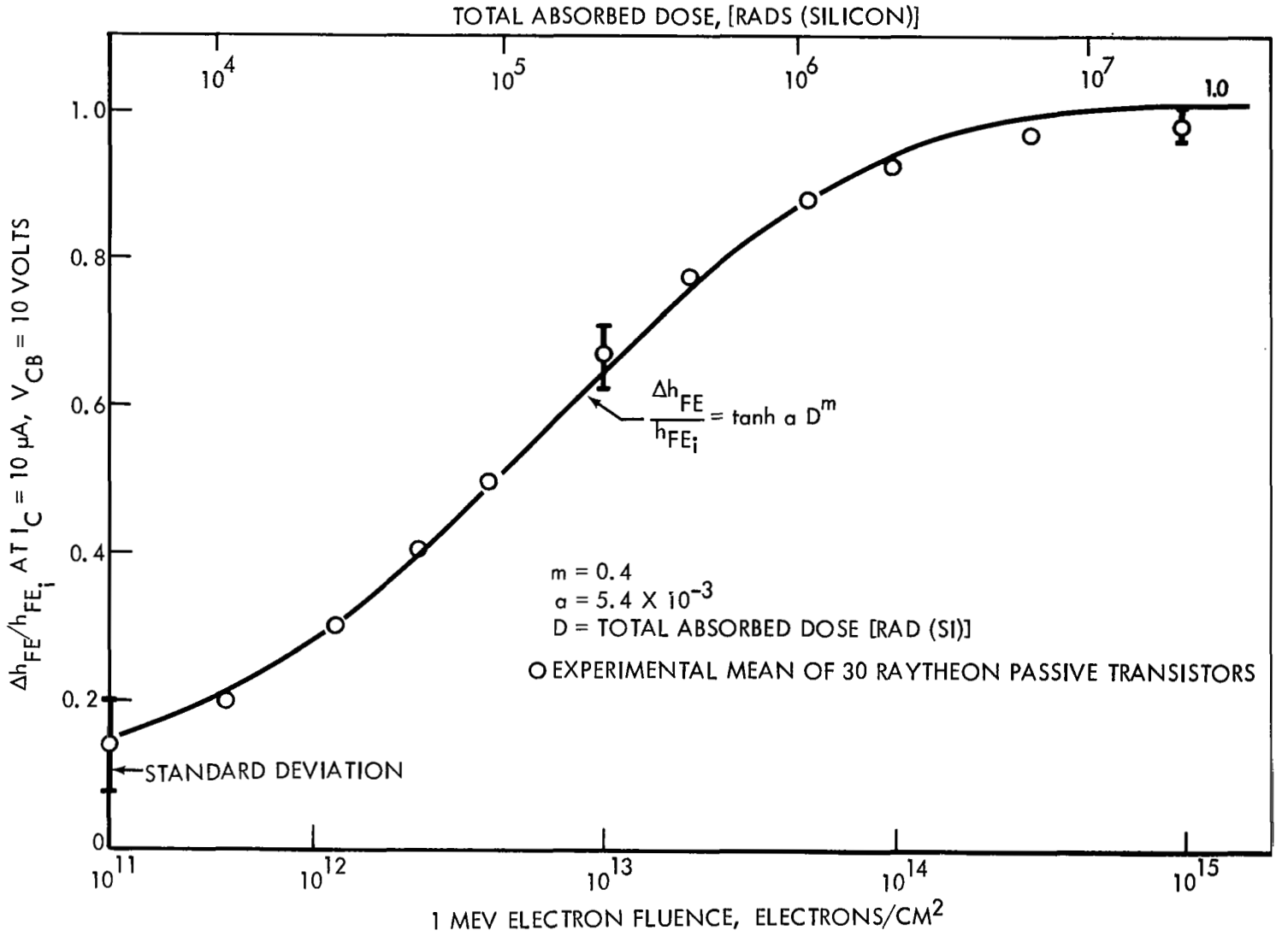

Figure 48. Empirical Formulation for Nonlinear Damage (2N1132)

Table 8. Damage Constants for a Hyperbolic Tangent Empirical Fit for Mean Relative Gain Loss (at I_C = 10 μamp)

Type	Manufacturer	f_s	K $(\text{rad Si})^{-1}$	K' $(\text{rad Si})^{-0.4}$
2N1613	Fairchild	0.88	1.8×10^{-6}	5×10^{-3}
2N1613	Raytheon	0.9	1.0×10^{-6}	4×10^{-3}
2N1132	Fairchild	0.9	1.0×10^{-6}	4×10^{-3}
2N1132	Raytheon	1.0	2.1×10^{-6}	5.4×10^{-3}

An example of a fit for a transistor condition where damage saturates at f_s = 0.75 is shown in Figure 49. That data was plotted for a collector current of 0.1 ma. The dependence of damage on collector current was discussed in section 2.3.1. Since only two transistor types were studied for empirical fitting no profound generalization of the applicability of Equation 19 to other device types is claimed at this time. However, at least variations of this form of equation look promising for expressing the nonlinear damage buildup with dose.

2.3.4 Ionization Equivalence for Passive Transistors

The apparent radiation equivalence for nonlinear damage based on total absorbed dose from the ionization phenomenon was described in early papers (Ref. 7 and 8) and the final report of phase I work under contract NAS5-9578 (Ref. 2). That data included results from X-ray, gamma ray, electron, and preliminary proton tests. Those findings indicated an independence of nonlinear damage on particle type or energy and only a dependence on the total dose absorbed at the transistor surface. The phase II test results verify in part those earlier findings . Figure 50 shows a comparison between damage to passive 2N1613 transistors caused by Cobalt-60 gamma ray exposure (Ref. 9) and phase II 1 MeV electron exposure. Collector current levels

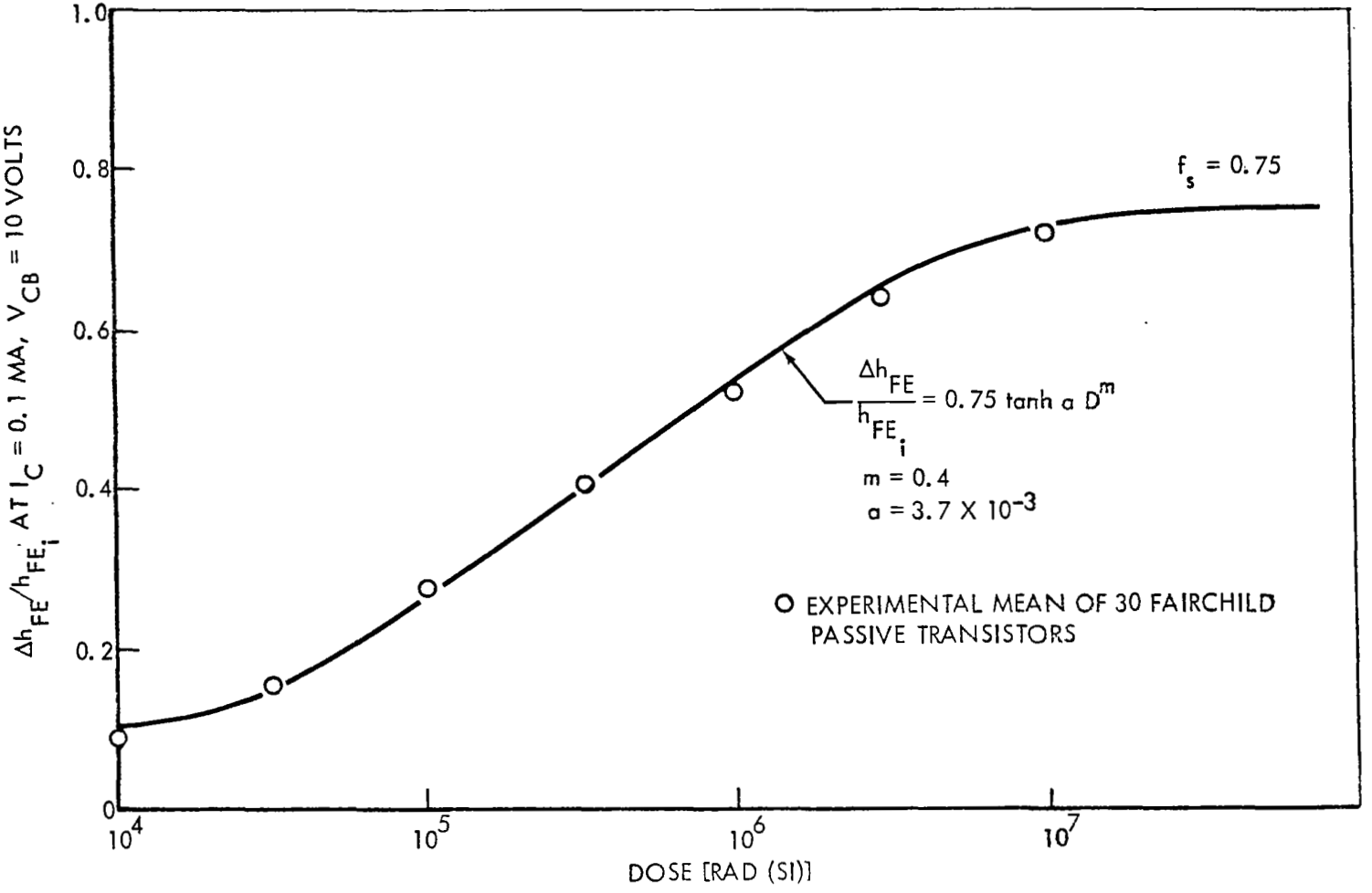

Figure 49. Empirical Formulation for 2N1613 at I_C = 0.1 ma

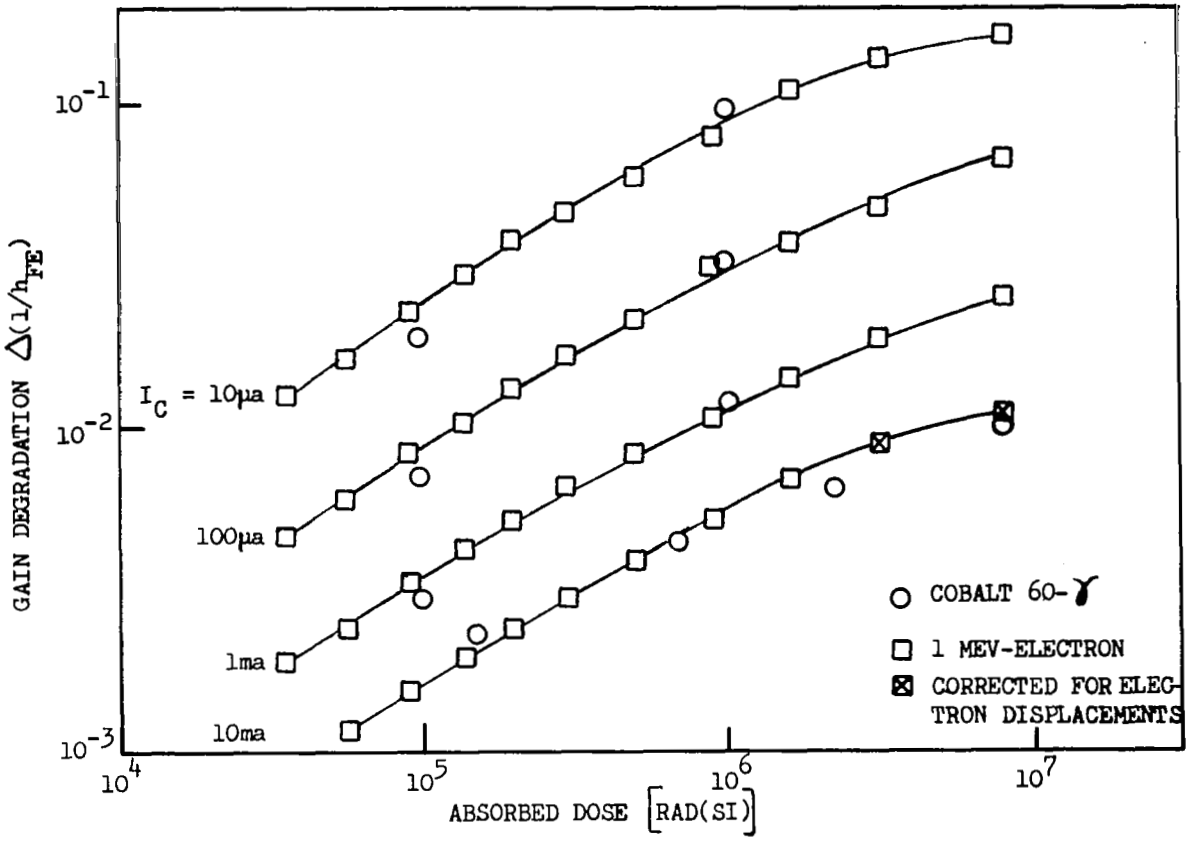

Figure 50. Nonlinear Damage of Passive 2N1613 Transistors

shown are at 10 μa, 0.1, 1.0, and 10 ma. Figure 51 illustrates comparable damage to passive pnp 2N1132 transistors for the present 1 MeV electron and 15 MeV proton tests.

An anomalous exception to the total dose equivalence concept for passive transistors was observed for 15 MeV proton damage to npn 2N1613 transistors. In that case, described in detail in section 2.5, more severe damage was observed at lower total dose for protons than for any other type of radiation and saturation of the damage was not evident except at very high exposures. The ionization equivalence concept does not appear to hold for active transistors either as described in more detail in section 2.4.

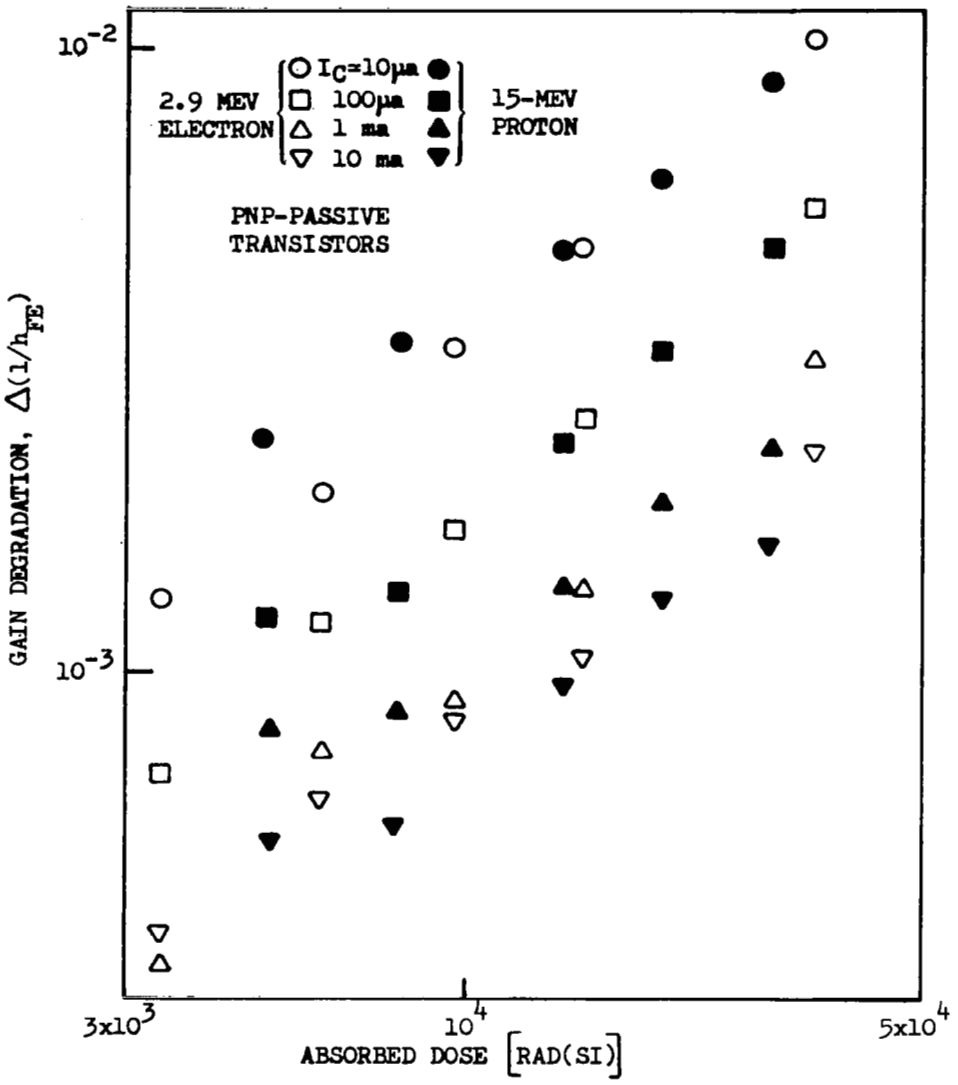

Figure 51. Comparison of Electron and Proton Ionization of 2N1132 Transistors

2.3.5 Exploration of the Source of Nonlinear Damage

At this point reference to Appendix I would be appropriate in order to review the theoretical background (References 10 - 18) for our further studies on the source of nonlinear damage. Most of the data discussed in this section was generated from the special measurements discussed in Section 2.1.3.2 and listed in Table 3. Damage to transistors exposed both passively and under active bias during exposure will be considered in this section. For an overall treatment of active bias damage see Section 2.4. Typical examples on the interpretation of these measurements are given below for selected devices where each device is a representative of a small group. The devices discussed are good representatives of the four main groups of transistors used in our experiment namely, the passive and active NPN's and PNP's. At least, the measurements which were common to all transistors (h_{FE}, I_{EBO}, I_{CBO}) seem to bear this assumption out. Consequently the conclusions drawn should essentially apply to the particular group containing the device in question.

The measurements will be interpreted on the basis of the theoretical discussion given in Appendix I since the data are analyzed in terms of the effect of the charge accumulation and of the creation of the new interface states on the Si surface where possible. Since the effect of the charge accumulation is different in the presence or absence of inversion, we will always start the discussion of the figures with the C_{BE} vs. fluence measurements. These curves can tell us immediately whether or not inversion has taken place. Conclusions drawn then can be substantiated by other measurements.

In discussing parameters such as I_B, I_R, h_{FE}, which are affected by both charge accumulation and the creation of new interface states, we have to be content with considering only the combined effects of these two phenomenon since on the basis of our measurements their effects cannot be separated. One can nevertheless draw some indirect conclusions about their relative importance under certain conditions. Gain degradation in this section will be expressed in terms of $\Delta 1/h_{FE}$ vs. Φ curves. The pros and cons of different methods of presenting gain degradation data was discussed in Section 2.3.3.

NPN-unbiased during irradiation: As discussed (Appen. I) it is the p type base which is affected primarily by the positive charge accumulation and the new interface states, thus leads to transistor degradation in an NPN structure.

The C_{BE} and C_{BC} vs. Φ curves are shown in Figure 52 for Fairchild 2N1613, device #1. For passive 2N1613 transistors there was no indication of any inversion of the base surface due to the accumulated charge since C_{BE} and C_{BC} remained approximately constant. The absence of inversion is also supported by the I_B vs. V_{BE} curves of the type shown in Figure 53 where the slopes yield n values ≤ 1.9 (n comes from Equation A7 of Appendix I).

I_B vs. Φ (Figure 54), or what is essentially the same, $\Delta 1/h_{FE}$ vs. Φ (Figure 55) and the I_{EBO} vs. Φ , I_{CBO} vs. Φ curves (Figure 56) can be qualitatively understood by assuming an increased surface recombination velocity due to irradiation on the base surface, in the vicinity of the junctions. This assumption as the reason for increased I_B, is in accordance with the n values determined from Figure 53, where $1.4 \leq n \leq 1.9$. There seems to be some discrepancy, however, if we also assume that I_{EBO} was likewise dominated by the surface generation current. Namely, such a current component is presumed to be approximately independent of voltage (Ref. 15). In the I_{EBO} vs. reverse voltage, V_R curves of Figure 57 this is true only above 0.2 volts. Essentially similar arguments apply for the I_{CBO} vs. V_R curves of Figure 58.

NPN - biased during irradiation: (Bias: V_{CB} = 10 V, I_E = 10 ma).

Just as in the passive NPN case, it is the surface condition of the base, affected by the positive charge accumulation and the new interface states which determines the transistor degradation. However, due to the active bias on the transistor during exposure, the amount of charge accumulation can be significantly increased due to the fringing electric fields influencing charge migrations. It is not yet clear how the creation of the new interface states is affected by biases across the junctions. Although it is claimed to be independent of the electric field (Ref. 14), it could conceivably be injection dependent. All in all, the combined effect of the charge accumulation and of the new interface states on active NPN transistors

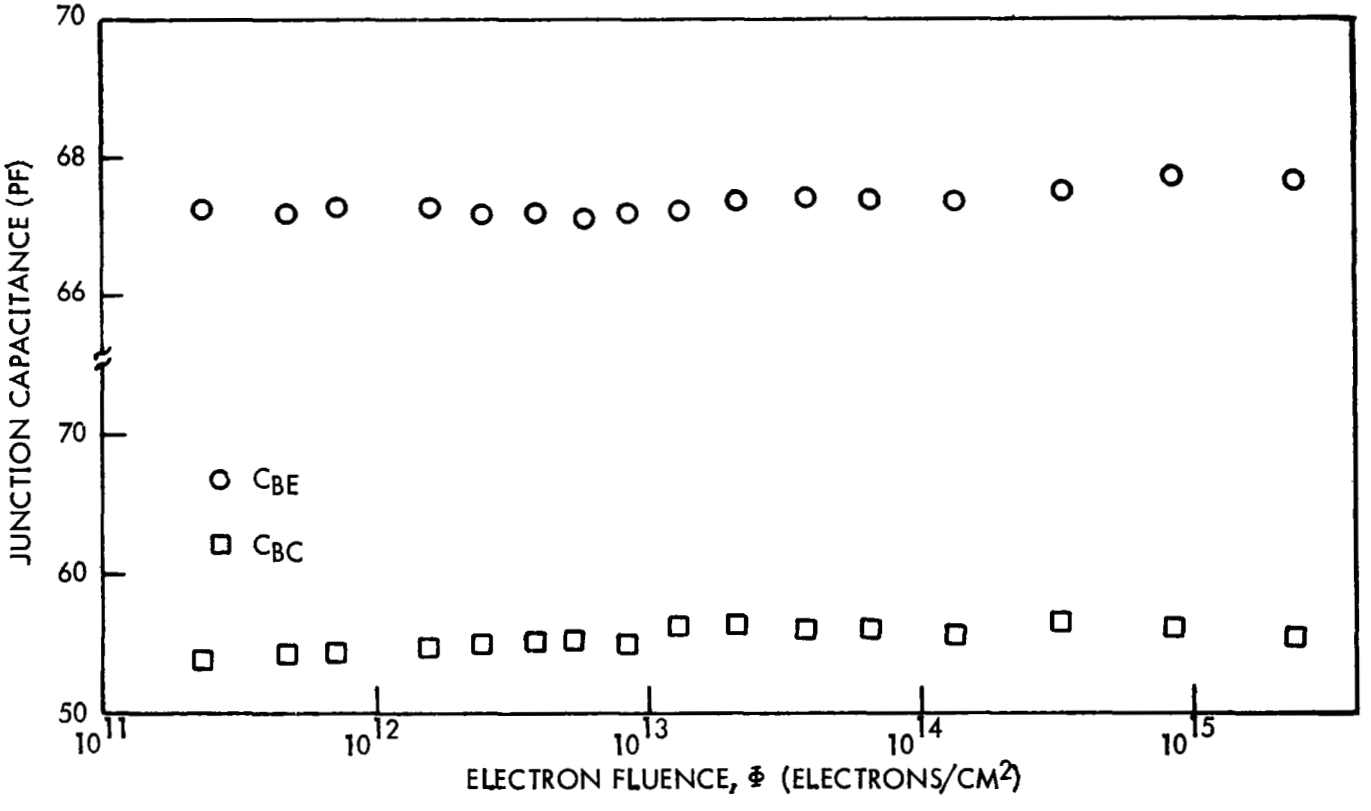

Figure 52. C_{BE} and C_{BC}(Zero Bias) Versus Fluence (Fairchild 2N1613, Passive During Irradiation)

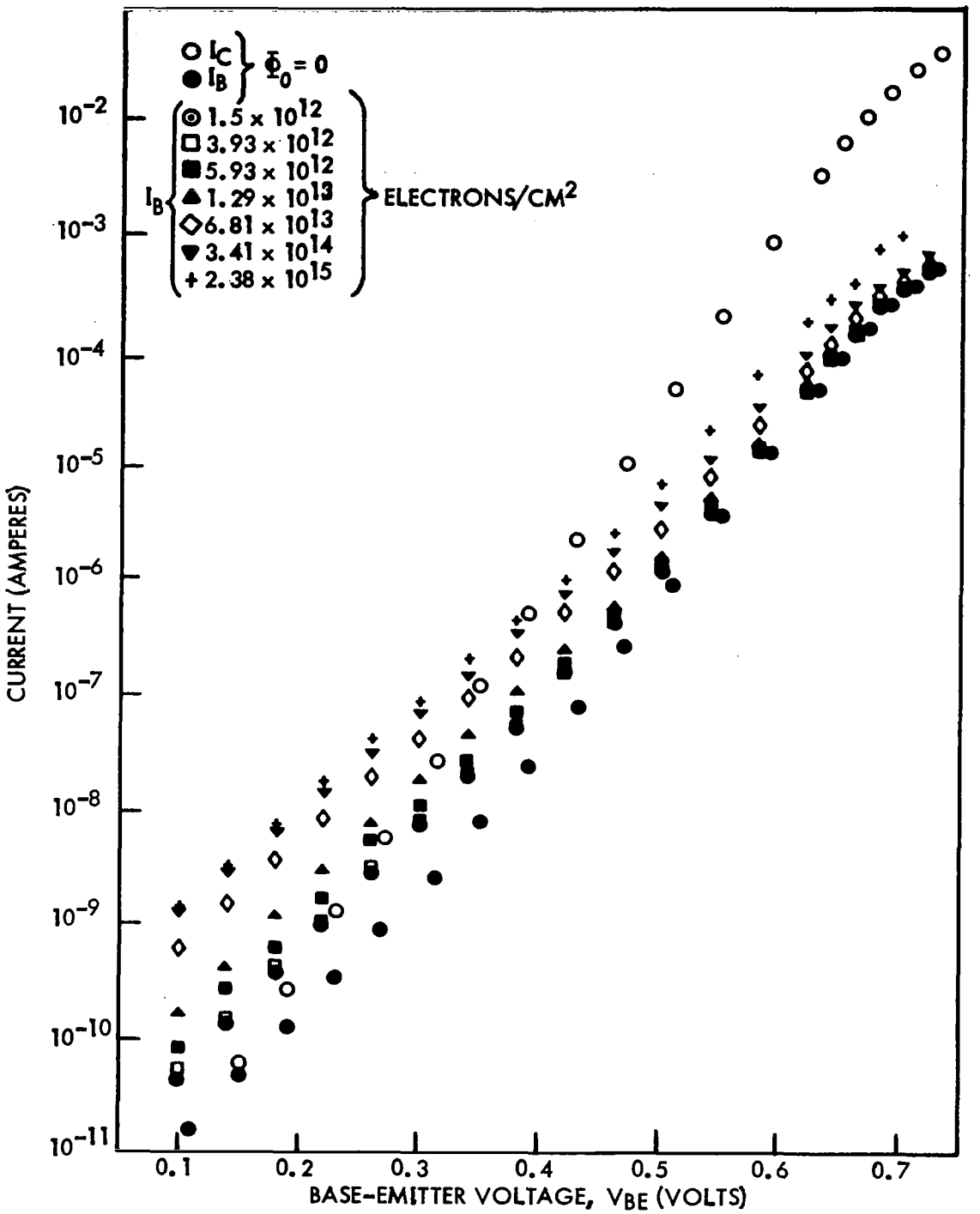

Figure 53. I_B and I_C Versus V_{BE} Curves, Taken at Different Stages During Exposure (Fairchild 2N1613, Passive During Irradiation)

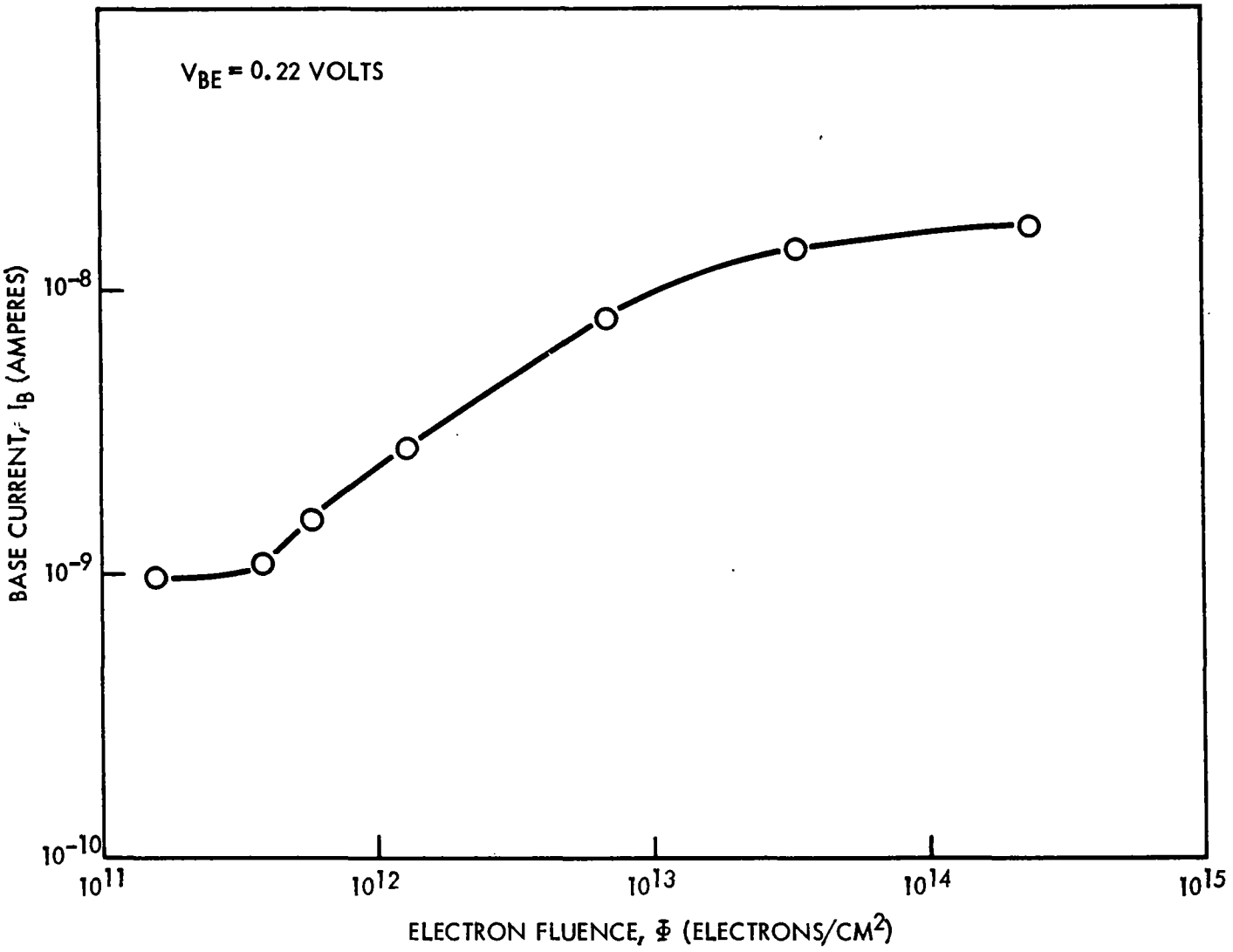

Figure 54 I_B Versus Fluence (Fairchild 2N1613, Passive During Irradiation)

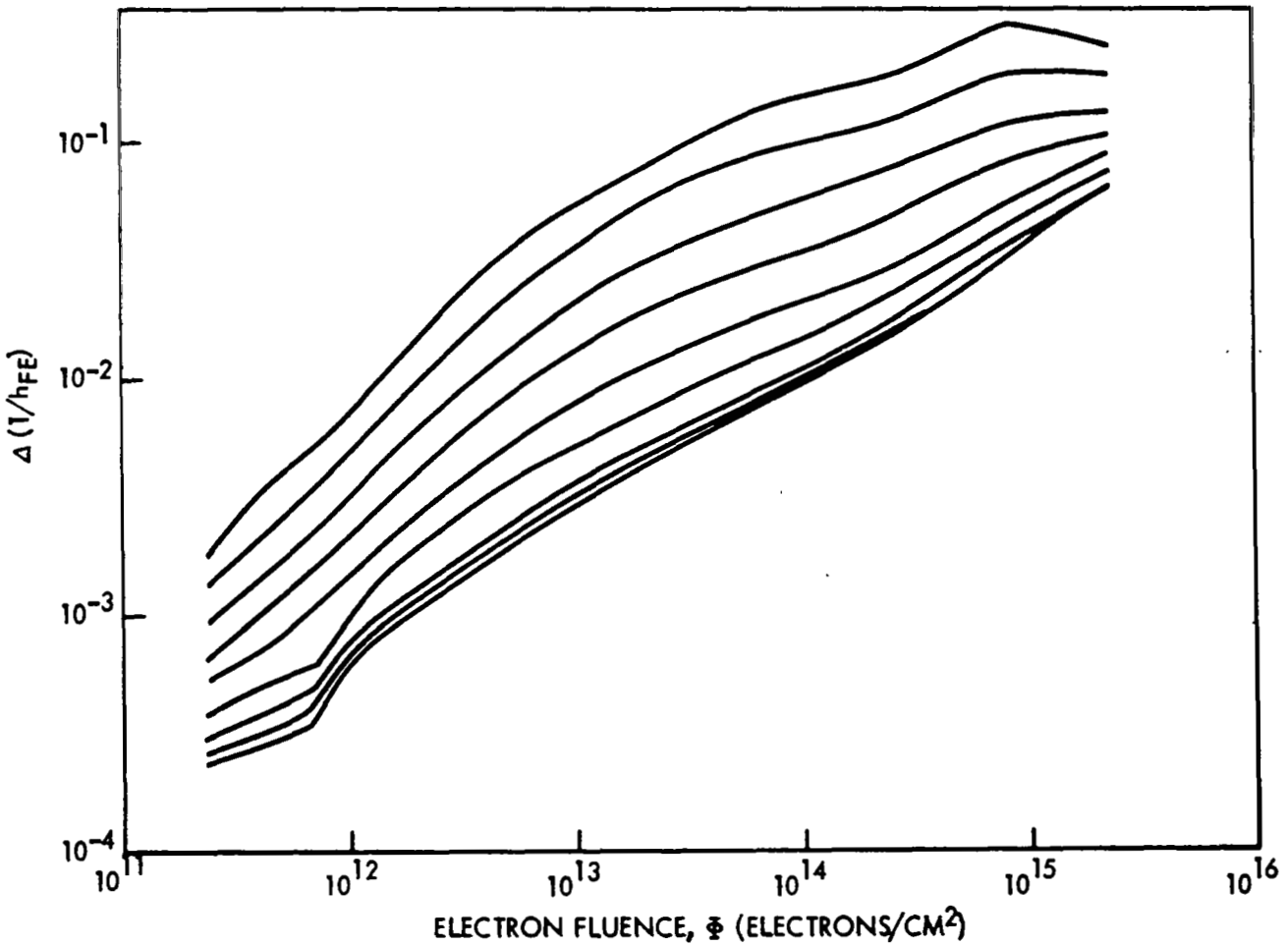

Figure 55. $\Delta (1/h_{FE})$ Versus Fluence (Fairchild 2N1613, Passive During Irradiation) (Measurement Current, I_E, From Top to Bottom: 10μa, 30μa, 100μa, 300μa 1 ma, 3 ma, 10 ma, 20 ma, 40 ma)

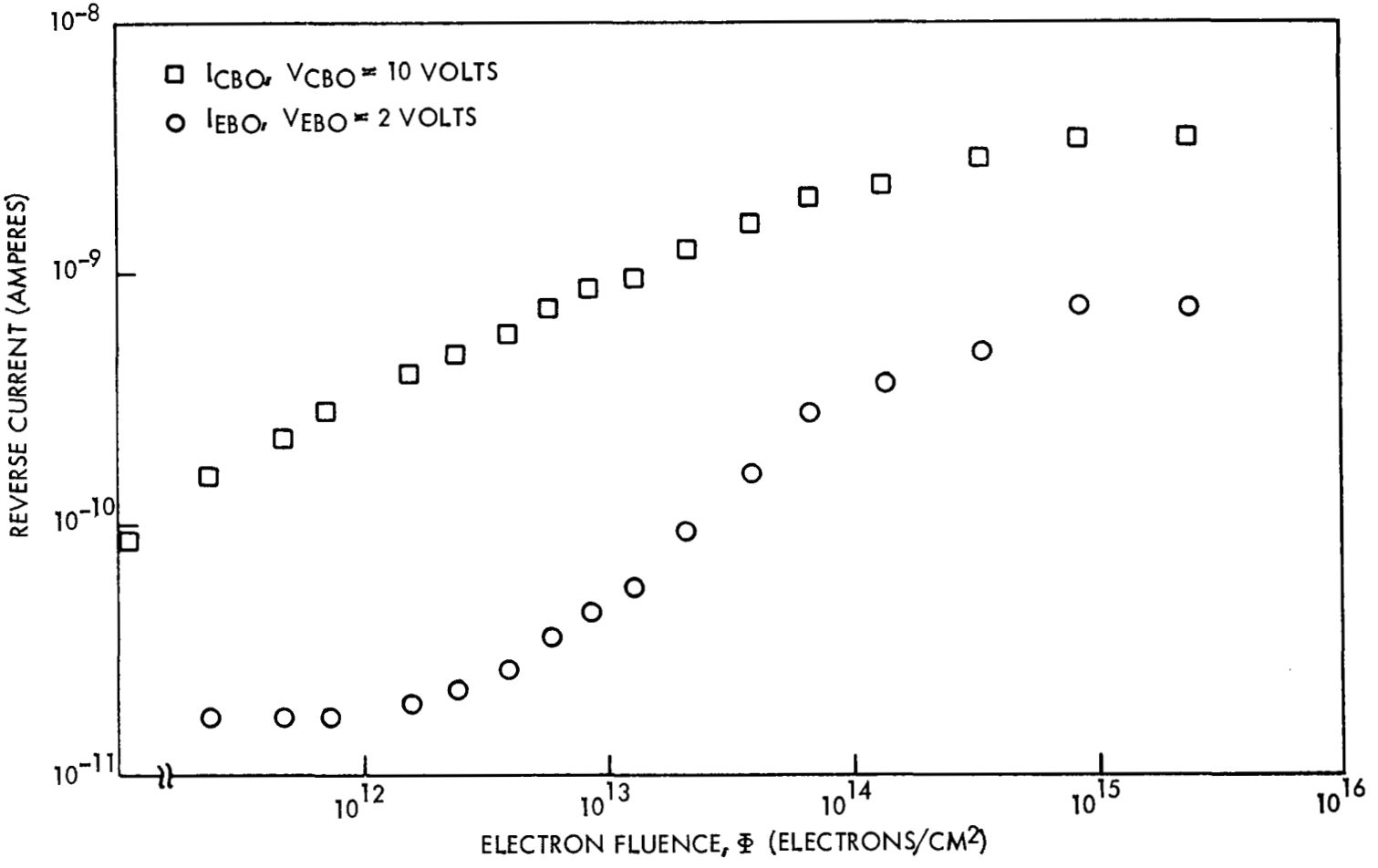

Figure 56. I_{EBO} and I_{CBO} Versus Fluence (Fairchild 2N1613, Passive During Irradiation)

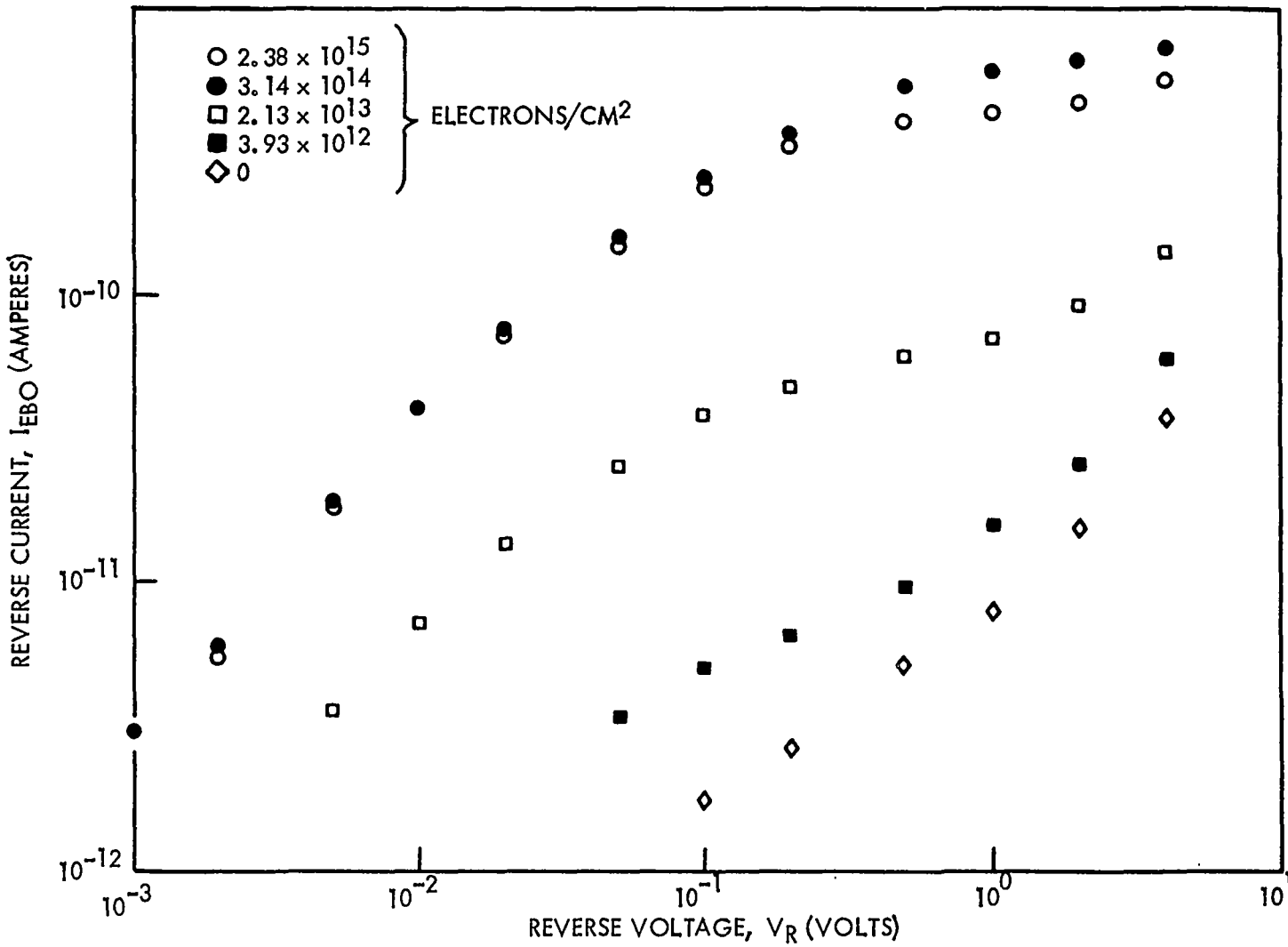

Figure 57 I_{EBO} Versus Reverse Voltage, V_R, Curves, Taken at Different Stages During Exposure (Fairchild 2N1613, Passive During Irradiation)

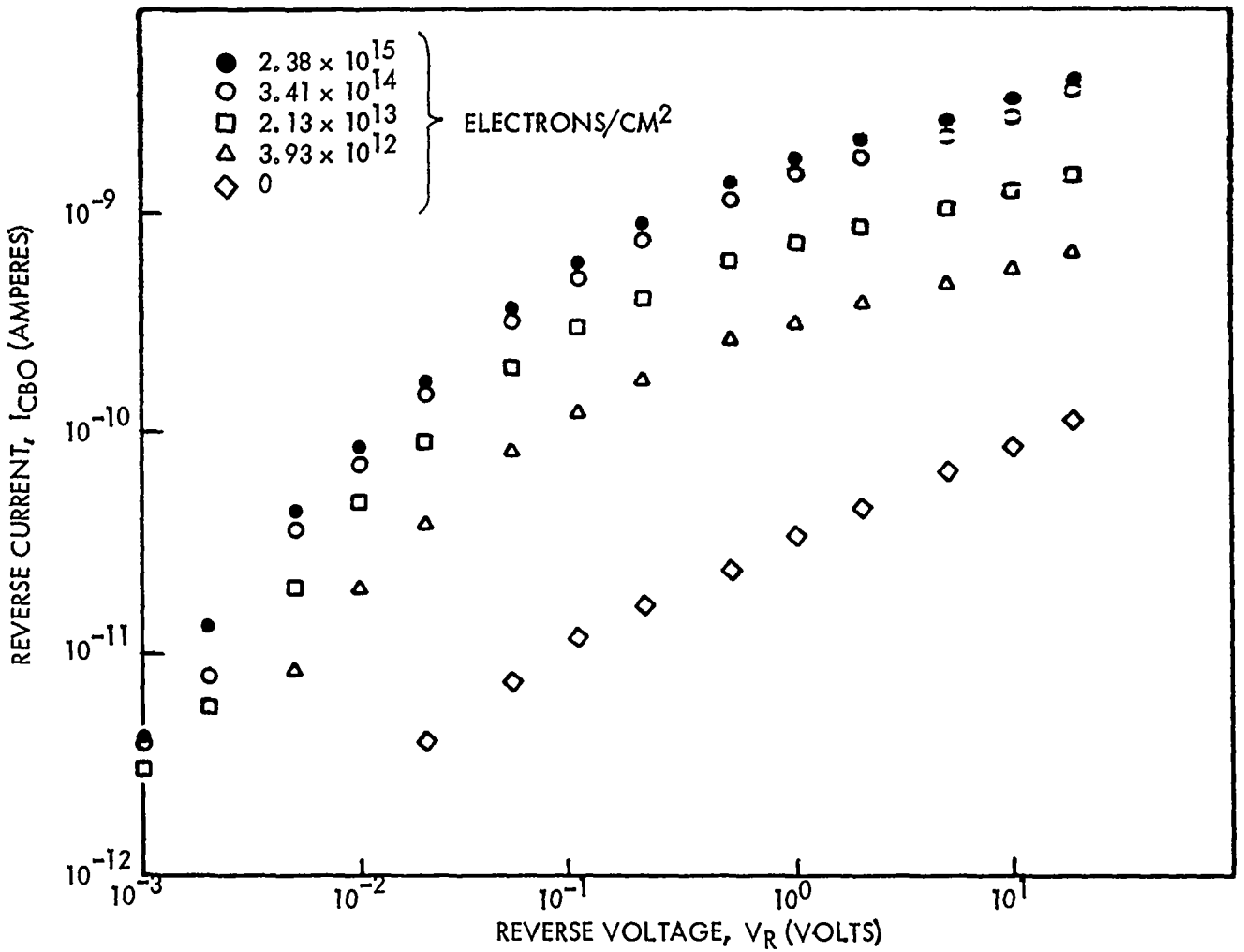

Figure 58. I_{CBO} Versus V_R Curves, Taken at Different Stages During Exposure (Fairchild 2N1613, Passive During Irradiation)

is drastic indeed. E.g., the $\Delta 1/h_{FE}$ vs. Φ figures will exhibit a significantly faster gain degradation with exposure than those for the respective passive devices. Also the formation of an inversion layer over the base will be noted.

C_{BE} vs. Φ curve in Figure (59) shown for Fairchild 2N1613, device #13, indicates inversion layer formation and also the receding of the layer with fluence. Inversion layer formation results in a substantial increase of the junction capacitance since the capacitance due to the field induced junction will add to that of the metallurgical junction. The reason for the receding of the inversion layer is discussed shortly; it is indicated by the broken lines in Figures 59 and 61. This conclusion is in accordance with the n values determined from the I_B vs. V_{BE} curves of Figure 60 where $n > 2$ in the similar fluence region.

The effect of inversion in I_{EBO} is strikingly illustrated by the similarity of the I_{EBO} vs. Φ curve of Figure (61) to the C_{BE} vs. Φ plot. The physical mechanism by which the inversion affected I_{EBO} appears to be channeling, it will be treated shortly. The initial, substantial rise in I_{EBO} prior to inversion is due to the increased surface recombination velocity caused by the irradiation. Incidentally, the values of I_{EBO} became quite high above $\phi \approx 5 \times 10^{14}$ electrons/cm^2 and one might wonder if tunneling took place across the field induced junction. This speculation is ruled out, however, because the presence of a breakdown voltage associated with tunneling (value expected is approximately 0.5-volt for our base doping) of the field induced junction was <u>not</u> observed as shown in the I_{EBO} vs. V_R curves, Figure (62). In fact, the shape of these curves did not change at all by the onset of inversion.

Now the question arises whether the positive charges inducing the observed inversion layer originated within or on the SiO_2. It appears that most of them were collected <u>on</u> the outer surface of the oxide layer (through the ionization of the gas inside the transistor can and the electric field between the base and the can which was connected to the collector). Namely we observed quite significant "Telstar type" effects, i.e., slow drifts, resulting in recovery of the transistor parameters with time after the

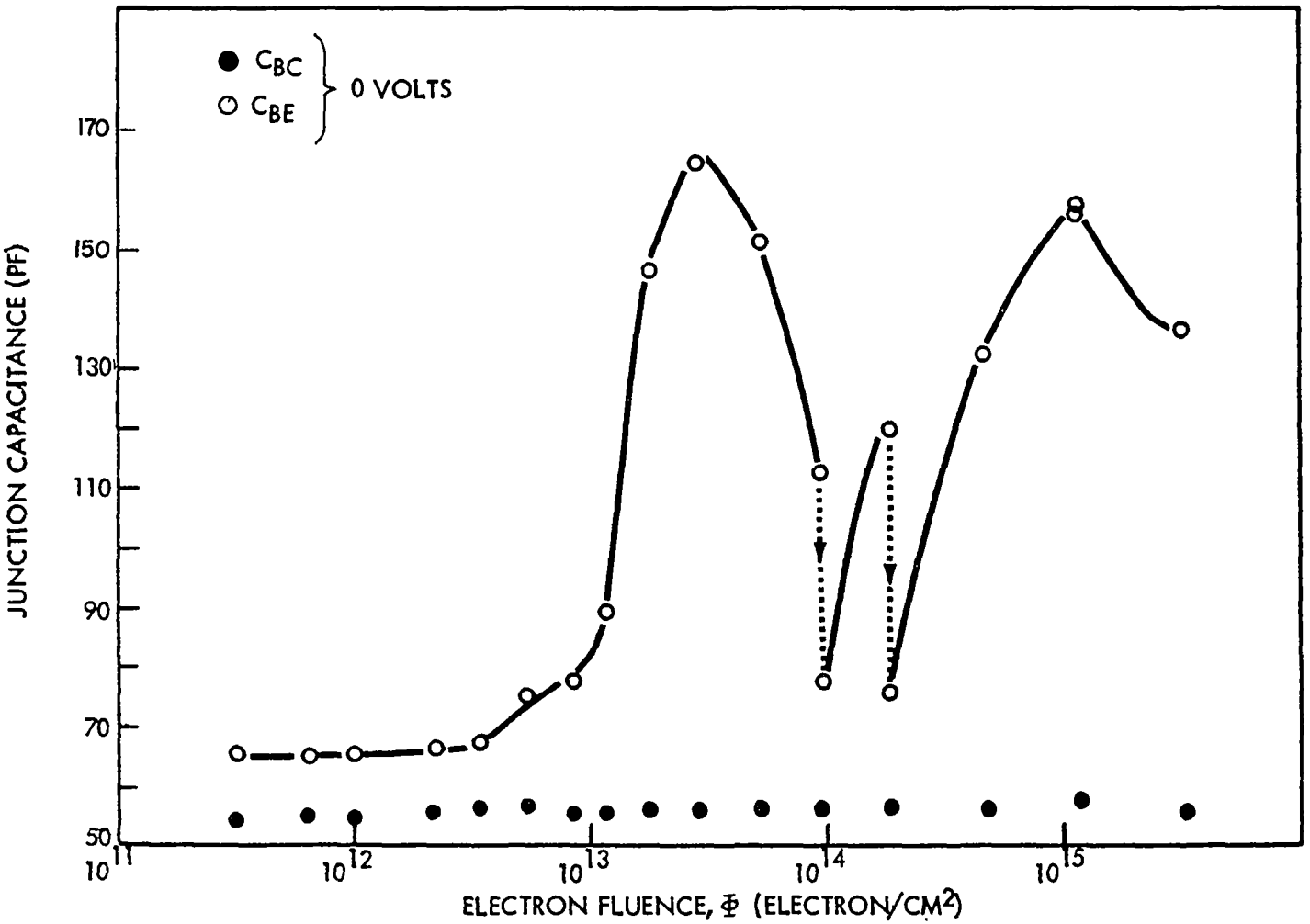

Figure 59. C_{BE} and C_{BC} (Zero Bias) Versus Fluence (Fairchild 2N1613, Active Bias During Irradiation V_{CB} = 10 V, I_E = 10 ma)

The broken lines indicate "Telstar-type" transient changes with time (usually overnight) after the irradiation has stopped and the bias was turned off.

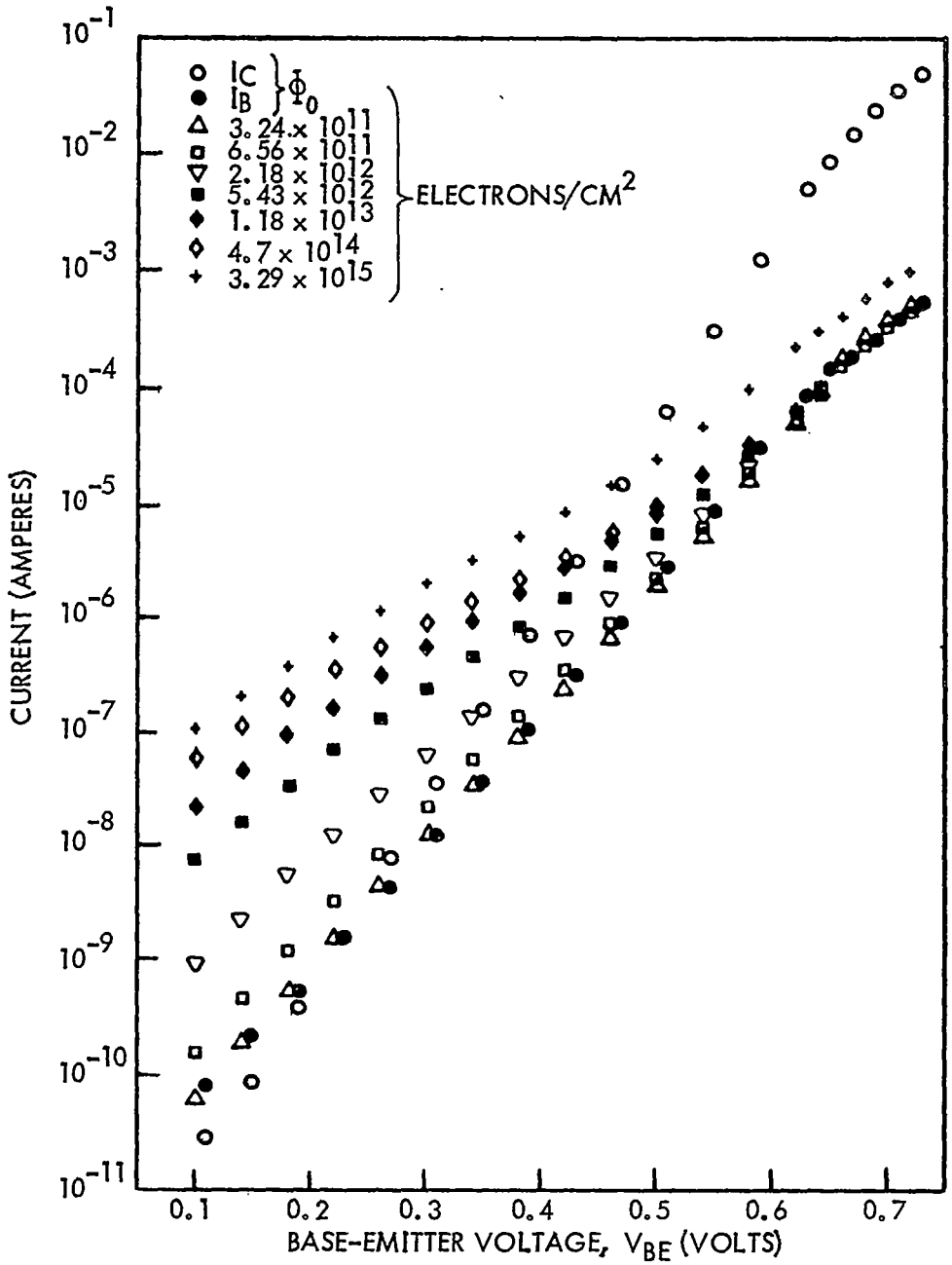

Figure 60. I_B and I_C Versus V_{BE} Curves, Taken at Different Stages During Exposure (Fairchild 2N1613, Active Bias During Irradiation: V_{CB} = 10 V, I_E = 10 ma)

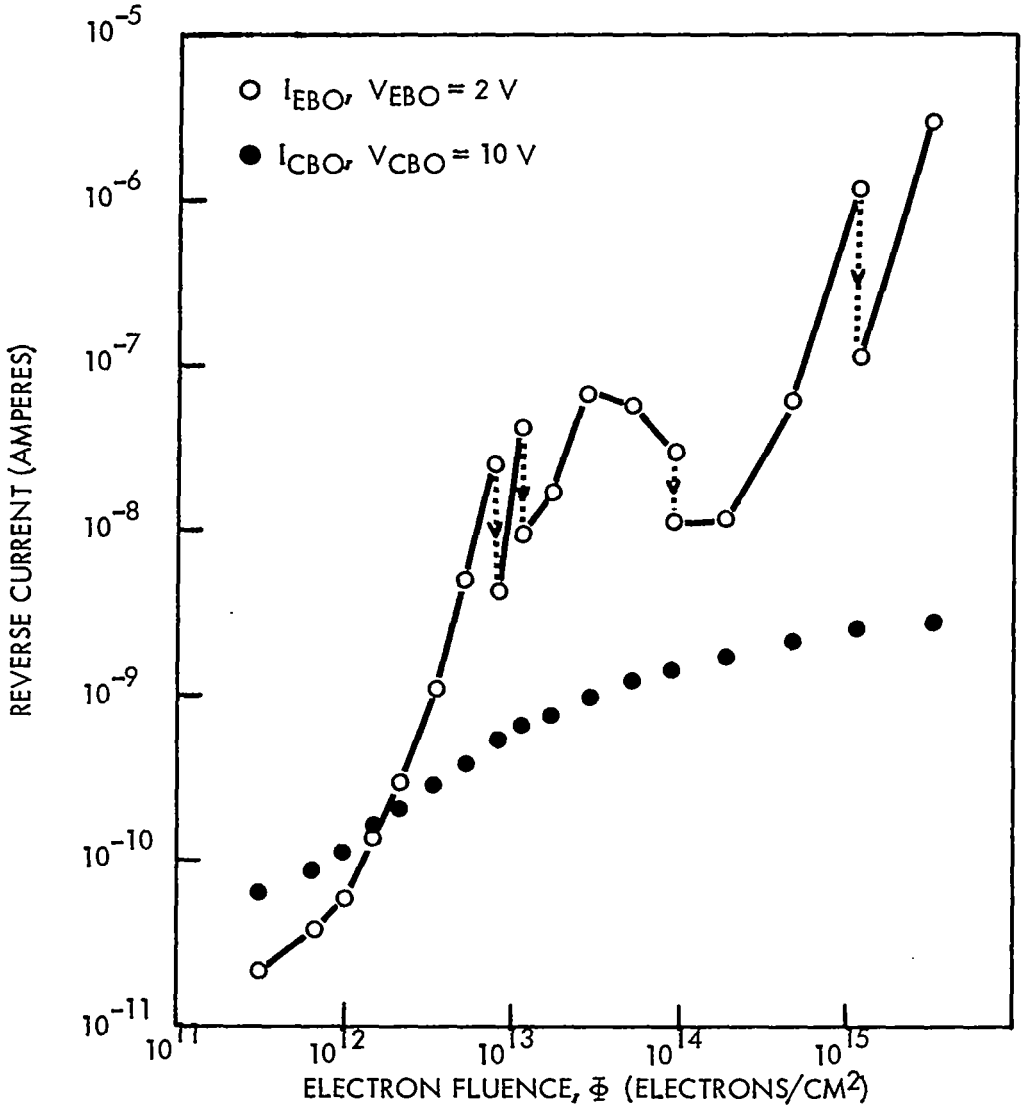

Figure 61. I_{EBO} and I_{CBO} Versus Fluence (Fairchild 2N1613, Active Bias During Exposure)

The broken lines indicate "Telstar-type" transient changes with time (usually overnight) after the irradiation has stopped and the bias was turned off.

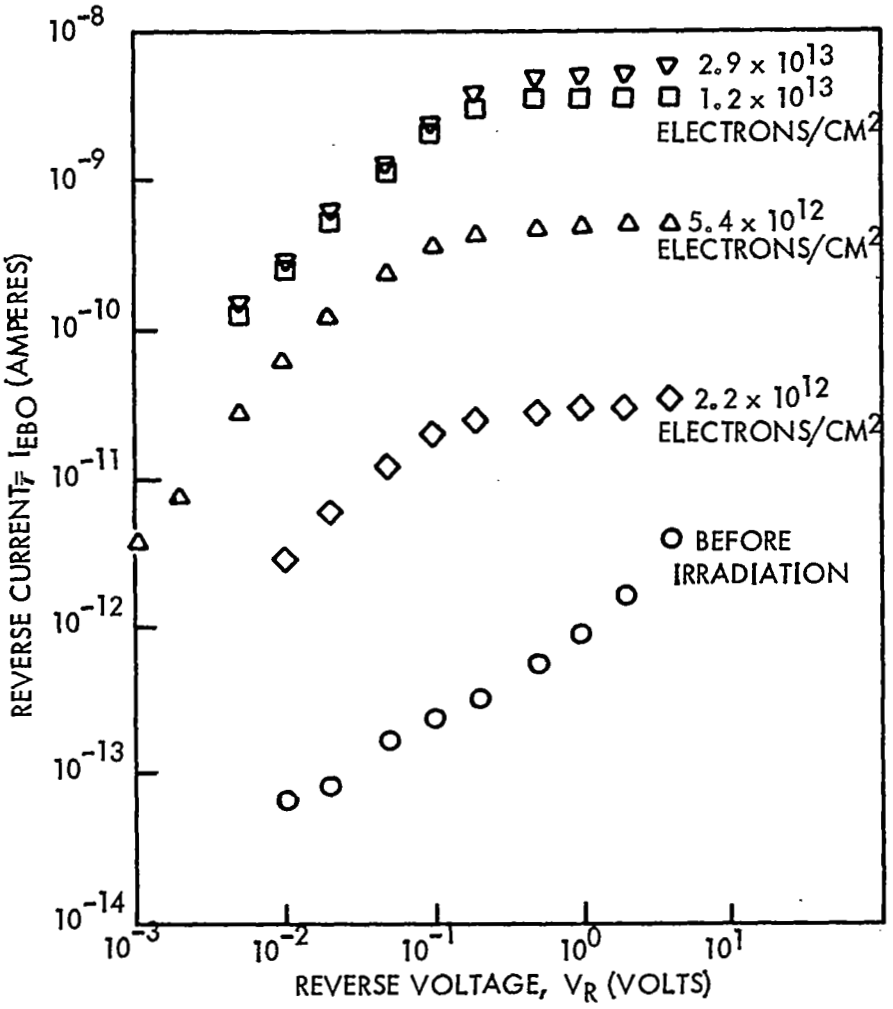

Figure 62. I_{EBO} Versus V_R Curves, Taken at Different Stages During Exposure (Fairchild 2N1613, Active Bias During Irradiation: $V_{CB} = 10$ V, $I_E = 10$ ma)

irradiation was stopped and the bias was disconnected. These effects are indicated in Figures (59) and (61) by the broken lines as mentioned earlier. The recoveries of C_{BE} and I_{EBO} with time after exposure were often substantial. (Such effects were observed essentially on all biased NPN devices.) In the past, such effects were found to be related to the redistribution of charges on the outer surface of the SiO_2.

Note by comparing Figure (59) and Figures (63) or (64) that quite significantly most of the gain degradation took place before the onset of inversion since $\Delta 1/h_{FE}$ or I_B went into saturation above $\approx 2 \times 10^{13}$ electrons/cm^2. Although the amount of positive space charge on the SiO_2 kept changing as indicated by the onset and the recession of the inversion layer, the correspondingly changing surface potential did not appreciably affect the rate of surface recombination thus I_B. All these can be qualitatively understood since the surface effects play a dominant role on I_B and I_R only before inversion occurs, after inversion their role becomes less and less significant because then the effects by the bulk transition region of the field induced junction take over. However, this latter event is usually not too serious in affecting I_B and I_R unless tunneling occurs.

Now since tunneling was absent nevertheless I_{EBO} was drastically affected during inversion, "channeling" or the formation of an ohmic path between base and emitter must have taken place. This would explain the large changes in I_{EBO} as well as the relative constancy of I_B, thus h_{FE}, during inversion, because channeling does not have much effect on a forward biased junction.

The C_{BC} vs. ϕ data in Figure (59) show an absence of inversion, also confirmed by I_{CBO} vs. ϕ on Figure (61), for device constructional reasons. According to the manufacturer the base metal contact overlaps the collector-base junction hence prevents charge accumulation on the surface of the oxide.

Although the assumption of an increased surface recombination velocity explains the increase in I_{CBO} with fluence (Figure 61) it is partially at variance with the I_{CBO} vs. V_R curves on Figure (65). Namely, I_{CBO} is approximately voltage independent only above ≈ 0.2 volt and not over the whole measurement range as it is theoretically claimed.

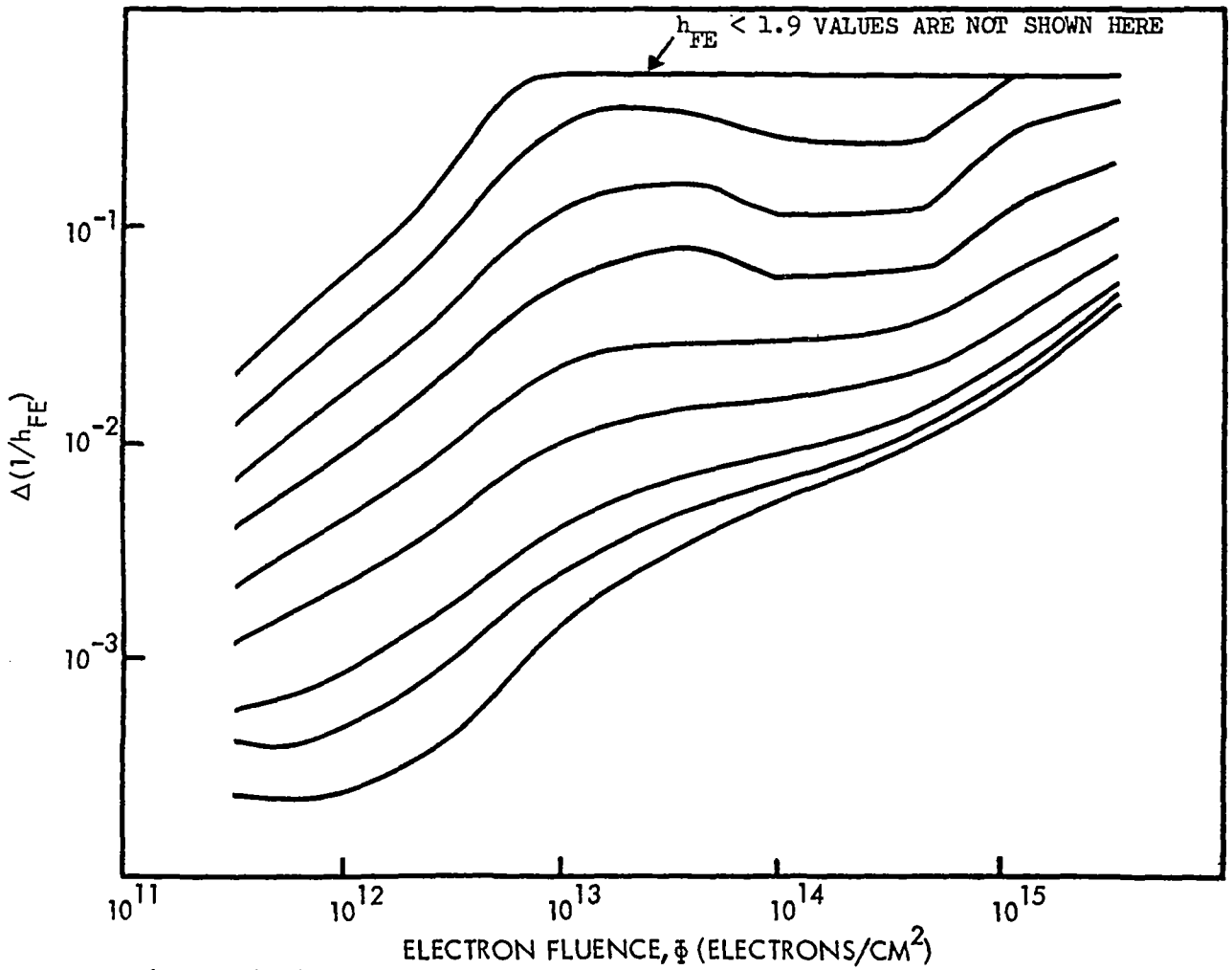

Figure 63. $\Delta(1/h_{FE})$ Versus Fluence (Fairchild 2N1613, Active Bias During Irradiation: V_{CB} = 10 V, I_E = 10 ma; Measurement Current, I_E, From Top to Bottom: 10μa, 30μa, 100μa, 300μa, 1ma, 3ma, 10ma, 20ma, 40 ma)

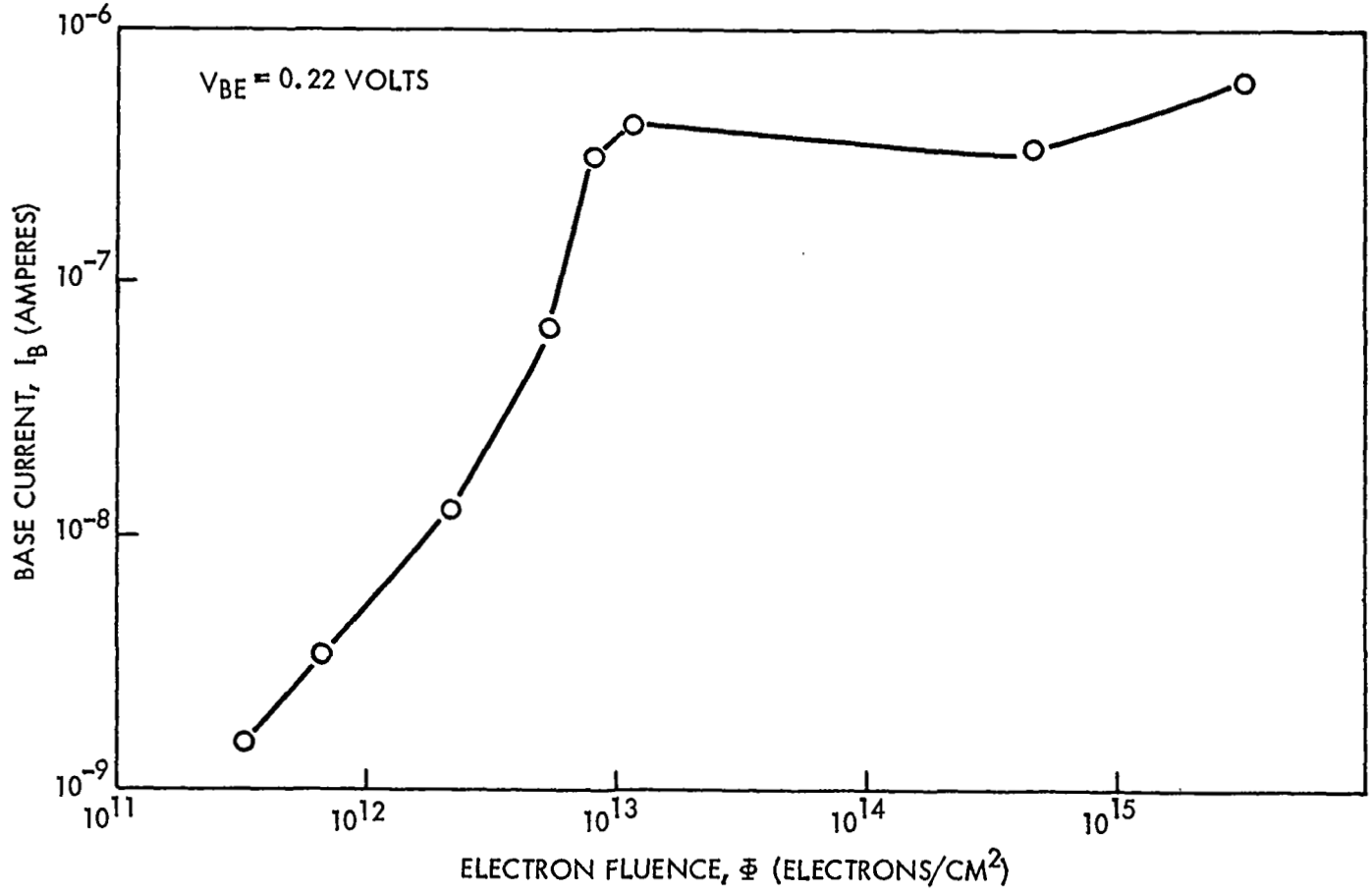

Figure 64. I_B Versus Fluence (Fairchild 2N1613, Active Bias During Irradiation: V_{CB} = 10 V, I_E = 10 ma)

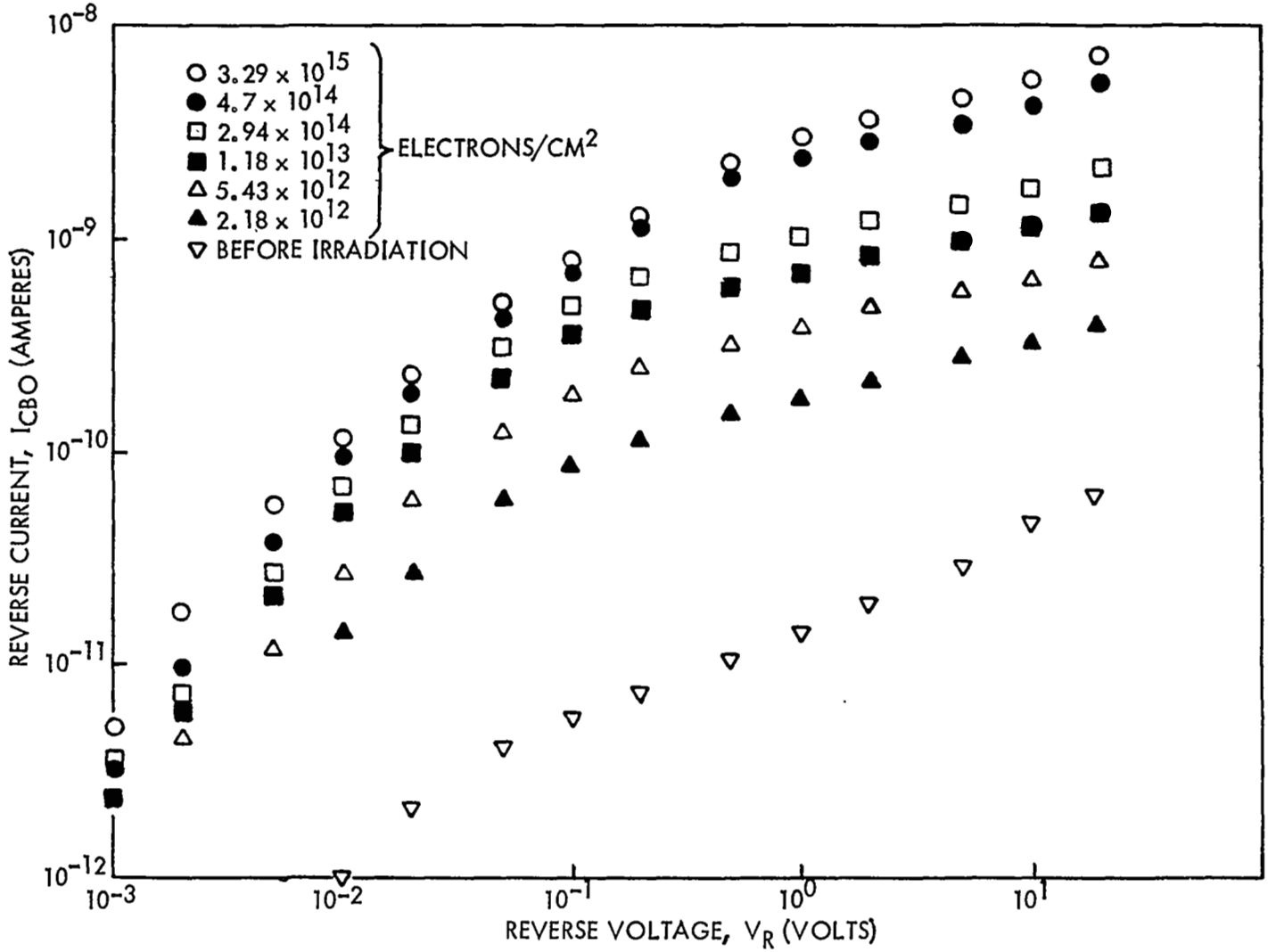

Figure 65. I_{CBO} Versus V_R Curves, Taken at Different Stages During Irradiation (Fairchild 2N1613, Active Bias During Irradiation: $V_{CB} = 10$ V, $I_E = 10$ ma)

PNP - unbiased during irradiation: As stated (Appendix I), it is a small part of the emitter region (close to the base-emitter junction) which is primarily affected by the positive charge accumulation and the new interface states, and subsequently leads to gain degradation in a PNP structure. For I_{CBO} degradation the collector surface in the vicinity of the base-collector junction is the important region.

C_{BE} vs. Φ is shown in Figure (66) for Raytheon 2N1132, device #111. There is no sign of inversion of part of the emitter region. This is in accordance with the n values of 1.24 - 1.55 obtained from the I_B vs. V_{BE} curves (Figure 67). Similarly, inversion is apparently absent over the collector region, (see C_{BC} vs. Φ on Figure 66), which is somewhat surprising in view of the low surface doping normally found in collectors. Increases in I_B, $\Delta 1/h_{FE}$, I_{EBO}, I_{CBO} as a function of Φ shown on Figures (68), (69), and (70) respectively, can be qualitatively understood in terms of increased surface recombination over the respective junctions. This assumption is in accordance with the $1.24 \leqslant n \leqslant 1.55$ values obtained from Figure (67). However, the I_{EBO} vs. V_R (Figure 71) and I_{CBO} vs. V_R (Figure 72) curves show very little if any saturation tendency with voltage which is at variance with the theoretical predictions of the voltage independence of the surface generation component of current.

PNP - biased during irradiation (Bias: V_{CB} = 10 V, I_E = 0.1 ma):

We saw previously the tremendous difference in irradiation behavior between the passive and active NPN devices. No such significant differences were observed between the passive and active PNP transistors. It is true that, due to the reverse biased collector base junction, an increased charge accumulation thus more severe I_{CBO} degradation was expected and indeed observed in active PNP devices (see Figures 70 and 77). Differences, however, practially disappeared when the gain degradation curves were compared. Although the detailed arguments to account for this observation are not clear, at present, certain tentative ideas can be presented. For one thing, the charge accumulation on the SiO_2 surface must surely be different from the NPN case, since the direction of the fringing electric field between the can and the base or the emitter surface (due to the reverse biased collector-base junction) is such now that the positive gas ions, generated inside the

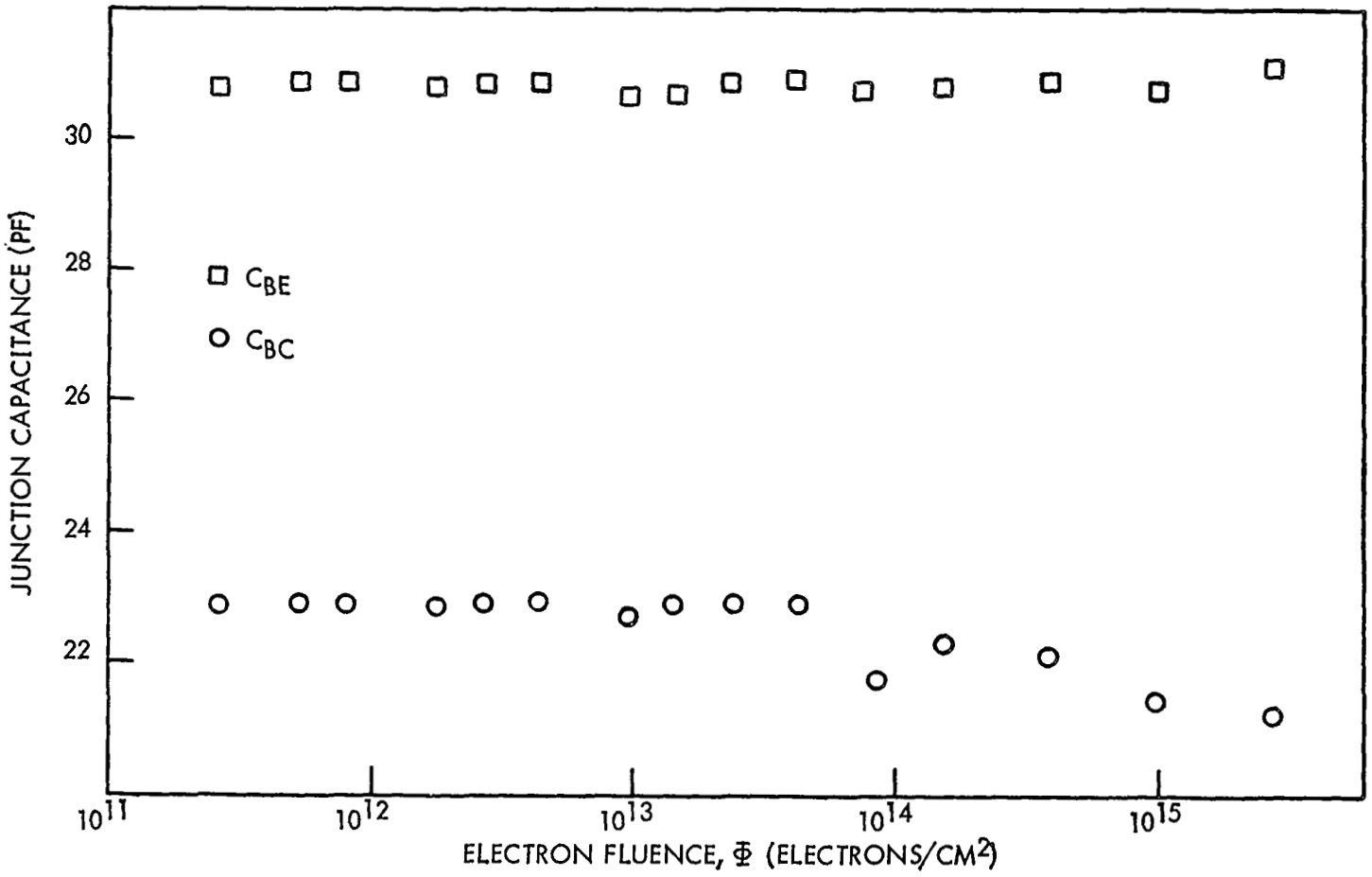

Figure 66. C_{BE} and C_{BC} (Zero Bias) Versus Fluence (Raytheon 2N1132, Passive During Irradiation)

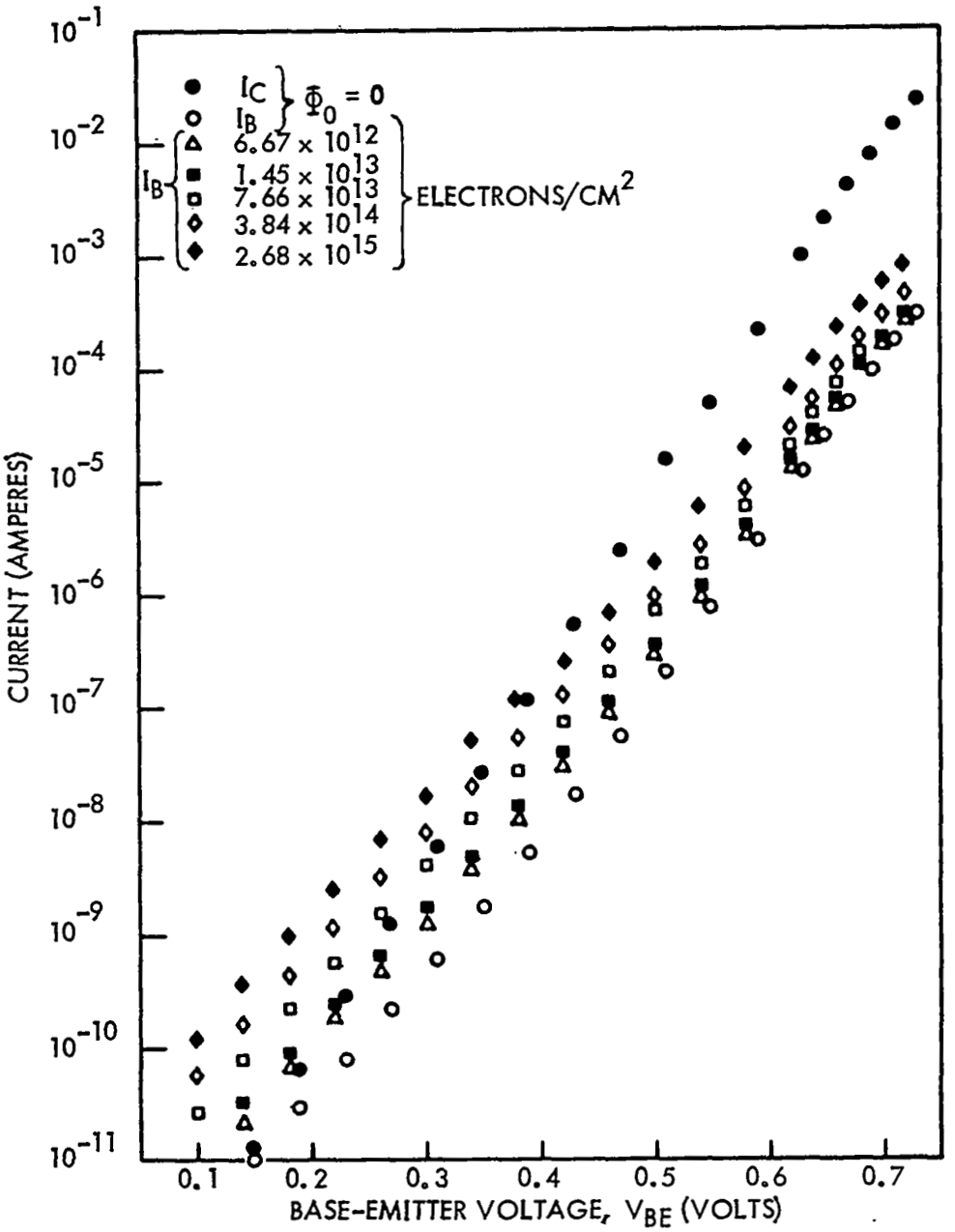

Figure 67. I_B and I_C Versus V_{BE} Curves, Taken at Different Stages During Exposure (Raytheon 2N1132, Passive During Irradiation)

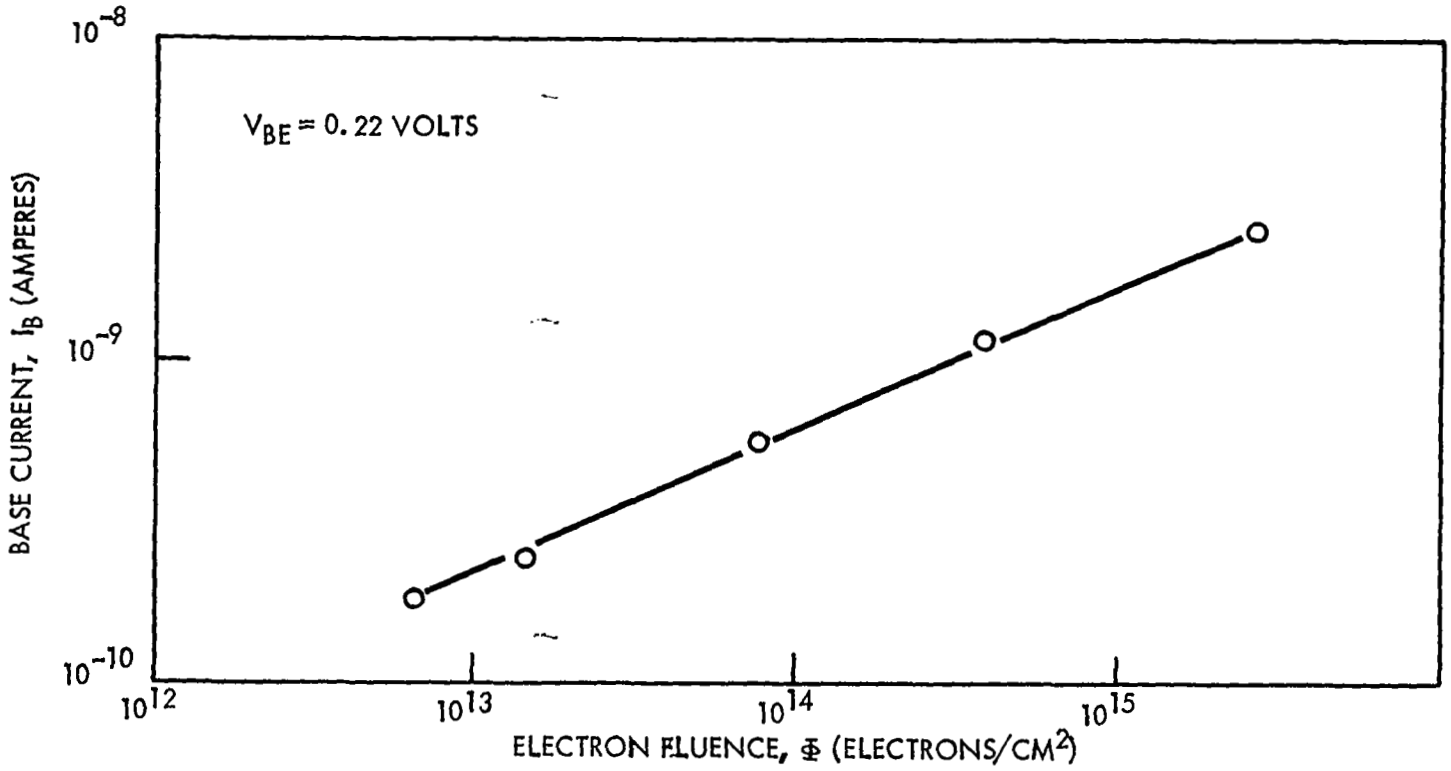

Figure 68. I_B Versus Fluence (Raytheon 2N1132, Passive During Irradiation)

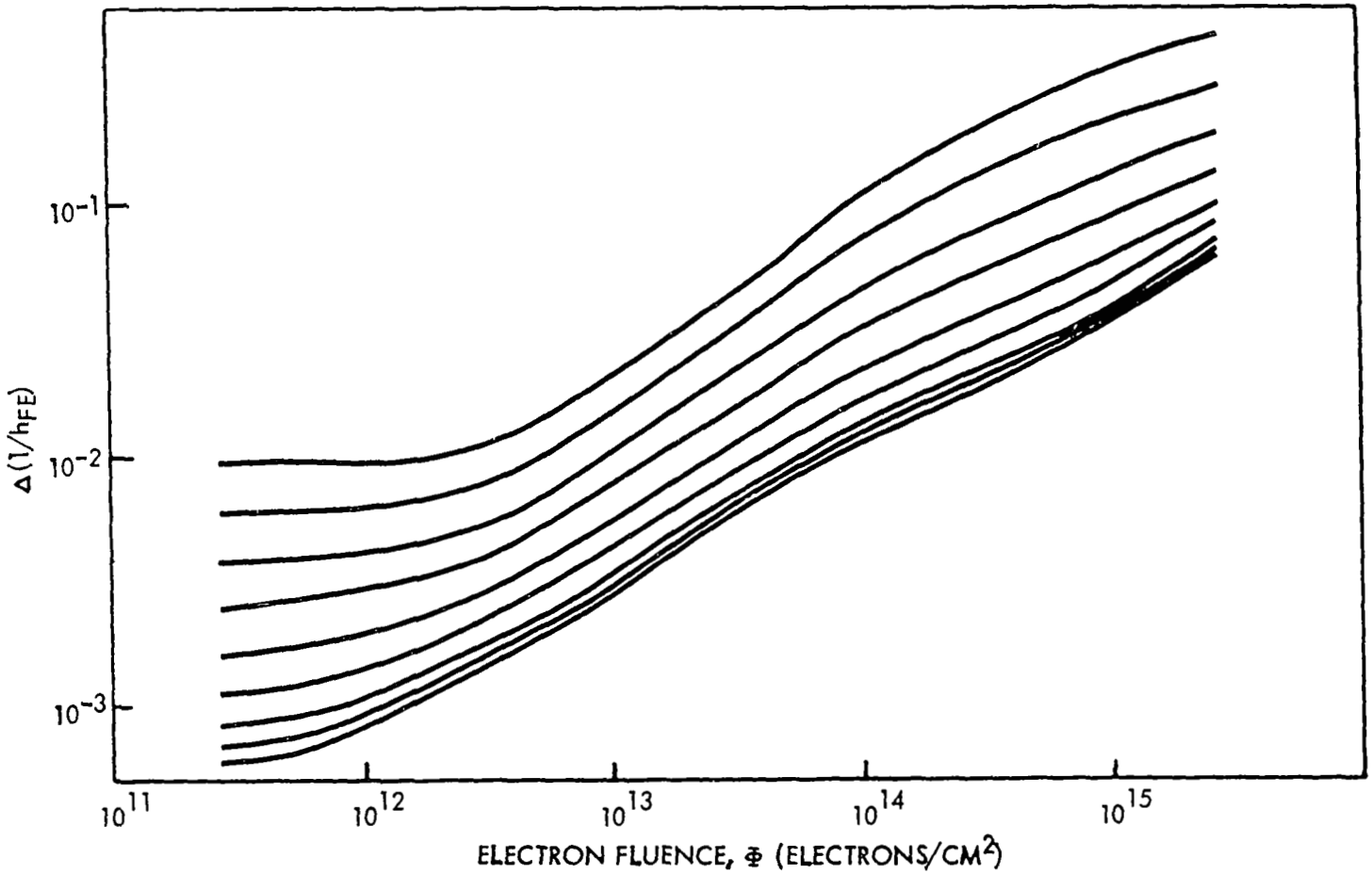

Figure 69. $\Delta(1/h_{FE})$ Versus Fluence (Raytheon 2N1132, Passive During Irradiation)
(Measurement Current, I_E, From Top to Bottom: 10μa, 30μa, 100μa, 300μa, 1ma, 3ma, 10ma, 20ma, 40ma)

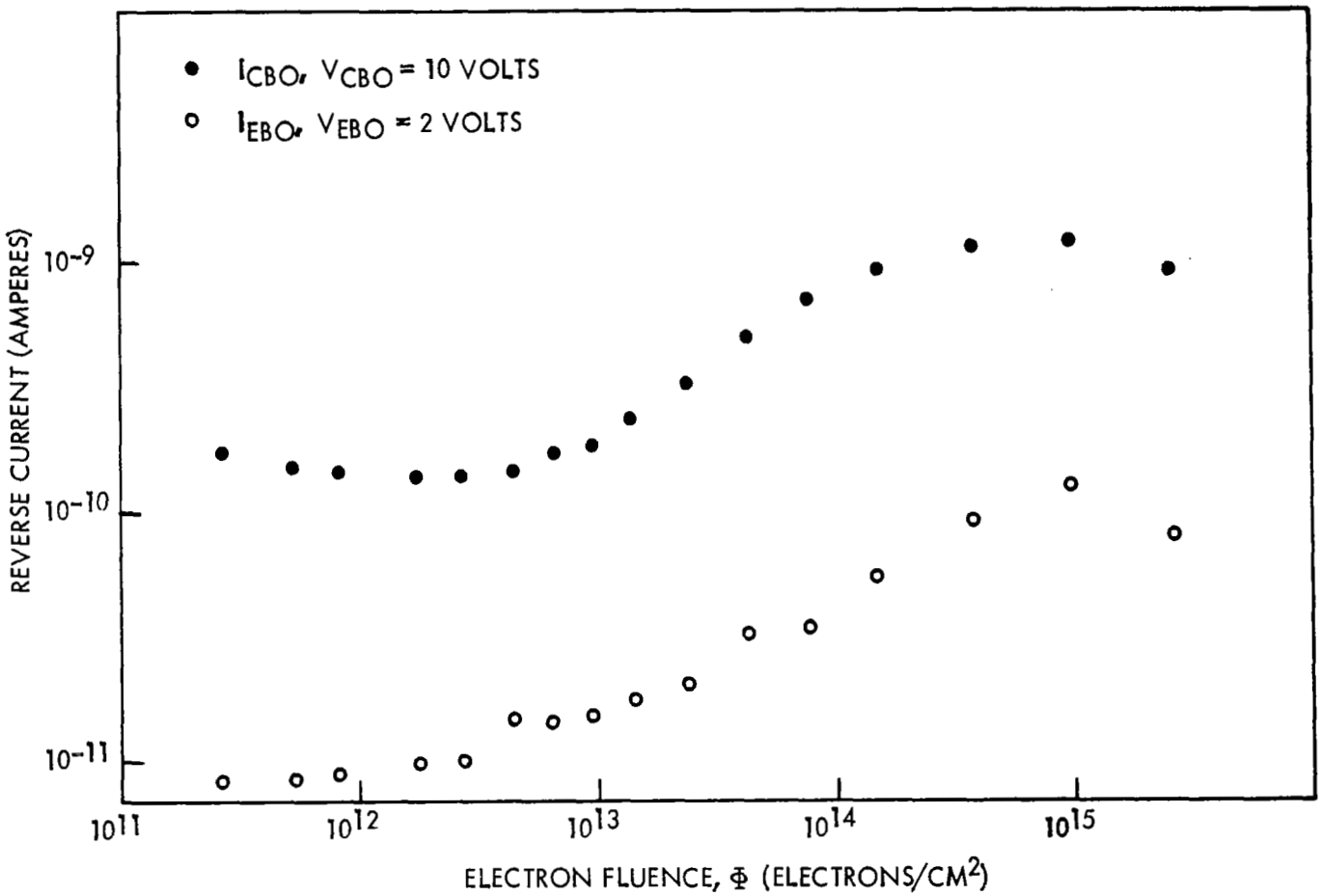

Figure 70. I_{EBO} and I_{CBO} Versus Fluence (Raytheon 2N1132, Passive During Irradiation)

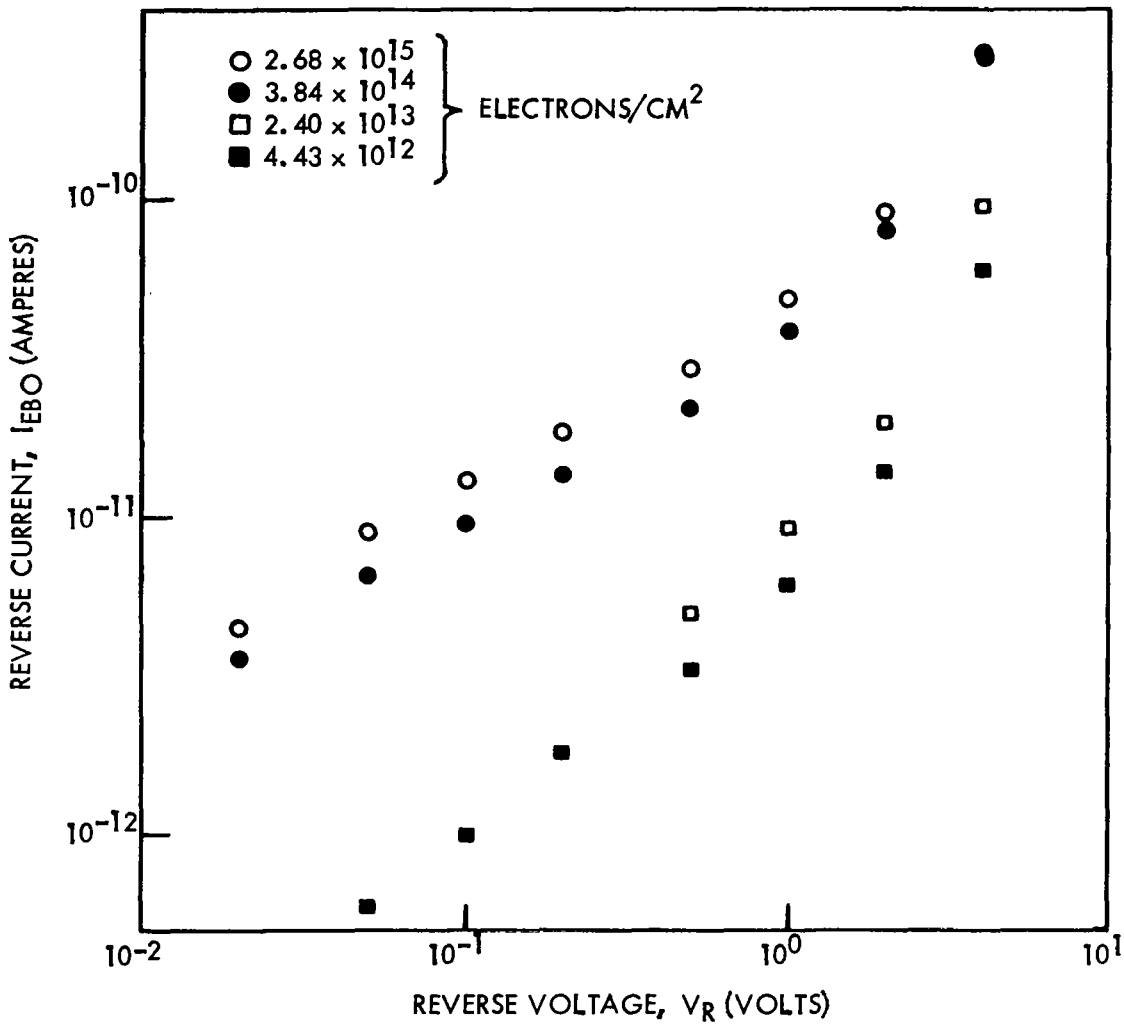

Figure 71. I_{EBO} Versus V_R Curves, Taken at Different Stages During Exposure (Raytheon 2N1132, Passive During Irradiation)

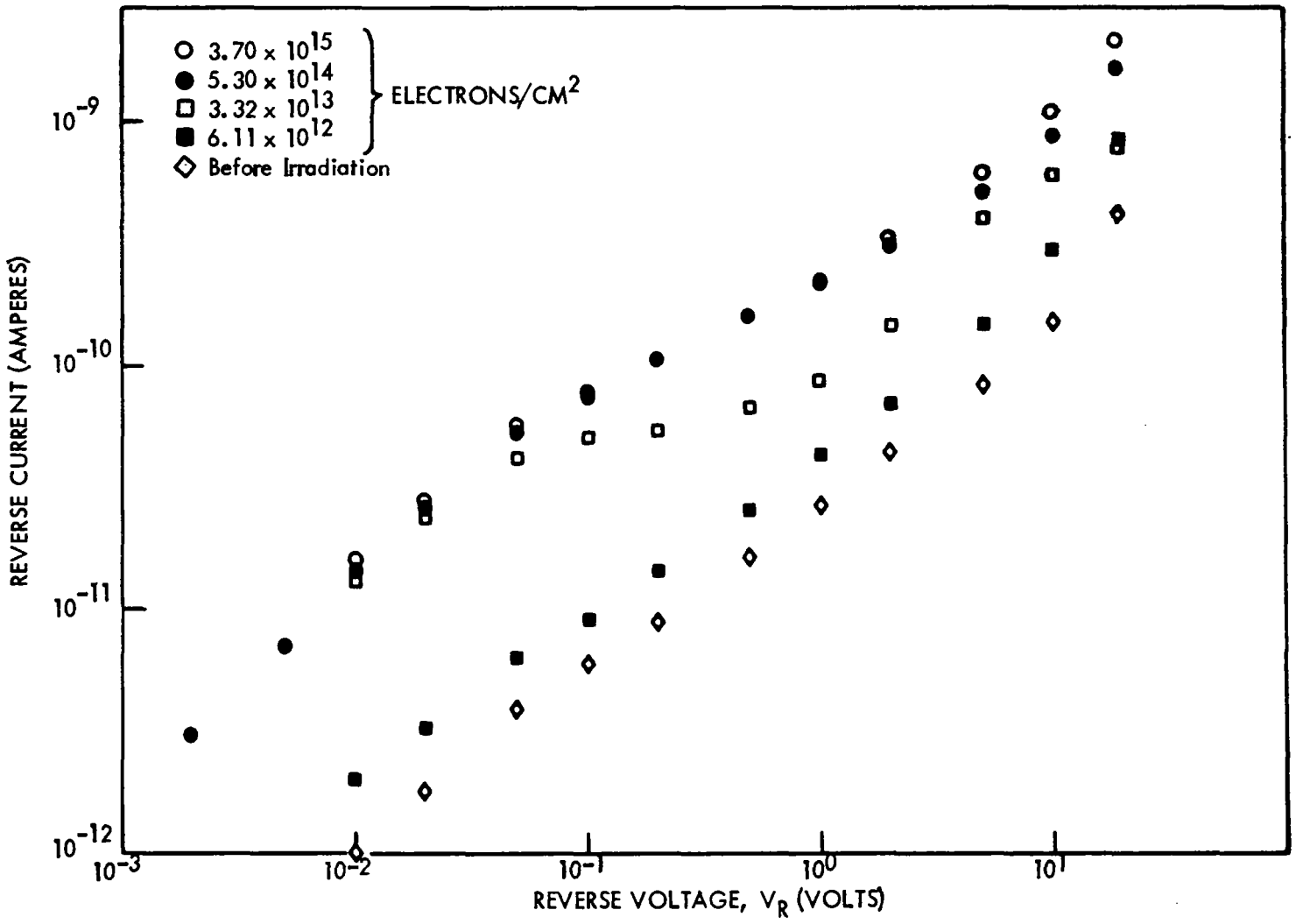

Figure 72. I_{CBO} Versus V_R Curves, Taken at Different Stages During Exposure (Raytheon 2N1132, Passive During Irradiation)

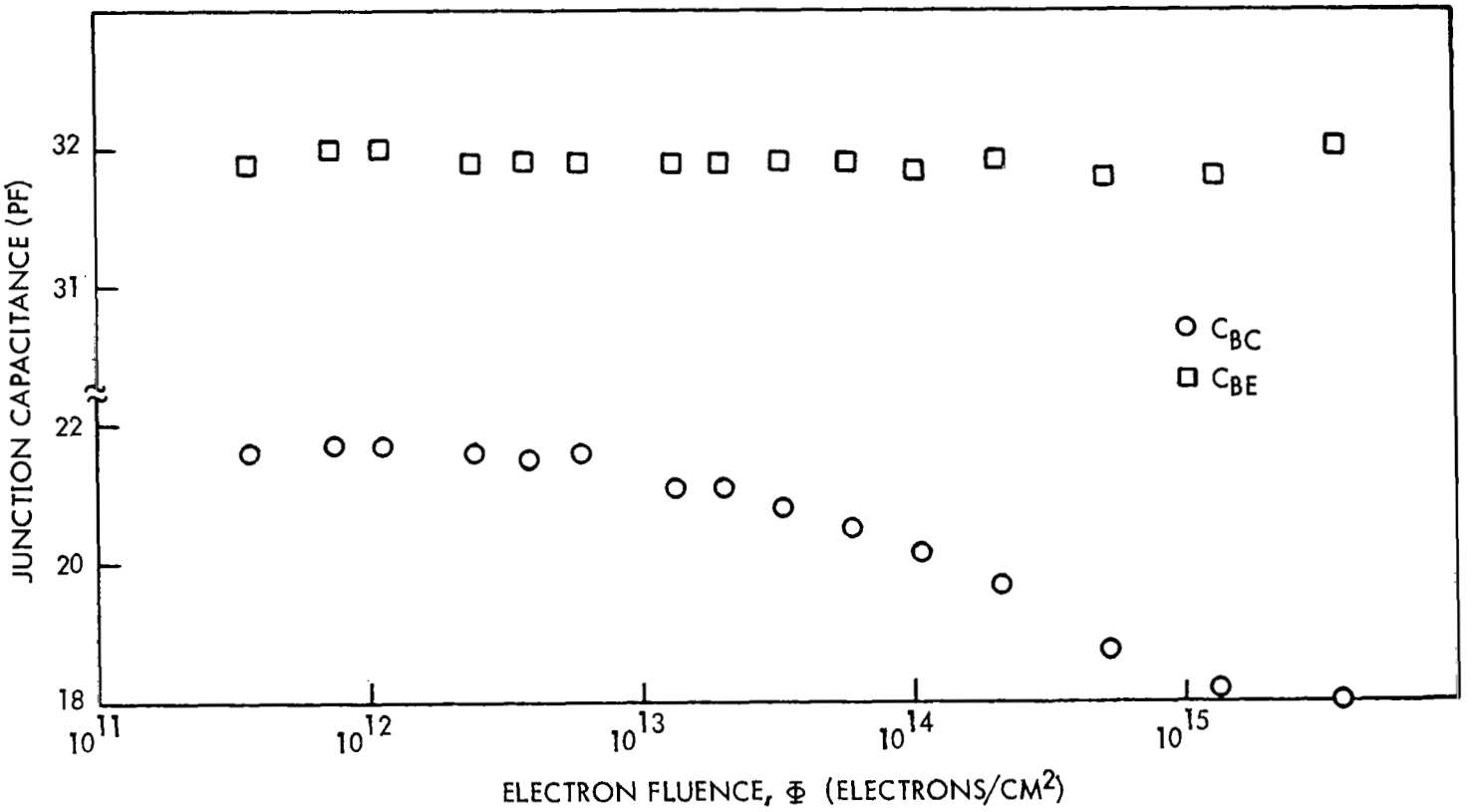

Figure 73. C_{BE} and C_{BO} (0 Volts) Versus Fluence (Raytheon 2N1132, Active Bias During Irradiation: $V_{CB} = 10$ V, $I_E = 0.1$ ma)

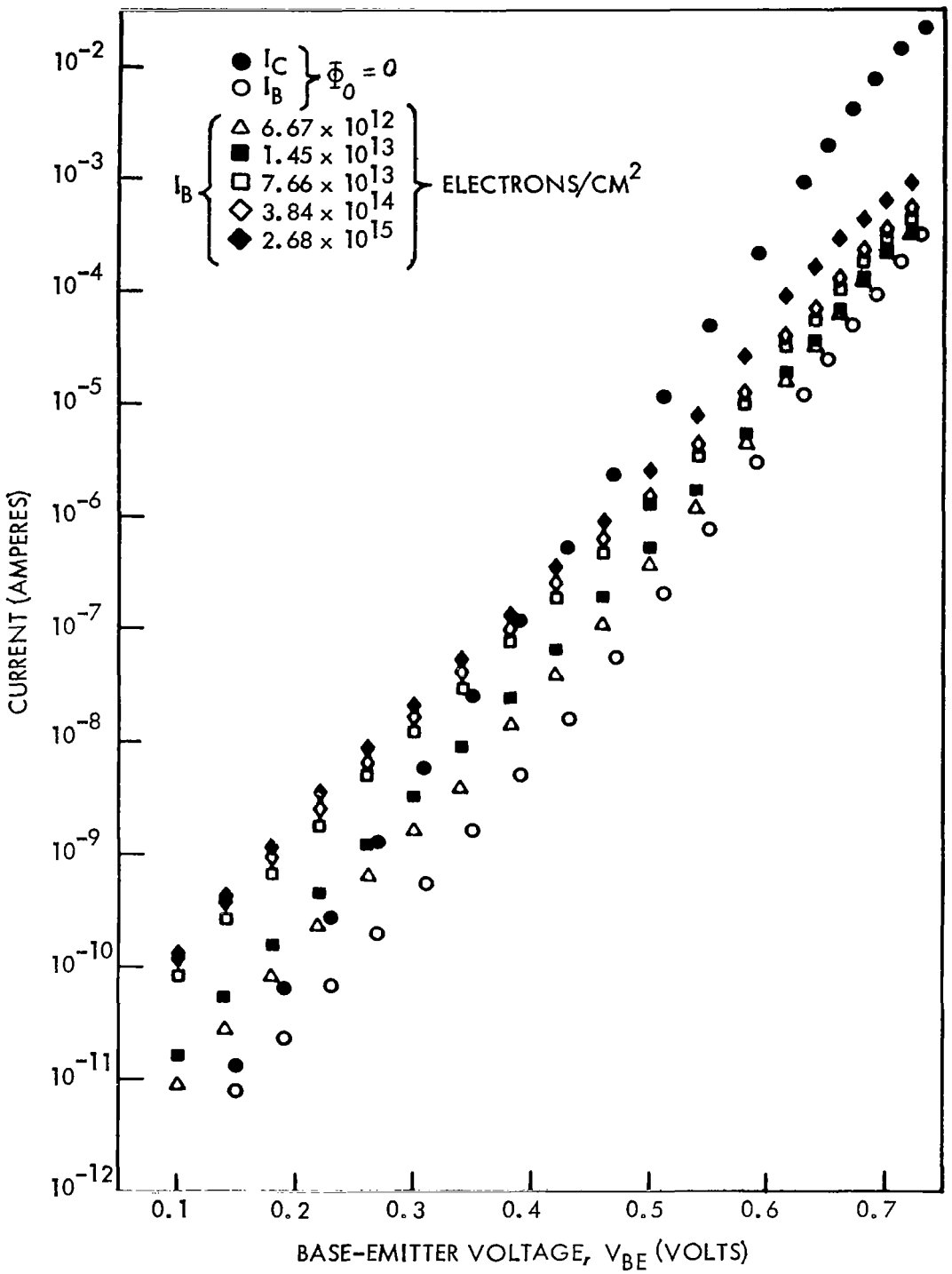

Figure 74. I_B and I_C Versus V_{BE} Curves, Taken at Different Stages During Exposure (Raytheon 2N1132, Active Bias During Irradiation: $V_{CB} = 10$ V, $I_E = 0.1$ ma)

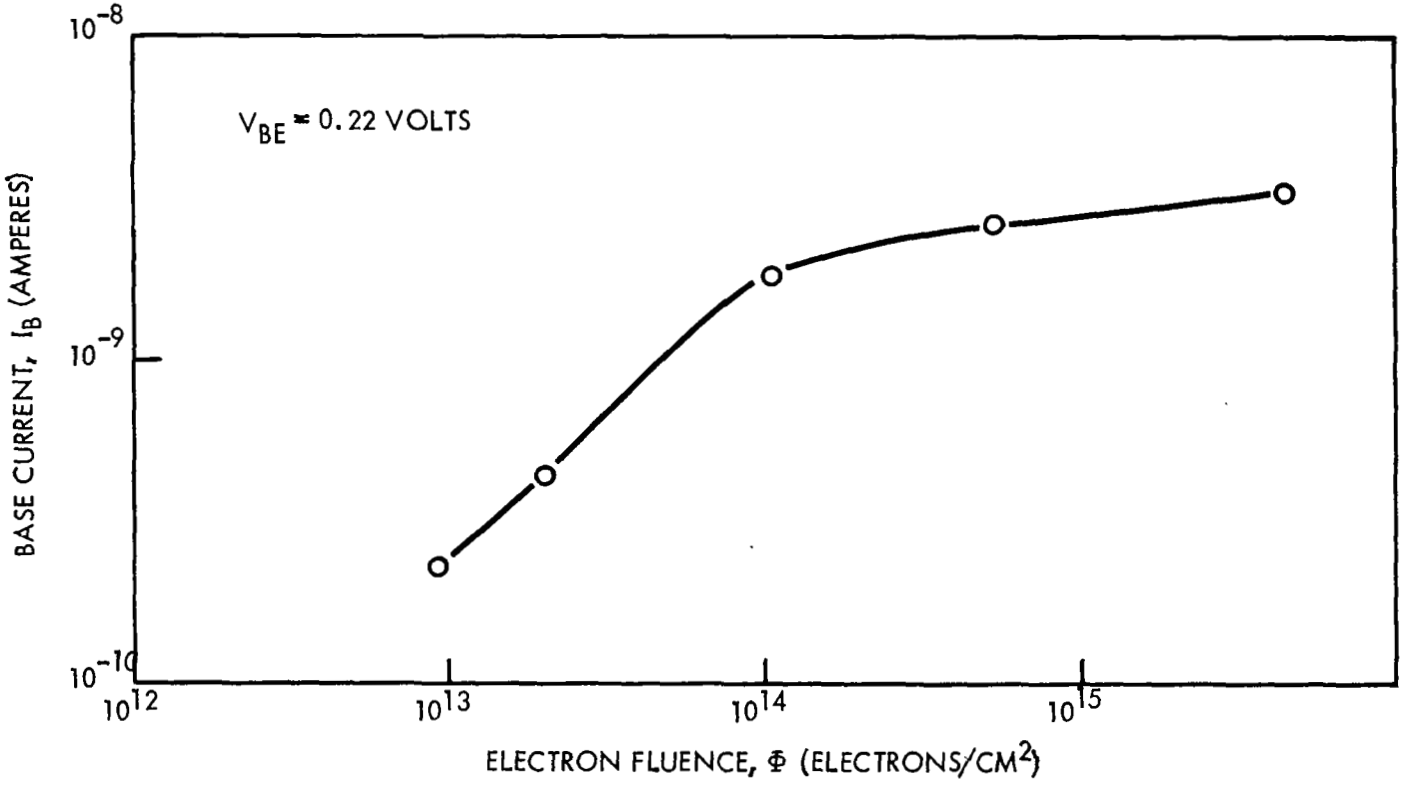

Figure 75. I_B Versus Fluence (Raytheon 2N1132, Active Bias During Irradiation: V_{CB} = 10, I_E = 0.1 ma)

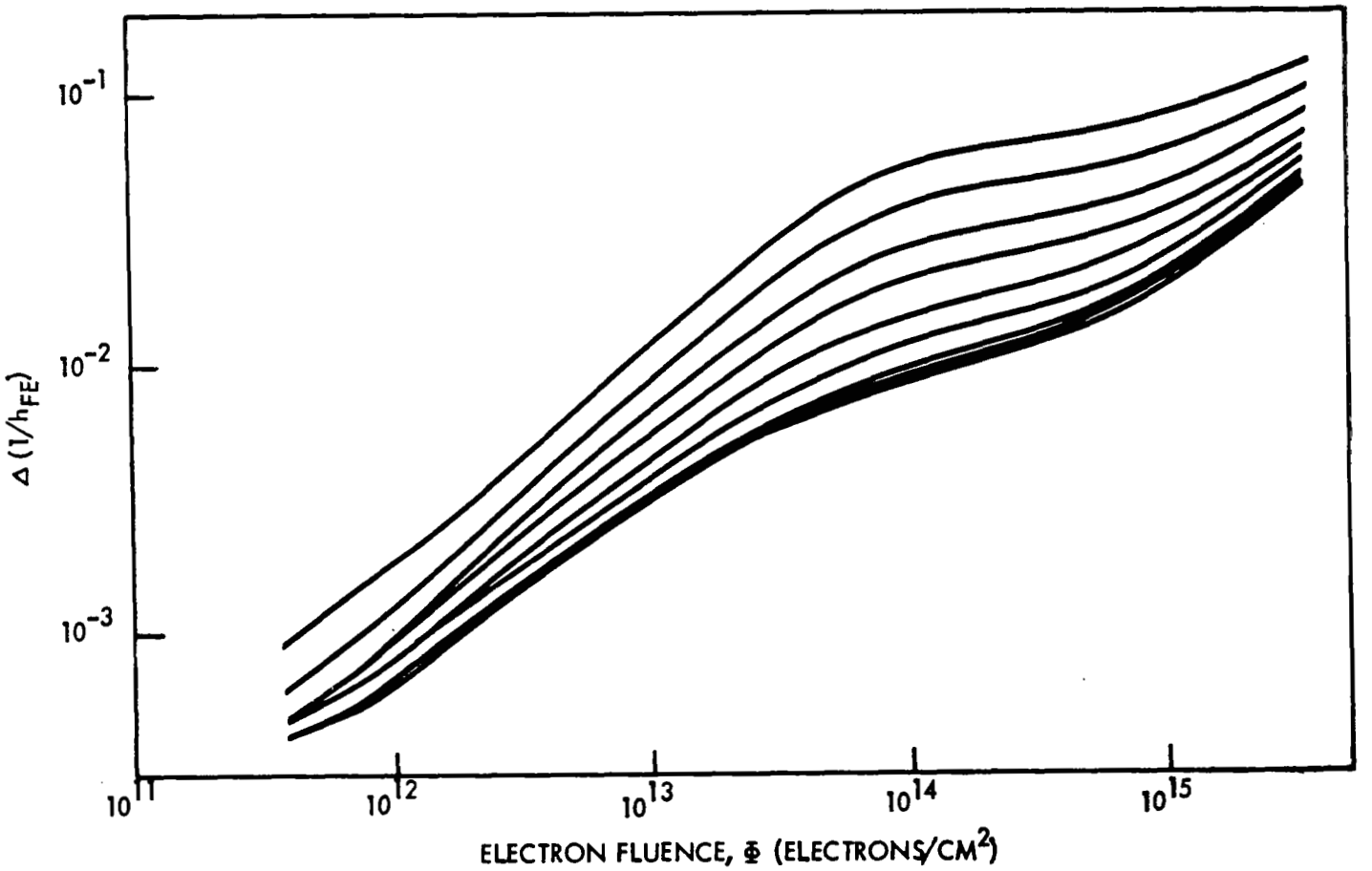

Figure 76. $\Delta(1/h_{FE})$ Versus Fluence (Raytheon 2N1132, Active Bias During Irradiation: V_{CB} = 10 V, I_E = 0.1 ma; Measurement Current, I_E, From Top to Bottom: 10μa, 30μa, 100μa, 300μa, 1 ma, 3 ma, 10 ma, 20 ma, 40 ma)

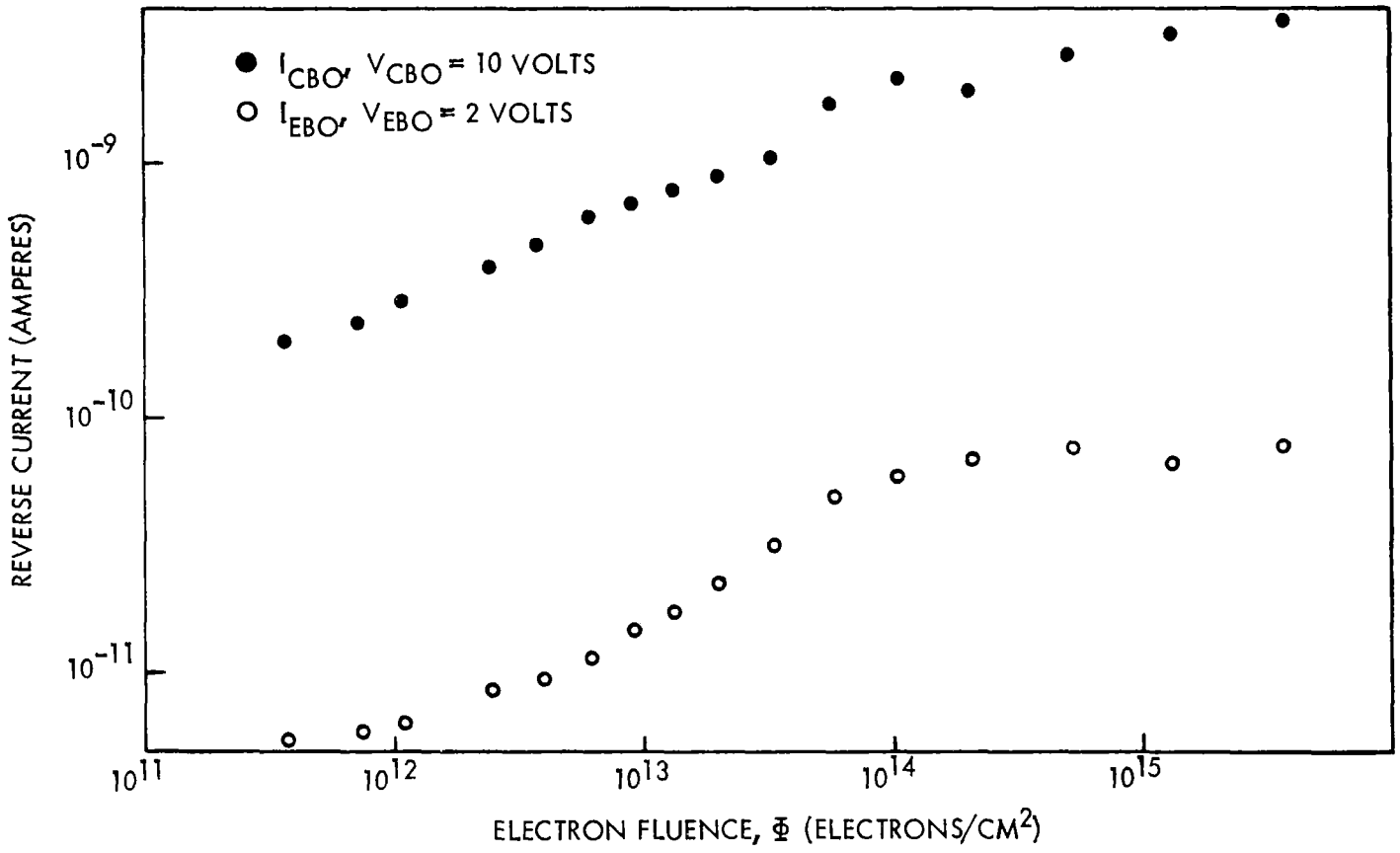

Figure 77 I_{EBO} and I_{CBO} Versus Fluence (Raytheon 2N1132, Active Bias During Irradiation: V_{CB} = 10 V, I_E = 0.1 ma)

can, are moved toward the transistor can. But then the positive charge accumulation on the SiO_2 could be small which is essentially the case also for the passive PNP devices. Secondly, in an NPN device the depletion of the silicon surface and the creation of new interface states occur coincidentally at the base surface. Hence their effect can reinforce each other significantly. This may not be the case for the emitter region of a PNP device. If, e.g., the creation of the new interface states over the base of an active NPN structure were enhanced by electron injection then such an enhancement would not occur in the emitter region of an active PNP transistor, due to the absence of such an injection. Then the differences in irradiation response between passive and active PNP transistors could be restricted essentially to slight differences in charge accumulation within the SiO_2, the net effect of which might be small. Clearly, further speculation is not justified without the benefit of additional experimental data.

The remarks on the figures are very similar to the PNP - unbiased case. Both C_{BE} vs. Φ and C_{BC} vs. Φ (Figure 73), shown for Raytheon 2N1132, device #121, indicate the absence of inversion in the emitter and collector regions respectively. The n values of 1.25 - 1.64 obtained from the I_B vs. V_{BE} curves (Figure 74) support the conclusion. The assumption of increased surface recombination over the junctions as the main reason for the increase in I_B (Figure 75), $\Delta\ 1/h_{FE}$ (Figure 76), I_{EBO} (Figure 77), I_{CBO} (Figure 77) are also in accordance with the quoted n values. However, the presumed voltage independence of the surface dominated I_{CBO} is demonstrated on the I_{CBO} vs. I_R curves in Figure (78) only above 0.1 volt (at large fluences). Worst yet, the I_{EBO} vs. V_R curves in Figure (79) are at variance with the theoretical predictions over the whole voltage range.

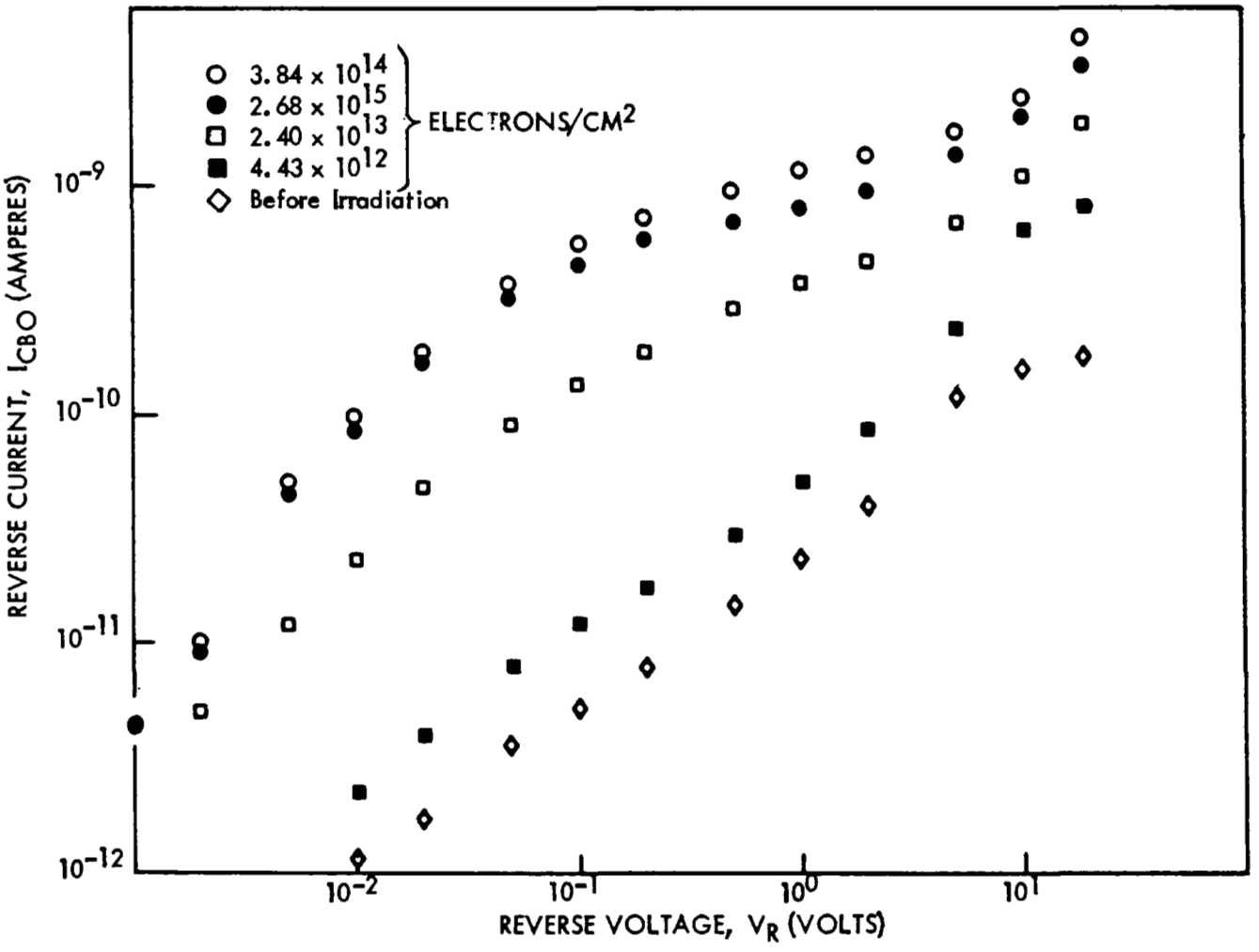

Figure 78. I_{CBO} Versus V_R Curves, Taken at Different Stages During Exposure (Raytheon 2N1132, Active Bias During Irradiation: V_{CB} = 10 V, I_E = 0.1 ma)

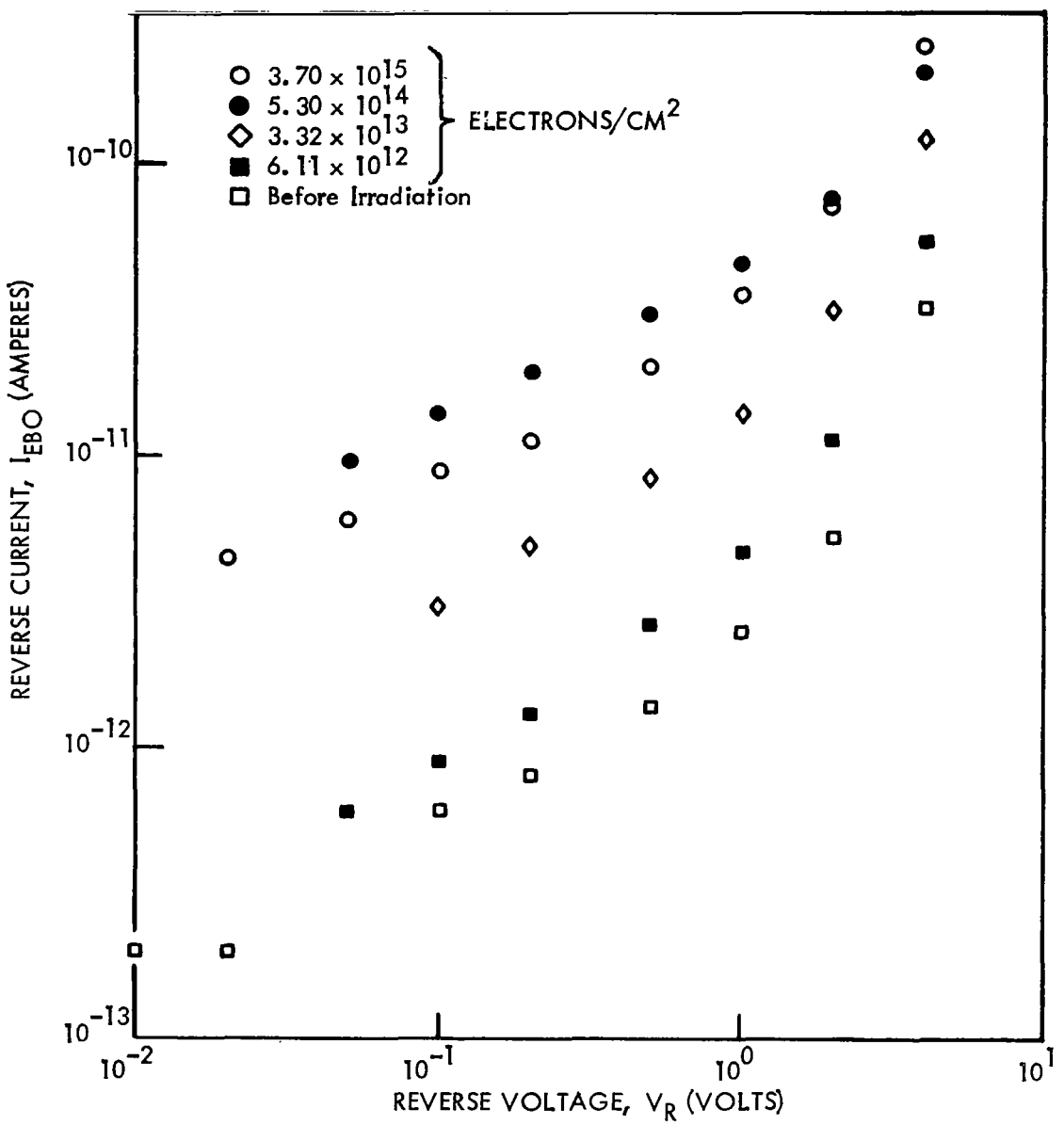

Figure 79 I_{EBO} Versus V_R Curves, Taken at Different Stages During Exposure (Raytheon 2N1132, Active Bias During Irradiation: V_{CB} = 10 V, I_E = 0.1 ma)

2.4 Task B - Influence of Active Operation During Exposure

Active operation during exposure significantly enhanced the sensitivity of NPN transistors to nonlinear damage. Latin Cube computer analysis (Reference 19) of a multifactor experimental design not only provided data on this dependence of damage on electrical biasing (during the 1 Mev electron exposure) but also data on the possibilities of any interdependence of test variables such as current, voltage, and dose. Because of the increase of damage for active NPN devices and because of post irradiation recovery, pulse tester techniques were developed for the 2.9 Mev linac test and the 15 Mev proton test. With the pulse tester, measurements were made in situ without disconnecting any bias voltages. In the 15 Mev proton test important anomolies in the ratio of active to passive NPN transistor damage was observed.

2.4.1 Enhanced Damage in NPN Transistors

NPN transistors showed much more damage when they were operated actively during exposure rather than passively. Electron results on biasing dependence observed in this phase II contract are in general agreement with Boeing Cobalt -60 gamma results obtained earlier. (References 9 and 20). Bias conditions for comparative studies are shown in Table 9 for those devices that received special measurements such as those listed in Table 3. Details of the results of those special measurements on active and passive transistors were described in Section 2.3.5. Additional biasing conditions were used in the multifactor experimental design described in Section 2.4.2.

Typical computer plots of NPN and PNP damage with active biasing during exposure are shown in Figures 80 and 81 respectively. Fairchild 2N1613 Transistors with operating conditions of I_E = 0.1 ma, and V_{CB} = 10 volt, showed enhanced damage at all nine current levels (Figure 80) when compared with similar devices that were exposed passively (Figure 40). (Using the low current gain module on the Fairchild Series 500 transistor testor, gain values below 1.9 were observed and shown on Figure 80). Figure 81, showing results of a Raytheon 2N1132 transistor operated at I_E = 5 ma and

Table 9

Numbers of Transistors
Receiving Special Measurements
for Bias Comparison

Bias Condition During Exposure	2N1613		2N1132	
	Fairchild	Raytheon	Fairchild	Raytheon
I_E = 0.1 ma V_{CE} = 10v	5	-	-	5
I_C = 10 m V_{CE} = 10v	5	-	-	5
No Bias (Passive)	5	5	5	5

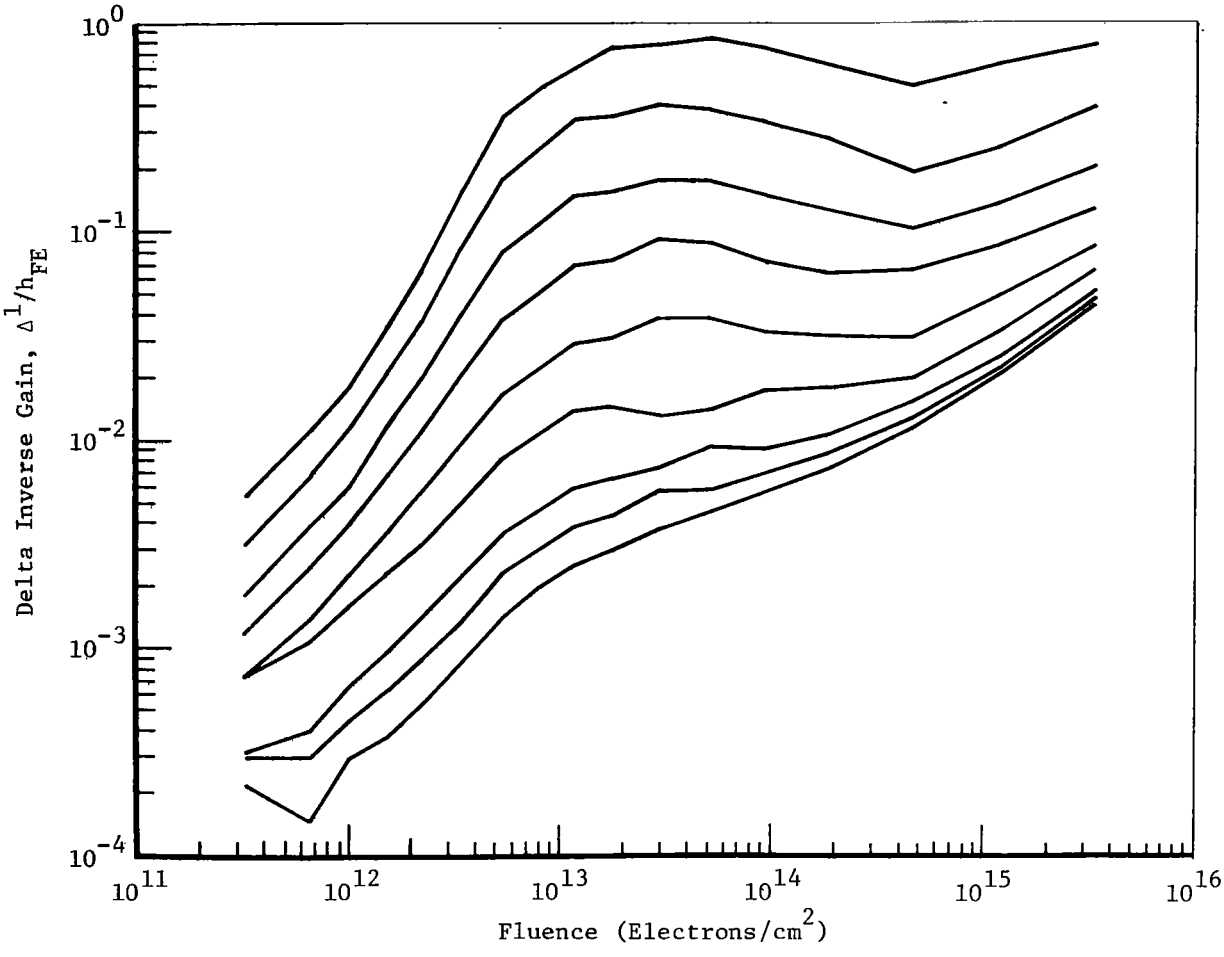

DC Gain vs Fluence, Family of Collector Currents, Type 2N1613, No. 71

(On the flattened-out 10-μa curve---see text)

Figure 80: DEPENDENCE OF NONLINEAR DAMAGE ON THE INJECTION LEVEL DURING MEASUREMENTS IN PARAMETRIC FORM (FAIRCHILD 2N1613 ACTIVE GROUP; MEASUREMENT CURRENTS FROM TOP TO BOTTOM: 10-30-100-300 μa, 1-3-10-20-40 ma)

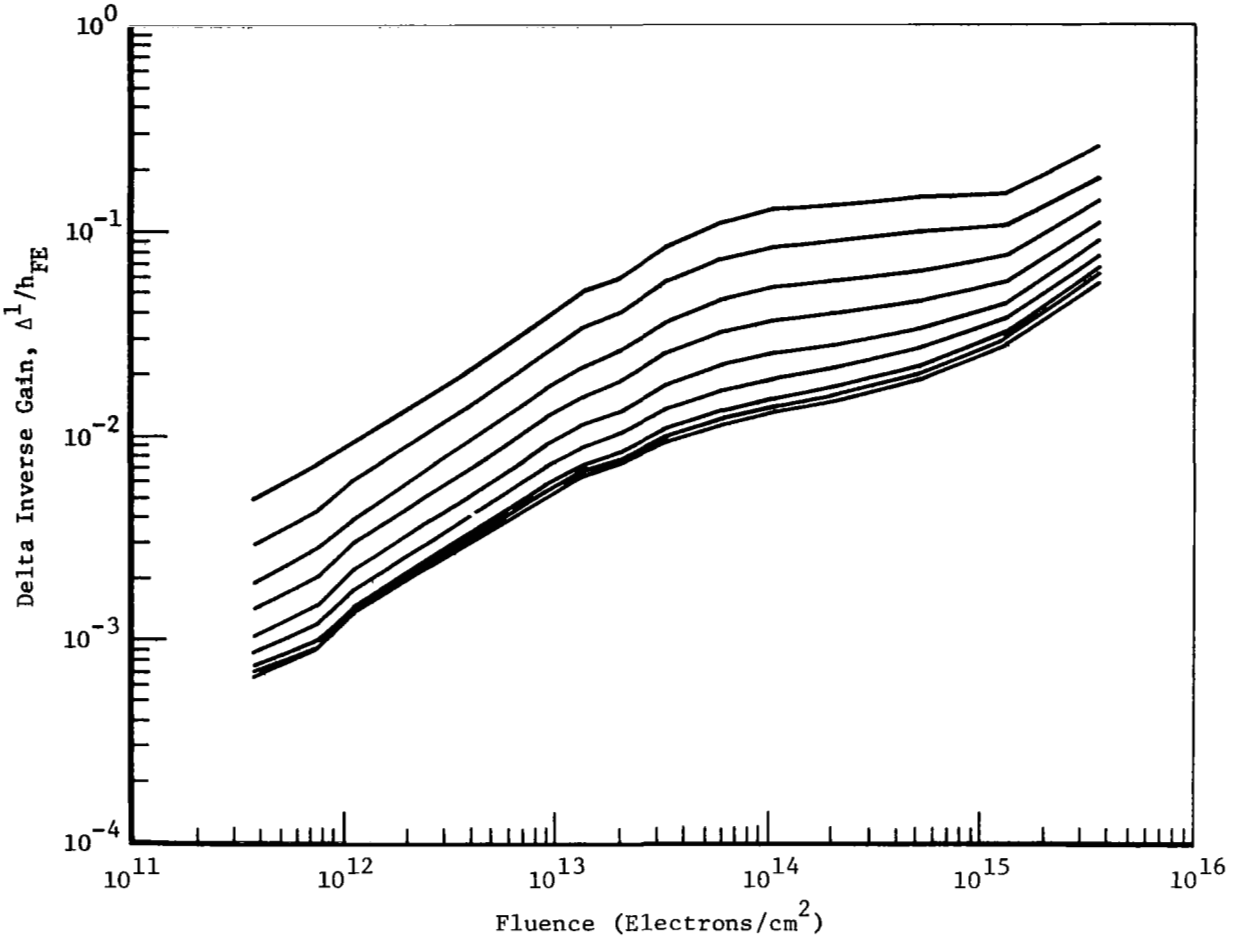

DC Gain vs Fluence, Family of Collector Currents, Type 2N1132, No. 129

Figure 81: DEPENDENCE OF NONLINEAR DAMAGE ON THE INJECTION LEVEL DURING MEASUREMENTS IN PARAMETRIC FORM (RAYTHEON 2N1132, ACTIVE GROUP; MEASUREMENT CURRENTS FROM TOP TO BOTTOM: 10-30-100-300 μa, 1-3-10-20-40 ma)

V_{CB} = 2 volts (one of the latin cube devices of Section 2.4.2), illustrates the reduced damage of active PNP transistors when compared with similar passive PNP transistors (Figure 42). Figures 80 and 81 are, in general, typical of all of the groups of active devices tested.

No statistical study was carried out to ascertain differences between different date codes and manufactures when exposed under identical bias conditions. At least not in the comprehensive manner discussed for the passive devices in Section 2.3.2. For each active bias condition (Table 9 and the latin cube conditions of Section 2.4.2) only 5 devices were tested. These were taken from the three different date codes(2 + 2 + 1 = 5) to make the results more general in nature. A far greater statistical spread was evident for active device damage than for passive. Those survey results indicate the desirability for a statistical study of active devices.

The average values of gain degradation for five 2N1613 Fairchild transistors with V_{CB} = 10v, I_E = 0.1 ma during exposure is shown in Figure 82 and can be compared with the corresponding average values for passive 2N1613 transistors shown much earlier in Figure 18. Differences between active and passive devices are clearly illustrated in Figures 83 for measurement collector currents of 0.1 ma and 1 ma. About an order of magnitude greater damage for active devices is seen at 10^6 rad Si measured at I_C = 0.1 ma. Differences between active and passive transistors (nonlinear) $\Delta 1/h_{FE}$ passive subtracted from $\Delta 1/h_{FE}$ active are plotted in Figure 84 showing the very definite peaking at 10^6 rad Si already evident in Figures 80 and 82. Differences at high exposure levels where displacement damage is present is not shown in this Figure.

Electron nonlinear damage to active transistors can be compared with Cobalt -60 gamma ray damage shown in Figure 85. It can be seen that 1 Mev electrons (Figure 82) appear to cause greater damage to active devices than a corresponding absorbed dose of Cobalt -60 gamma rays. Although the curves are close at low and high exposures, there is about a factor of 2 more damage from electrons at the damage peak. Exposure rates for electrons and gamma rays were comparable for low exposures but ultimately at high exposures elec-

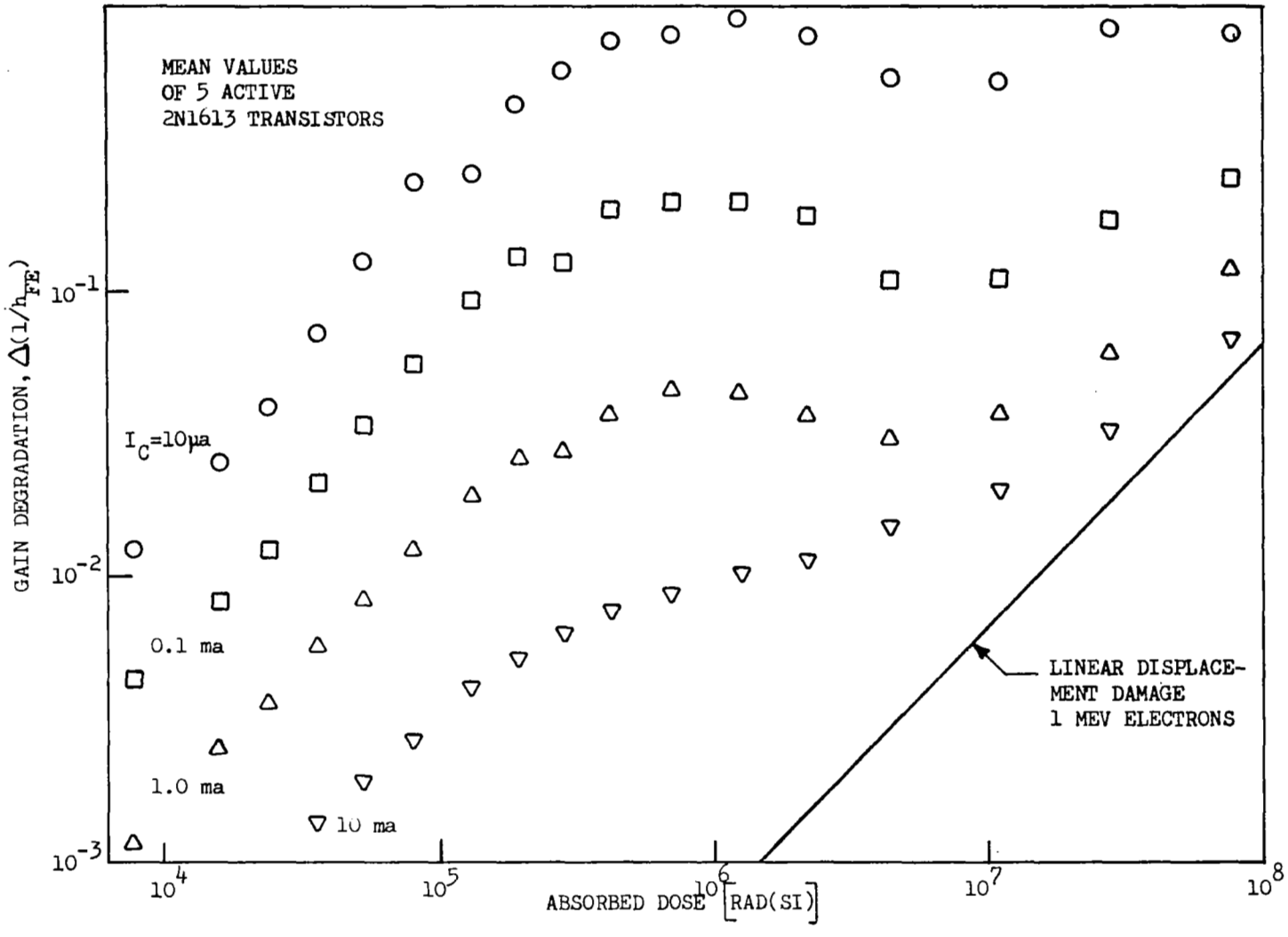

Figure 82. Enhanced Nonlinear Damage in NPN Transistors

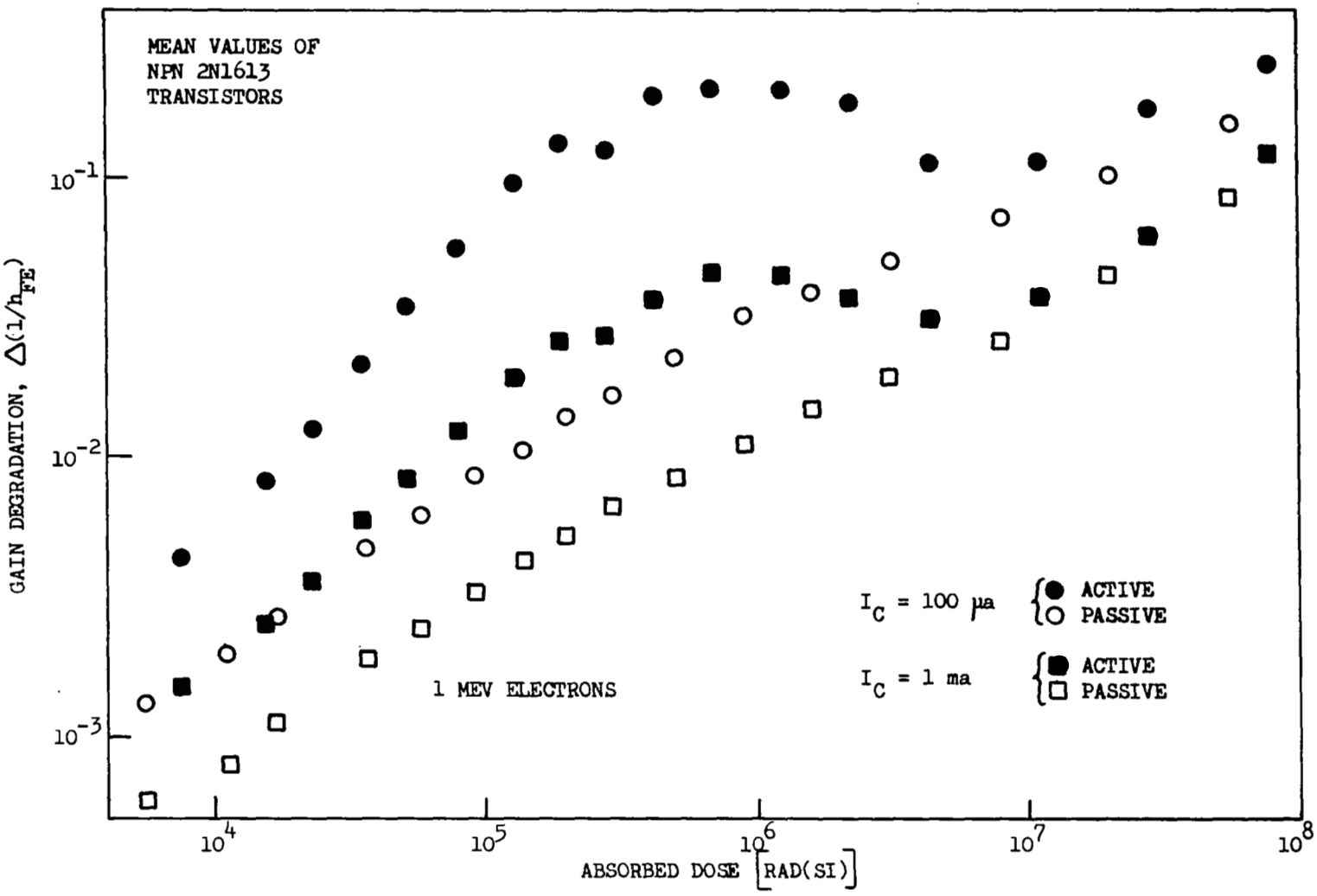

Figure 83. Comparison of Passive and Active Nonlinear Damage

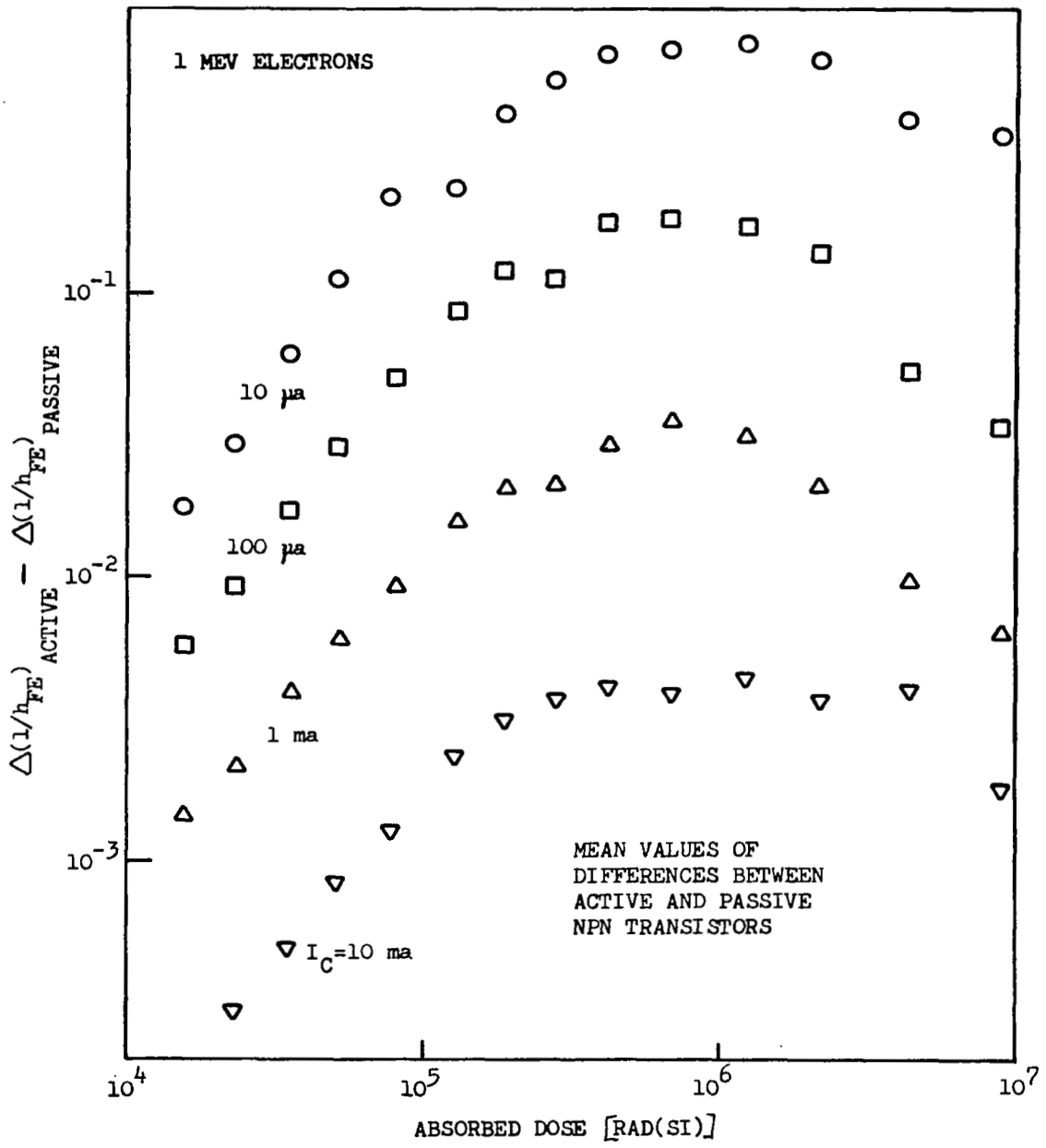

Figure 84. Difference Curves for Active Bias Effect

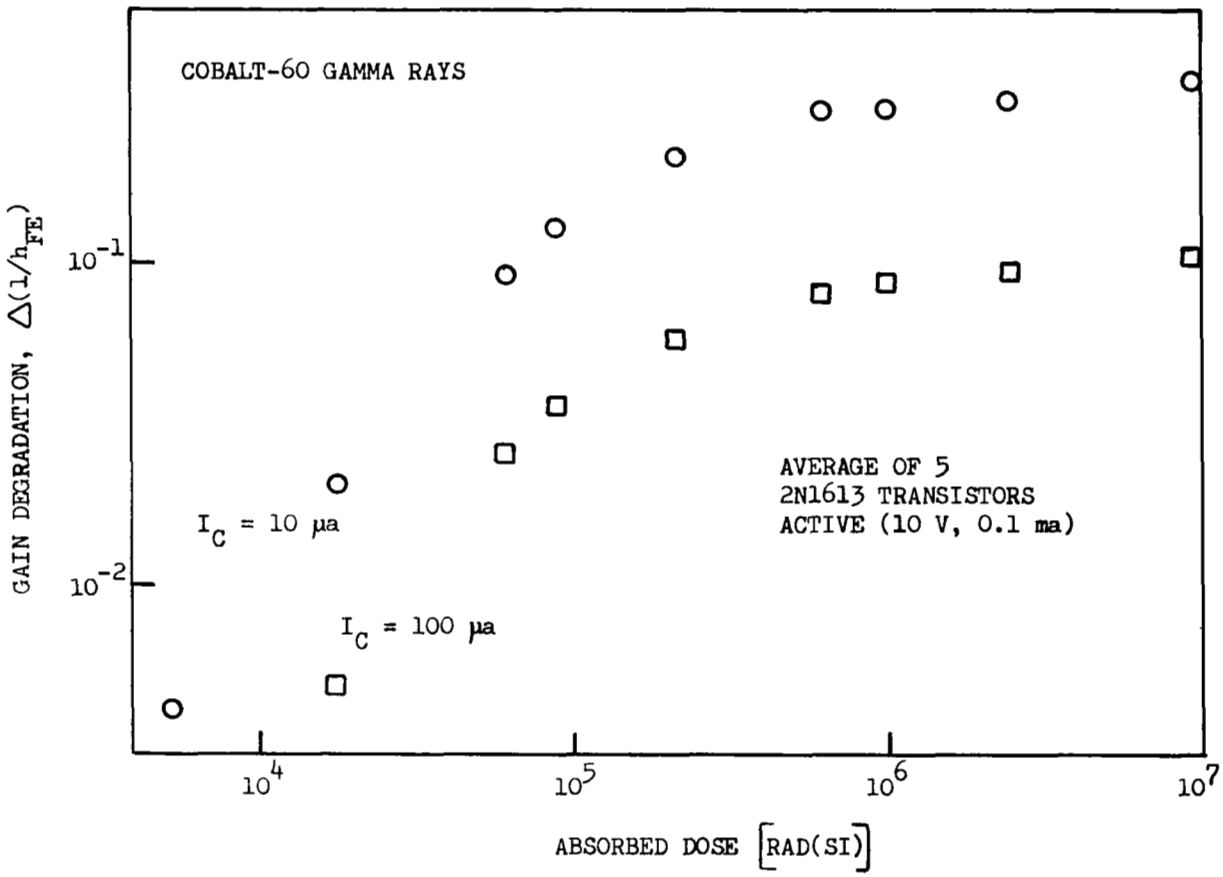

Figure 85. Nonlinear Gamma Damage to Active Devices

tron rates were much higher than gamma rates (see Sections 2.2.1 and 2.2.2). Equivalent amounts of absorbed dose from gamma rays and electron caused equivalent damage in transistors exposed passively (Figure 50). The lack of rate effects for passive transistors was established by inhouse Boeing tests, however rate effects on active devices should be studied in some detail.

The steeper dependence of $\Delta 1/h_{FE}$ on fluence or dose for active devices as opposed to passive generally would require a value of X>1 for the power law assumption of equation 12 (Section 2.3.3). Because of the limited number of devices tested and the obvious importance of statistical spread no attempt will be made at this time to fit active devices to an empirical formula such as that developed earlier in equation 19. Indications are that again a formulation using relative gain loss would be best (see Section 2.3.3) since correlations between Δh_{FE} and h_{FE_i} do appear to be present for active devices as well as passive. Figure 86 shows a fairly good correlation (rank coefficient of 0.89) for active 2N1613 transistors.

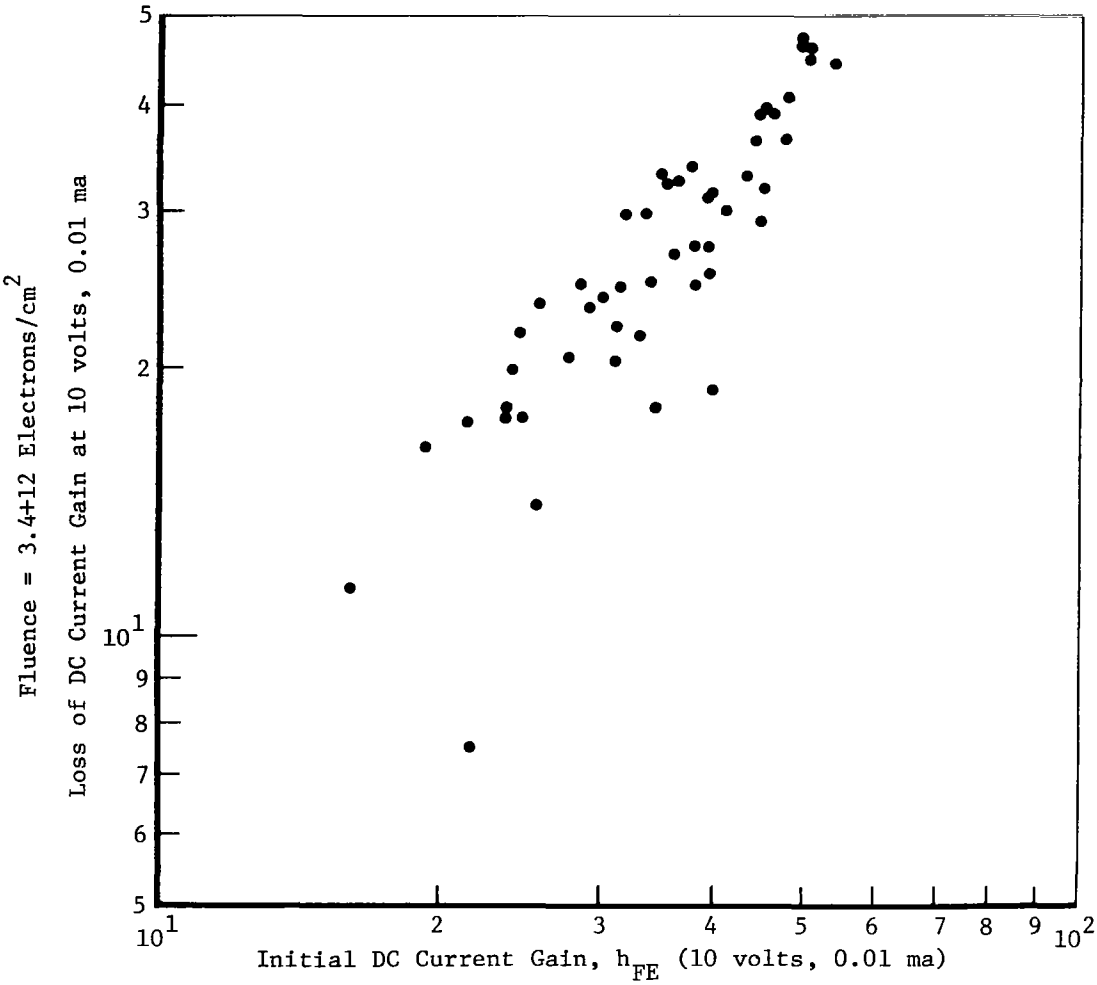

Figure 86: CORRELATION OF GAIN LOSS WITH INITIAL GAIN (2N1613 ACTIVE)

2.4.2 Multifactor Experimental Design

In order to investigate whether interactions between operating current, bias voltage, and fluence affect the radiation-induced damage observed in transistors, an experiment was designed to measure the effects of these factors both singly and in combination. A second-order model with central composite design based upon the work of Box and Hunter (Ref. 19) was chosen. This approach assumes that the significance of the interdependence of factors can be examined in a precursory manner by expressing damage as a second-order polynomial in current, I , voltage, V, and fluence, Φ.

$$\frac{\Delta h_{FE}}{h_{FE_i}} = C_o + C_1 I + C_2 V + C_3 \Phi + C_4 I^2 + C_5 V^2 + C_6 \Phi^2 + C_7 IV + C_8 I\Phi + C_9 V\Phi \qquad (20)$$

The set of coefficients [C] is chosen to give a minimum least-squares error fit to the observed data.

By suitable selection of the measurement points (I, V, Φ), the least-squares equations can be greatly simplified (Ref. 21). Since there are three variables of interest in this case, a suitable design model will take the form of a cube.

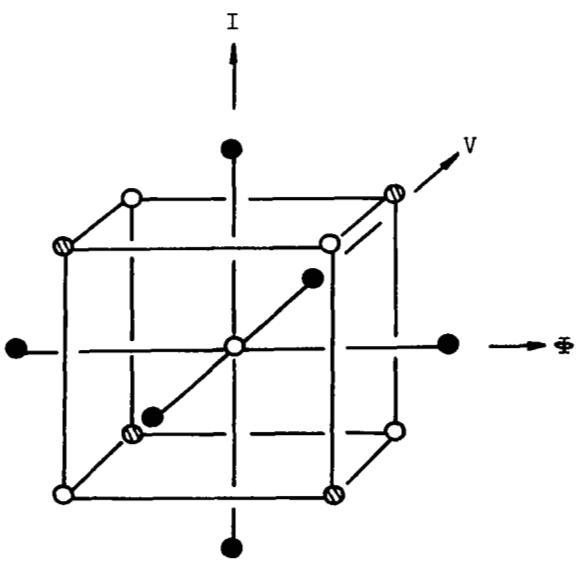

Central composite design in three dimensions

A minimum of twenty measurements must be made for each experiment: eight measurement points lie at the corners of the cube; six points lie along the axes; six measurements are made at the center of the cube. If the variables are normalized so that the center of the cube lies at (o, o, o) and one corner lies at (1, 1, 1) in the normalized coordinate system, then the measurement points on the axes lie at the points ($\pm$ 1.68, o, o), (o, $\pm$ 1.68, o), and (o, o, $\pm$ 1.68). The values used for current, voltage, and fluence are listed in Table 10. These electrical conditions were dictated by symmetry requirements on the Latin Cube computer analysis described in the proposal document D2-125398-1 (Ref. 1). Test circuitry to provide these operating conditions were designed and fabricated as shown in Figure 87. Five devices of a given type were specified at each bias condition. Two each were taken from batch number 1, 2 each from batch number 2, and 1 each from batch number 3.

An analysis of variance table was constructed to measure the fit of the polynomial and the adequacy of the model. Since the component of the residual due to lack of fit was comparable in magnitude to the component due to experimental error, we can conclude that the variability of data about the polynomial is similar to that which is expected due to experimental errors alone.

Table 10. Design Matrix

Normalized Coordinates*			True Values			
i	v	ø	I_C (ma)	V_{CB} (volts)	Φ_{NPN} (e/cm^2)	Φ_{PNP} (e/cm^2)
-1	-1	-1	2.2	5.0	9.97×10^{11}	2.46×10^{12}
1	1	-1	7.8	15.0	9.97×10^{11}	2.46×10^{12}
1	-1	1	7.8	5.0	2.18×10^{12}	2.00×10^{13}
-1	1	1	2.2	15.0	2.18×10^{12}	2.00×10^{13}
0	0	0	5.0	10.0	1.51×10^{12}	9.21×10^{12}
0	0	0	5.0	10.0	1.51×10^{12}	9.21×10^{12}
1	1	1	7.8	15.0	2.18×10^{12}	2.00×10^{13}
-1	-1	1	2.2	5.0	2.18×10^{11}	2.00×10^{12}
-1	1	-1	2.2	15.0	9.97×10^{11}	2.46×10^{12}
1	-1	-1	7.8	5.0	9.97×10^{11}	2.46×10^{12}
0	0	0	5.0	10.0	1.51×10^{12}	9.21×10^{12}
0	0	0	5.0	↓	↓	↓
-α	0	0	.3			
α	0	0	9.7	↓		
0	-α	0	5.0	1.6		
0	α	0	↓	18.4		
0	0	-α		10.0	3.24×10^{11}	3.64×10^{13}
0	0	α		↓	3.37×10^{12}	3.32×10^{12}
0	0	0			1.51×10^{12}	9.21×10^{12}
0	0	0	↓	↓	1.51×10^{12}	9.21×10^{12}

*$\alpha = 1.68$

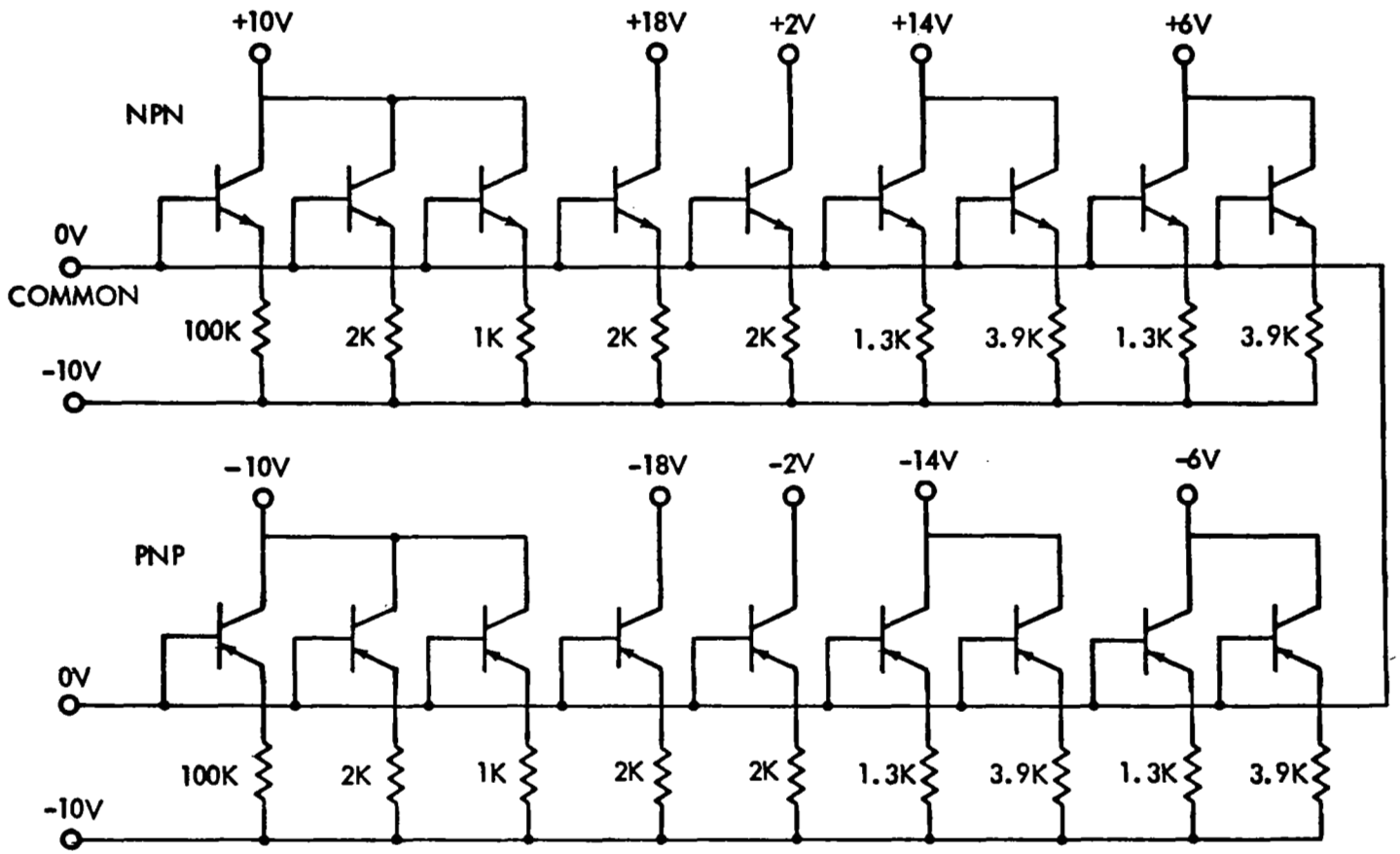

Figure 87. Test Circuitry for Transistor Biasing

In Latin Cube space coefficients can be evaluated for equation (20) using normalized coordinates in Table 10.

$$\Delta h_{FE}/h_{FE_i} = B_o+B_i i+B_v v+B_\phi \phi+B_{i^2} i^2+B_{v^2} v^2+B_{\phi^2} \phi^2+B_{iv} iv+B_{i\phi} i\phi+B_{v\phi} v\phi \qquad (21)$$

The magnitude of the coefficients in coordinate space indicate the relative importance of each term. Differences in evaluation of B_i were noted as shown in Table 11.

Table 11. Evaluation of B_i, B_v and B_ϕ

Transistor Type	Current of Gain Measurement	Injection Level During Exposure	B_i	B_v	B_ϕ
npn 2N1613	I_C = 10 μa	See Table 10	-.0001	+.054	+.136
pnp 2N1132	I_C = 10 μa	See Table 10	-.0004	+.016	+.171
npn 2N1613	Bias Conditions of Table 10	See Table 10	-.065	+.015	+.042
pnp 2N1132	Bias Conditions of Table 10	See Table 10	-.047	+.011	+.115

The B_i values in Table 11 indicate that if a fixed collector current is used to measure gain then there is no significant dependence of gain loss on injection current (from 0.3 to 9.7 ma). If, however, gain is measured at the same collector current as the injection level during exposure then there is a significant dependence on measurement current (for the range from 0.3 to 9.7 ma). Current gains were measured at a fixed collector to base voltage (V_{CB} = 10 volts). The magnitude of the values of B_v in Table 11 indicate that there is a dependence of $\Delta h_{FE}/h_{FE_i}$ on the voltage at which devices are biased during exposure (for the range of 1.6 to 18.4 volts). This dependence is weaker than that due to collector current at which gain was measured. The strongest dependence in general was upon electron dose as indicated by the magnitude of B_ϕ values. Negative values for B_i indicate (as was expected) greater damage for gain at lower measurement currents. Positive values of B_v and B_ϕ indicate greater damage for larger bias voltages applied during

exposure and for high levels of radiation exposure, respectively. Average values for the cross terms were as follows:

$$B_{v\phi} = +.008,\ B_{i\phi} = -.0024,\ B_{ie} = +.0028$$

The magnitude of the values of cross terms indicates that, although interdependences between I, V, and may modify damage, in general they are relatively insignificant between the limits of: 013 to 9.7 ma, 1.6 to 18.4 volts, 3×10^{11} to 3×10^{12} e/cm^2 (npn), and 3×10^{11} to 3×10^{13} e/cm^2 (pnp).

The Latin Cube normalized coordinate equation (Eq. 21) can be transformed to real space.

$$h_{FE}/h_{FE_i} = A_o + A_I I_C + A_V V_{CB} + A \quad + A_{I^2} I_C^2 + A_{V^2} V_{CB}^2 \qquad (22)$$
$$+ A_{2}{}^{2} + A_{IV} I_C V_{CB} + A_I I_C \quad + A_V \quad V_{CB}$$

Using the real coordinate values of Table 10 the dependence on each of the real variables separately (I_C, V_{CB}, and) can be determined about the center point of the cube (I_C = 5 ma, V_{CB} = 10 volts and = 1.5×10^{12} e/cm^2 for npn transistors). An example is now worked out for the I_C dependence of npn transistors.

$$\Delta h_{FE}/h_{FE_i} = \begin{cases} 0.19 - .054\ I_C + .004(10V) + 2.44\times10^{-13}(1.5\times10^{12}\ e/cm^2) + .004\ I_C^2 \\ + .0002(10V)(10V) - 3.7\times10^{-26}(1.5\times10^{12}\ e/cm^2)\ (1.5\times10^{12}\ e/cm^2) \\ + .0009(10V\ I_C + 1.3\times10^{-15}(1.5\times10^{12}\ e/cm^2)\ I_C \\ + 1.4 \times 10^{-15}(10V)\ (1.5 \times 10^{12}\ e/cm^2) \end{cases} \qquad (23)$$

(The real coefficients computer evaluated for equation 23 can be deciphered from the terms above.)

This reduces to

$$h_{FE}/h_{FE_i} - \frac{1}{2}\ 1 - 0.1\ I_C + 0.01\ I_C^2 \qquad (24)$$

for npn transistors (for V_{CB} and ● space from 1.6 to 18.4 volts, 3×10^{11} to 3×10^{12} e/cm^2). The dependence on I_C is in general agreement with $\Delta 1/h_{FE} = \text{const } I_C^{(1/n - 1)}$ as discussed in section 2.3.1 as well as typical results of figure 20 shown in that section. As seen from the last three terms of equation 23, the interdependence coefficients A_{IV}, $A_{V\emptyset}$ and $A_{I\Phi}$ are small but interesting (see Φ dependence on I_C plots of figure 20).

The dependence of damage on collector to base voltage applied during exposure, V_{CB}, reduces to

$$\Delta h_{FE}/h_{FE_i} \simeq 1/3 \left[1 + .03\ V_{CB} + .0003\ V_{CB}^2\right] \tag{25}$$

for npn transistors (for I_C and Φ space from 0.3 to 9.7 ma and 3×10^{11} to 3×10^{12} e/cm^2).

The dependence of damage on electron fluence, Φ, reduces to

$$\Delta h_{FE}/h_{FE_i} \simeq 1/8 \left[1 + 2 \times 10^{-12}\ \Phi - 0.3 \times 10^{-24}\ \Phi^2\right] \tag{26}$$

for npn transistors (for I_C and V_{CB} space from 0.3 to 9.7 ma and 1.6 to 18.4 volts respectively). Equation 26 in general fits the fluence dependence described in section 2.3.3. A further than second order polynomial expansion in Φ might well have approximated the empirical form for damage discussed in section 2.3.3. The series expansion for tanh $k\Phi$ is

$$\tanh k\Phi = k\Phi - \frac{(k\Phi)^3}{3} + \frac{2(k\Phi)^5}{15} \tag{27}$$

The general form of each of the pnp equations for dependence on I_C, V_{CB}, and ● were similar to equations 24 through 26.

2.4.3 Pulsed h_{FE} Tester Techniques

To lessen the time required between irradiation and h_{FE} measurement, thus making feasible the taking of more data points and lessening any annealing which might occur during a prolonged delay, a plan was devised to make in situ h_{FE} measurements. Two of the ten transistors of each type tested were actively biased during 15 MeV proton and 2.9 MeV electron irradiation. The circuitry for these transistors was a simple emitter follower circuit with the emitter taken to $\pm$ 10 volts (depending on the transistor type) through a one-megohm resistor, the base taken to ground (common to the emitter and collector supplies) through a 100 kilohm resistor and the collector taken to $\mp$ 10 volts (depending on the transistor type). This curcuit biased the transistors to conduct approximately ten microamperes of emitter current. Emitter and base current (and thus h_{FE}) could be monitored continually by measuring the voltage drop across the emitter and base resistors which were mounted external to the scattering chamber. The remaining eight of the ten transistors of each type were passive during irradiation and h_{FE} was measured using the pulsed h_{fe} test set up shown in Figure 88. The emitter and base of each passive transistor was switched inside the scattering chamber using a leadex switch which was controlled externally. The transistor under test was pulsed with a constant emitter current (10, 100 μa, 1 or 10 ma) pulse and a corresponding base current which was monitored to determine the transistor h_{FE}. A pulse width of 300 microseconds was used to provide a pulse width which was long compared to the rise and fall times of the system thus permitting the system to reach DC test conditions while allowing a minimum of junction heating.

Consider the operation of the h_{FE} tester with the switches in positions shown in Figure 88 (NPN). A negative emitter pulse of approximately 10 volts (the zener voltage of the 1N825 plus the IR drop of the zener current across the 500 ohms base resistor) drives the emitter current source generator which supplies a constant current pulse that is determined by the value of the emitter resistor (550 K for 10 μa of current) in the current source. The base current driver amplifier is an operational amplifier with the transistor under test in the feedback loop. When the current source is pulsed, the

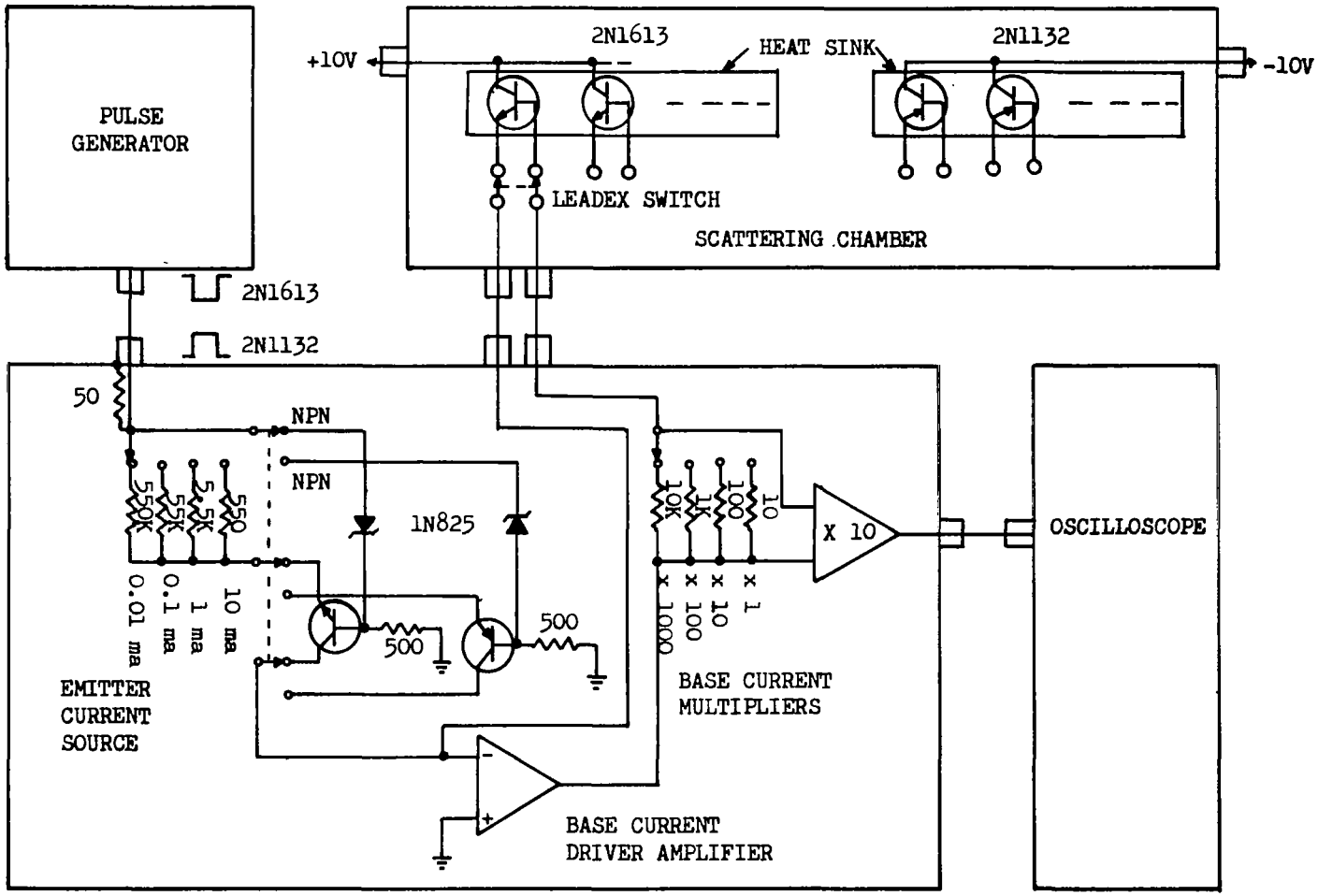

Figure 88. Pulsed h_{FE} Test Set Up

summing junction or inverting input (indicated (-) in Figure 88) of the base current driver amplifier is driven negative which drives the output positive turning on the transistor under test. The driver amplifier continues to turn-on the transistor under test until sufficient base drive is provided for the transistor under test to conduct the full 10 μa of current which is then limited to this value by the emitter current source. At this time the inverting input has been forced to assume the potential of the non-inverting input (ground) and the emitter of the transistor under test is at a virtual ground. Thus the V_{CE} is simply the 10 volts applied to the collector. The base drive current necessary to force the transistor under test to conduct 10 μ a of emitter current is measured by amplifying the voltage dropped across the base current sampling resistor and observing the voltage pulse on an oscilloscope. The sensitivity of the base current measuring circuit is changed by switching to different sampling resistors. Figure 89 is a photograph of the actual test set up.

The transistors in the scattering chamber were press fitted into a heat sink which was cooled by tap water. The heat sink temperature was monitored using chromel-constantan thermocouples. The temperature varied no more than three degrees centigrade from the beginning to the end of either the 2.9 MeV electron or 15 MeV proton tests. In terms of temperature variation per decade increment of fluence, the temperature varied no more than one half of one degree centigrade and the change in base current due to the temperature variation was small compared to the change induced by the radiation.

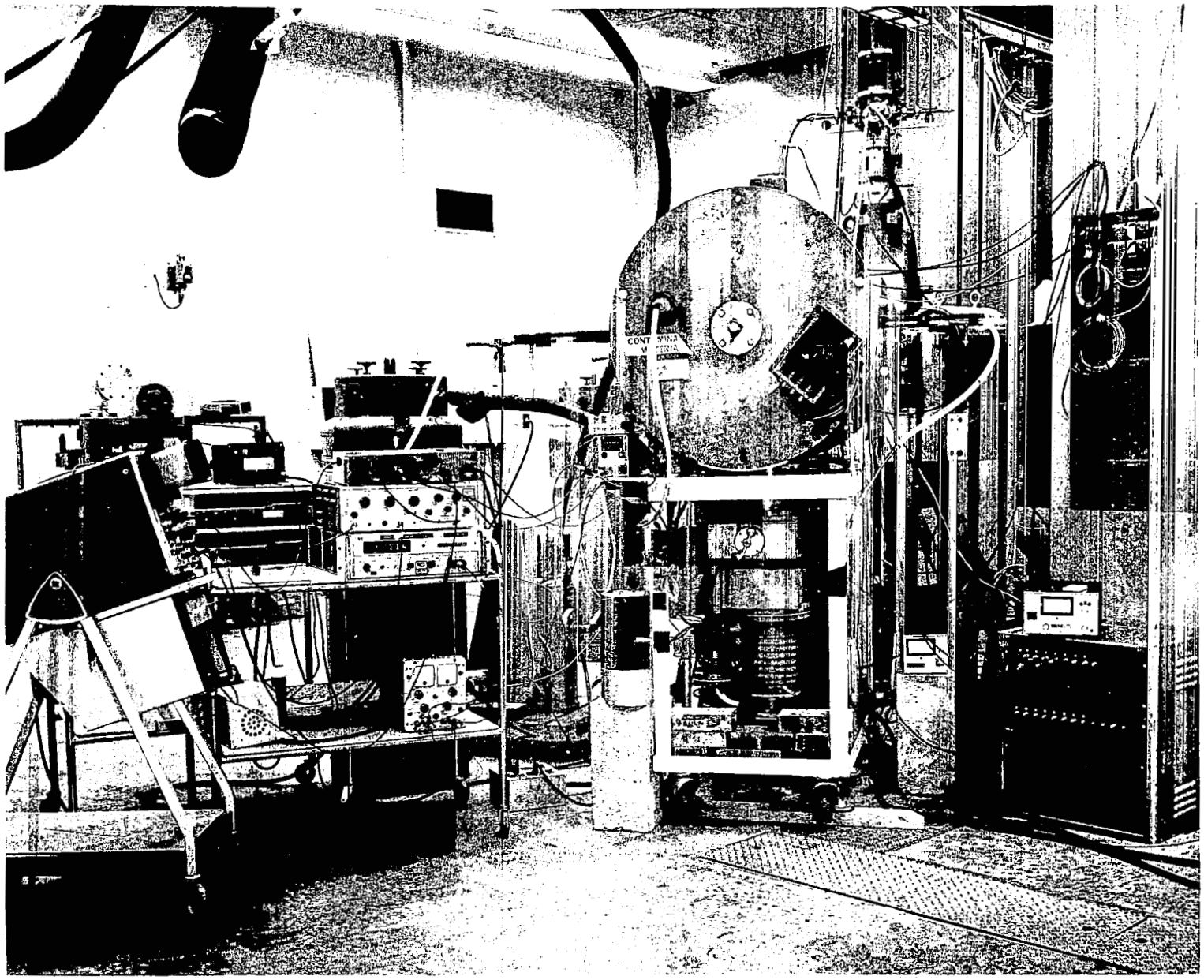

Figure 89: ACTIVE MEASUREMENT EQUIPMENT

2.4.4 Anomalous Bias Dependence for Proton Damage

PNP transistors, under active bias during radiation exposure, generally suffer less damage than when they are passive during irradiation (as indicated in section 2.4.1 for electron exposure). The results of proton exposure of pnp transistors were similar to electron damage both in magnitude for equivalent absorbed dose (see radiation equivalence section 2.3.4) and in the relative damage sensitivity between active and passive devices. That result is indicated in Figure 90. (The dashed line of Figure 90 indicates the slight deviation between I_E and I_C gain measurements at damage greater than $\Delta(1/h_{FE}) = 0.1$.

NPN transistors, under active bias during exposure generally show greatly enhanced damage over that of passive devices (Ref. 9) (also discussed in section 2.4.3 for gamma rays and electrons). When npn transistors were exposed to 15 MeV protons, however, the nonlinear gain degradation was greater than that expected on the basis of ionization equivalence. Proton damage to passive npn transistors was actually closer to the enhanced electron damage observed on active npn transistors while devices operated at 10 volts V_{CB} and 10 μamps I_E during exposure were actually damaged less than passive devices in the same exposure test. This result is apparent from a comparison between proton test results of Figure 91 and the active and passive electron results in Figures 82 and Figure 18, respectively. The significance of these results will be discussed further in section 2.6 when the desirability and feasibility of combined testing is discussed.

The anomalous dependence on bias conditions for proton damage to npn transistors was not expected and should be studied further in order to provide insight into damage mechanisms (the interplay between the creation of interface sites and charge buildup - see section 2.3.5). It appears that a detailed bias study (different injection levels and voltages during exposure) ought to be conducted for proton effects as has already been performed for electron (section 2.4.2) and gamma exposure (Ref. 9).

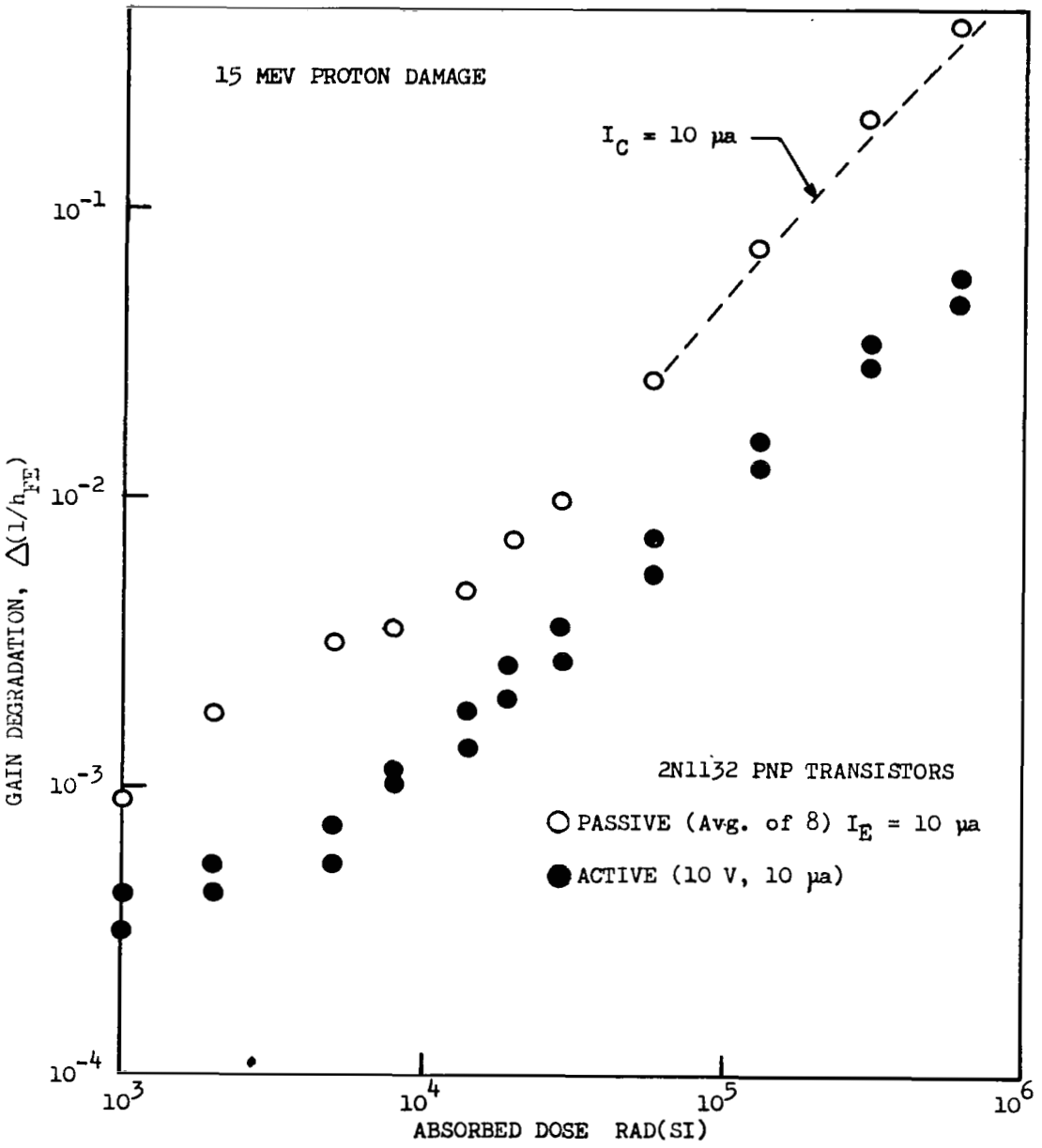

Figure 90. Bias Dependence for Proton Damage to 2N1132 Transistors

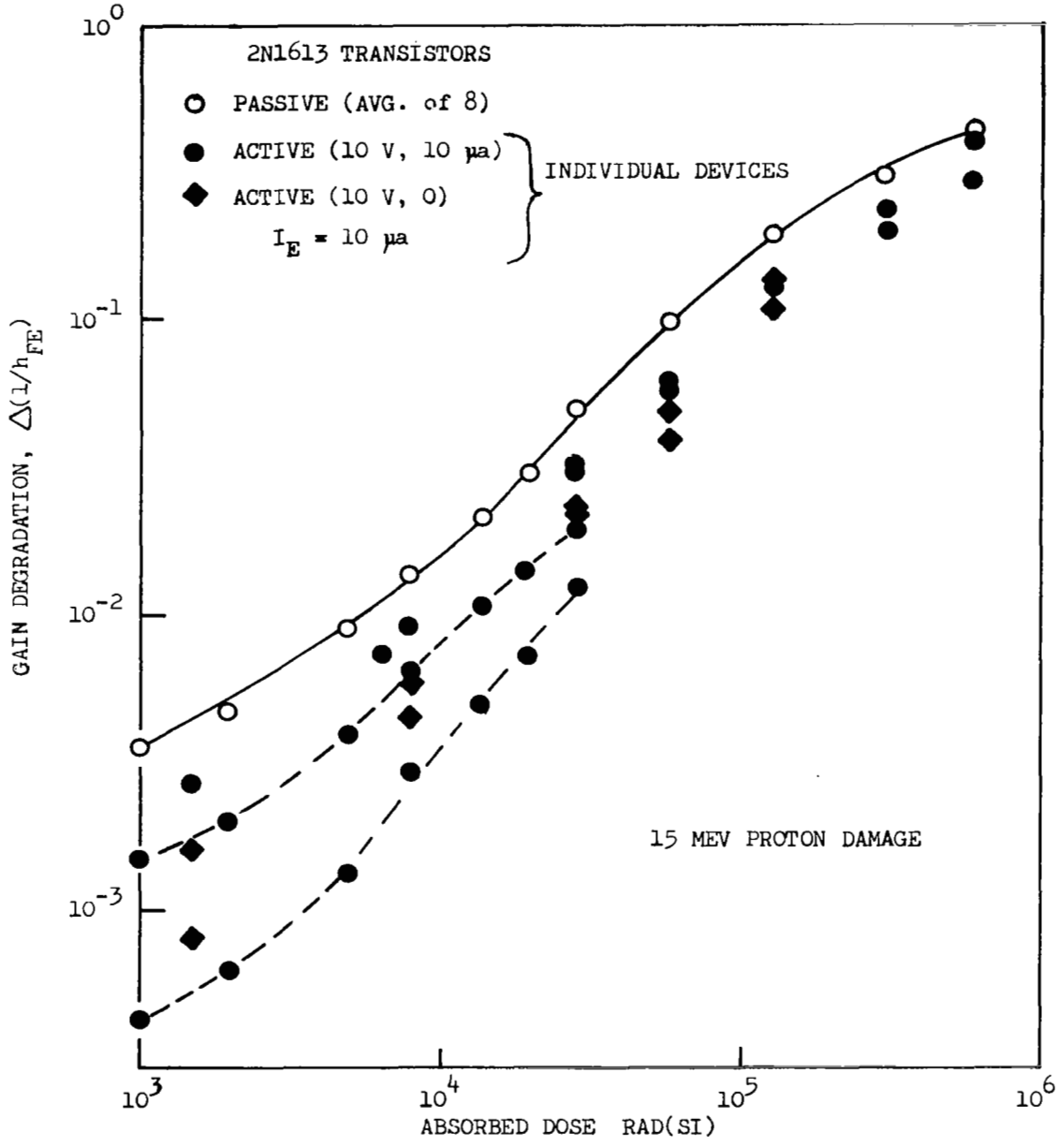

Figure 91. Anomalous Bias Dependence for Proton Damage 2N1613 Transistors

2.5 UPDATING OF DISPLACEMENT EQUIVALENCES

Efforts to update displacement equivalence values under this contract included: (1) The remeasurement of transistors heavily irradiated by electrons under an earlier contract, NAS5-9578 (Ref. 2), (2) the extension of gamma ray irradiation of transistors exposed to lower levels under contract NAS5-9578, and (3) the extension of 15 MeV proton testing under this contract in place of combined electron and proton tests (to be discussed in more detail in section 2.6).

2.5.1 Remeasurement of Transistors (Irradiated in Phase I)

Neutron studies (Ref. 22) have shown that displacement damage can have a weak dependence on collector current at which the common emitter current gain is measured. This phase II study of nonlinear damage did not include a program of extended electron testing to linear damage regions where displacements dominate. Thus in order to verify that displacement equivalence values of phase I tests (at I_C = 10 ma) were valid for other currents, further analysis of heavily damaged devices was conducted.

The base transit times, t_b, at I_E = 2.8 ma and 5.0 ma were determined for transistors tested in the phase I program in order to accomplish the following specific objectives:

1. Obtaining damage constants at selected values of I_E which then furnished equivalence values between the different types of radiation. Base transit times at the same I_E values were necessary for the normalization of the $\Delta(1/h_{FE})$ versus Φ curves.

2. Separation of the nonlinear damage from the linear type at three collector currents (2.8 ma, 5.0 ma, 10 ma). Again, normalization of the $\Delta(1/h_{FE})$ versus Φ curves was required, which in turn required the knowledge of the t_b (2.8 ma), t_b (5.0 ma), t_b (10 ma) data.

Since during the previous contract (NAS5-9878) only the t_b (10 ma) values were required hence known, the t_b (2.8 ma), t_b (5.0 ma) values have had to be determined. Actually, in order to obtain self-consistent data the t_b (10 ma) values were redetermined as well. Needless to say, one could not predict the relation between the different t_b (I_E) values. t_b (2.8), t_b (5.0),

t_b (10) might or might not have been different from each other for transistors of a given type. Transistors within a given type were expected to behave similarly.

The following program was carried out on all the transistors involved to obtain reasonably good consistent t_b (2.8), t_b (5.0), t_b (10) data:

1. h_{FE}(db) data were measured at room temperature with Fairchild Model 7515S h_{FE} tester at many different current values. (Typical set: I_E = 0.7, 0.8, 1.0, 1.2, 1.6, 2.5, 5.0, 10, 20, and 40 ma.) The frequency of measurements, f, was selected sufficiently low to produce reasonably high gain even at low currents in order to improve the relative accuracy. Frequency was usually 30 MHz.

2. A computer program determined the gain-bandwidth frequency, f_T, for each device at all currents from the h_{FE}(db) versus log frequency plots in a routine manner (i.e., by drawing a 6 db/octave line from the measured h_{FE}(db) point and reading the frequency at the intersection of this line with the 0 db line).

3. From the tabulated $f_T(I_E)$ data for each transistor, the computer prepared $1/f_T$ versus $1/I_E$ plots.

4. t_b was determined from the f_T^{-1} versus I_E^{-1} plots in the usual manner. However, the straight line which was drawn across the "low" current points to give the presumably current independent t_b (by the intersection of the f_T^{-1} axis) was <u>handdrawn</u> and not computer constructed. This step was done on each plot individually after careful examination of the position of the points. (t_b data obtained by using computer constructed "least-square" fitted straight lines were generally useless.)

Plots of the type discussed are shown in Figures 92 and 93. Interestingly, transistor 2N1711 exhibits the "Kirk" effect, i.e., t_b increases with current at high current values.

As expected, there was found to be no set rule to decide beforehand if t_b (2.8), t_b (5.0), t_b (10) differed from each other. In general some transistors did exhibit common values of t_b at two or more I_E values, however many others showed that t_b must be determined separately for each I_E value.

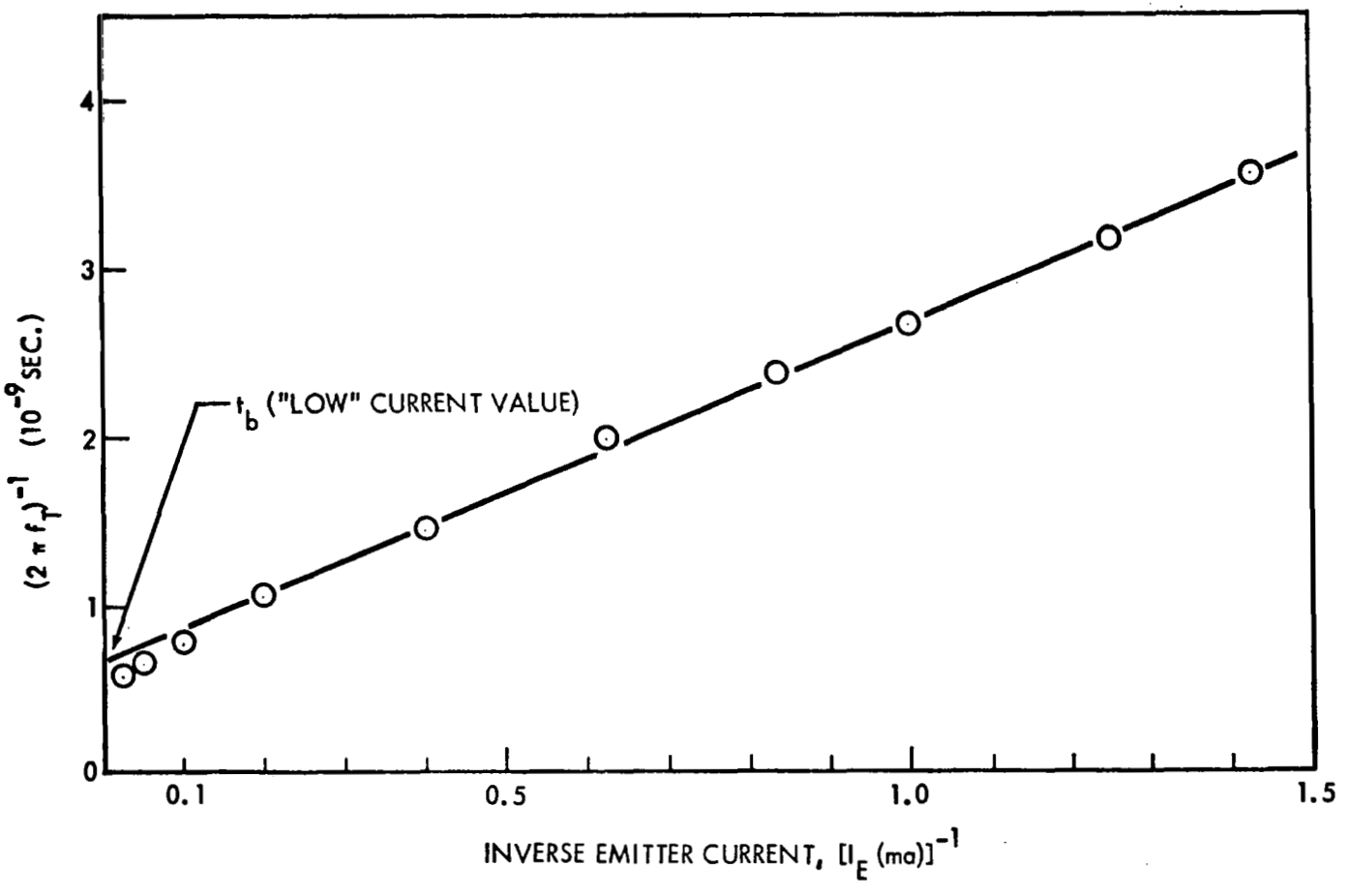

Figure 92. Determination of Base Transit Time From $(2\pi f_T)^{-1}$ Versus (I_E^{-1}) Plot (2N1132)

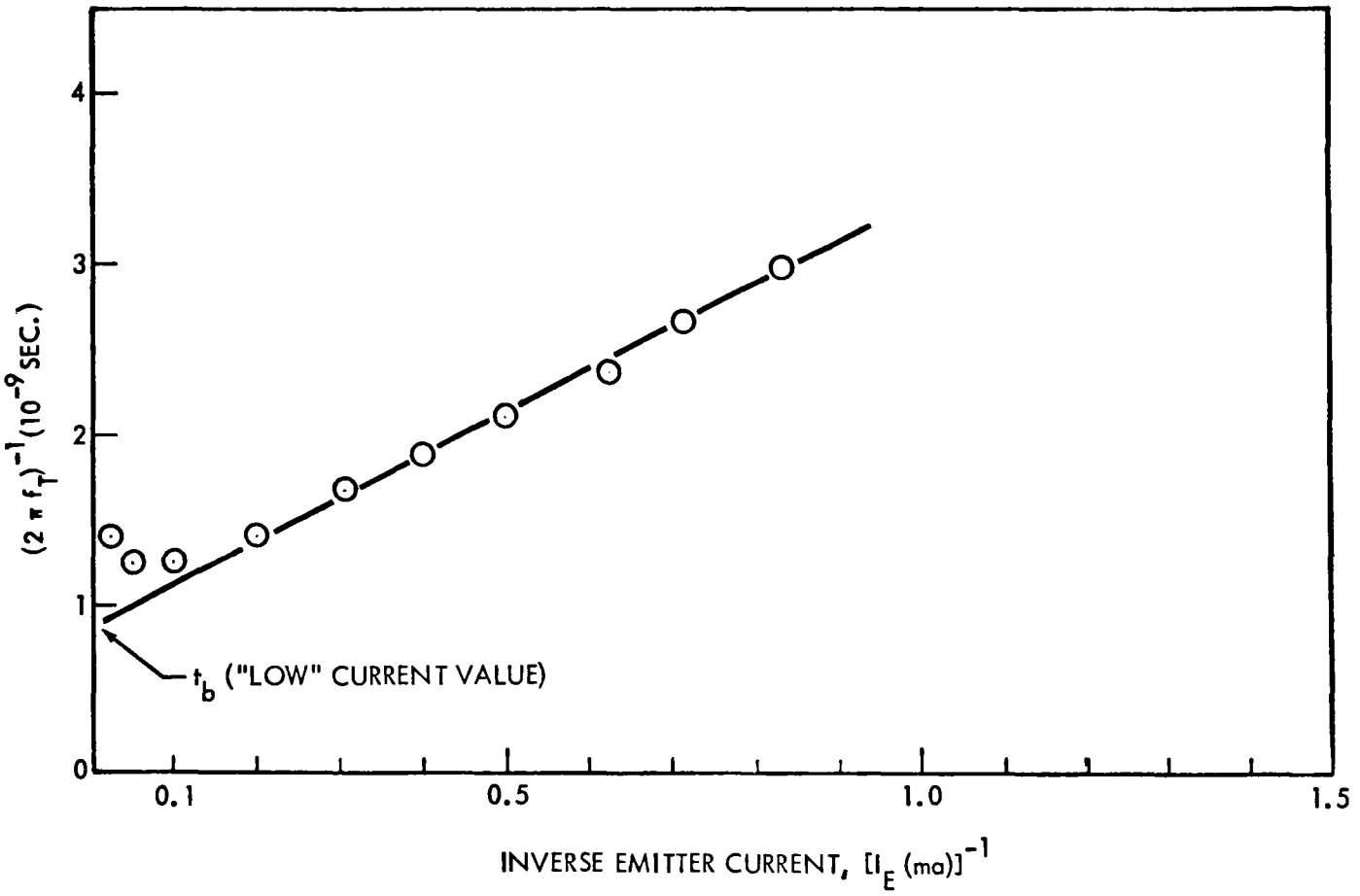

Figure 93. Determination of Base Transit Time From $(2\pi f_T)^{-1}$ Versus (I_E^{-1}) Plot (2N1711)

A computer analysis of old data (NAS5-9578) yielded damage constants at I_E = 2.8 ma (Tables 12 and 13) from which equivalence values between the different types of radiation can be determined. New measurements of base transit time at 2.8 and 10 ma were used in this work. Comparison of these equivalence values with those originally obtained at 10 ma showed no significant difference between the two. It is significant to note that these equivalence values were not significantly dependent on emitter current between 2.8 and 10 ma thus a broader validity of the equivalence concept is verified.

Further data on the validity and updating of damage constants and radiation equivalence values for displacements will be discussed as extended gamma ray test results (section 2.5.2) and extended 15 MeV proton tests (section 2.5.3). Equivalence values in section 2.5.3 will reflect the revised displacement values for cobalt-60 gamma ray tests and for 15 MeV proton tests.

Table 12. Transistor Damage Constants for Proton Tests (I_E = 2.8 ma)

Freq f_N (Mc)	Transistor Type	Test 24 1 MeV		Test 26 8-17 MeV		Test 27 100 MeV	
		K' $(\text{protons/cm}^2)^{-1}$	K_D $\text{Mc}(\frac{\text{protons}}{\text{cm}^2})^{-1}$	K' $(\text{protons/cm}^2)^{-1}$	K_D $\text{Mc}(\frac{\text{protons}}{\text{cm}^2})^{-1}$	K' $(\text{protons/cm}^2)^{-1}$	K_D $\text{Mc}(\frac{\text{protons}}{\text{cm}^2})^{-1}$
87.9	2N1613	7.0×10^{-14}	6.2×10^{-12}	3.8×10^{-14}	3.3×10^{-12}	9.0×10^{-15}	7.9×10^{-13}
109.4	2N1711	3.2×10^{-14}	3.5×10^{-12}	1.9×10^{-14}	2.1×10^{-12}	2.5×10^{-15}	2.7×10^{-13}
505.3	2N2219	7.2×10^{-15}	3.6×10^{-12}	4.2×10^{-15}	2.1×10^{-12}	8×10^{-16}	4.0×10^{-13}
213.3	2N1132	1.7×10^{-14}	3.6×10^{-12}	2.2×10^{-14}	4.7×10^{-12}	4×10^{-15}	8.5×10^{-13}
303.6	2N2801	2.1×10^{-14}	6.4×10^{-12}	2.2×10^{-14}	6.6×10^{-12}	3.3×10^{-15}	1.0×10^{-12}
271.8	2N2411	4.5×10^{-15}	1.2×10^{-12}	6.8×10^{-15}	1.8×10^{-12}	1.8×10^{-15}	4.9×10^{-13}

Table 13. Transistor Damage Constants for Electron Tests (Only for Linear Displacement Component) (I_E = 2.8 ma)

Freq f_N (Mc)	Transistor Type	Test 21 2.0 MeV		Test 22 1.3 MeV		Test 23 0.53 Mev	
		K'	K_D	K'	K_D	K'	K_D
87.9	2N1613	4.8×10^{-17}	4.23×10^{-15}	2.6×10^{-17}	2.29×10^{-15}	1.7×10^{-17}	1.39×10^{-15}
109.4	2N1711	2.3×10^{-17}	2.51×10^{-15}	9.0×10^{-18}	9.8×10^{-16}	7.1×10^{-18}	7.8×10^{-16}
505.3	2N2219	5.3×10^{-18}	2.7×10^{-15}	3.3×10^{-18}	1.67×10^{-15}	2.9×10^{-18}	1.46×10^{-15}
213.3	2N1132	3.9×10^{-17}	8.3×10^{-15}	3.8×10^{-17}	8.1×10^{-15}	1.8×10^{-17}	3.8×10^{-15}
303.6	2N2801	2.8×10^{-17}	8.5×10^{-15}	2.4×10^{-17}	7.3×10^{-15}	1.8×10^{-17}	5.5×10^{-15}
271.8	2N2411	2.2×10^{-17}	6.0×10^{-15}	7.9×10^{-18}	2.1×10^{-15}	5.0×10^{-18}	1.4×10^{-15}

2.5.2 Cobalt-60 Gamma Ray Damage Constants

Four each of the following types of transistors: 2N1613, 2N1711, 2N2219, 2N1132, 2N2801, and 2N2411 were selected from phase I for extended Cobalt-60 gamma exposure. The extended exposure of these devices was started on June 2, 1967 following full characterization by the Fairchild 500 Series Transistor Tester. This characterization included: h_{FE} at a collector voltage of 10 volts and emitter currents at 10 μa, 30 μa, 100 μa, 300 μa, 1 ma, 3 ma, 10 ma, 20 ma, and 40 ma; I_{EBO} at V_{CE} of 1.0, 1.5, 2.0, 3.0, 4.0, 5.0, 6.0, and 7.0 volts; and I_{CBO} measurements for different transistor types as listed below.

2N1613 2N1711	2N1132 2N2219 2N2801	2N2411
V_{CB} (volts)	V_{CB} (volts)	V_{CB} (volts)
1.0	1.0	1.0
5.0	5.0	3.0
10.0	10.0	7.0
20.0	20.0	15.0
40.0	40.0	20.0
60.0	50.0	30.0
80.0	65.0	40.0
100.0	80.0	50.0

Transistors were recharacterized periodically until a total dose of 6×10^8 rad Si was absorbed. Dose rate information and test conditions were described in Section 2.2.2.

Increases in leakage currents due to the extended testing (6×10^7 to 6×10^8 rad Si) were not appreciable. The significant permanent changes in leakage current had occurred prior to the extended tests as indicated in Table 14 and Figure 94.

An example of the results of degradation of current gain during the extended Cobalt-60 gamma ray tests is shown in Figure 95 for passive 2N1711 transistors. The linear displacement line is shown on the plot for comparison purposes, as well as the nonlinear damage buildup at selected collector currents of 10 μa, 100 μa, 1 ma, and 10 ma for the extended tests. Earlier phase I test

Table 14. Leakage Currents for Gamma Exposure

Dose (rad Si)	0	6×10^7 r	6×10^8 r	0	6×10^7 r	6×10^8 r
V_{CB} (volts)	1.0 V	1.0 V	1.0 V	40 V	40 V	40 V
2N1613 1	0.13 nA			1.11 nA		
22		0.66 nA	1.27 nA		2.62 nA	4.22 nA
23		0.45	1.02		1.64	3.21
24		0.54	0.95		2.10	3.53
25		0.54	1.06		2.16	3.60
2N1711 1	0.05			0.30		
20		0.40	4.41		1.11	9.11
21		1.02	1.63		4.41	6.41
22		0.64	1.46		2.37	4.77
23		0.58	1.46		2.20	4.21
2N2219 1	0.01			0.25		
20		0.31	0.62		1.43	2.60
21		0.21	0.42		0.96	2.15
22		0.31	0.70		1.51	2.69
23		0.28	0.46		1.44	3.99
2N2801 1	0.15			1.19		
20		1.57	5.60		17.00	42.00
21		1.09	4.53		13.10	41.00
22		1.21	5.03		16.70	50.00
23		1.25	5.71		12.40	50.00
2N1132 1	0.06			0.22		
20		0.96	1.07		6.75	8.51
21		0.08	0.24		2.71	3.38
22		0.09	0.22		3.47	3.64
23		0.09	0.28		11.20	38.90
2N2411 1	0.40			9.75		
20		0.59	0.52		29.40	25.00
21		0.60	2.77		25.30	24.60
22		0.63	0.61		28.50	26.10
23		0.57	0.58		20.50	26.60

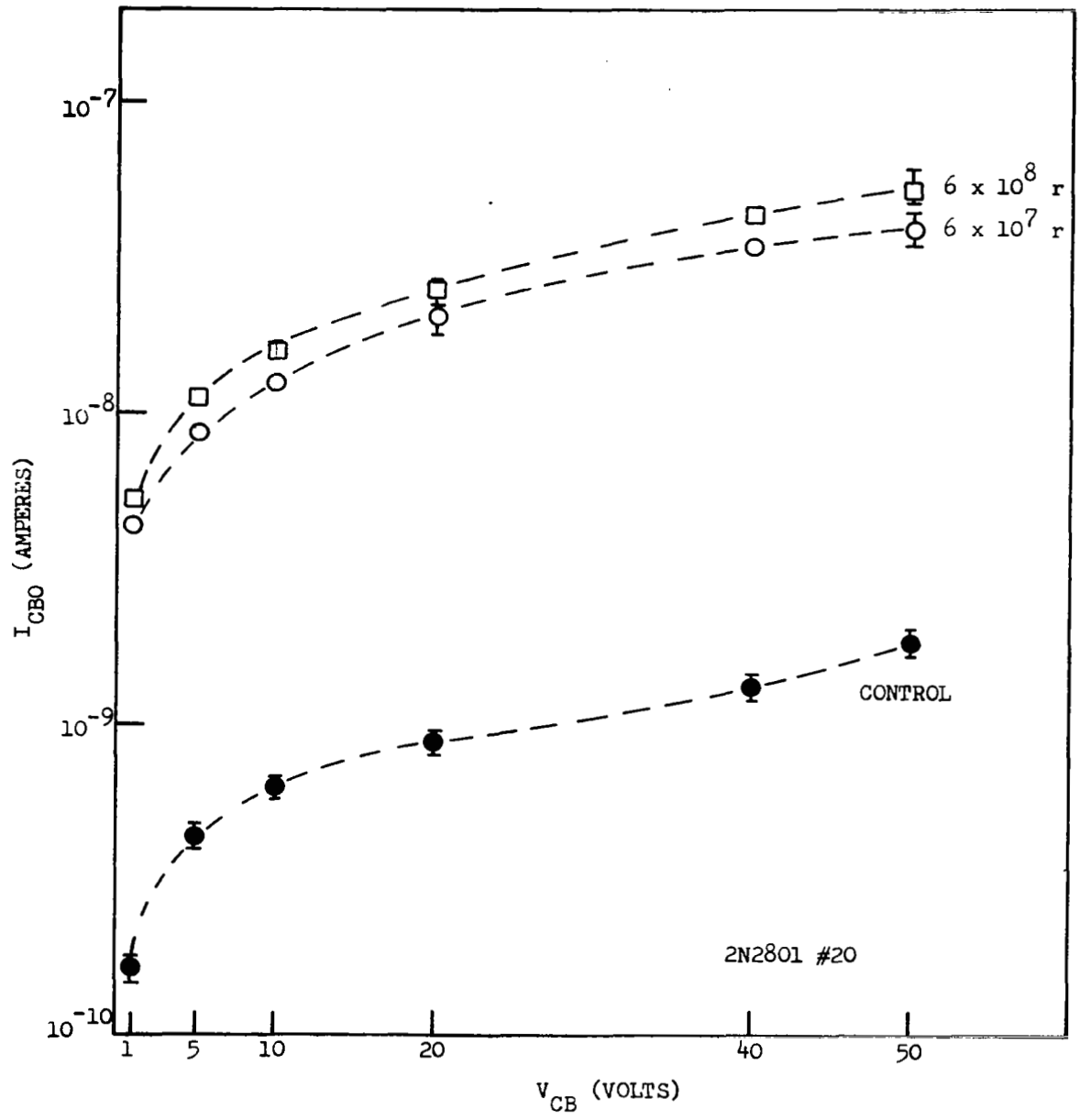

Figure 94. Increased Leakage Current as a Function of V_{CB}

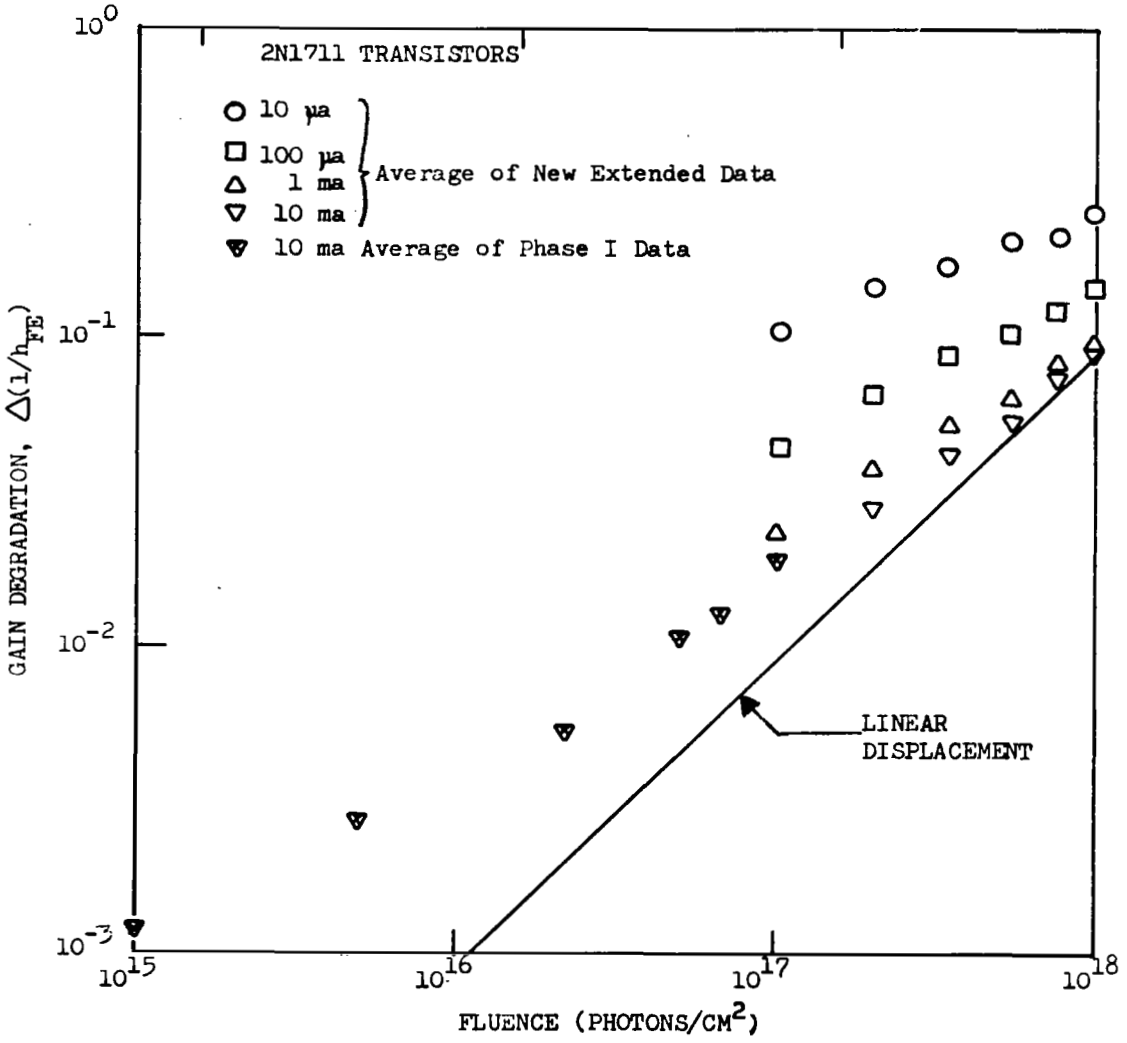

Figure 95. Extended Cobalt-60 Testing to the Linear Displacement Region

data is also shown on the figure. Linear displacement damage dominated (at 10 ma) only after the devices had suffered severe nonlinear gain degradation. Note the compression of the I_C = 10 ma and I_C = 1 ma damage curves in Figure 95 as displacement damage sets in, showing less dependence on I_C for displacement damage than for nonlinear damage.

Verification of the domination of damage by displacements (10 ma) at high levels of exposure can also be seen in Figure 96. Slope values of n = 1 indicate bulk displacement damage while the slopes of n = 1.7 are more typical of that observed for nonlinear surface effects (Section 2.3.1). From the extended tests it was evident that phase I extrapolations for Cobalt-60 gamma ray displacement damage needed significant revision. Earlier values were extrapolated from much lower levels of exposure where nonlinear damage was still dominant. A comparison of the earlier estimates and the revised damage constants from the extended tests are shown in Table 15. Even with extended exposures out to 6×10^8(rad Si) some transistor types were still dominated by nonlinear damage making extrapolation still necessary. A revised equivalence table is shown at the end of Section 2.5.3.

Table 15. Transistor Damage Constants for Gamma Ray Displacements

Transistor Type	K'		K_D	
	Phase I Estimate	Updated Phase II	Phase I Estimate	Updated Phase II
2N1613	7.1×10^{-19}	2.5×10^{-19}	6.7×10^{-17}	2.35×10^{-17}
2N1711	1.8×10^{-19}	9.0×10^{-20}	2.7×10^{-17}	1.33×10^{-17}
2N2219	5.0×10^{-20}	1.7×10^{-20}	2.2×10^{-17}	7.47×10^{-18}
2N1132	3.4×10^{-19}	1.7×10^{-19}	1.3×10^{-16}	6.74×10^{-17}
2N2801	3.0×10^{-19}	7.5×10^{-20}	9.7×10^{-17}	2.43×10^{-17}
2N2411	7.7×10^{-20}	$<5.0 \times 10^{-20}$	2.7×10^{-17}	$<2.04 \times 10^{-17}$

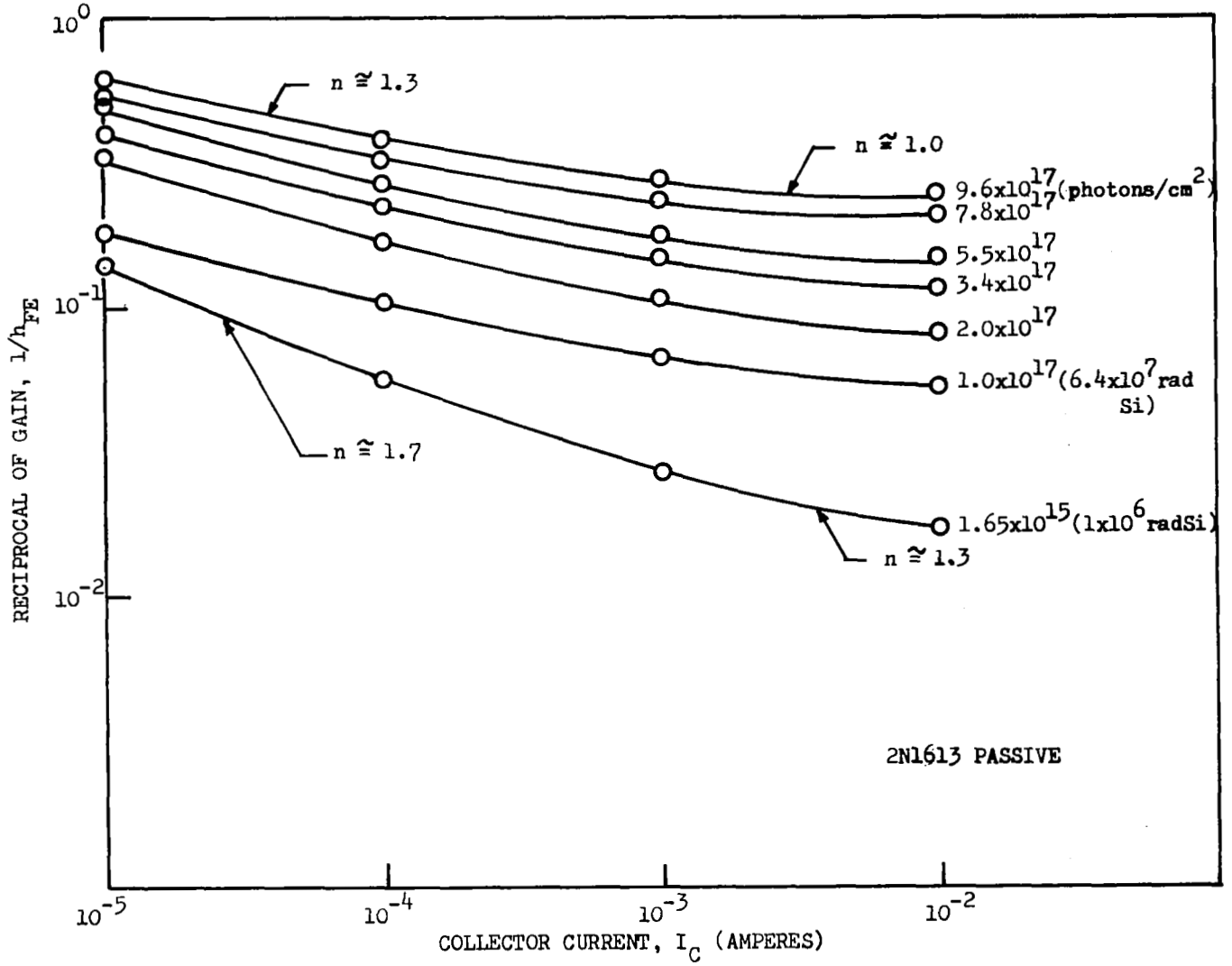

Figure 96. $\Delta 1/h_{FE}$ Versus I_C for Cobalt-60 Extended Testing

2.5.3 Extended 15 MeV Proton Testing

In the original technical proposal (Ref. 1) tests were planned to cover a wide enough proton exposure range to include damage regions dominated both by nonlinear surface effects (low level exposures) and displacement damage (high level exposures). From those tests it was planned that the relative contributions of both types of damage could be assessed. At the time of contract negotiation, however, the 15 MeV proton tests were reduced to low level exposures in order to correspond with limitations of available funding by NASA GSFC. After contract award exposure tests were conducted for absorbed doses from approximately 10^3 to 2×10^4 rad Si.

As partially revealed in Section 2.4.4, "Anomalous Bias Dependence for Proton Damage," some very interesting but unexpected results were observed for those tests. Those findings demonstrated the need for resolving whether or not nonlinear damage dominates for low level exposure before beginning any combined test program. By mutual agreement between the Boeing technical leader and the NASA GSFC technical monitor, the contract work statement was formally altered to provide for extended proton testing by delaying combined testing for possible inclusion in a later program.

In Section 2.6, "Feasibility of Combined Testing," the results of extended tests are viewed in terms of the resolution of proton damage mechanisms. In this section data from the extended proton testing is used to evaluate damage constants for displacement effects. 15 MeV proton linear displacement damage (at I_C = 10 ma) is shown for NPN and PNP transistors by the solid lines in Figures 97 and 98 respectively. (The dashed lines in Figure 97 indicates that differences between gain measured at fixed I_C and I_E are small for this damage region). Displacement values found for the extended testing agree fairly well with those determined in the phase I program as indicated in the comparison between dash (10 ma) and solid lines on Figure 98.

A comparison between displacement lines for purposes of evaluating equivalences is shown in Figure 98 for PNP devices.. A comparable figure for NPN devices is shown later in Section 2.6, where implications for combined radiation tests are discussed. Based on the overall results from Section 2.5,

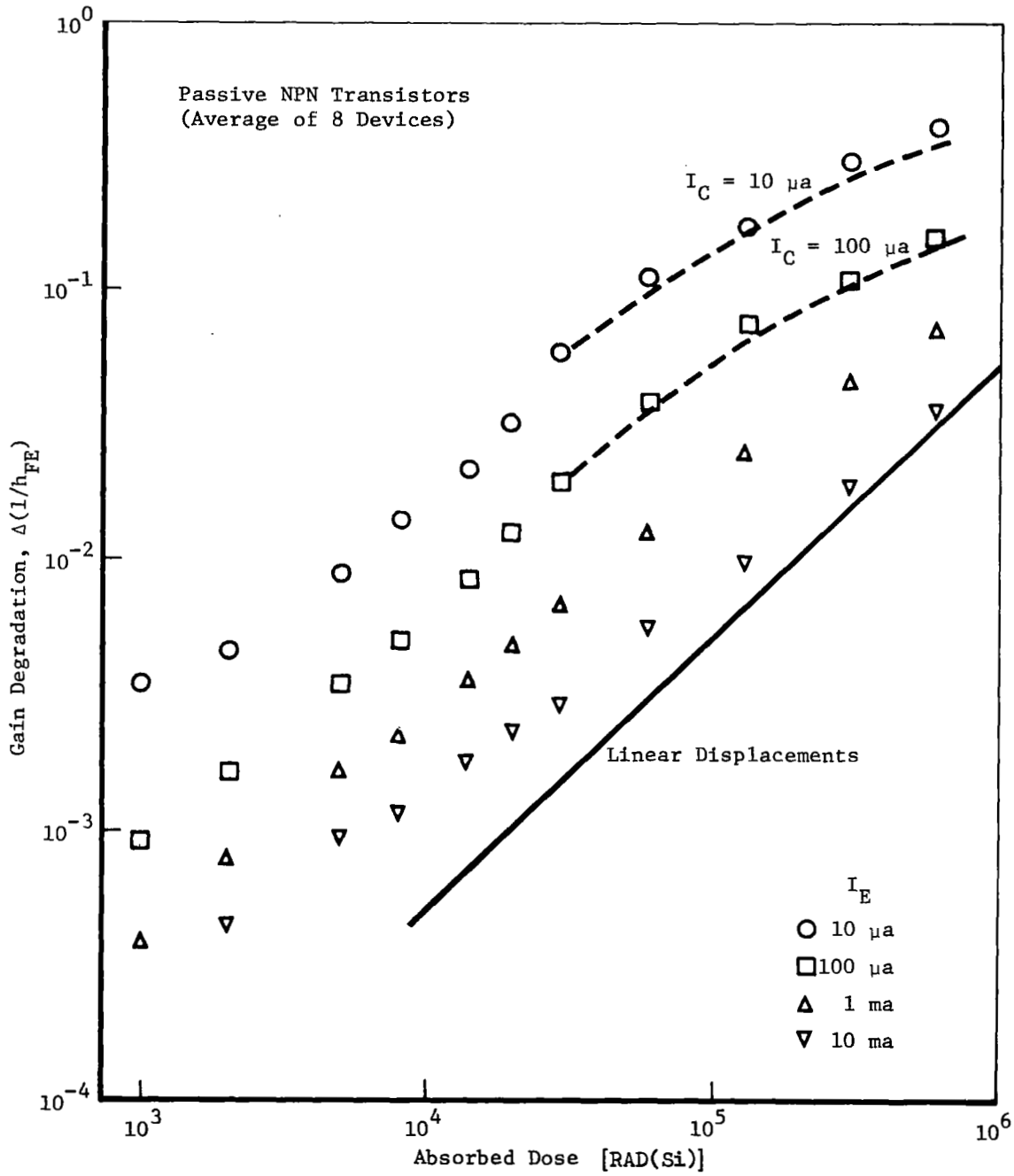

Figure 97: EXTENDED 15-MEV PROTON TESTING 2N1613 TRANSISTORS

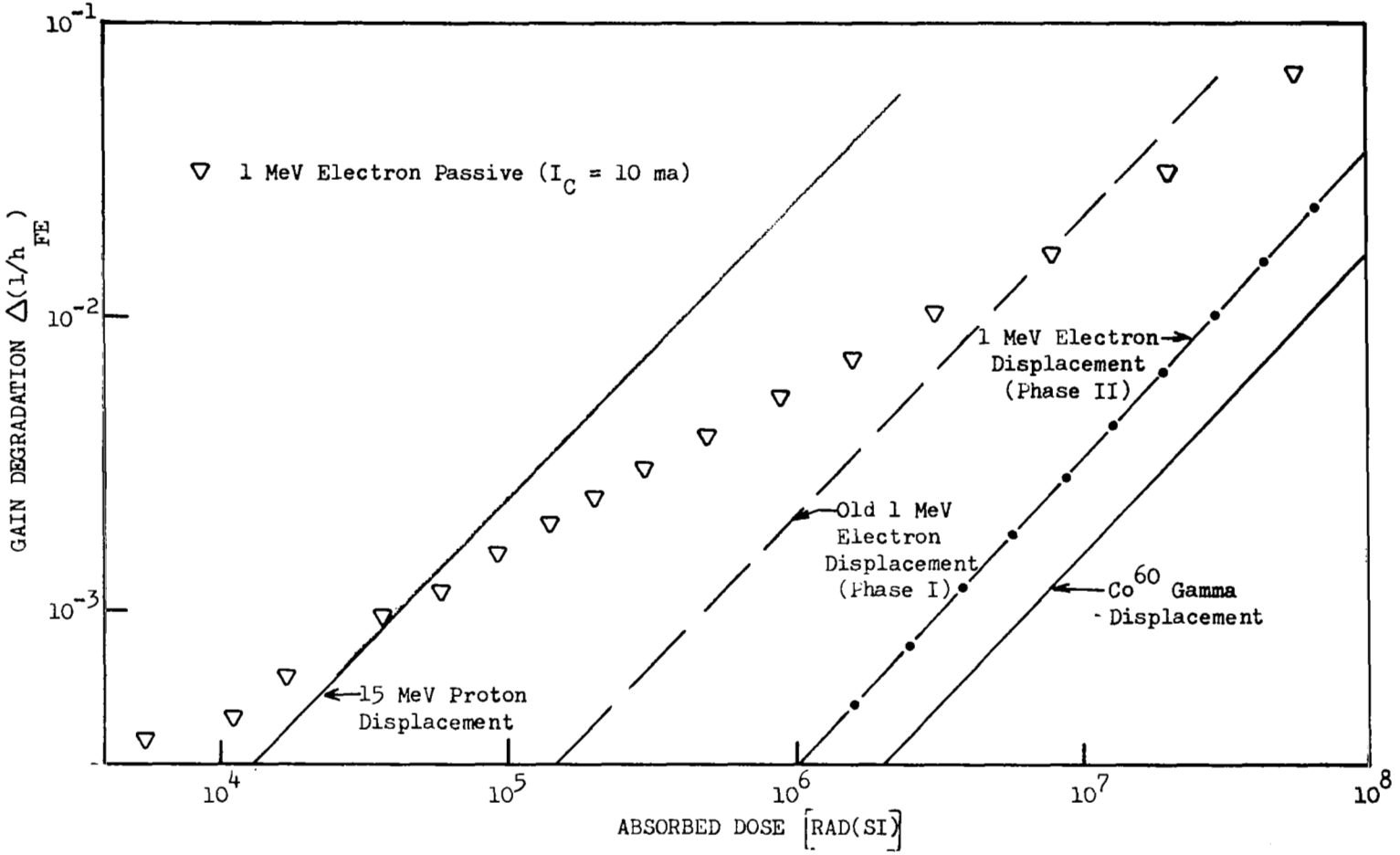

Figure 98. Comparison of Damage Profiles (2N1132)

a set of revised equivalence values for displacement effects is presented in Table 16. During the 1 MeV electron nonlinear tests, exposure levels were extended in order to better extrapolate displacement effects. Those results indicated that a shift in the extrapolated displacement lines for electron damage to PNP 2N1132 transistors be made in the direction of agreement between equivalences obtained for NPN transistors (Ref. 2).

Table 16. Revised Values for Displacement Equivalences

Particle Type and Energy	Alpha* 5 MeV	Proton 15 MeV	Neutron TRIGA Reactor	Electron 1.3 MeV	Gamma Rays Cobalt-60
Alpha* (5 MeV)	1	4.1	1.4×10^{2}	3.75×10^{3}	3.75×10^{5}
Proton 15 MeV	2.5×10^{-1}	1	3.3×10^{1}	9.0×10^{3}	9.0×10^{4}
Neutron (Reactor)	7.1×10^{-3}	3.1×10^{-2}	1	2.8×10^{1}	2.8×10^{3}
Electron 1.3 MeV	2.7×10^{-4}	1.1×10^{-3}	3.6×10^{-2}	1	1.0×10^{2}
Gamma Rays Cobalt-60	2.7×10^{-6}	1.1×10^{-5}	3.6×10^{-4}	1.0×10^{-2}	1

*Transistor Cans off for 5 MeV Alpha Particles

2.6 FEASIBILITY OF COMBINED TESTING

The contract for this program, before modification for extended proton testing, included the requirement for conducting a simultaneous electron-proton exposure test to determine synergistic effects for nonlinear damage. Consequently, a combined test set up was assembled. Before starting any combined tests the test setup was used to conduct separate electron and proton exposures of transistors. The results of high rate Linac electron tests at 2.6 MeV energy agreed well with steady state 1 MeV electron results. 15 MeV proton tests revealed anomalous results that obscured resolution of the relative importance of ionization and displacement effects. To overcome this difficulty the contract was modified in order to extend proton test data to higher exposures and thus determine enough about the damage profile to recommend a proper combined test program for later phase III studies. Differences observed between proton and electron damage indicates that combined tests are imperative in order to perform the proper assessment of radiation damage to electronics on board orbital systems.

2.6.1 Combined Test Setup

Details of the radiation test configuration, in particular the description of separate proton and electron exposures, were discussed in Section 2.2. The plan view for combining the electron beam from the Linac and protons from the helium-deuterium reaction is shown in Figure 99. The axes of the Dynamitron and Linac beam handling systems converge at an angle of 30 degrees inside the scattering chamber. The deuterated titanium target is positioned at the convergence point (Figure 100) at an angle of 20 degrees to the He^3 beam just as it was in the separate proton tests. Dosimetry for the combined tests would have been accomplished as in the separate proton and electron tests (see Sections 2.2.3 and 2.2.4). A photograph of an overall view of the combined beam setup is shown in Figure 101.

2.6.2 High Rate Linac Results

Electron exposure tests of 2N1132 and 2N1613 transistors were performed at 2.6 MeV using the Linac accelerator. Exposure conditions in Section 2.2.3 indicated that high instantaneous rates were employed (pulsed beam) as compared

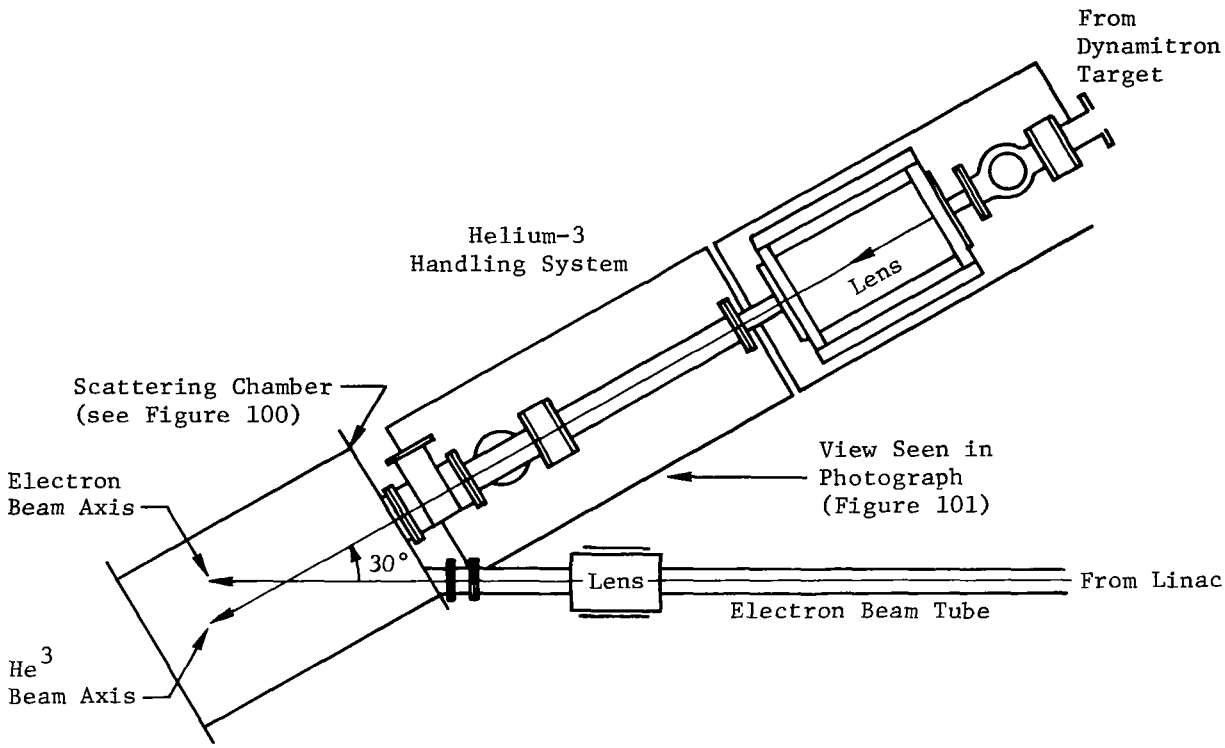

Figure 99: PLAN VIEW OF THE DUAL-BEAM TEST SETUP

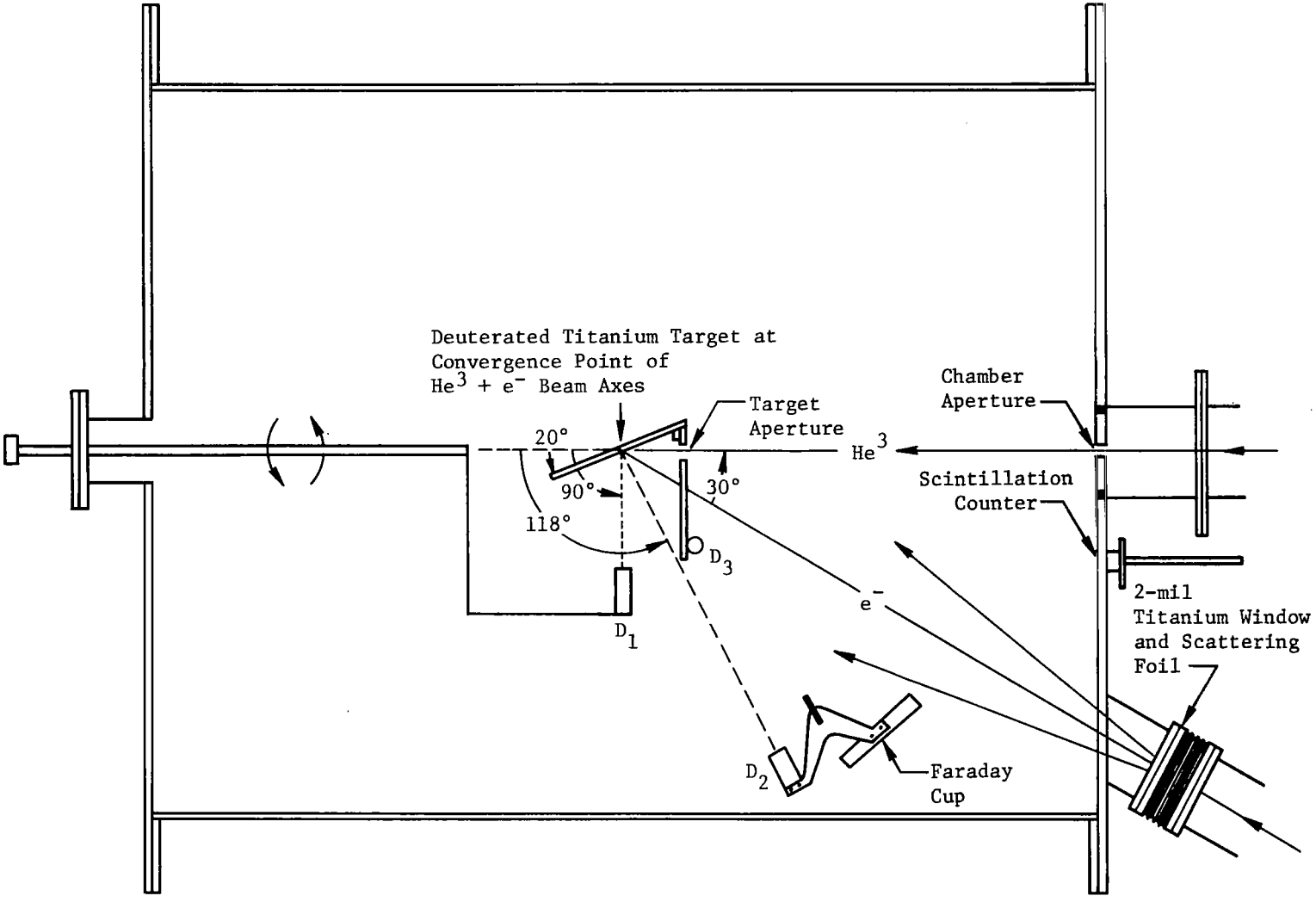

Figure 100: OVERHEAD PLAN VIEW OF THE SCATTERING CHAMBER

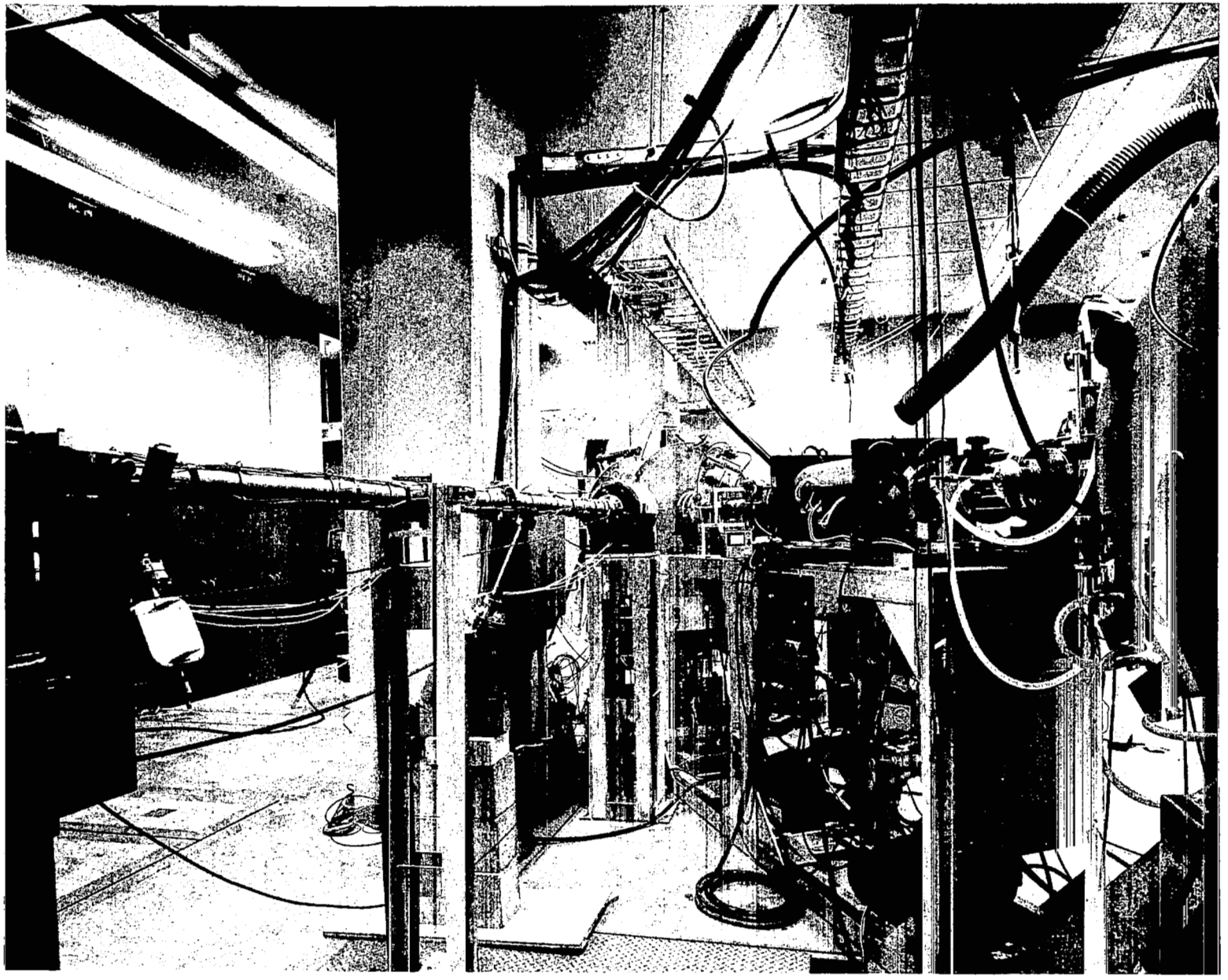

Figure 101: SIMULTANEOUS EXPOSURE BEAM HANDLING SYSTEM

with earlier 1 MeV steady state electron tests. The purpose of separate testing of transistors using the Linac was to validate the use of pulsed exposure at high rates to simulate low rate steady state exposure typical of space radiation environments. Test results were quite favorable as indicated in Figures 102 through 105. Linac results on passive 2N1613 transistors of Figure 102 can be compared with steady state exposure of Figure 18. The results are essentially equivalent. Active NPN transistors exposed to 2.6 MeV electrons show enhanced damage over passive NPN transistors as in the case of steady state electron exposure. Agreement between the 10 μamp curve of Figure 82 and the active curve of Figure 104 is clear. It can be concluded that equivalent nonlinear damage to transistors (active or passive) is obtained independent of the rate of electron exposure. Thus pulsed Linac electrons should be adequate for combination with steady state protons in future synergistic tests.

2.6.3 Resolution of Proton Damage and the Proposed Synergistics Test Plan

In order to properly plan a combined test it was necessary first to determine the relative importance of ionization and displacement damage over the fluence range of interest. At the end of the originally planned low fluence 15 MeV proton test (2.9×10^4 Rad Si) a number of apparent inconsistencies existed in determining whether damage was due to displacement or ionization. Those inconsistencies were as follows:

Inconsistent with normal displacement effects

1. The n values in $\Delta(1/h_{FE}) \cong KI_C^{(1/n - 1)}$ for both NPN and PNP transistors corresponded to those found for ionizing electron and gamma ray nonlinear damage, i.e., $1.3 \leq n \leq 1.8$.
2. Values of alpha cutoff frequency, transit time, or f_T were ineffective in normalizing the gain degradation.
3. Passive PNP transistors were more sensitive to proton damage than were active transistors, similar to electron or gamma ray nonlinear damage.
4. Isothermal fractional annealing of the damage was similar to nonlinear gamma ray damage. (See Figures 106 and 107.)

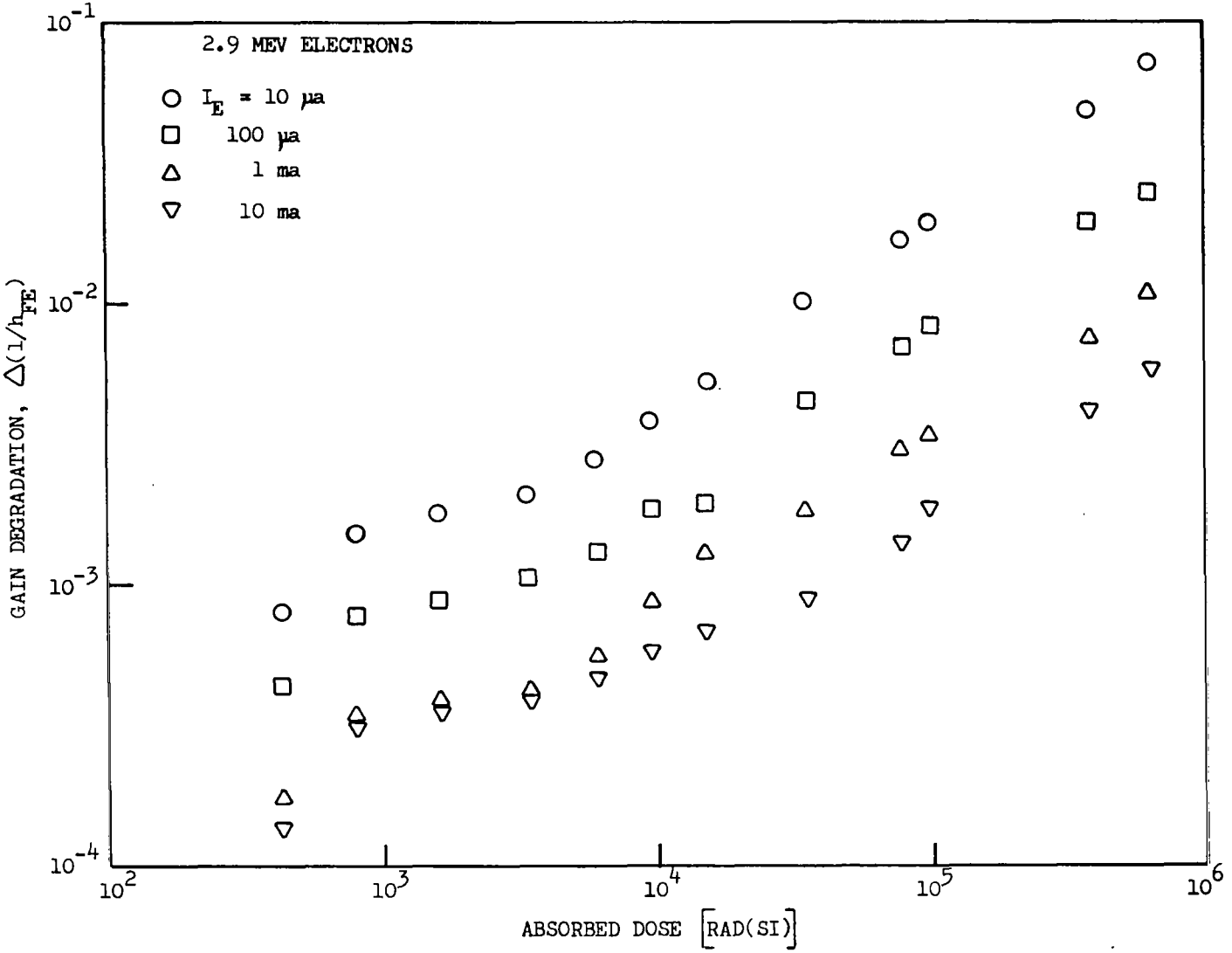

Figure 102. High Rate Linac Test Results Passive Transistors (2N1613)

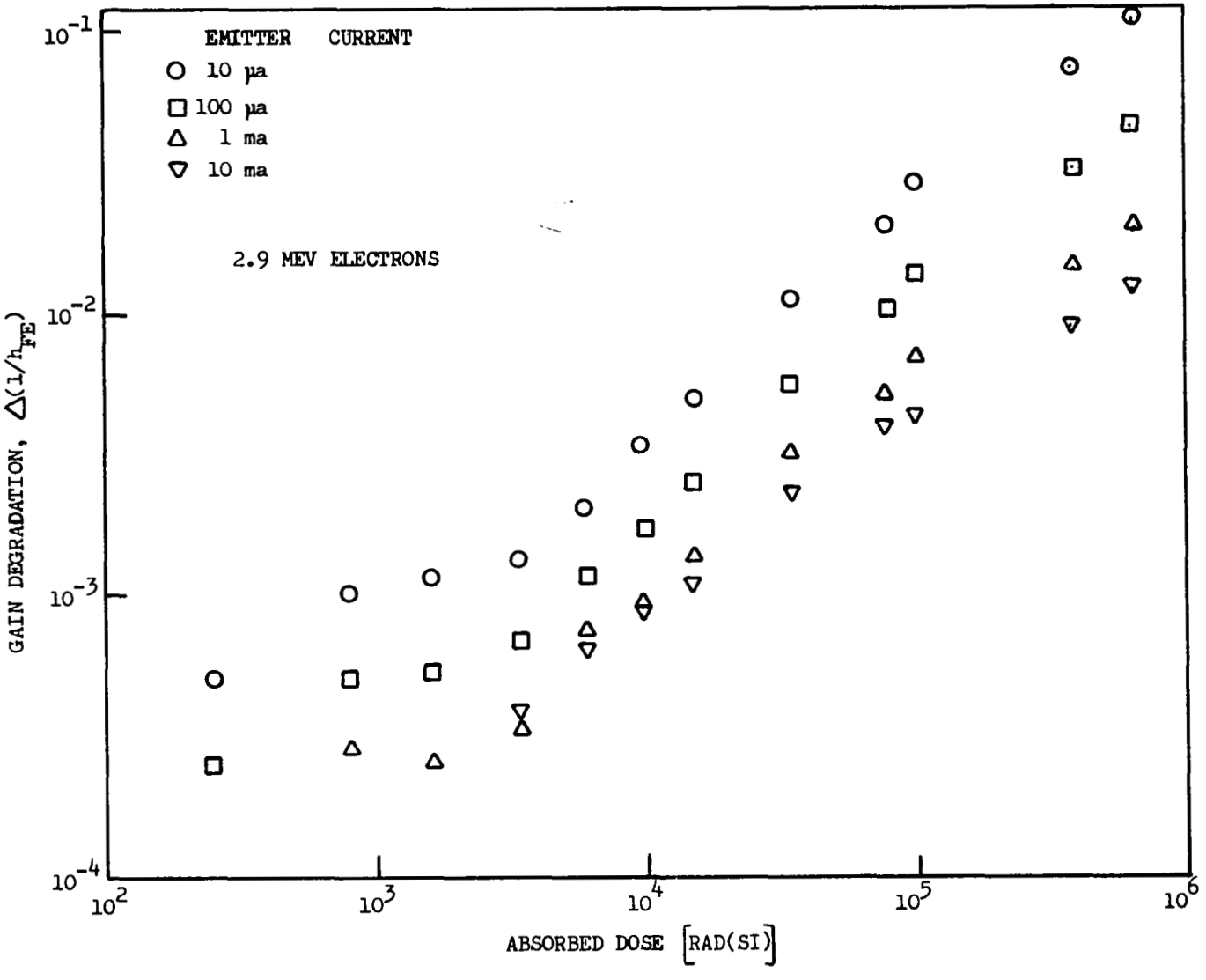

Figure 103. High Rate Linac Test Results Passive Transistors (2N1132)

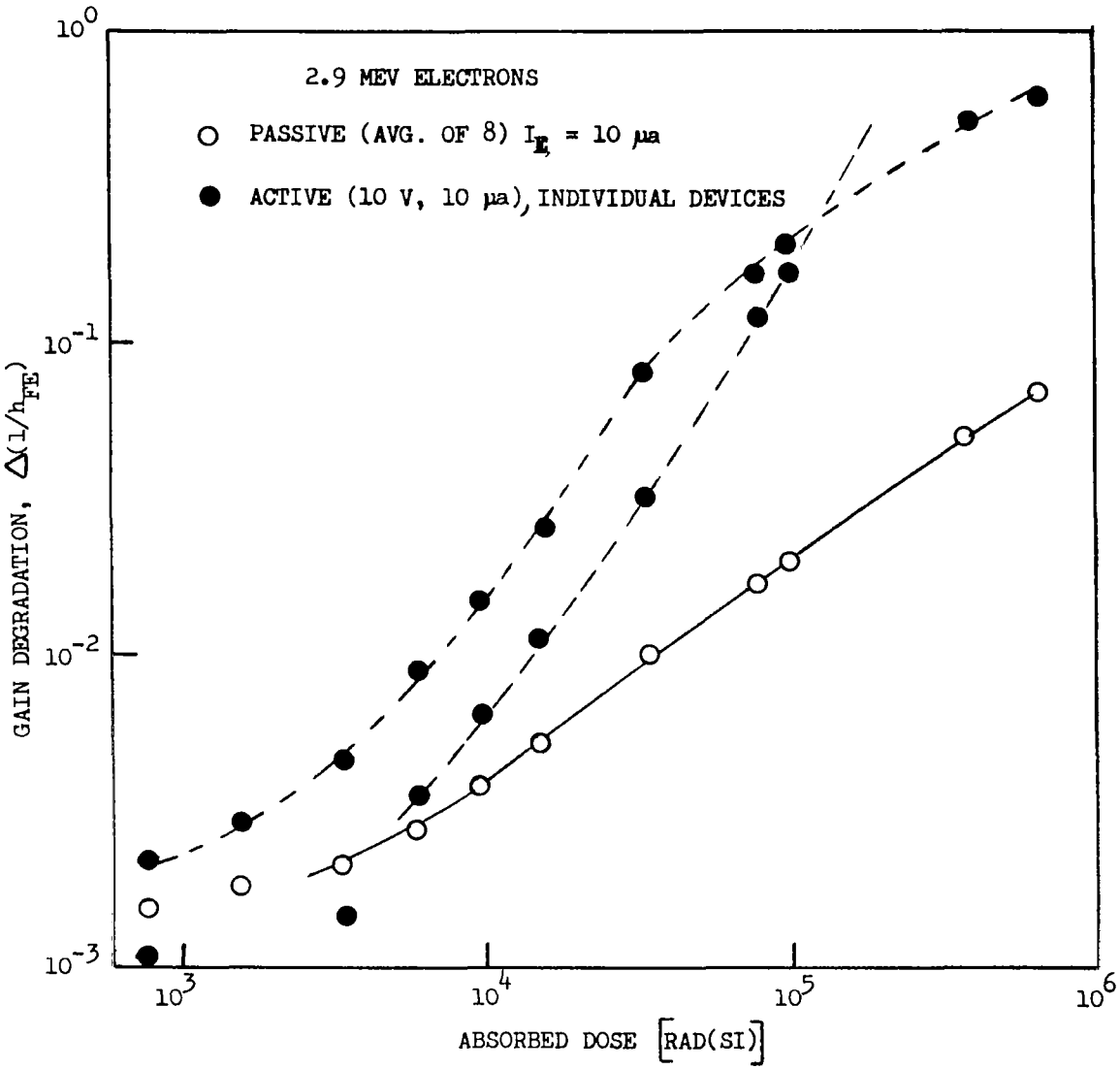

Figure 104. Active Bias Linac Test Results (2N1613)

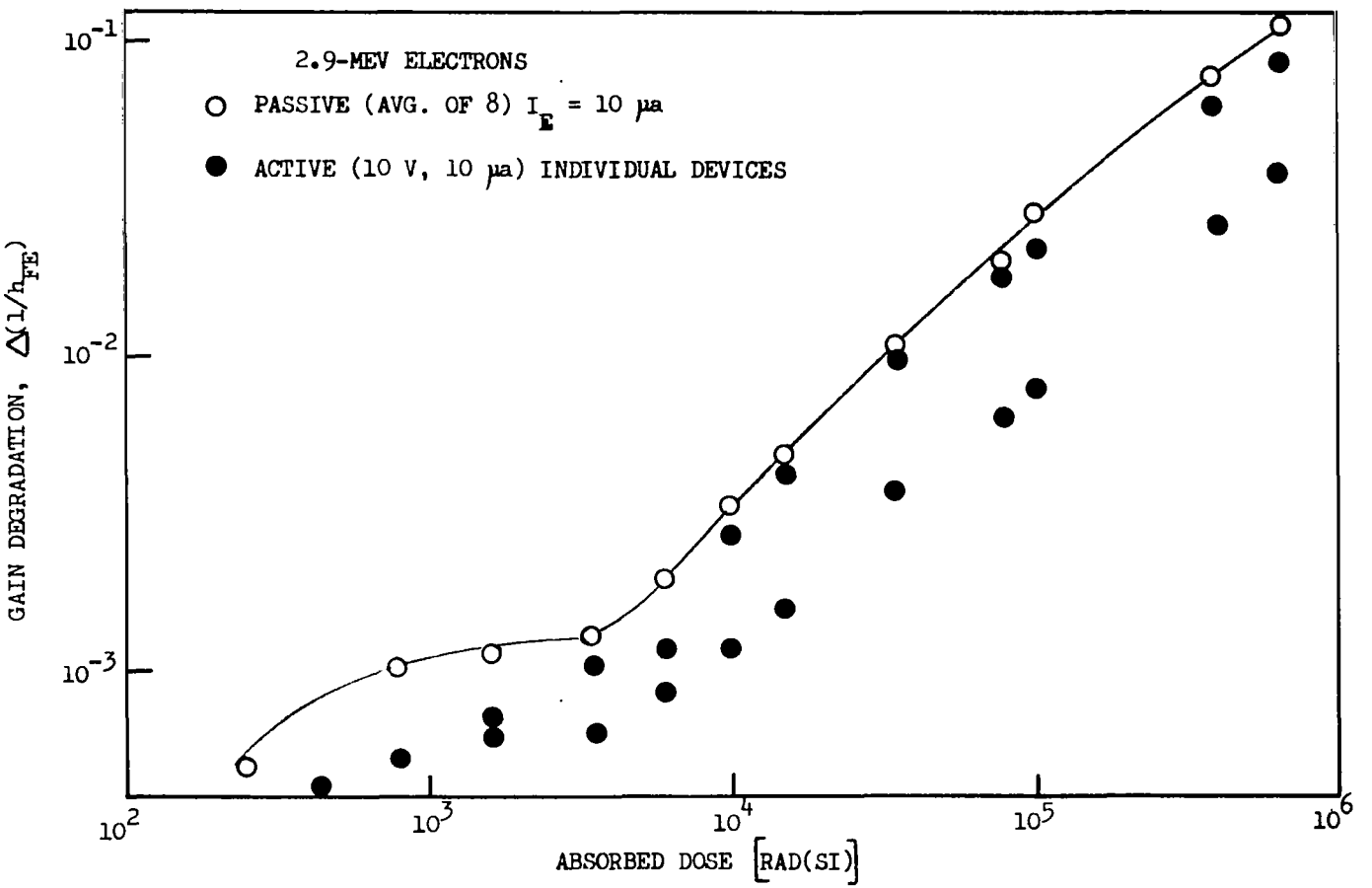

Figure 105. Active Bias Linac Test Results (2N1132)

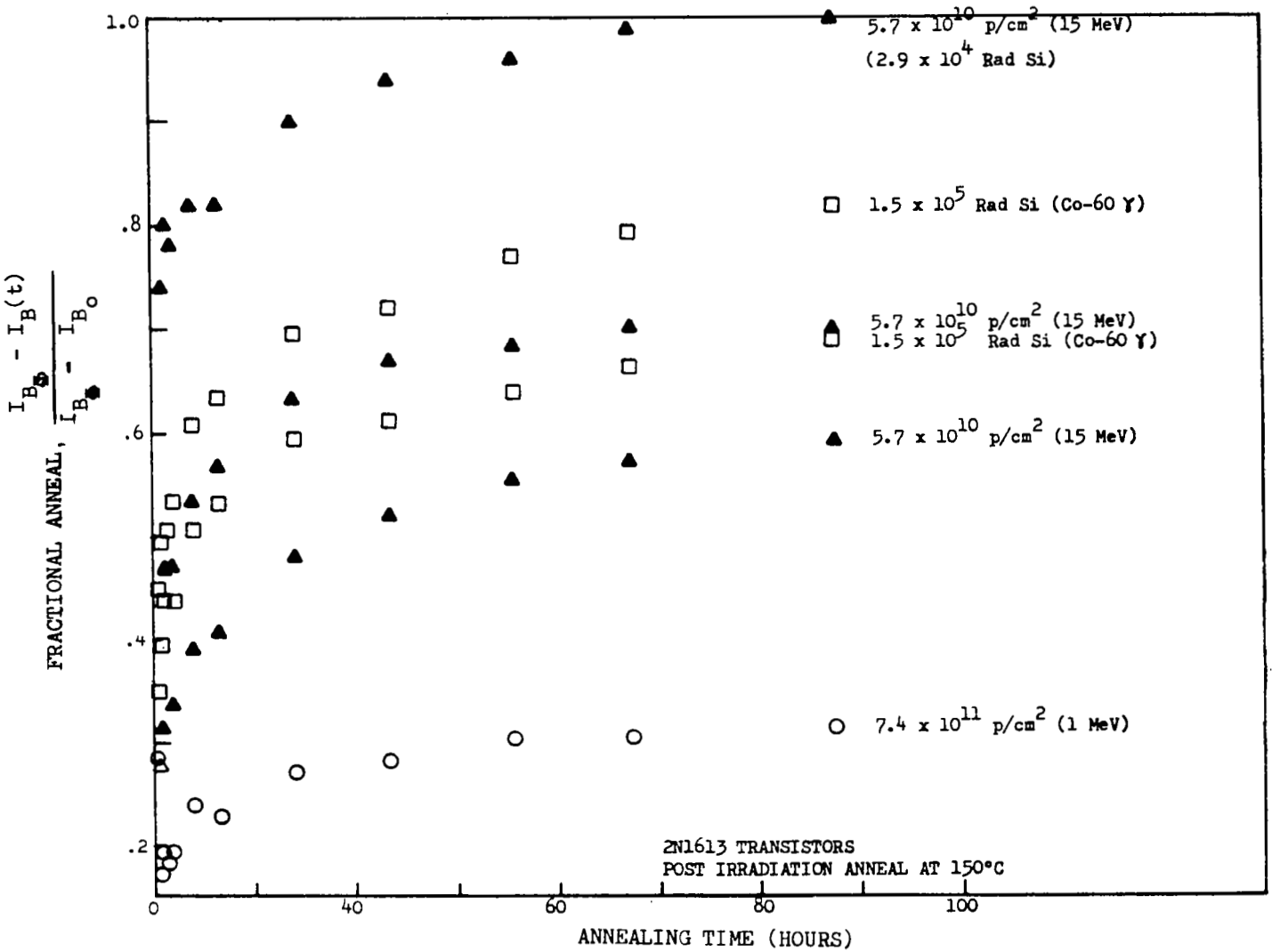

Figure 106. Isothermal Fractional Annealing at 1 ma

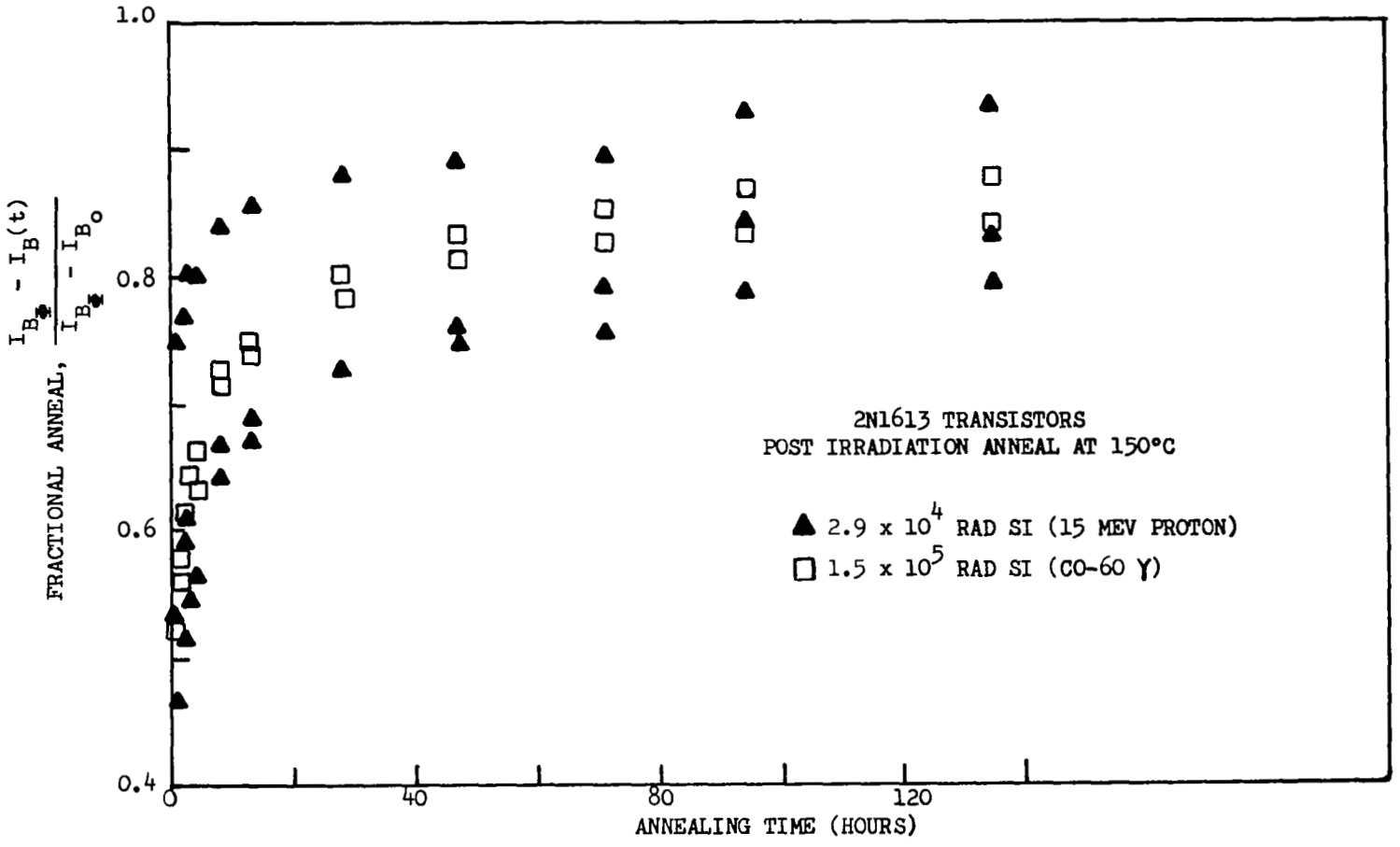

Figure 107. Isothermal Fractional Annealing at I_E = 10 ua

5. Damage showed a very large dependence on collector current ($n \sim 1.7$) considerably greater than that observed in neutron displacement damage or in the 1 MeV proton damage observed in the earlier phase I equivalence study. (See Figure 108.)

6. A large spread in 2N1132 device response was observed typical of nonlinear damage from electron testing.

Apparent inconsistencies with normal nonlinear damage

1. Damage appeared to be linear rather than nonlinear in profile, i.e., $\Delta 1/h_{FE} \cong K \Phi$

2. The "linear" damage line for protons agreed fairly well with proton equivalence values (at 10 ma) from the NAS5-9578 study.

3. Proton damage to passive 2N1613 transistors was greater than that for an equivalent absorbed dose from electrons or protons (ionization equivalence did exist however for PNP 2N1132 transistors).

4. At the low exposure of 2.9×10^4 Rad Si there was as yet no tendency for the damage to saturate.

5. Isochronal fractional annealing data did not agree exactly with gamma ray results indicating the possibility of displacements. (See Figures 109 and 110.)

6. Proton damage to active NPN transistors was less than that to passive transistors, opposite of that observed in electron or gamma ray nonlinear damage.

Based on these inconsistencies no combined tests were performed since the following dilemma arises in selecting between approach A and B.

A. If the protons cause nonlinear surface damage then the synergistics test should use equivalent dose and dose rates for both the electrons and protons, otherwise one would expect one particle type to dominate. (This approach would be worthless if the proton damage were due to displacements, since an equivalent amount of electron dose would also be dominated by proton displacements.)

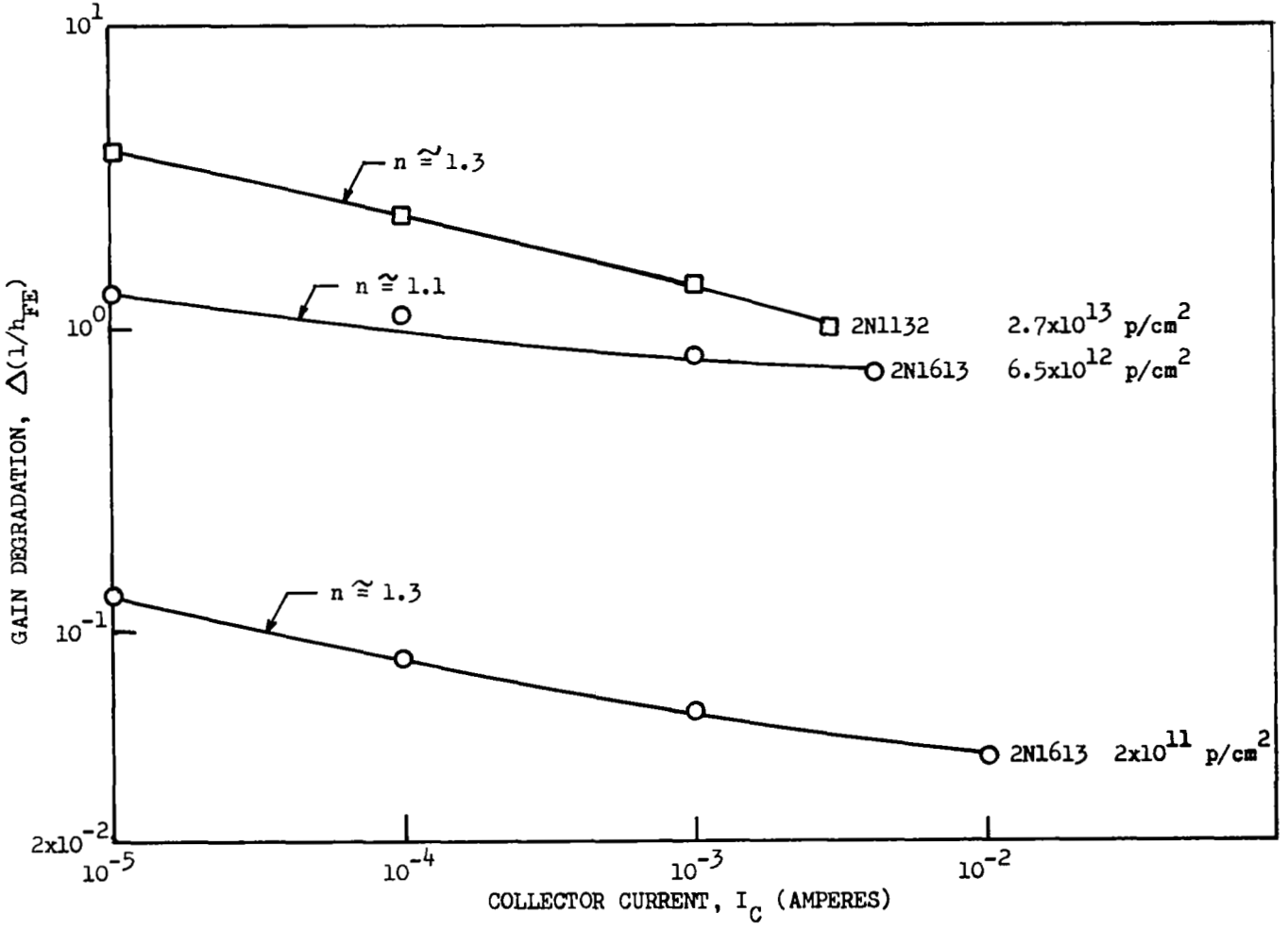

Figure 108. $\Delta(1/h_{FE})$ Versus I_C Plot for 1 MeV Proton Displacement Damage

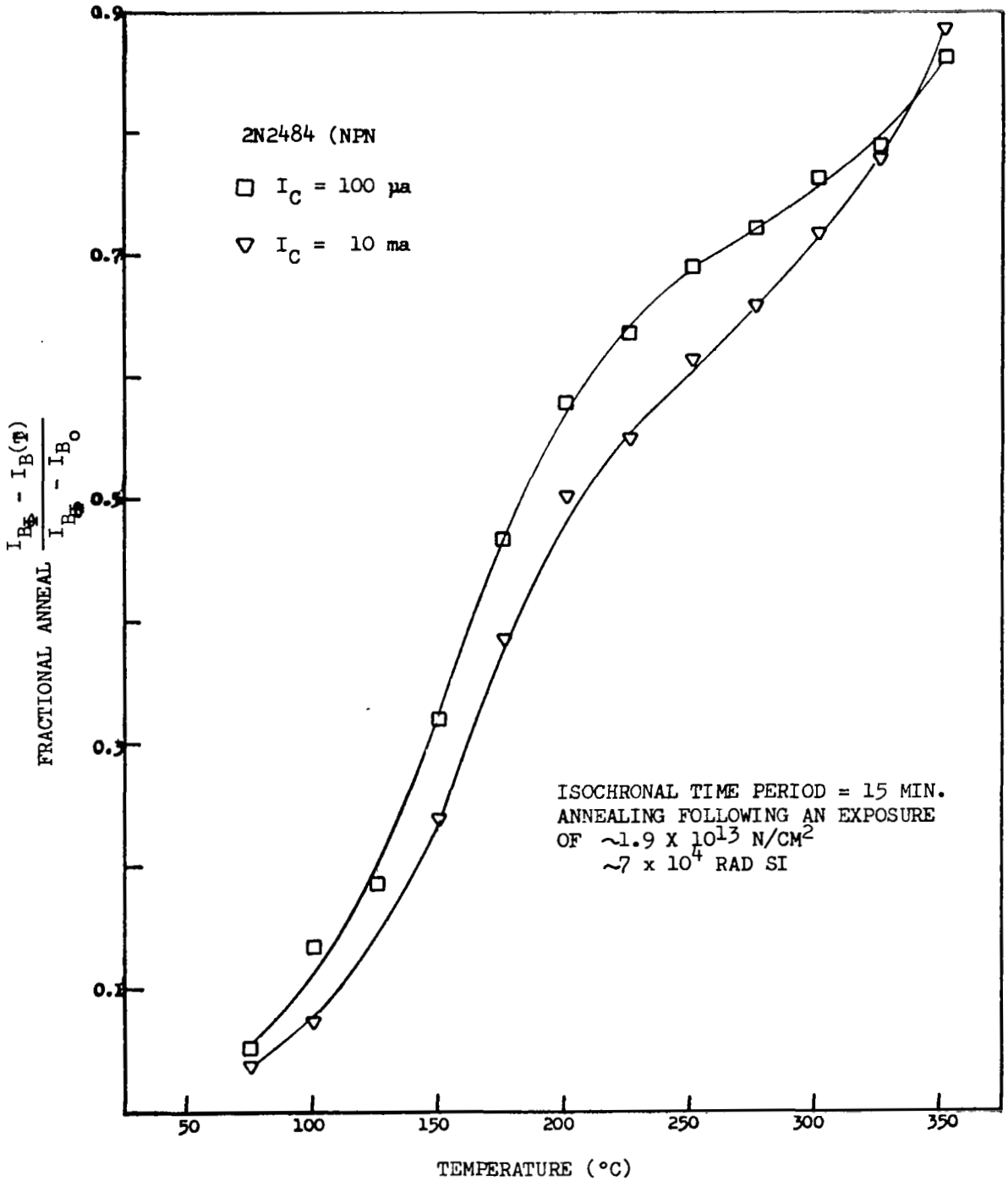

Figure 109. Neutron Isochronal Annealing

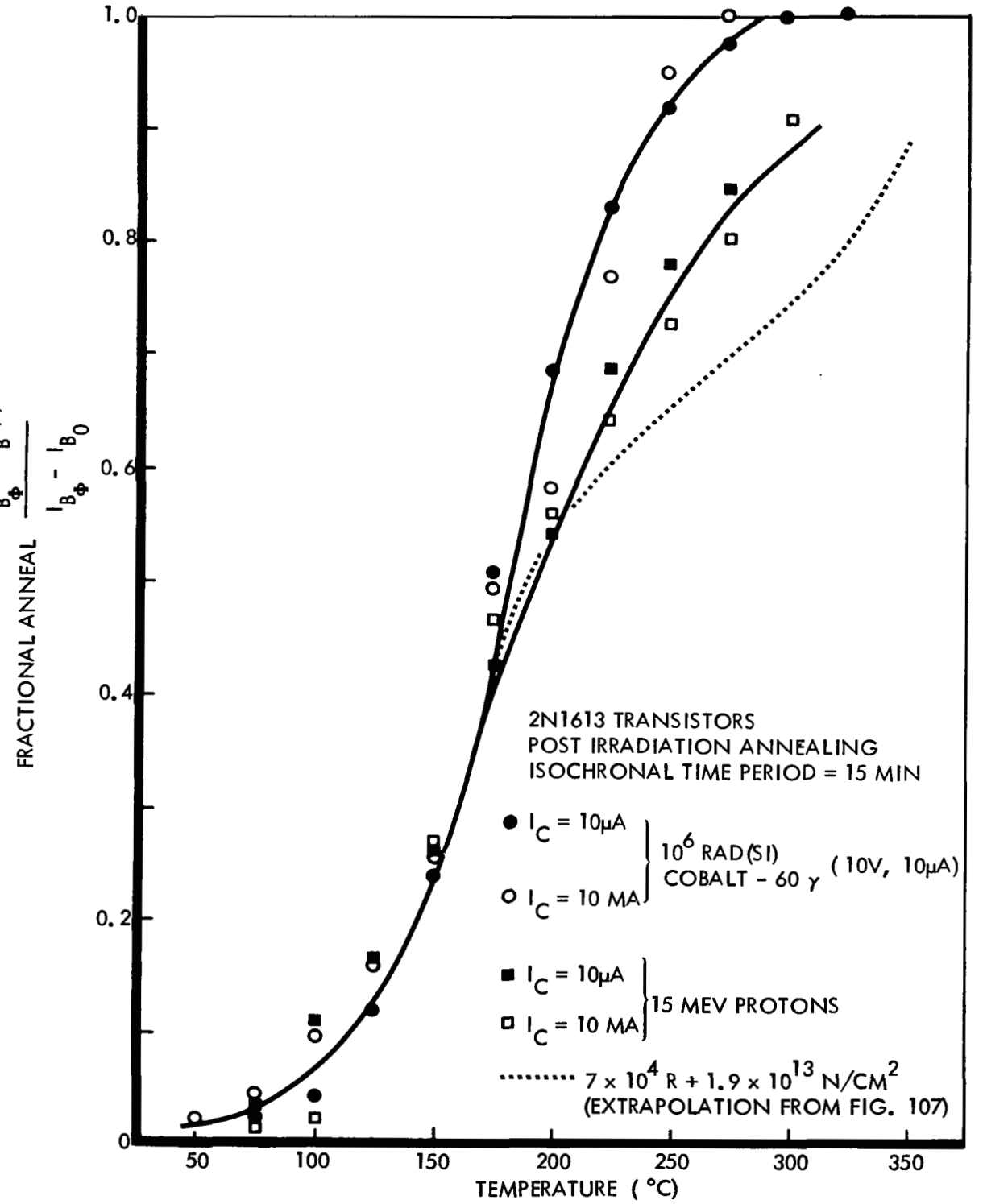

Figure 110. Nonlinear Damage Isochronal Annealing

B. If 15 MeV proton damage at low fluences is due to displacements then in a synergistics test a much higher dose and dose rate for electrons (several orders of magnitude) should be used to determine if ionization can influence displacement damage, otherwise proton displacements would dominate electron dose as it dominates proton dose effects. (This approach is worthless if the proton damage is due to "nonlinear" surface effects since the electron dose would then dominate the proton dose and no synergistic effects would be expected.)

Because of this dilemma the combined tests were postponed until later and extended proton testing was performed up to an absorbed dose of 6×10^5 Rad Si. The results of those tests were shown earlier in Figures 51, 90, 97, and 98 as well as now in Figures 111, 112, and 113. The results of the extended tests in no way removed any of the inconsistencies with displacement damage, as listed, but rather strengthened them. As an example, Figure 111 shows that the strong dependence of 2N1613 damage on I_C remains similar to surface effects (i.e., $n \cong 1.7$) for exposures up to 1.3×10^5 rad Si. Only above that exposure level is there a definite indication (with $n = 1.4$ at 10 ma) of the onset of the dominance of displacement damage at high currents for 2N1613 transistors. Figure 112 shows that for 2N1132 transistors displacement damage appears to be competitive with ionization damage at high currents (10 ma) even at low exposures.

Two of the apparent inconsistencies with nonlinear surface effects have been removed:

1) Damage at high exposures no longer appears to be linear for 2N1613 transistors (see Figure 113).

2) There is a definite indication of the beginning of saturation of the damage at high exposures for 2N1613 transistors (see Figure 113).

Furthermore, the linear damage line for proton effects (at 10 ma), as shown in Figure 112, still agrees fairly well with the phase I equivalence results. Finally, anomalous proton damage, i.e., damage to passive NPN transistors being greater than that to active NPN or passive PNP devices is not only inconsistent with ionization effects but also with displacement effects.

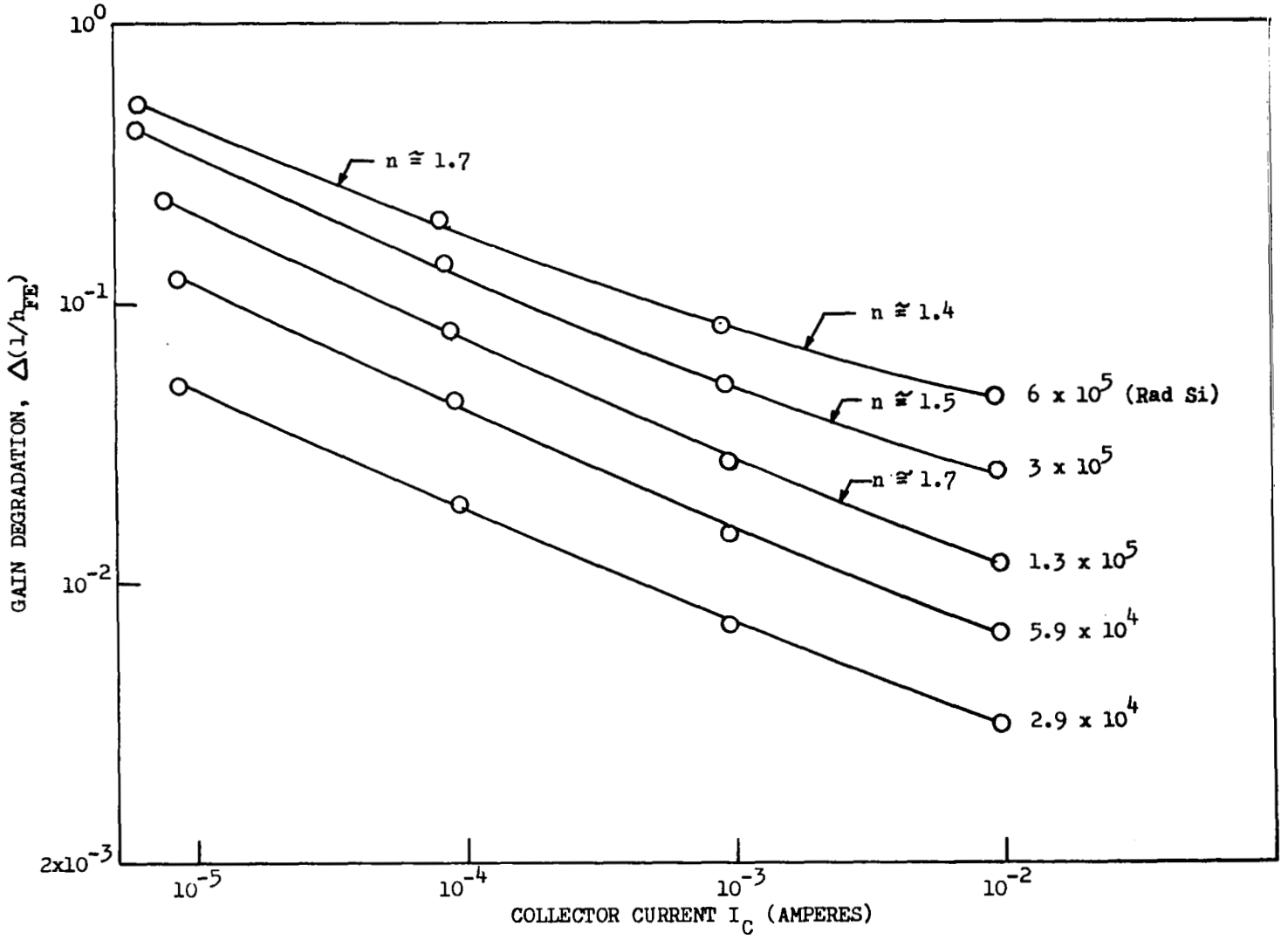

Figure 111. $\Delta(1/h_{FE})$ Versus I_C Plot for Extended 15 MeV Proton Testing

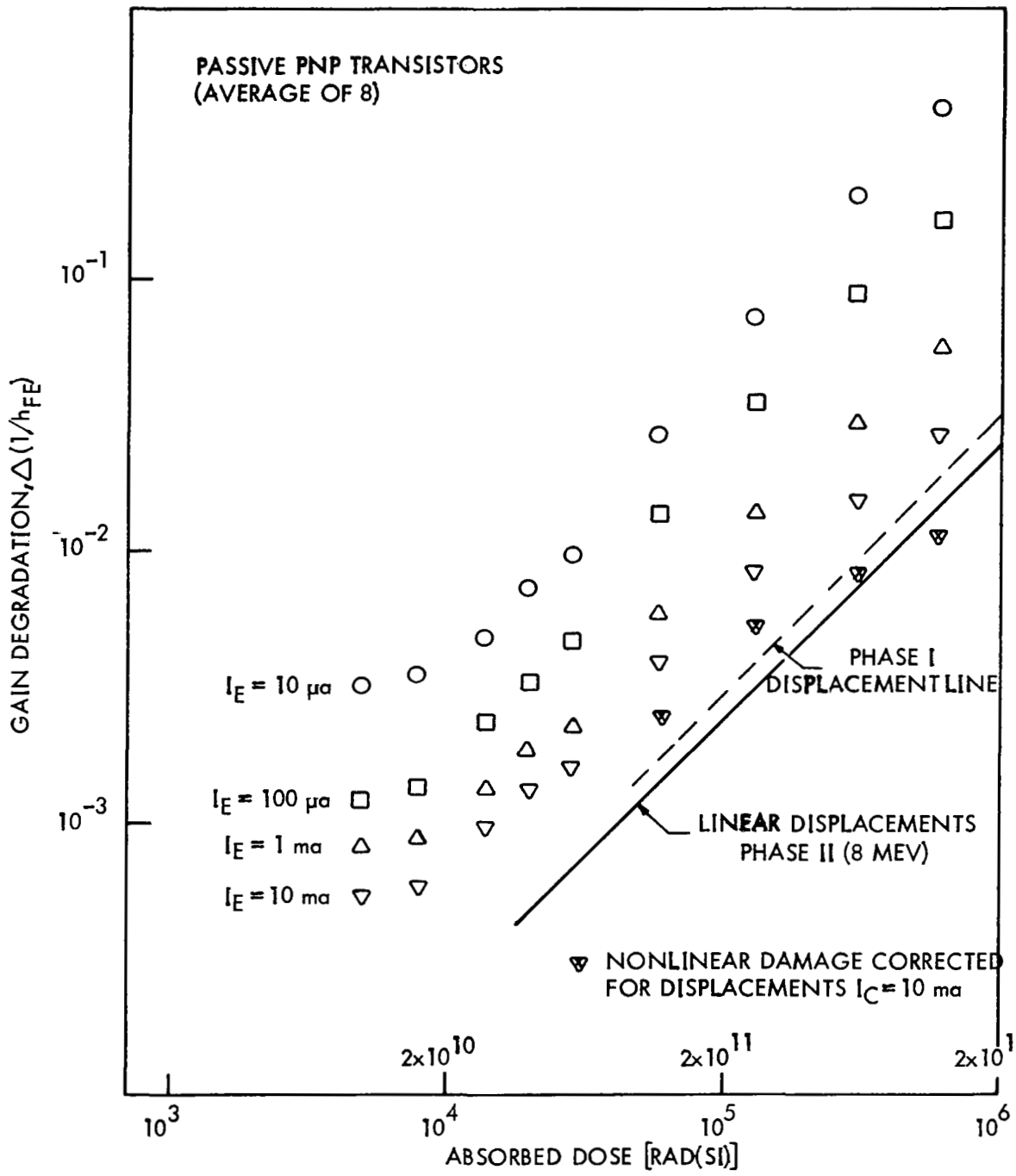

Figure 112. Extended 15 MeV Proton Testing of 2N1132 Transistors

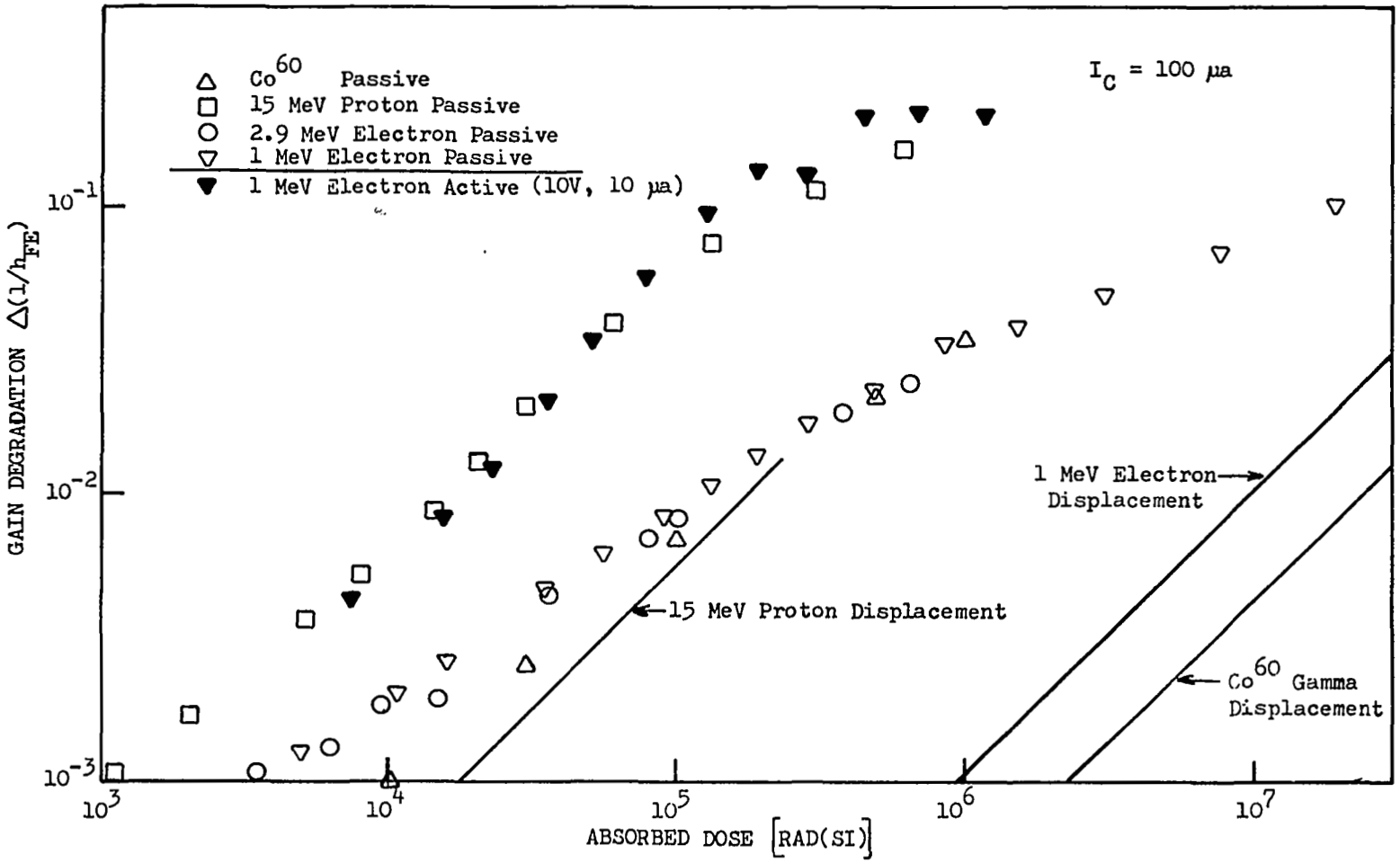

Figure 113. Comparison of Damage Profiles (2N1613)

Thus, it appears that the gain degradation caused by 15 MeV protons most resembles nonlinear damage (ionization induced surface effects). Based on this assumption, it is recommended that test approach A described in Section 2.6.3 be used in future combined tests. Since anomolous proton damage does not obey the ionization equivalence concept and since dependence on active biasing is the opposite of that observed by electrons, it is deemed highly desirable to conduct combined protcn-electron tests.

3.0 NEW TECHNOLOGY

The research work performed on this contract has been reviewed and to the best of our knowledge no new technology is reportable.

4.0 CONCLUSIONS AND RECOMMENDATIONS

Significant conclusions based on the results of this study are briefly summarized in this section along with appropriate recommendations for future study.

4.1 CONCLUSIONS

1) Dependence of Nonlinear Damage on Measurement Current

In general, nonlinear damage to passive transistors when presented in the form of $\Delta(1/h_{FE})$ versus particle fluence (or dose) resulted in parallel curves for a family of I_C values at which h_{FE} is measured. (The reason for this result is explained qualitatively in Section 2.3.1 and does not apply to transistors operated actively during exposure.) It was further verified that for both electrons and protons the current dependence is as theoretically expected

$$\Delta(1/h_{FE}) = \text{constant } I_C^{(1/n-1)}$$

where n is the exponent in

$$I_B \cong I_{B_o} \exp (qV_{BE}/n\ k\ T)$$

Raytheon 2N1132 and 2N1613 transistors both had a "surface effects n value" of approximately 1.5, while Fairchild transistors of both types had n values closer to 1.7 for nonlinear damage. Transistors of both registered types for both manufacturers demonstrated a change in n value toward n = 1 when displacement damage began to dominate surface damage. (15 MeV proton damage to Fairchild devices showed a slope of n = 1.7 for doses up to 1×10^5 Rad Si.)

2) Statistical Spread in Device Response

Devices of the same register number, but different batches (even between different manufacturers) generally showed similar sensitivity to radiation. Devices of the same batch generally degraded in a similar manner. Interesting differences in sensitivity of damage were observed for devices of different date codes from the same manufacturer. In general for better

normalization of damage for different date codes of the same manufacturer was obtained when damage was examined in terms of relative gain loss, $\Delta h_{FE}/h_{FE_i}$, rather than $\Delta(1/h_{FE})$. 2N1613 Fairchild devices demonstrated less statistical spread in sensitivity than did Raytheon devices. The gain loss of Fairchild devices was in between that of the extremes of the Raytheon batches. Significantly, devices from one of the later date codes proved to be the most sensitive. 2N1132 transistors had approximately the same statistical spread in damage independent of the manufacturer.

Active devices were also tested but in smaller lots. Test results indicate that the spread in the radiation sensitivity of active devices is much greater than that for passive devices.

3) Correlations and Empirical Formulation

Gain degradation was analyzed in several mathematical expressions to investigate empirical formulations. Although a simple power law

$$\Delta(1/h_{FE}) = \text{constant } \Phi^{x} \qquad 0 < x < 1$$

holds in some cases, it was generally only over a very limited fluence range, if at all. For actively biased devices during exposure, values of $x > 1$ were even observed. Correlation studies, furthermore, appear to indicate that excess base current ΣI_{B_x} is related to I_{B_i}. Consequently, the reduction of statistical spread using a formulation in terms of relative gain loss would be expected. An empirical relationship of the following form

$$\Delta h_{FE}/h_{FE_i} = f_s \tanh \left[K D\right]^{0.4}$$

was found to best fit the experimental data over the full dose, D, range up to and including saturation damage, f_s.

4) Ionization Equivalence for Nonlinear Damage

The hypothesis of ionization equivalence for nonlinear damage to passive transistors was found to be violated. In general equivalence on the basis of todal dose appears to hold for X-ray, gamma ray, electron and proton exposure of passive PNP transistors and indeed for exposures of passive NPN

transistors by all except protons. An anomalous exception to the total dose equivalence concept for passive transistors was observed with far greater 15 MeV proton nonlinear damage to 2N1613 transistors.

5) The Source of Nonlinear Damage

The problem of the source of nonlinear damage seems to narrow down to the fact that the relative importance of charge accumulation and creation of interface states under the various bias conditions during exposure has not been thoroughly studied hence resolved. Work carried out in this area has been somewhat fragmentary so far. In particular the results by the Fairchild group on passive (only) NPN transistors and by Maier on reverse biased (only) NPN transistors demonstrated the dominance of the new interface states over the charge accumulation. (See references 5 and 6 in App. II.) The results of Boeing in-house research on active and passive, normal (i.e., gas filled) and evacuated Fairchild 2N1613 transistors showed, on the other hand, that the charge accumulation due to gas ionization inside the can was the primary factor for the enhanced degradation of the normal active NPN devices. Nevertheless the passive gas filled, as well as the passive and active evacuated devices seemed to indicate the predominance of the degrading effect of the new interface states over that of the charge accumulation. A more detailed description of the Boeing work is given in Appendix II.

6) Active Biasing and Latin Cube Analysis

Active operation during exposure significantly enhances the sensitivity of NPN transistors to electron or gamma ray induced nonlinear damage. Furthermore this enhanced damage depends on the type of radiation causing the damage although it does not depend on the rate of exposure. 1 MeV electron damage to active NPN transistors is greater than that caused by a corresponding absorbed dose from Cobalt 60 gamma rays. On the other hand, active proton damage to NPN transistors is less than passive proton damage. 15 MeV proton damage to passive transistors was actually very close to enhanced (on active devices) electron damage providing a definite anomaly in the bias dependence correlations.

The Latin cube computer analysis of the multifactor experimental design provided a determination of the weak interactions between the three test variables--injection current, collector voltage, and particle fluence. While cross dependences between current and fluence or current and voltage are close to negligible a stronger interdependence between collector voltage during exposure and fluence (or dose) was observed. Latin cube binomial empirical formulations for the separate dependences on current, voltage, and fluence were

$$\left(\Delta h_{FE}/h_{FE_i}\right)_{V_C,\Phi} \simeq 1/2 \left[1 - 0.1\ I_C + 0.01\ I_C^2\right]$$

$$\left(\Delta h_{FE}/h_{FE_i}\right)_{I_C V_C} \simeq 1/8 \left[1 + 2 \times 10^{-12}\ \Phi - 0.3 \times 10^{-24}\ \Phi^2\right]$$

$$\left(\Delta h_{FE}/h_{FE_i}\right)_{I_C \Phi} \simeq 1/3 \left[1 + 0.03\ V_{CB} + .0003\ V_{CB}^2\right]$$

over the ranges of 0.3 to 9.7 ma, 1.6 to 18.4 volts and 3×10^{11} to 3×10^{12} e/cm^2 (for NPN transistors).

7) Updating of Equivalence Values for Displacements

Equivalence values (from early phase I data) were analyzed and found not to be significantly dependent on emitter current between 2.8 and 10 ma. Thus, a broader validity of the equivalence concept was verified. Gamma radiation testing extended to very high doses provided the means for replacing earlier lower dose extrapolations to determine damage constants. The extension of proton testing to high exposures also provided increased confidence in equivalence numbers presented in Section 2.5.

8) Feasibility of Combined Testing

The integrated test setup (2.9 MeV electrons from the Linac and 15 MeV protons from the Helium 3 - deuterium reaction using the Dynamitron) worked quite well in separate electron and proton tests. The transistors were exposed in the same position on the sample holder for each test indicating that simultaneous exposure at the desired rates is feasible. Results from the separate 2.9 MeV Linac test (pulsed) agreed very well, for both active and passive transistors, with earlier results from the 1 MeV electron Dynamitron test (steady state) indicating that simulation by the Linac was feasible. Extended proton testing indicated that 15 MeV proton damage to NPN transistors (2N1613) is dominated by nonlinear damage (at

low currents up to 10 ma and for exposures up to 1 x 10^5 Rad Si). This damage was anomalous, however, in that active devices were damaged less than passive devices by protons (opposite to electron induced damage). This result would seem to indicate that simultaneous electron and proton exposures (synergistic), typical of exposure of space systems in the Van Allen belts, would be expected to show nonadditive results (on the basis of total dose deposited).

4.2 RECOMMENDATIONS

It appears that, based on conclusions listed in Section 4.1, the following recommendations should be implemented in a future phase III program in order to allow for computerized prediction of effects in transistors caused by exposure to space radiation of complex spectra.

1) Based on the results of statistical tests on passive transistors, it is recommended that in the procurement of transistors for future testing important surface properties be identified, specified, and controlled during manufacture. This should be done in order to generate data that can be extended to a generalization of effects in other transistor types. Furthermore, it is recommended that a statistical test of actively biased transistors be conducted similar to that for passive transistors.

2) Further investigation of the empirical formulation appears to be desirable to determine whether an expression involving the hyperbolic tangent has general validity for different types of devices and whether a theoretical basis exists. When a formulation is validated it will provide a basis for standard evaluation of surface effects damage constants for different types of transistors.

3) The generalization of the proton violation of the concept of dose equivalence for exposure of NPN transistors should be explored by proton irradiation of other types of NPN transistors.

4) It is recommended that studies should be conducted to determine the relative role of charge buildup and the creation of new interface states in producing nonlinear gain degradation.

5) The anomalous dependence on bias condition for proton nonlinear damage to NPN transistors was not expected and should be studied further in order to provide insight into damage mechanisms. A detailed bias study (different injection levels and voltages during exposure) ought to be conducted for proton effects as have already been performed for electron and gamma ray exposure.

6) It is finally recommended that the combined tests originally planned for this program be included in a future study. The desirability of synergistic tests to determine the method of computer integration of effects from separate particle types and energies has increased because of the lack of ionization equivalence between protons and electrons.

5.0 REFERENCES

1. Brown, R. R. and Horne, W. E., "Radiation Induced Nonlinear Degradation of Transistor Gain," Technical Proposal D2-125398-1 to NASA Goddard Space Flight Center, June 1967.

2. Brown, R. R. and Horne, W. E., "Space Radiation Equivalences for Displacement Effects on Transistors," Final Report for NASA Contract NAS 5-9578, Document D2-84088-2, November 1966, NASA CR-814, July 1967.

3. Horne, W. E. and Brown, R. R., "Correlation of Electron Induced Changes in Transistor Gain with Components of Recombination Current," IEEE Trans. on Nuc. Sci., NS-13, 6, pp. 181-187, December 1966 (Nuclear and Space Radiation Effects Conference, Stanford, California).

4. Brucker, G. J., et al., "Ionization and Displacement Damage in Silicon Transistors," IEEE Trans. Nuc. Sci., NS-13, 188 (1966).

5. Poch, W. J. and Holmes-Siedle, A. G., "A Prediction and Selection System for Radiation Effects in Planar Transistors," presented at the Nuclear and Space Radiation Effects Conference, Missoula, Montana, July 1968.

6. Brown, R. R. and Horne, W. E., "Study of Semiconductor Reliability Following an Exposure to Nuclear Weapon Gamma Radiation," Final Report to NRDL contract NOO 22867 C0292, Document number D2-125743-1, USNRDL-TRC-68-32, June 1968.

7. Brown, R. R., "Proton and Electron Permanent Damage in Silicon Semiconductor Devices," paper presented at the Joint ANS and ASTM Conference: Radiation Effects on Electronics, Nuclear News, ANS-7, 8, 43, August 1964, and Radiation Effects in Electronics, STP 384, American Society for Testing and Materials, May 1965.

8. Taulbee, C. D., Nelson, D. L., and Southward, B. G., "The Effects of Ionizing Radiation on Transistor Gain," Radiation Effects in Electronics, STP 384, American Society for Testing and Materials, May 1965.

9. Measel, P. R. and Brown, R. R., "Low Dose Ionization-Induced Failures in Active Bipolar Transistors," presented at the 1968 IEEE Conference on Nuclear and Space Radiation Effects, July 1968.

10. For good reviews, see e.g. Mitchell, J. P. and Wilson, D. K., "Surface Effects of Radiation on Semiconductor Devices," Bell Syst. Techn. J. 46, 1 (1967), and Revesz, A. G. and Zaininger, K. H., "The Si-SiO_2 Solid-Solid Interface System," RCA Review, 29, 22 (1968).

11. Mitchell, J. P., "Radiation-Induced Space-Charge Buildup in MOS Structures," IEEE Trans. El. Dev., ED-14, 764 (1967).

12. Kooi, E., "Influence of Heat Treatments and Ionizing Irradiations on the Charge Distribution and the Number of Surface States in the Si-SiO_2 System," IEEE Trans. El. Dev., ED-12, 238 (1966). See also Revesz, A. G., et al., "Interface States and Interface Disorder in the Si-SiO_2 System," J. Phys. Chem. Solids, 28, 197 (1967).

13. Goetzberger, A., et al., "Surface States in Silicon from Charges in the Oxide Coating," Appl. Phys. Let., 12, 95 (1968).

14. Snow, E. H., et al, "Effects of Ionizing Radiation on Oxidized Si Surfaces and Planar Devices," IEEE, 55, 1168 (1967).

15. See e.g., Grove, A. S., Physics and Technology of Semiconductor Devices (J. Wiley, New York, 1967).

16. Fitzgerald, D. J. and Grove, A. S., "Surface Recombination in Semiconductors," Surf. Sci., 9, 347 (1968).

17. See e.g., Reddi, V. G. K., "Influence of Surface Conditions on Silicon Planar Transistor Current Gain," Sol. State Electr., 10, 305 (1967).

18. Grove, A. S. and Fitzgerald, D., "The Origin of Channel Currents Associated with P^+ Regions in Silicon," IEEE Trans. El. Dev., ED-12, 619 (1965).

19. Box, G. E. P. and Hunter, J. S., "Multi-factor Experimental Designs for Exploring Response Surfaces," Annals of Math. Stat., vol. 28, pp. 195-241, March 1957.

20. Brown, R. R. Horne, W. E., and Hamilton, A. E., "Recovery of Gamma Dose Mil. Spec. Failures During Low and High Power Life Testing of Silicon Transistors," presented at the IEEE Conference on Nuclear and Space Radiation Effects, July 1968.

21. Hunter, J. S., "Some Applications of Statistics to Experimentation," Chemical Engineering Progress Symposium Series, vol. 56 no. 31, pp. 10-26, 1960.

22. Caldwell, R. S. and Rosenberg, C., "Improvements in Transistor Models and Circuit Hardening for TREE Applications," AFWL TR-67-71, August 1967.

APPENDIX I

THEORETICAL BACKGROUND

OF THE SOURCE OF NONLINEAR DAMAGE

The following is a brief review of the effects of ionizing radiation on oxide passivated Si surfaces and on the subsequent physical events leading to planar transistor degradation. This step is necessary because our experimental results will be discussed and analyzed against this background.

A1. Effects of Ionizing Radiation on Oxide Passivated Si Surfaces

According to numerous investigators an oxidized Si surface when exposed to ionizing irradiation undergoes the following changes:[10]*

i) Positive charge is accumulated within and sometimes on the SiO_2.

ii) New energy levels are introduced into the forbidden band of Si at the Si-SiO_2 interface. In short, new "interface states" are created.

Let us discuss the physics of these two events briefly in turn:

i) Physical origin of the accumulated charges and their buildup with dose:

The accumulation of positive charge within the SiO_2 in the presence of a uniform electric field across the oxide (during irradiation), is quite satisfactorily explained by Mitchell[11]. His model assumes that hole-electron pairs are created in the SiO_2 by the radiation and that some of the electrons thus created drift out of the SiO_2 layer under the action of an applied potential across the oxide, V_G, while the corresponding holes become trapped. The analysis predicts 1) a dependence of charge buildup on radiation dose D,

* References 10 - 18 of Appendix I are listed in Section 5.0.

approximately of the form $1 - \exp(-\beta D)$ where β is a material dependent constant; 2) a linear dependence of the charge buildup at saturation on V_G, for both polarities of V_G; and 3) the dependence of the charge buildup on the total dose absorbed and not on the rate at which the dose was received.

Experiments by Mitchell himself as well as by others on MOS structures (NOT on bipolar transistors) support the type of charge buildup process predicted by the equation $1 - \exp(-\beta D)$. We will also make an attempt to correlate our gain degradation vs. dose curves with the predicted charge buildup vs. dose relation.

Another important case we should try to understand is the experimentally observed positive charge accumulation within the SiO_2 when there is no electric field across the oxide layer during irradiation ($V_G = 0$). Unfortunately there is no satisfactory treatment accounting for the charge accumulation under zero bias conditions. Only some tentative ideas have been proposed so far.[11]

An understanding of charge collection on the SiO_2 surface of a planar transistor is relatively easy. It occurs only when the collector base junction is reverse biased during irradiation. It is due to the irradiation induced ionization of the gas within the transistor can and the subsequent collection of the positive ions over the base or the collector by the electric field existing between the can and the base (the can is connected to the collector).

ii) Physical Origin of the Interface States and Their Buildup with Dose:

At the present time there is no theoretical treatment predicting the functional form of buildup of new interface states with dose, like the one worked out for charge accumulation. The primary reason is probably that even the identity or the physical origin of the defects responsible for the interface states, both original and new, is in question. Some workers claim that the new states are due to the breakup of Hydrogen-Si bonds at the interface by the irradiation.[12] Hence, the states are independent of the accumulated charges within the oxide. Other researchers[13] propose that the interface states are due to some positive and negative charges located in the oxide within a certain distance from the $Si-SiO_2$ interface. There are a number of valid arguments for

or against either proposition. It is very likely that there are several sources of the original and the new interface states, including the two ideas presented.

For the purpose of this report, we conclude that the creation of new interface states is a fact, although the physical origin of the states is still uncertain. In any case it is shown experimentally that the buildup of new states with dose will also go into saturation not unlike the buildup of positive charges. It is claimed, however, that the buildup of the new states is independent of the applied gate bias during irradiation in MOS structures.[14]

A2. Degradation of Transistor Parameters

Next, we would like to discuss the expected degradation of a passivated planar transistor in terms of the surface changes caused by ionizing irradiation presented previously. The two main degradations we are concerned with are the increase of I_{CBO} and the decrease of h_{FE}. To be more general, we will talk about the increase in the reverse current, I_R. Also, instead of the degradation of h_{FE} we will discuss the increase of the base current, I_B. These latter two events are equivalent because

$$h_{FE} = \frac{I_C - I_{CEO}}{I_B} = \frac{I_C}{I_B}\left(1 - \frac{I_{CBO}}{I_B}\right) \qquad A(1)$$

where

$$I_{CEO} = \left(\frac{I_C}{I_B}\right) \times I_{CBO}$$

Since I_C changes very little during ionizing irradiation it is the increase in I_B which is primarily responsible for the gain loss.

Now we wish to find out the controlling variables of currents I_R and I_B in order to assess and understand the effect of the charge accumulation and the creation of new interface states on the appropriate variables hence on currents I_R and I_B. Reiterating some of the results of semiconductor device physics it is well established that in terms of their physical origin I_R and I_B are given by:[15]

$$I_R = \sum_i I_R^i = \sum_i I_{gen}^i \quad \text{and} \quad I_B = \sum_i I_B^i = \sum_i I_{rec}^i \qquad A(2)$$

The equations above tell us first that both I_R and I_B are made up of several different components designated as I_R^i and I_B^i, each component having a different spatial origin in the transistor. The regions in question are: bulk of the emitter and of the base; surface of the emitter and of the base; bulk of the junction transition region; surface of the transition region; channel (inversion) region, if present. (The appropriate components originating at the surface of the junction will be designated as I_B^s, I_R^s, I_{rec}^s, I_{gen}^s.) The relative importance of these regions in contributing to I_B or I_R depends on many factors including the injection level (for I_B). As an example, it is the surface of the transition region which is the most important in determining the value of I_B thus the current gain at low injection. More will be said about the empirical equations representing the different I_B components in section A3.

It is also shown in Equation A(2) that the separate components can be identified with thermal generation (I_{gen}^i) and recombination (I_{rec}^i) currents respectively as to their physical origin. Equations A(2) then simply express the fact that in a given region of the transistor a thermal generation current will result whenever the thermal generation rate of hole-electron pairs is made excessive over the recombination rate of those pairs. (The thermal generation is due to the electromagnetic radiation, called "thermal radiation", present in any material at temperature T.) Similarly, a recombination current will result whenever the recombination rate becomes excessive over the generation rate. In thermal equilibrium these two rates are equal of course, but by external means (e.g. reverse bias, forward bias, illumination...) the balance can be destroyed and one ends up either with current sources furnishing the I_R or with current sinks representing I_B.

By taking into account the fact that according to the Shockley-Read-Hall theory the generation and recombination of hole-electron pairs takes place through some energy levels located in the forbidden energy band, serving as "stepping stones" for the particular process, we can now list the variables controlling I_R and I_B.

$$J^i_{rg} = f\,(N_t,\ E_t, \sigma_e, \sigma_h,\ n_o,\ p_o,\ T,\ V,\ n,\ p) \qquad A(3)$$

where J^i_{rg} is the recombination or generation current density in a given region of the transistor (hence $J^i_r = I^i_B$ and $J^i_g = I^i_R$). By writing J_{rg} instead of J_r and J_g we want to emphasize the intimate relation between J_r and J_g since the same energy levels serve as stepping stones for either the recombination or the generation process.

N_t: Density of energy levels in the energy gap promoting the generation and recombination; E_t is their energy position; σ_{el}, σ_h are the electron and hole capture cross-sections respectively

n_o, p_o: Equilibrium electron and hole concentrations in the bulk

T: Temperature

V: Applied voltage

n, p: Electron and hole concentrations in the particular region in question

The explicit functional form of J^i_{rg} is somewhat different in different regions of the transistor it is also different for J^i_r and J^i_g (i.e. for I^i_B and I^i_R). At the surface of the transition region for both J^s_r and J^s_g the dependence on N_t is linear. The dependence on n and p is much more complicated, containing hyperbolic cosine functions. J^s_r will have a maximum when $n = p \cong n_i \exp(q|V_F|/2KT)$ and J^s_g has a maximum when $n, p \ll n_i$ i.e. for a depleted surface. n_i is the intrinsic carrier concentration, V_F is the applied forward bias. Incidentally, the semi-empirical expressions for $(J^s_r)_{max}$ and $(J^s_g)_{max}$ are[16]

$$(J^s_g)_{max} = q \times S_o \times n_i \qquad A(4)$$

where S_o has been defined as the surface recombination velocity of a depleted surface. It is proportional to the density of the interface states. (Actually $S_o = S_{max}$ here since the n_s, $p_s \ll n_i$ condition made S reach its maximum value in the reverse biased case. Of course S_o is still a function of N_t, E_t, σ_{el}, σ_h, T, n_o, p_o as listed in EquationA(3).) Also,

$$(J_r^s)_{max} \cong \frac{2}{\pi} \times q\, S_o \times n_i \frac{q|V_F|}{2KT} \exp\,(q|V_F|/2KT) \qquad A(5)$$

$$\text{for } |V_F| \gg KT/q$$

It is significant to note that surprisingly $(J_g^s)_{max}$ i.e. $(I_R^s)_{max}$ is independent of the reverse voltage in EquationA(4).

Another interesting result comes by taking the ratio of EquationsA(5) andA(4).

$$\frac{(J_r^s)_{max}}{(J_g^s)_{max}} = \frac{2}{\pi} \times \frac{q|V_F|}{2KT} \exp\,(q|V_F|/2KT) \qquad A(6)$$

I.e. the ratio of $(I_B^s)_{max}/(I_R^s)_{max}$ is a constant at a given forward bias and temperature. Consequently if, for example, the maximum surface generation current, $(I_R^s)_{max}$, increases by a factor of two because of new interface states then so does approximately the maximum surface recombination current, $(I_B^s)_{max}$. (Hence the h_{FE} will also decrease by a factor of two.) Similar approximate results are obtained by taking the ratios I_B^i/I_R^i for other current components, signifying a close relation between them, although the ratio in those cases will depend on the reverse bias, V_R, as well.

Having found the variables controlling I_B and I_R in EquationA(3) we can now discuss the effect of the charge accumulation and of the new interface states on these currents in terms of their variables.

The introduction of the new interface states will increase the density of the recombination - generation levels, N_t, in EquationA(3). Consequently both I_R and I_B will be enhanced since their surface components I_B^s and I_R^s are increased linearly with N_t. Although the energy positions and respective capture cross-sections of the new levels may be different from those of the levels originally present, it is an experimental fact that the new energy

levels themselves are very efficient recombination-generation states. It should be pointed out that whenever I_B^s is affected seriously as the case here, then the gain degradation is most significant at low injection levels where usually $I_B \simeq I_B^s$ even before irradiation.

The effect of the charge accumulation (either within or on the SiO_2 or both) on I_B and I_R in terms of their variables will be somewhat different in the following cases therefore treated separately in turn:

i) No inversion, only depletion of the substrate Si occurs. The charge accumulation will modify n and p at the surface of the transition region (n_s, p_s) in Equation A(3) by changing the surface potential hence J_r^s or J_g^s will be modified. I_B^s and I_R^s may or may not reach maximum as a function of the surface potential (thus n_s and p_s) depending upon the extent of depletion of the substrate.

ii) Inversion of the substrate Si occurs, thus a junction, called the "field induced junction", is formed. This case has to be divided into the following three subcases: (In the first two it is assumed that the extent of inversion is not sufficient to cause "channel" formation discussed in γ.)

α) There is no breakdown across the field induced junction during applied bias:

The two new regions which affect I_B and I_R in this inversion case are the surface of the inversion layer and the bulk transition region of the field induced junction. However, the effect of the surface decreases rapidly with surface inversion and will be negligible under large inversion.[17] (Since J_r^s and J_g^s as functions of the surface potential have already passed their maximum when the inversion set in.) On the other hand, the bulk transition region of the field induced junction will serve as an extra source of current for either I_R or I_B thus contributing to their degradation.

β) There is a voltage breakdown of the field induced junction during applied bias:

The breakdown can be either an avalanche or a Zener breakdown depending upon the surface doping of the inverted substrate.[18] Avalanche occurs below approximately 3×10^{18} cm^{-3}. Zener breakdown or tunneling occurs

when the surface doping is approximately between 3×10^{18} cm^{-3} and 8×10^{18} cm^{-3}. Either of these breakdowns give rise to a tremendous increase in I_R. In addition, the tunneling can significantly increase I_B hence degrade h_{FE} both at low and high injection levels. This effect, when it occurs, is so drastic that it overrides every other cause of gain degradation especially at high injection levels.

γ) "Channel" or ohmic path formation between the contacts of the base-emitter, base-collector, emitter-collector.

This event specifically refers to the case of base inversion of such an extent in area that a direct ohmic path between the different terminals of the transistor develops. Depending upon the size of the channel the resulting increase in I_{CBO} or I_{CEO} may completely disrupt further device operation. (Fortunately the effect of a channel across the base-emitter junction alone is not too serious for gain degradation because this junction is forward biased and the channel path is usually highly resistive.)

Since the accumulated charges in the SiO_2 are positive it follows that the depletion and inversion occurs on a P type substrate only. This is the base of an NPN transistor and the emitter and collector of a PNP transistor. Therefore, a different response is expected to ionizing irradiation by NPN and PNP transistors. The difference in behavior is further amplified by the fact that the surface doping of the base and emitter regions is quite different. The emitter region is usually very highly doped ($> 10^{20}$ cm^{-3}), consequently only a very narrow region in the vicinity of the junction, where there is a lateral concentration gradient, can be depleted and inverted. Nonetheless, since tunneling can usually occur through part of the small inverted region, the degradation of I_B hence h_{FE} can still be very significant for a PNP transistor as we will see later during the presentation of our experimental results.

A3.. . Empirical Equations for I_B^i

Previously in EquationA(3), we indicated the variables controlling I_B^i by taking into account the physical mechanisms causing the current. Next we write down some empirical equations for I_B^i, which say very little about the physical origin of the current but emphasizes its approximate voltage and temperature dependence.

$$I_B = \sum_i I_B^i \qquad \text{and} \qquad I_B^i = I_O^i \exp \frac{qV}{n_i(V,T)kT} \qquad A(7)$$

where I_O^i is an empirical constant for the i^{th} component of the base current, $n_i(V,T)$ is the "identifying" component number for the i^{th} component. In general, it may be a function of injection level and of temperature. The value or the range of values of n for the different base current components are as follows:

n = 1: Bulk recombination current in the emitter and base region. Or, surface recombination current on the emitter and base region.

1<n<2: Bulk recombination current in the junction transition region. Or, surface recombination current over the transition region. It is significant to note that in this important case the meaning of a given n value is unfortunately ambiguous, unless complemented by some other measurements.

2<n<4: Recombination current in the channel (inversion) regions, if present, and the adjacent bulk material.

In a given V and T range it is usually true that one of the base current components is dominant. Then by determining the n value we may be able to identify the component in question. The identification of the spatial origin of the current is usually important in complementing and supplementing the conclusions of some other measurements. Two different techniques were used to obtain "n":

i) V_{BE} analysis: n can be determined from the slopes of the log I_B vs. V_{BE} plots as seen from EquationA(7) and is well discussed in the literature. We emphasize again that a changing n value at different V_{BE} points may still represent one dominant I_B component. The variation in n in such a case may simply reflect its injection level dependence.

ii) $1/h_{FE}$ vs. I_C plots: n can also be determined from the slopes of the log $1/h_{FE}$ vs. log I_C plots at a given fluence since

$$\frac{1}{h_{FE}} \simeq \frac{I_B}{I_C} \cong \text{constant } I_C^{\frac{1}{n}-1} \qquad A(8)$$

This is valid if the base current consists of one dominant component, i.e. $I_B = I_{BO} \exp(qV/nkT)$. Then since $I_C = I_{CO} \exp(qV/KT)$ we can write $I_B = \text{constant } I_C^{1/n}$ and consequently obtain Equation A(8).

If one is interested in identifying only the additional base current component(s) introduced by the irradiation then the log ($\Delta 1/h_{FE}$) vs. log I_C plots have to be used instead. In practice there was very little difference between this and the log $1/h_{FE}$ vs. log I_C plot when I_B increased by a factor of 20 or more.

Although method i) is more precise in obtaining n it is also far more tedious and time consuming than ii). In contrast the data necessary for method ii) are relatively easily obtained on a high speed automatic transistor gain tester like the Fairchild Series 500. Nevertheless, method i) also furnishes actual I_B vs. V_{BE} data while ii) does not. In certain analyses the knowledge of the I_B values is just as important as the knowledge of the "n" values.

APPENDIX II

"BIAS DEPENDENCE AND ORIGIN OF THE IONIZATION INDUCED SURFACE DEGRADATION OF NPN PLANAR TRANSISTORS"

In spite of the many excellent technical papers in the area of irradiation induced surface effects, some uncertainty still exists in the literature as to the cause, or even to the existence of the bias dependence of the surface degradation of NPN planar transistors. (We define bias dependence to mean that the amount of surface degradation is dependent on whether the transistor is reverse biased (C-B junction voltage)during exposure .

As an example, the Bendix group (Ref. II-1) observed the bias dependence of the surface degradation of NPN bipolar transistors but their finding was at variance with that of Schmid (Ref. II-2) who claimed no such dependence. Hughes (Ref. II-3) also reported no bias dependence, whereas a recent paper by Poch and Holmes-Siedle (Ref. II-4) calls the bias dependence "typical". The surface degradation in papers II-1, II-2, and II-3 was explained in terms of the charge accumulation on the SiO_2 or in the SiO_2 or both. Supplementing this model, the papers by Snow, et al (Ref. II-5), and by Maier (Ref. II-6) pointed out that the effect of the new interface states could be dominant over that of the charge accumulation in causing surface degradation of planar transistors. However, no study was carried out on the problem of bias dependence, if any.

Partially because of the contradictory claims as to the existence of bias dependence which is an extremely important problem for prediction purposes, but mainly because of the newly recognized role of the interface states, experiments were carried out to study the bias dependence of surface degradation. The experimental results were examined in terms of all the ideas used at present to explain the irradiation induced surface effects. These ideas include i) the

effect of the charge accumulation over the oxide surface with subsequent migration into the oxide (Ref. II-7), ii) the effect of the charge migration and accumulation within the SiO^2 due to the positive charges generated there, iii) the effect of the creation of the new interface states which may or may not be related to the positive charges within the oxide.

Type 2N1613 transistors from Fairchild were used in this study. The following parameters were measured as a function of exposure: I_B at V_{BE} = 0.26V, 0.38V, 0.50V, I_{EBO} at 2V reverse bias and C_{BE} at zero bias to monitor the surface conditions at the E-B junction; I_B^{inv} at V_{CB} = 0.26V forward bias (i.e., the base current in inverted transistor configuration), I_{CBO} at 10V reverse bias and C_{BC} at zero bias to monitor surface conditions at the C-B junction. The measurements of I_B and I_B^{inv}) at low V_{BE} resulted in a high sensitivity in monitoring the surface conditions which is ordinarily not possible with gain measurements.

Separate Co^{60}-γ rays and 1 MeV electrons were used to produce ionization. The evacuation of the transistors was accomplished by puncturing holes on the cans consequently the devices were under vacuum only during electron exposure. The different biases applied during exposure were turned off when the irradiation was stopped. Then the devices were transferred into a 35°C temperature chamber for all measurements but the C_{BE}, C_{BC}. Many of the devices were used over and over again in subsequent exposure runs by annealing the surface damage after each exposure.

As a result of these investigations we repeatedly observed a very large bias dependence of the surface damage on normal (gas filled) NPN transistors. Namely, devices with a reverse biased C-B junction (10V) or in the usual active state (reverse biased CB, forward biased EB) showed almost an order of magnitude higher radiation sensitivity than the passive ones during exposure. Note that

the final amount of damage for doses above$\approx 10^6$ rads(Si) was approximately the same for all the devices. I.e., the substantial differences in radiation sensitivity were evident only at the lower doses during measurements as a function of dose. (Incidentally, part of the high surface damage tends to decay with time after the irradiation is stopped and the bias is turned off. But after the partial recovery is completed the surface damage is still far more than that on the passive transistors.)

In sharp contrast to the behavior of the normal devices, no bias dependence of the surface damage was found on evacuated NPN transistors under otherwise identical exposure conditions. (Nevertheless, the surface degradation was still substantial; the same as those of the passive devices normal or evacuated). It appears then that the strong bias dependence of the surface degradation was entirely due to the ionization of the gas within the can and to the fringing electric field between the header and the base. Although this is a familiar explanation, proposed almost 6 years ago, it is quite a surprising result in view of the current models of radiation damage on oxidized Si surfaces. It means that somehow we have to explain the observed bias (i.e., electric field) independence of the surface degradation in the evacuated devices in terms of one or both of the two degrading factors: the positive charge generation within the SiO_2 and the new interface states. Keeping in mind that the base surface in the vicinity of the EB junction would be subjected to a weak fringing field due to the reverse biased CB junction we believe that the implications are the following:

i) The charge accumulation was sufficient to cause surface damage either by modifying the surface potential or by the effect of the charge related interface states or both.

This charge accumulation, however, was not affected by the fringing electric field due to the biases (e.g., the diffusion was the dominant factor.)

ii) The charge accumulation, although affected by the fringing electric field, was insignificant to cause damage through the modification of the surface potential. Then apparently the primary cause of surface degradation was the creation of the new interface states which were independent of the charge accumulation in the SiO_2. This last conclusion would be at variance with the proposal by Goetzberger, et al (Ref. II-9) that the new interface states around the middle of the bandgap are due to double charges or charge clusters in the SiO_2.

Significantly, the arguments presented in i) and ii) above also follow from the studies of I_B^{inv} and I_{CBO}. Since the base contact overlaps the CB junction in the Fairchild 2N1613 transistors, no charge accumulation on the surface did take place. Nevertheless, a substantial degradation of both I_B^{inv} and I_{CBO} was usually observed for both normal and evacuated devices. However, this degradation was always independent of reverse bias (10V) across the CB junction. This result can be understood only by argument similar to i) and ii).

Since it is difficult to see how the charge accumulation as presented in i), could not be influenced by the high fringing fields (as caused by a 10-volt reverse bias across the CB junction) and since the important role of the new interface states in surface degradation is well established, we believe that proposal ii) has higher credibility than i).

Figures (II-1) through (II-4) show some typical curves. To reduce confusion on these preliminary figures, only the data of one transistor is shown to represent a given test condition. The feasibility of using evacuated transistors in a radiation environment to make them more radiation resistant should be explored and re-examined.

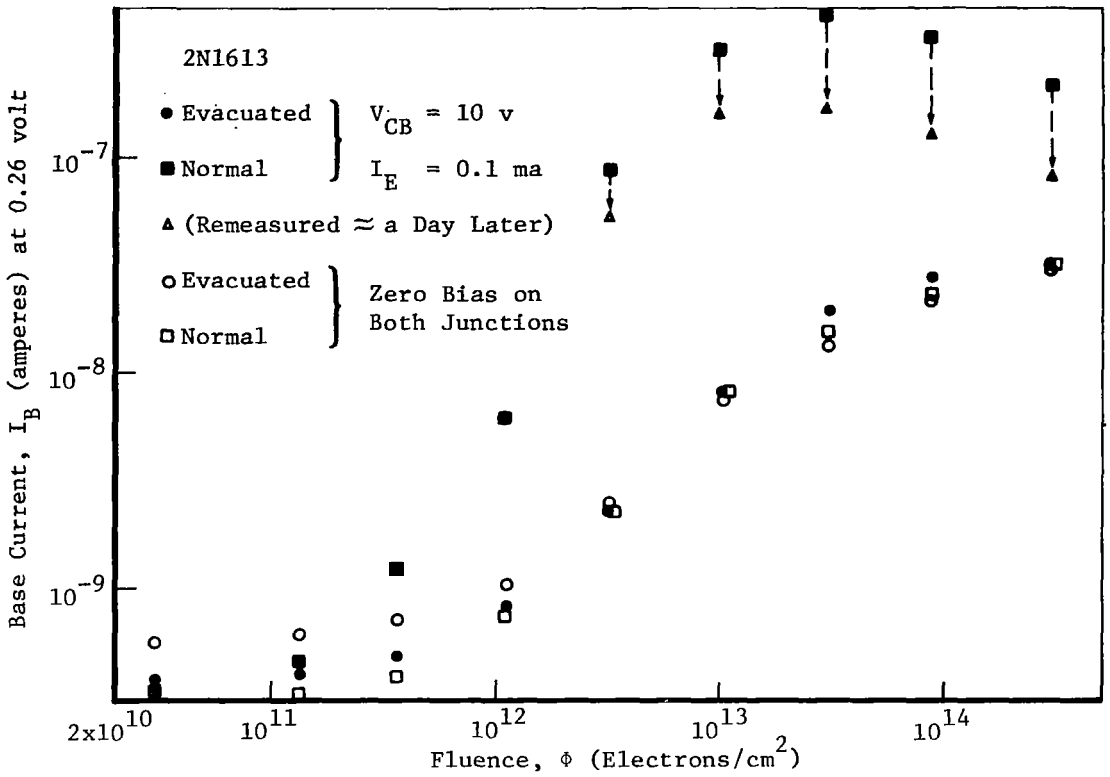

Figure 1: BASE CURRENT, I_B VERSUS FLUENCE

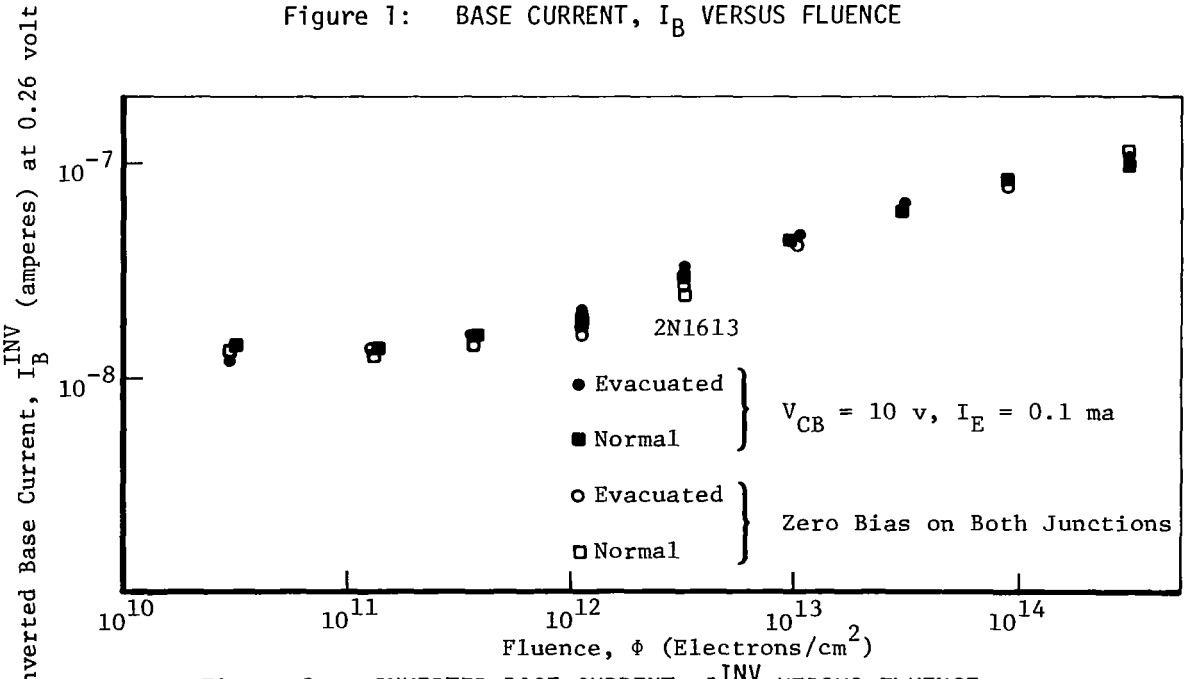

Figure 2: INVERTED BASE CURRENT, I_B^{INV} VERSUS FLUENCE

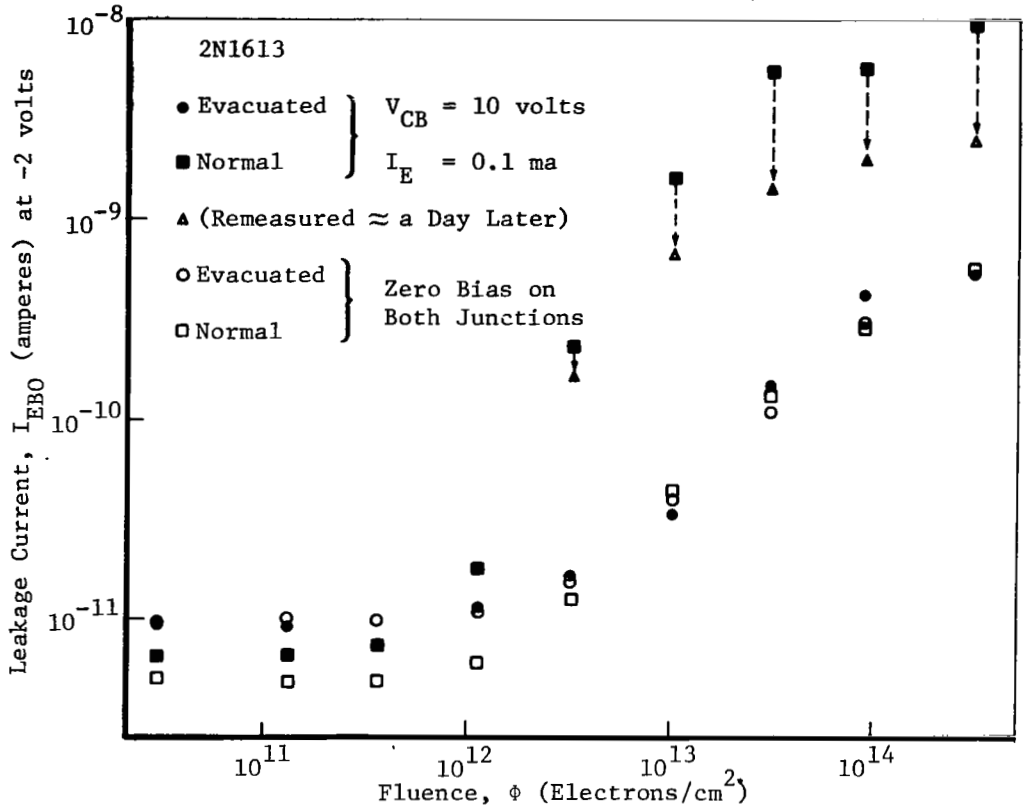

Figure 3: LEAKAGE CURRENT, I_{EBO} VERSUS FLUENCE

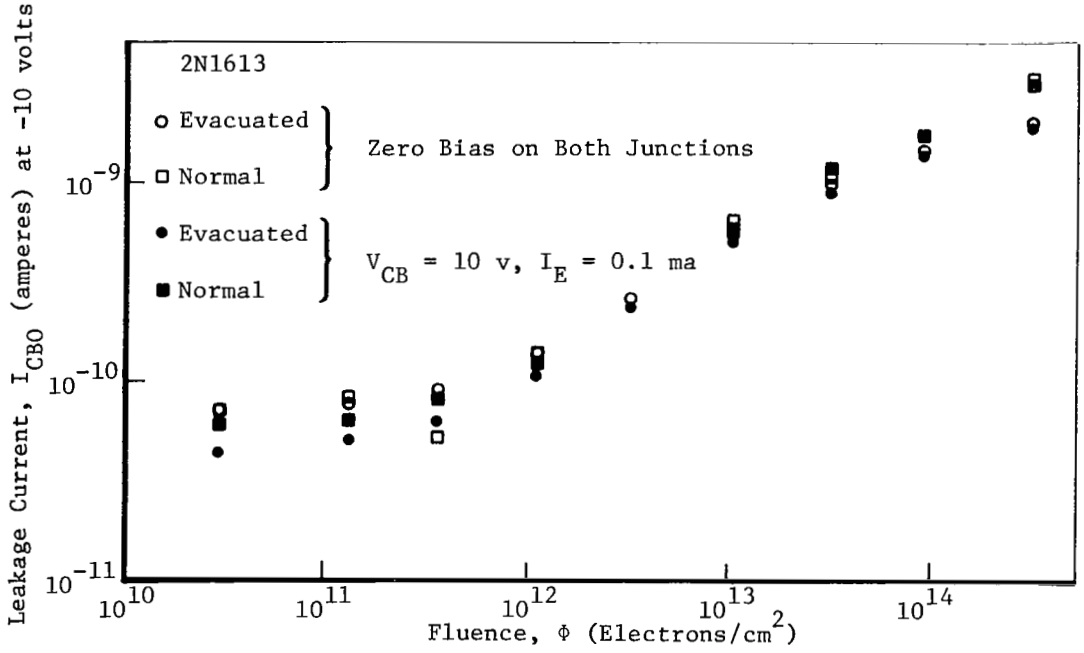

Figure 4: LEAKAGE CURRENT, I_{CBO} VERSUS FLUENCE

REFERENCES

II-1. C.D. Taulbee, et al., Radiation Effects in Electronics, ASTM Special Technical Publication, 384, 121 (1964).
D. L. Nelson and R. J. Sweet, IEEE Trans. Nucl. Sci. NS-13, 197 (1966).

II-2. E. R. Schmid's work have been quoted by J. P. Mitchell and D. K. Wilson, Bell Syst. Techn. J. XLVI, 1 (1967) on p. 48.

II-3. H. L. Hughes, IEEE Trans. Nucl. Sci. NS-12, 53 (1965).

II-4. W. Poch and A. G. Holmes-Siedle, IEEE Trans. Nucl. Sci. NS-15, 213 (1968).

II-5. E. H. Snow, et al., IEEE Proc. 55, 1168 (1967).

II-6. R. J. Maier, IEEE Trans, Nucl. Sci. NS-14, 252 (1967).

II-7. P. J. Estrup, Sol. State Electr. 8, 535 (1965).

II-8. See also:
P. R. Measel and R. R. Brown, IEEE Trans. Nucl. Sci. NS-15, 224 1968). L. L. Sivo and R. R. Brown, Contract NAS5-10443, Document No. D2-125680-2.

II-9. A. Goetzberger, et al., Appl. Phys. Letter, 12, 95 (1968).